LBL-19276
c.2

Lawrence Berkeley Laboratory

UNIVERSITY OF CALIFORNIA

RECEIVED
LAWRENCE
BERKELEY LABORATORY
APR 17 1985
LIBRARY AND
DOCUMENTS SECTION

CHEMICAL BIODYNAMICS DIVISION

I. KINETICS OF OLIGODEOXYNUCLEOTIDE DOUBLE STRAND FORMATION AND THE INTERACTION OF AN UNCHARGED INTERCALATOR WITH DNA. II. THE AQUEOUS PHOTOCHEMISTRY OF 4'Hydroxymethyl-4,5', 8-trimethylpsoralen

J.P.Y. Kao
(Ph.D. Thesis)

December 1984

TWO-WEEK LOAN COPY

This is a Library Circulating Copy which may be borrowed for two weeks.

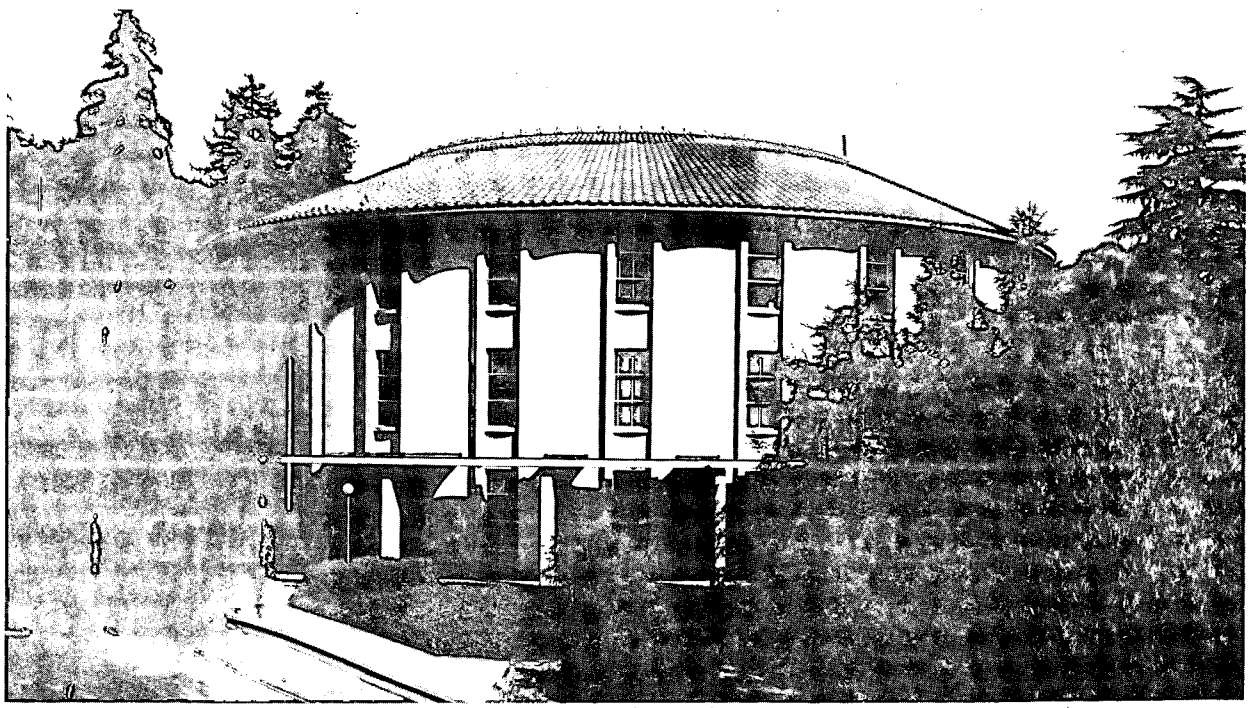

LBL-19276
c.2

Prepared for the U.S. Department of Energy under Contract DE-AC03-76SF00098

DISCLAIMER

This document was prepared as an account of work sponsored by the United States Government. While this document is believed to contain correct information, neither the United States Government nor any agency thereof, nor the Regents of the University of California, nor any of their employees, makes any warranty, express or implied, or assumes any legal responsibility for the accuracy, completeness, or usefulness of any information, apparatus, product, or process disclosed, or represents that its use would not infringe privately owned rights. Reference herein to any specific commercial product, process, or service by its trade name, trademark, manufacturer, or otherwise, does not necessarily constitute or imply its endorsement, recommendation, or favoring by the United States Government or any agency thereof, or the Regents of the University of California. The views and opinions of authors expressed herein do not necessarily state or reflect those of the United States Government or any agency thereof or the Regents of the University of California.

LBL-19276

I. Kinetics of Oligodeoxynucleotide Double Strand Formation and the Interaction of an Uncharged Intercalator with DNA

II. The Aqueous Photochemistry of 4'Hydroxymethyl-4,5',8-trimethylpsoralen

Joseph Pao Yung Kao

Ph.D. Thesis

Lawrence Berkeley Laboratory
University of California
Berkeley, California 94720

December 1984

I. Kinetics of Oligodeoxynucleotide Double Strand Formation and the Interaction of an Uncharged Intercalator with DNA

II. The Aqueous Photochemistry of 4'-Hydroxymethyl-4,5',8-trimethylpsoralen

by

Joseph Pao Yung Kao

ABSTRACT

Two deoxyoligonucleotide duplexes were studied by temperature-jump relaxation kinetic experiments: dCA_6G + dCT_6G, a completely base-paired duplex, and dCA_3CA_3G + dCT_6G, a "bulged" duplex containing an extra unpaired cytosine. The kinetics of forming the perfect duplex is simply described by a single step, characterized by a recombination and a dissociation rate constant. Kinetically, the perfect duplex is similar to the homologous duplex dCA_5G + dCT_5G studied previously (Nelson & Tinoco, 1982). Formation of the "bulged" duplex proceeds with a recombination rate constant which decreases with increasing temperature—recombination occurs with a negative activation energy. This lead to a two-step model for forming the "bulged" duplex: a rapid pre-equilibrium which generates a partially formed duplex, followed by a unimolecular "zipping-up to yield the complete "bulged" duplex.

HMT, a neutral furocoumarin, forms a complex with calf thymus DNA. The thermodynamics and kinetics of this process were studied. HMT binds to DNA ~100 times more weakly than the positively charged ethidium and proflavin. This difference is accounted for almost entirely by differences in the ethalpy of binding and not in the

entropy. Analyzing the binding of HMT to DNA in buffers varying over a range of sodium ion concentrations showed that HMT binds to DNA by intercalation. Studying the binding by temperature-jump techniques led to a sequential binding model. DNA intercalates directly into DNA in a bimolecular step. The intercalated complex may rearrange to an alternative form the nature of which is unknown. The bimolecular rate constant for intercalation is $5.44 \times 10^5\ M^{-1}s^{-1}$ at 25°C. This rather small rate constant is the result of a large and negative entropy of activation (-19 e.u.) for intercalation.

HMT undergoes photochemical reactions when irradiated with UV light. Investigations into the aqueous photochemistry of HMT revealed three principal products: two dimers formed by cycloaddition and one photoisomerized form of HMT. One dimer is formed by head-to-tail joining while the other results from head-to-head joining. Both dimers have <u>cis</u>-<u>syn</u> configuration. The photoisomer has been tentatively assigned as having a furan ring flipped 180° relative to the parent HMT.

DEDICATION

This meager work is dedicated to my parents

Kao Kung-Lu and

Kao Liu Wan-Yung

who gave me love and strength.

ACKNOWLEDGEMENTS

Acknowledgements could never fully express the debts I owe to all the people in my life; moreover, they are the type of thing which often have little significance except for the author. A couple of pages filled with expressions of gratitude serve to mark in a graduate career those events and associations I feel contributed positively to my being. As such, acknowledgements are in the end a form of self-affirmation: justifying six years of life through hind-sight. It was in such a mood that the following emotional laundry list was compiled.

A vague sense of chronology dictates an early mention of the lab members from the primordial ages. Steve Winkle was, loosely speaking, my direct predecessor. "The Hairy Little Midget", as he was fondly known, had a recklessness and a penchant for raucous fun that was inspiring. Art Pardi was at all stages a monitor and commentator on everyone's performance and often tried to prod us, with varying degrees of success, out of our lethargy. Ken Dahl occupies a special spot in my heart as the shy ogre with the good heart. His humor, wit, and a facility with language in its many forms made the lab habitable. Jeff Nelson is one of the smartest people I know. He was quite willing to lend the power of his mind to help anyone through a conceptual pinch. In the pantheon of "Super Post-Docs" sits Frank Martin, whose breadth and thoroughness of knowledge gave us a sense of coherence and direction. I should also thank Frank for the Corsicana fruit cakes. Carlos Bustamante, with his erudition and knowledge of the arts, enlivened and enlightened the lab.

Among my contemporaries I have Rob (Bob, at Pitt) Baseman and Rob Corn to thank for many restaurant-hunting expeditions around the Bay Area. Rob Corn is a good friend with a sense of the "done" and "not done". We share a warm friendship for which I am grateful. It is always with love that I think of Kathy Morden. She is to me an intelligent and zany sister and also no slouch when it comes to making exceptionally decadent chocolate cakes. Without her to fun and commiserate with, much of graduate life would have been unlivable.

David Keller deserves a special note of respect. He is a man devoted to being consistent with his principles. While I disagree with him on many points, I still find this effort toward consistency admirable. In a number of respects he is as good a true Christian as ever I have seen.

Jeff Cina, ex-member of the group and my roommate of three years, is a devoted friend. I thank him for being totally trusting and giving me the chance to be the same with him. I'm also indebted to him for having gotten me to start running regularly and keep it up for the last five years. Natalie Ahn never ceases to impress me with her readiness to learn anything and everything that will better her science. A woman of extraordinary persistence and endurance, she is awesome as she runs through a marathon kinetics experiment consisting of fifteen-second time points. She has been my confidante in many personal matters and has been that rarity—a good sympathetic listener. Milan Tomic is good-hearted by nature, and when this is supplemented by his will to be kind in action, he often approaches

being saintly (but not in the common sickening way). He delights in the joys of others as much as his own. There is nothing forced about him. He is always willing to sooth and protect. I am happy to count him among my friends, Vulcan back-rubs notwithstanding.

Now I come to the woman of a thousand talents—Robi Mulford. Her every anecdotal account is a fine short story. If only she'd set everything down, she could be published in a month. She has never failed to be witty and knowledgeable on any subject. She is always honest—a truly frightening quality which few possess. For being loving and thoughtful, I thank her.

It was fortunate for me that Emil Scoffone joined the lab during the last throes of my graduate career. He is a man of intense concentration and once having set his mind to understand something, attacks it with an agonized persistence that is often painful for the on-looker. I have benefitted by his knowledge of history and literature and enjoyed the time we spent sampling Chinese and Italian "delicacies" fit only for old-world palates. I find him lovable for he, having accepted me as a friend, patiently endured my many ill-considered and injurious remarks. Growing up one in Padova and the other in Taipei, we seem to share much—presumably owing to having mothers who we believe must have graduated with honors from the same military academy!

Christa Hartmann arrived late but neverthleless impressed me with her sauciness. When she sheds her feisty mantle, she is gentle and understanding. She is one of the very few people I know who <u>will not</u>

stomach something she thinks is wrong and who will stand up for her rights and beliefs. In this she is an example for me. I hope I can catch up with her soon.

Phil Burns remained a good friend after his sojourn through our lab. He has had a profound effect on me. I thank him for having introduced me to weight training, a fine way to self-improvement, strangely enough. He has been caring even while demanding care from me. Ours has been a tortuous and fruitful friendship. With a measure of fairness, I should say that without Phil's understanding and concern, this work would have been completed long ago. (One is permitted one plagiarism)!

In the lab, there are three constancies: Barbara Dengler, David Koh and Helen Lok. Helen Lok was kind to me in the way that a Chinese mother is. We share some family history and find a common interest in Chinese literature. She has a strong faith in good and always sees the good in her coworkers. Barbara Dengler I have on occasion referred to as "Den Mother". She is generous and helpful. A firmness of character enables her to rein in generations of unruly thrashing graduate students. Barbara is the embodiment of order in the lab: in the most obvious way by ensuring the smooth running of the lab in matters of administration and routine, but more importantly she sits easily in a position of kind neutrality, partial to none, ministering to all that need her. It is thus belaboring the obvious to say that Barbara has my love and respect. In more material ways, I thank her for the yearly abundances of fresh produce from Brentwood and her

garden and the incessant flow of goodies from fine bakeries all around town. David Koh is a man I know by affinity. He has developed "easy-going" into a full, respectable way of life. He has never failed to sooth ruffled feathers and injured pride. In life he sits with the wise--this is trite except for those that know him. I'm very glad to have been accepted as a friend in the house of David and Nora.

I must thank my two uncles C. F. and C. H. Liu, who taught me science by example. They are inventive, clever and eclectic. The fun they have with their science often fill me with jealousy. Rarely also have I seen anyone with teaching abilities and styles even remotely approaching theirs. I'm forever indebted to these two men who have been at once fathers and teachers to me ever since my arrival in this country.

In some of my darkest moments at Berkeley, Carver Mead came to my rescue. A computer scientist by vocation and devilish punster by avocation, Carver has a mind which works at the physical limits of computation. When not listening to me discuss my work, he's always telling me about the newest developments in everything: vision, concurrent computation, patch-clamping... He knows all the finest eateries on the west coast, and damn near all the latrines accessible to the public on holidays and weekends. I thank Carver for leading me out of the smog and up Mount Waterman.

An enigmatic character is Nacho. Generations of students have told stories about what he is <u>really</u> like and I don't think anybody has a very good idea. I appreciated his <u>laissez-faire</u> direction which

at times, I must confess, appeared to be neglect and aroused in me a great resentment. To many in the past, Nacho is remembered for his dictum "Just figure out what you want to do and DO it!", which is maddening in the extreme but in the end is reasonable advice (providing that one lasts till the end). I thank Nacho for having paid me (no small favor, that) through all my thrashing about. I regret that I've never seen Nacho on a mountain.

Now for the business end of the matter. This work was supported in part by National Institutes of Heath Grant 10840 and by the Division of Biomedical and Evironmental Research of the U.S. Department of Energy under Contract 03-82ER60090.000. of DE-AC03-76SF00098.

TABLE OF CONTENTS

DEDICATION i

ACKNOWLEDGEMENTS ii

TABLE OF CONTENTS viii

CHAPTER I INTRODUCTION 1

CHAPTER II PERFECT AND BULGED DNA DUPLEXES: A KINETIC COMPARISON 11

1. Introduction 11
2. Experimental 12
3. Results 18
4. Discussion 51

CHAPTER III THE INTERACTION OF AN UNCHARGED MUTAGEN WITH DNA 67

1. Introduction 67
2. Experimental 69
3. Results 74
   A) Thermodynamics 74
   B) The Nature of the HMT-DNA Complex 88
   C) Relaxation Kinetics 94
4. Discussion 107

CHAPTER IV THE AQUEOUS PHOTOCHEMISTRY OF HMT 126

1. Introduction 126
2. Experimental 129
3. Results 132

A) HPLC Analyses 132

B) UV Spectra 142

C) Pyrolysis Experiments 150

D) Mass Spectral Results 151

E) NMR Spectral Information 166

4. Discussion 174

A) Compound HT 174

B) Compound HM 181

C) Compound I 185

APPENDIX 1 MISCELLANEOUS COMPONENTS FOR THE DIALOG TEMPERATURE JUMP INSTRUMENT 191

1. The Polarizer and Orientational Effects 191

2. Fluorescence Measurement: Improving the Signal to Noise 191

A) UV-Enhanced High Reflectivity Planar Mirror 192

B) Concave Mirror 193

C) Cut-Off Filters 193

3. The Arc Lamp 194

APPENDIX 2 THE ZERO-SUPPRESSION OPTION ON THE DIALOG TEMPERATURE JUMP INSTRUMENT 196

1. The Ability of the Discharge to Trigger the Gate Voltage Output of the Tektronix Time Base 199

2. High-Positive Z Output from the Control Unit as Function of Time in Zero-Suppression Mode 199

3. Behavior of the Gate Voltage in Zero-Suppression Mode 204

4. An Example Illustrating the Use of Zero-Suppression 204

APPENDIX 3 CALIBRATING THE TEMPERATURE JUMP INSTRUMENT 211

1. Determining the Size of the Temperature Jump 213

A) Absorbance of the Calibration Solution as a Function of Temperature 213

B) Size of the Temperature Jump as a Function of the Capacitor Voltage 214

2. Determining the Heating Time on the Instrument 216

BIBLIOGRAPHY 217

CHAPTER I

INTRODUCTION

Addition or deletion of small numbers of base pairs in DNA constitute the class of frameshift mutations. Studies of the DNA sequences involved in frameshift mutations have revealed that a large number of the mutations occur in repetitive sequences, e.g., the addition or deletion of an AT base pair in a run of five AT base pairs (Streisinger *et al.*, 1966; Okada *et al.*, 1966; Okada *et al.*, 1972). This observation, which was first made in studying the lysozyme gene of T4 phage, led Streisinger and others to propose a mechanism for generating frameshift mutations in repetitive sequences (Streisinger *et al.*, 1966). In the Streisinger model, a run of identical base pairs allows the two strands of the DNA to slip and be misaligned during replication, recombination, or repair. These slip-mismatched structures, if uncorrected, become frameshift mutations. The Streisinger model is depicted pictorially in Figure 1.1.

Consideration of certain frameshift mutations in the T4 lysozyme gene and the iso-1-cytochrome *c* gene of the yeast *Saccharomyces cerevisiae* prompted Ripley to propose a frameshift model involving near-palindromic DNA sequences (Ripley, 1982). In this model, imperfect sequence complementarity in the stem regions of the secondary structures formed by the near-palindromes give rise to small loops of unpaired bases. These loops are the potential sites of

Figure 1.1 Streisinger Model for Frameshift Mutations in Repetitive Sequences

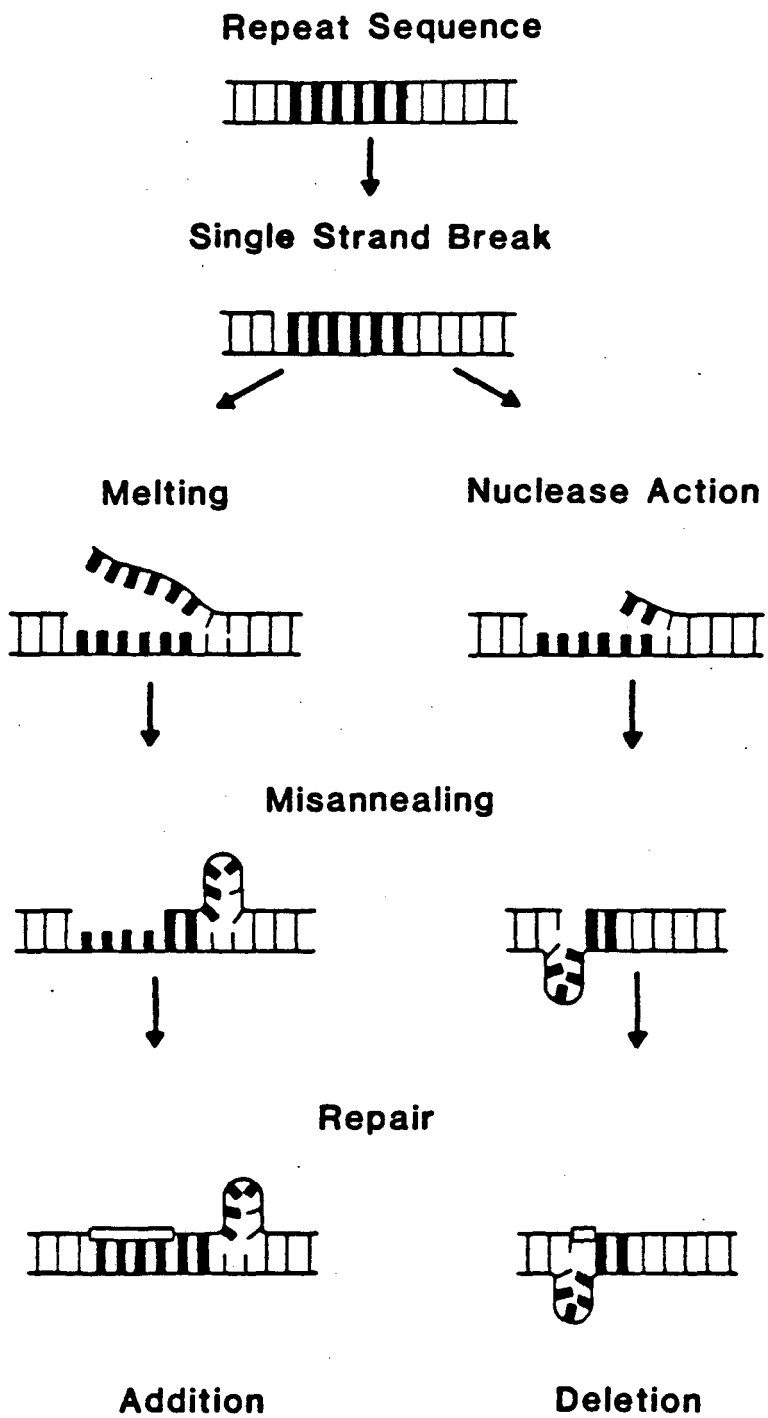
Repeat Sequence
Single Strand Break
Melting
Nuclease Action
Misannealing
Repair
Addition
Deletion

Figure 1.2 The Quasi-Palindrome Frameshift Model of Ripley: Pathway I produces deletions in the B region by the templated incorporation of a sequence complementary to the A region. Pathway II produces additions in the A region by the templated incorporation of a sequence complementary to the B region. (From Ripley, 1982).

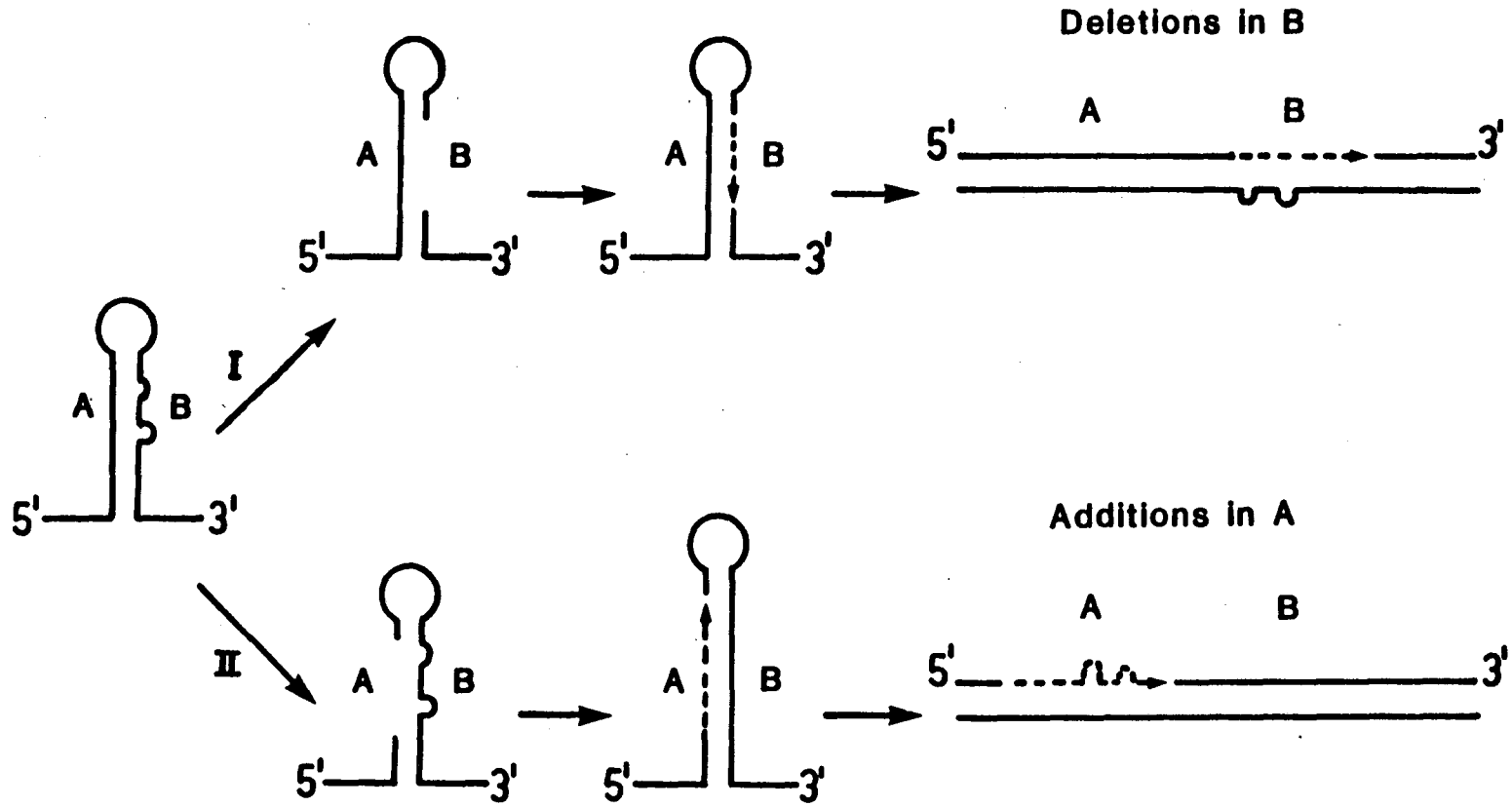
Deletions in B
A
B
5'
3'
I
II
Additions in A

frameshift mutations. The Ripley model is diagrammed in Figure 1.2. This model allows for both addition and deletion in DNA sequences which are not runs of identical bases and accounts for a substantial sub-class of frameshift mutations which previously had no rational mechanistic basis.

Comparing the two models, one sees that the feature common to both mechanisms is the loop or bulge of unpaired bases. In attempting to understand the models better, we can begin by examining the physical chemistry of various nucleic acid structures postulated in the models. Previous work in this laboratory has focussed on the behavior of perfectly based-paired nucleic acid helices. Recently, we have been able to synthesize by organic chemical techniques oligodeoxynucleotides which can form bulged structures akin to those postulated in the frameshift models. The second chapter of this work is a comparison of the kinetic behavior of a perfectly base-paired DNA duplex and a "bulged" duplex containing an extra cytosine on one strand. Thermodynamic and structural studies on the same duplexes have been presented elsewhere (Morden et al., 1983).

While frameshift mutations do occur spontaneously in nature, it is possible to increase the frequency of such mutations to many times above the natural frequency by challenging an organism with certain mutagens. Frameshift mutagens generally tend to be polycyclic aromatic or heteroaromatic compounds capable of intercalating into the DNA helix. Other workers have investigated the interactions between intercalators and nucleic acids. Two intercalators have been

particularly favored in previous studies and these are the ethidium ion and the protonated proflavin (Li & Crothers, 1969; Schmechel & Crothers,1971; Bresloff & Crothers,1975; Ramstein et al., 1980). The structures for these mutagens are displayed in Figure 1.3. These intercalators are characterized by their cationic charge, high aqueous solubility and the high stability of their complexes with DNA. There has been no detailed work on uncharged frameshift mutagens, which might be the more biologically relevant choices for study. The reasons for this will be elaborated in Chapter III, which contains thermodynamic and kinetic results on the interaction between calf thymus DNA and a neutral intercalator, 4'-hydroxymethyl,4,5',8-trimethylpsoralen (also known as 4'-hydroxymethyltrioxalen, or HMT). The structure of HMT is shown in Figure 1.3. HMT is a photoreagent which forms covalent adducts with thymine bases in DNA when irradiated with ultraviolet light.

In doing the temperature jump kinetic studies on HMT and calf thymus DNA, it became clear that exposure of the sample mixture to the UV light used to probe the sample generated chemical species which contributed unwanted signals. These signals were not due to the conventional DNA-HMT adducts which were produced only in negligible amounts under the conditions of the experiment. The chemical species responsible for the spurious signals proved to be photoreaction products of HMT alone. Chapter IV is an account of the experimental detour I made to isolate and characterize the major products generated by the aqueous photochemistry of HMT. Results

Figure 1.3 Structures of Proflavin and Ethidium Cations and HMT

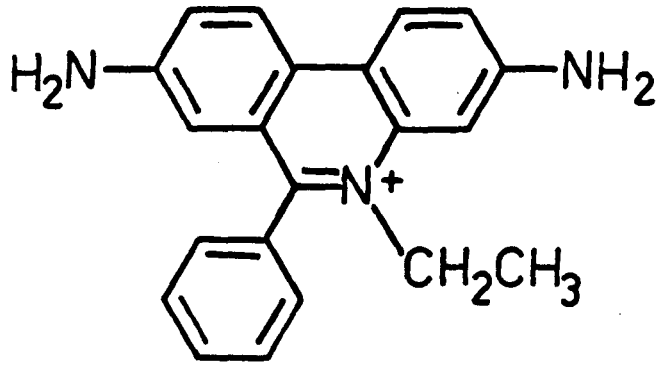

Ethidium Cation

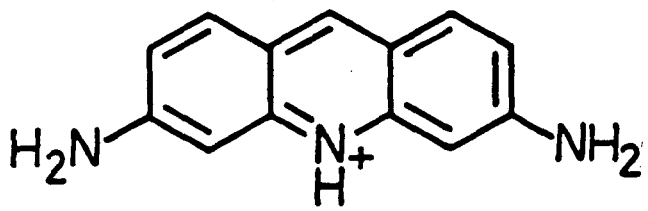

Proflavin Cation

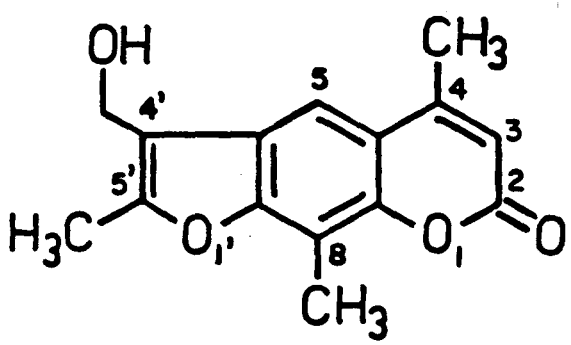

HMT

from the study include some new instances of classical organic photochemistry and some novel twists on photoisomerizations.

Also included are three appendices. Appendix 1 offers descriptions of various user-changeable components for the Dialog temperature jump instrument as well as instructions for their use. Ordering information for parts requiring occasional to frequent replacement can also be found in Appendix 1. In Appendix 2 are given reasonably detailed instructions on using the ZERO-SUPPRESSION option on the temperature jump instrument. One finds also in Appendix 2 several procedures for verifying that the instrument is operating properly in the zero-suppresion mode. At the end of Appendix 2 is an example illustrating the proper use of the zero-suppresion option. Appendix 3 outlines methods for calibrating temperature jump sizes and for calibrating the heating time (limiting rise time) of the instrument.

Finally, I made no attempt to give detailed derivations for various equations and mathematical expressions used in analyzing results from temperature jump experiments. The theory underlying relaxation kinetic methods can be found in the text written by Bernasconi (Bernasconi, 1976). The book provides good treatments of almost all the topics in which one is likely to be interested. Furthermore, the author has compiled for the book a list of references which includes both seminal original publications as well as documentation on applications.

CHAPTER II

PERFECT AND BULGED DNA DUPLEXES:

A KINETIC COMPARISON

1. Introduction

In the course of DNA replication and repair, a class of mutations known as frameshift mutations can occur. A frameshift mutation is the insertion of extra bases into or the deletion of bases from the daughter DNA strand. Such insertions and deletions cause the triplet reading frame of the DNA to be shifted out of register (Crick et al., 1961), hence the name for this class of mutations. Two conformational models for how frameshift mutations arise have been proposed (Streisinger et al., 1966; Ripley, 1982). Commmon to both models is the requirement that some bases on one DNA strand must be "bulged out" and thus unpaired with bases on the opposing DNA strand. In the case of deletions on the daughter strand, the bulges form on the parent strand; whereas bulging on the daughter strand leads to additions on the daughter strand. An important feature of these frameshift models is the bulged structure. In order to render such structures accessible to physical study, attempts have been made to synthesize oligodeoxynucleotides with well-

defined sequences. These oligonucleotides are such that the double-stranded structures they form contain bases which have no complementary bases on the opposing strand. Previous to this work, the self-complementary tridecamer dCGCAGAATTCGCG, which forms a helix with two unpaired adenines, has been studied by calorimetric, NMR and temperature jump kinetic techniques (Patel et al., 1982b; Chu & Tinoco, 1983).

In the present study, a comparison is made between the perfect helical duplex formed by the oligonucleotides dCA_6G and dCT_6G and the duplex formed by dCA_3CA_3G and dCT_6G, which contains an extra unpaired cytosine. By examining the relaxation kinetics of these two systems, especially in the light of existing knowledge on oligonuleotides, one can hope to gain insight into the behavior of structurally imperfect DNA helices. Structural studies by NMR techniques as well as thermodynamic studies on the two duplexes used in this work have been reported elsewhere (Morden et al., 1983).

2. Experimental

The oligomer dCT_6G was synthesized using the solution diester method (Khorana, 1968). The molecules dCA_3CA_3G and dCA_6G were prepared using the phosphoramidite method modified for use on solid supports (Matteucci & Caruthers, 1981). All syntheses were carried out by Dr. Francis Martin. All oligonucleotides were desalted at least twice on Biogel P-2

columns and then frozen for storage.

Extinction coefficients for the oligomers were calculated using the ε_{260} values of mononucleotides and dinucleoside monophospates (CRC Handbook of Biochemistry and Molecular Biology, 1975). The extinction coefficients at 25°C and 260nm, per mole of single strands, are $66 \times 10^3\ l \cdot mol^{-1} \cdot cm^{-1}$ for dCT_6G, $91 \times 10^3\ l \cdot mol^{-1} \cdot cm^{-1}$ for dCA_6G, and $98 \times 10^3\ l \cdot mol^{-1} \cdot cm^{-1}$ for dCA_3CA_3G. Sample solutions of the duplexes were always prepared by mixing appropriate amounts of the single stands from aqueous stock solutions. These solutions were lyophilyzed and then taken up in the desired buffer. The buffer used for all experiments consisted of 28mM phosphate, 0.1mM EDTA and 0.2M NaCl, at pH 7.0.

The samples were filtered through Bio-Rad Uni-Pore polycarbonate membranes (pore size 3μm). Dissolved gasses were swept from the samples by purging the samples for 3-5 minutes with helium gas which had been saturated with water vapor. Because of a limited stock of the oligonucleotides, each sample was used for relaxation measurements at two temperatures. Thus, data at the two lower temperatures were gathered using one set of samples while data at the two higher temperatures were collected using a different set of samples.

The temperature jump instrument was manufactured by Dialog (Garching, West Germany). Detailed descriptions of the instrument have been published previously (Rigler et al., 1974;

Nelson, 1982). All relaxation data were recorded using spectrophotometric detection at 250nm. Temperature jumps of magnitude 1.8°C were produced by discharging a 20nf capacitor, charged to 20kV, through the sample. A detailed procedure for calibrating the size of temperature jumps is included in Appendix 3. The initial temperature of the sample was monitored to an accuracy of 0.2°C with the aid of a copper-constantan digital thermocouple (Fluke model 2100A) in contact with the upper electrode of the temperature jump cell.

The relaxation data were first stored digitally on a Biomation model 805 Transient Recorder. The data set from each jump consisted of 2048 time points. Via a PET microcomputer, each data set was transferred to a VAX 11/780 minicomputer for analysis. The data were analyzed using the program DISCRETE, written by S. W. Provencher (Provencher, 1976a,b). The program determines the number of exponential relaxation components which will yield the best fit to the relaxation data. The program was allowed to search for up to three components.

In analyzing the kinetic data, a simple two-state equilibrium can be used to describe the reaction between the oligonucleotides:

$$A + B \underset{k_d}{\overset{k_r}{\rightleftharpoons}} AB \qquad (2.1)$$

In this scheme, A and B represent the single-stranded oligodeoxynucleotides and AB, the duplex formed from the single strands. The unimolecular rate constant for dissociating the duplex is k_d, while k_r is the bimolecular rate constant for forming the duplex. When the equlibrium is perturbed by applying a temperature jump to the system, the system relaxes exponentially to a new equilibrium at the final temperature. This exponential process is characterized by a relaxation time, τ, given by

$$\tau^{-1} = k_r([A] + [B]) + k_d \qquad (2.2)$$

where [A] and [B] are the equilibrium concentrations of the single strands at the final temperature. Since in these experiments, the samples always contained the two single strands at equal concentrations, equation 2.2 reduces to

$$\tau^{-1} = 2k_rC_s + k_d \qquad (2.3)$$

where $C_s = [A] = [B]$. If one uses C_{tot}, the total concentration of either single strand, one can square equation 2.3 and eliminate the equilibrium concentration C_s to give

$$\tau^{-2} = 4k_rk_dC_{tot} + k_d^2 \qquad (2.4)$$

Two methods are thus available for analyzing the relaxation time data. First, we can measure $1/\tau$ for a series of total concentrations. Using a thermodynamically determined

Figure 2.1 Relaxation signal for dCA_6G + dCT_6G at 8.75 μM total concentration and a final temperature of 19°C

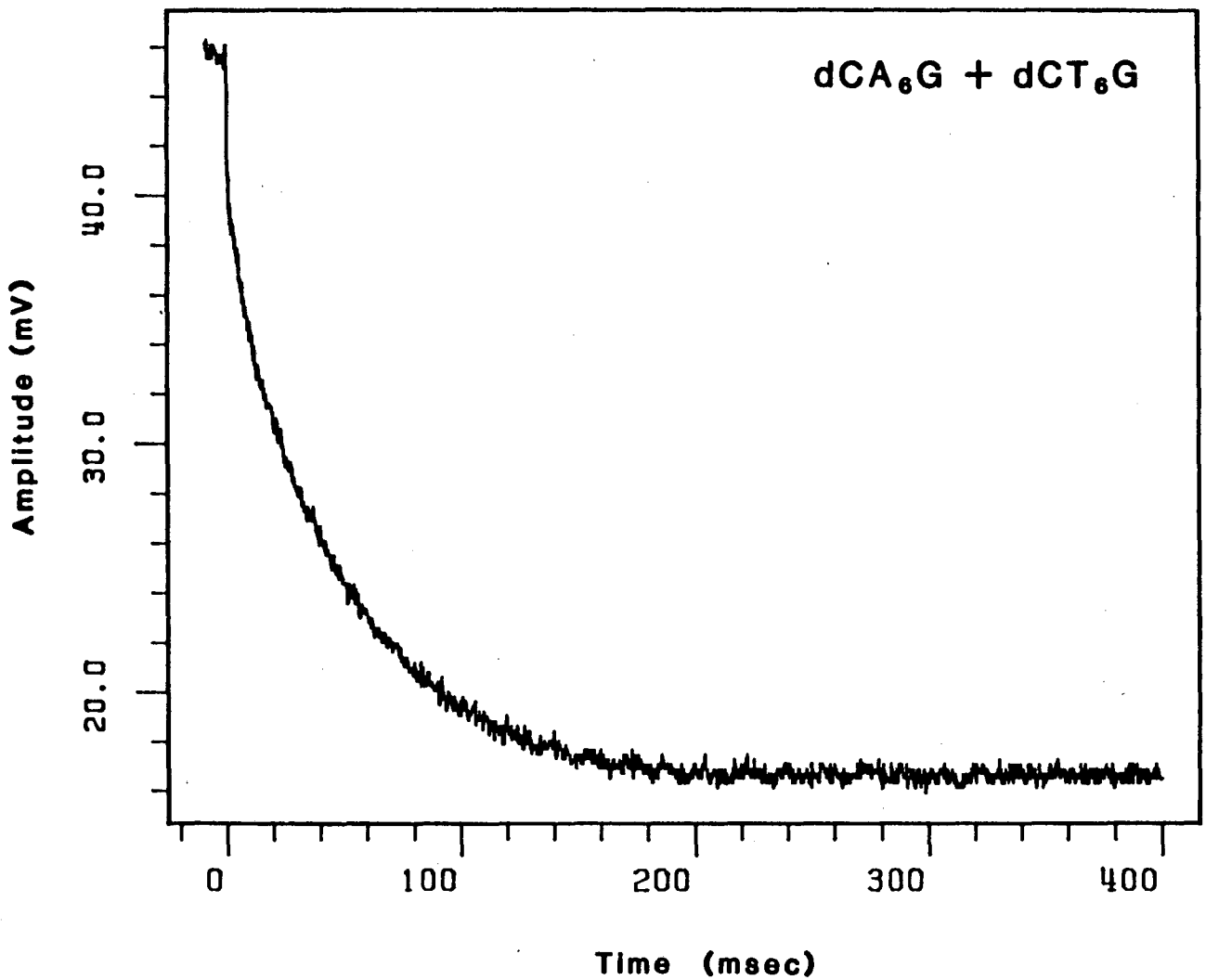
dCA6G + dCT6G
Amplitude (mV)
40.0
30.0
20.0
0
100
200
300
400
Time (msec)

equilibrium constant, or an estimate of it, C_s can be calculated at each C_{tot}. With this set of trial C_s values, a plot of $1/\tau$ vs C_s yields estimates of k_r and k_d. Using $K_{kinetic} = k_r/k_d$, a new set of C_s values is calculated and the linear fit of $1/\tau$ vs C_s repeated. Applying this procedure iteratively results in a set of C_s, k_r and k_d values consistent with the kinetic data.

An alternative method is to plot $1/\tau^2$ vs C_{tot}. By equation 2.4, k_r and k_d values can be extracted from the plot. Once the rate constants are known at various temperatures, plots of $\log_e(k)$ vs $1/T$ yield the activation parameters.

3. Results

Shown in Figure 2.1 is a trace of the relaxation signal for the system $dCA_6G + dCT_6G$ at 8.75μM total concentration and a final temperature of 19°C. The initial (baseline) signal was set equal to 5V. For data sets such as this example, a single exponential component was almost always found, although occasionally, a second fast relaxation component of very small amplitude was also revealed by the analysis. The small-amplitude fast component was most likely the result of initial transient disturbances caused by the temperature jump and was not included in subsequent kinetic analyses. The relaxation times used in the kinetic analyses were averages of five to ten relaxation measurements for each sample.

Plots of the fit of the inverse relaxation times to

Table 2.1 Kinetic Results for $dCCA_3CA_3G$ + dCT_6G Using Different Analytical Methods

	$k_r x10^{-6}$ $[M^{-1}s^{-1}]$		k_d $[s^{-1}]$	
	Iterate		Iterate	
	τ^{-1} vs C_s	τ^{-2} vs C_{tot}	τ^{-1} vs C_s	τ^{-2} vs C_{tot}
5°C	6.72 ± 0.05	6.80 ± 0.82	8.3 ± 0.3	8.2 ± 0.9
10°C	2.07 ± 0.03	2.11 ± 0.04	82.6 ± 0.5	82.0 ± 0.6
13°C	2.23 ± 0.06	2.22 ± 0.07	196 ± 1	196 ± 1
16°C	1.07 ± 0.17	1.08 ± 0.18	489 ± 5	489 ± 5

Table 2.2 Kinetic Results for $dCA_6G + dCT_6G$ Using Different Analytical Methods

	$k_r x10^{-6}$ $[M^{-1}s^{-1}]$		k_d $[s^{-1}]$	
	Iterate		Iterate	
	τ^{-1} vs C_s	τ^{-2} vs C_{tot}	τ^{-1} vs C_s	τ^{-2} vs C_{tot}
14°C	0.65 ± 0.20	0.75 ± 0.60	4.4 ± 1.2	4.1 ± 2.1
19°C	1.5 ± 0.1	1.4 ± 0.4	7.1 ± 0.9	7.4 ± 1.6
24°C	2.5 ± 0.3	2.5 ± 0.7	24 ± 3	24 ± 4
29°C	2.0 ± 0.2	2.0 ± 0.2	117 ± 2	117 ± 3

Figure 2.2-2.5 $1/\tau$ vs C_s plots for $dCA_6G + dCT_6G$ at 14°C, 19°C, 24°C and 29°C, respectively.

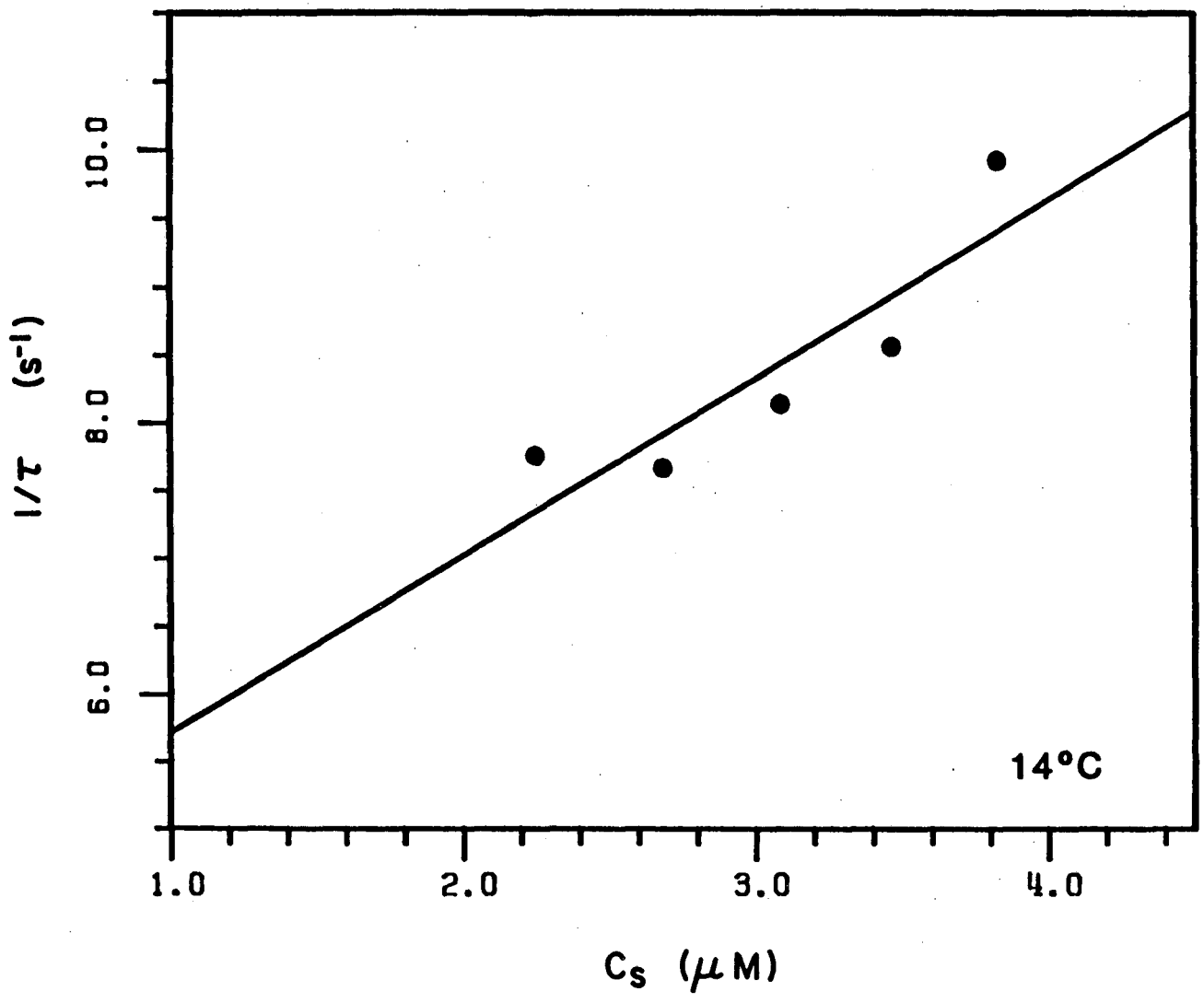
10.0
8.0
6.0
1/τ (s⁻¹)
14°C
1.0
2.0
3.0
4.0
Cs (μM)

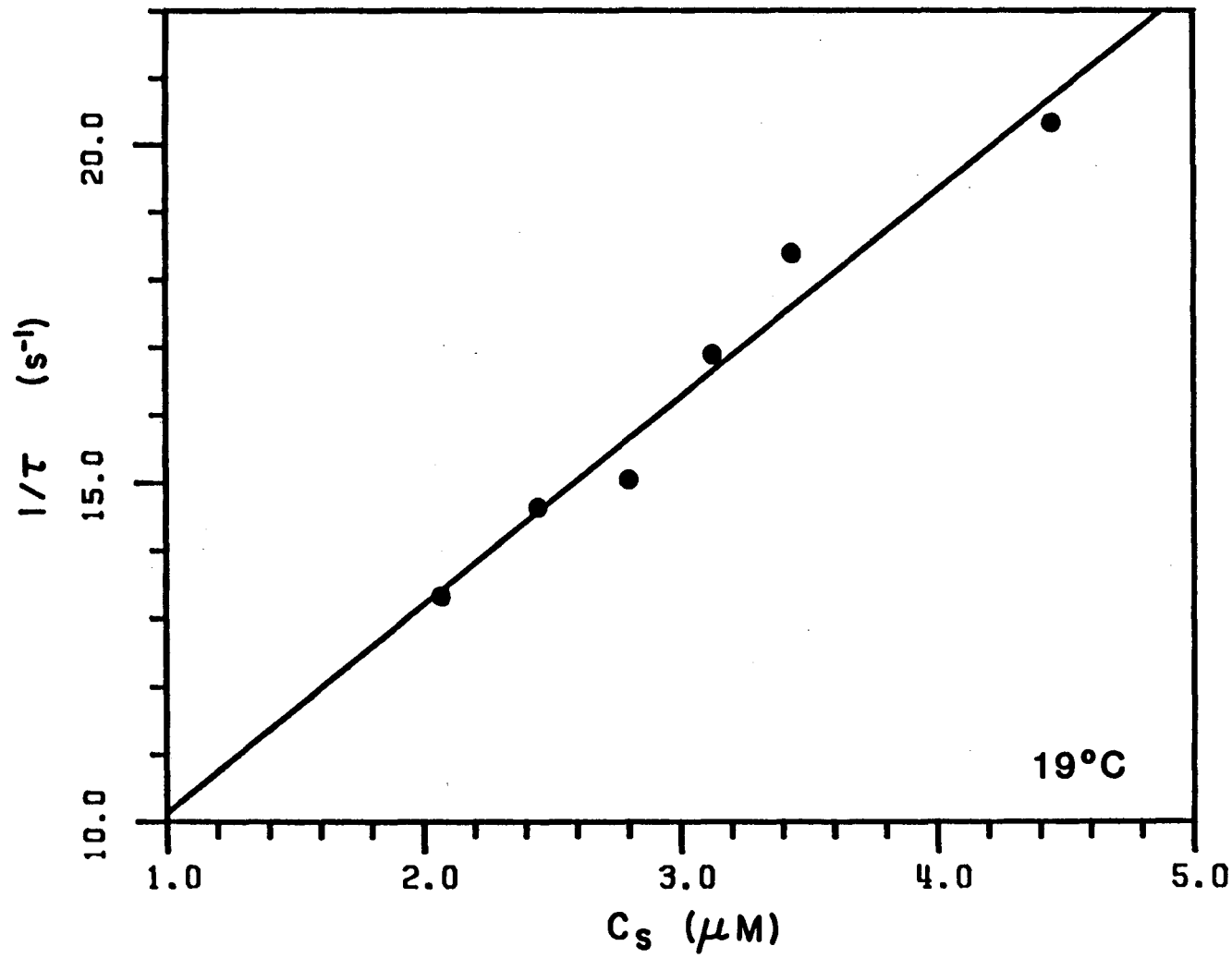
20.0
15.0
10.0
1/τ (s⁻¹)
1.0
2.0
3.0
4.0
5.0
Cs (μM)
19°C

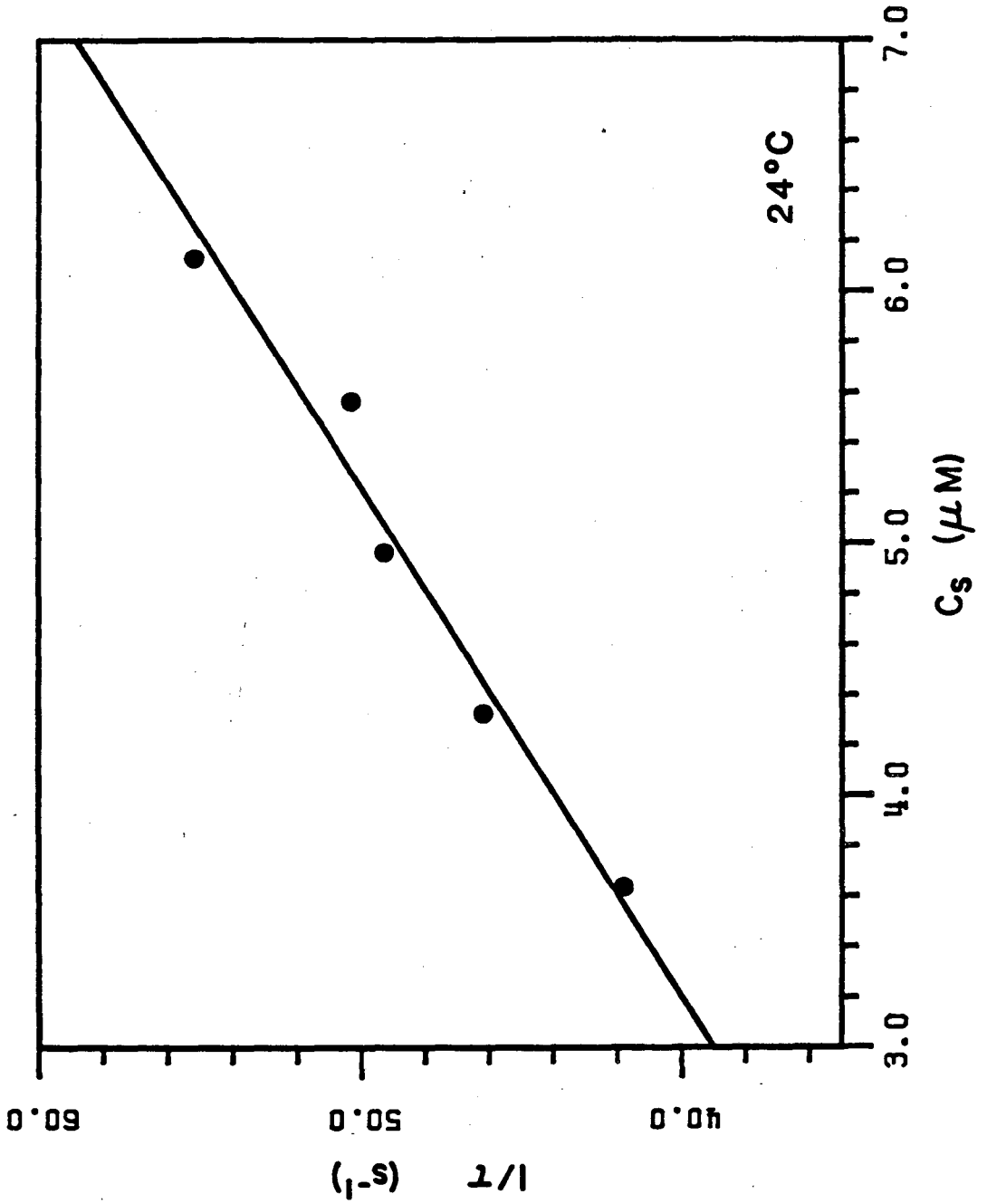
24°C
3.0
4.0
5.0
6.0
7.0
C_s (μM)
40.0
50.0
60.0
$1/\tau$ (s^{-1})

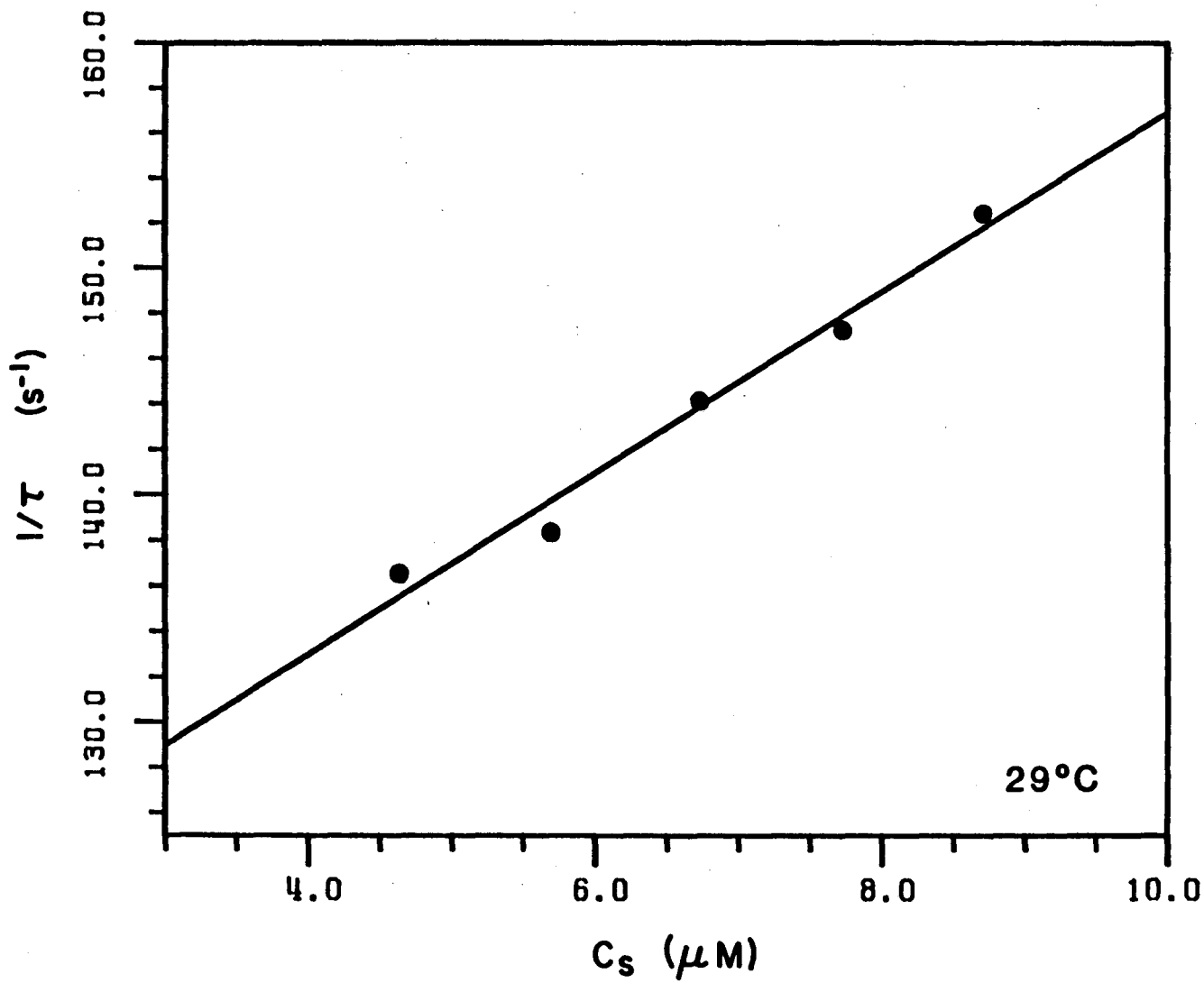
160.0
150.0
140.0
130.0
1/τ (s⁻¹)
29°C
4.0
6.0
8.0
10.0
Cs (μM)

Figure 2.6-2.9 Plots of $1/\tau^2$ <u>vs</u> C_{tot} for $dCA_6G + dCT_6G$ at 14°C, 19°C, 24°C and 29°C, respectively.

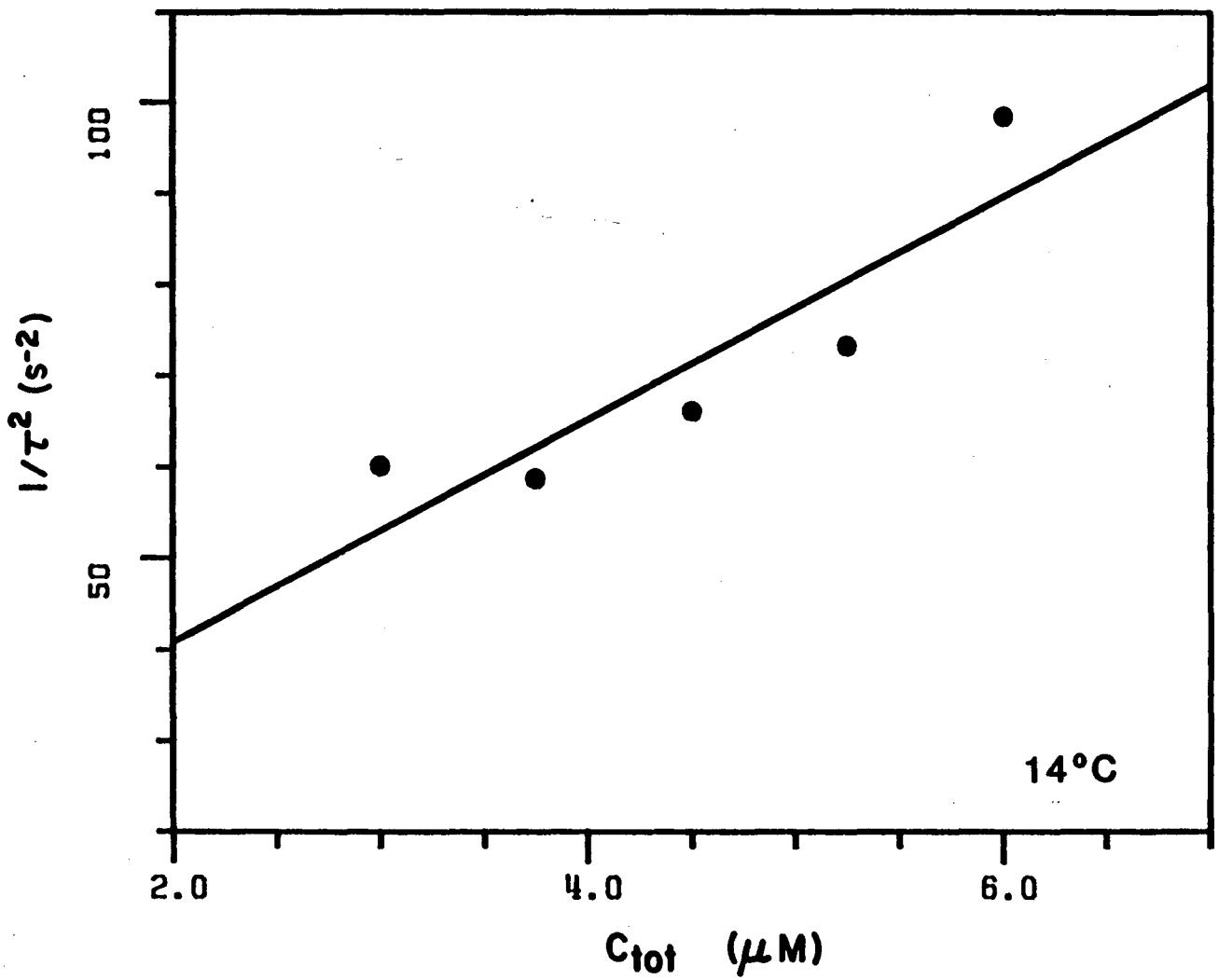
100
50
$1/\tau^2$ (s^{-2})
14°C
2.0
4.0
6.0
C_{tot} (μM)

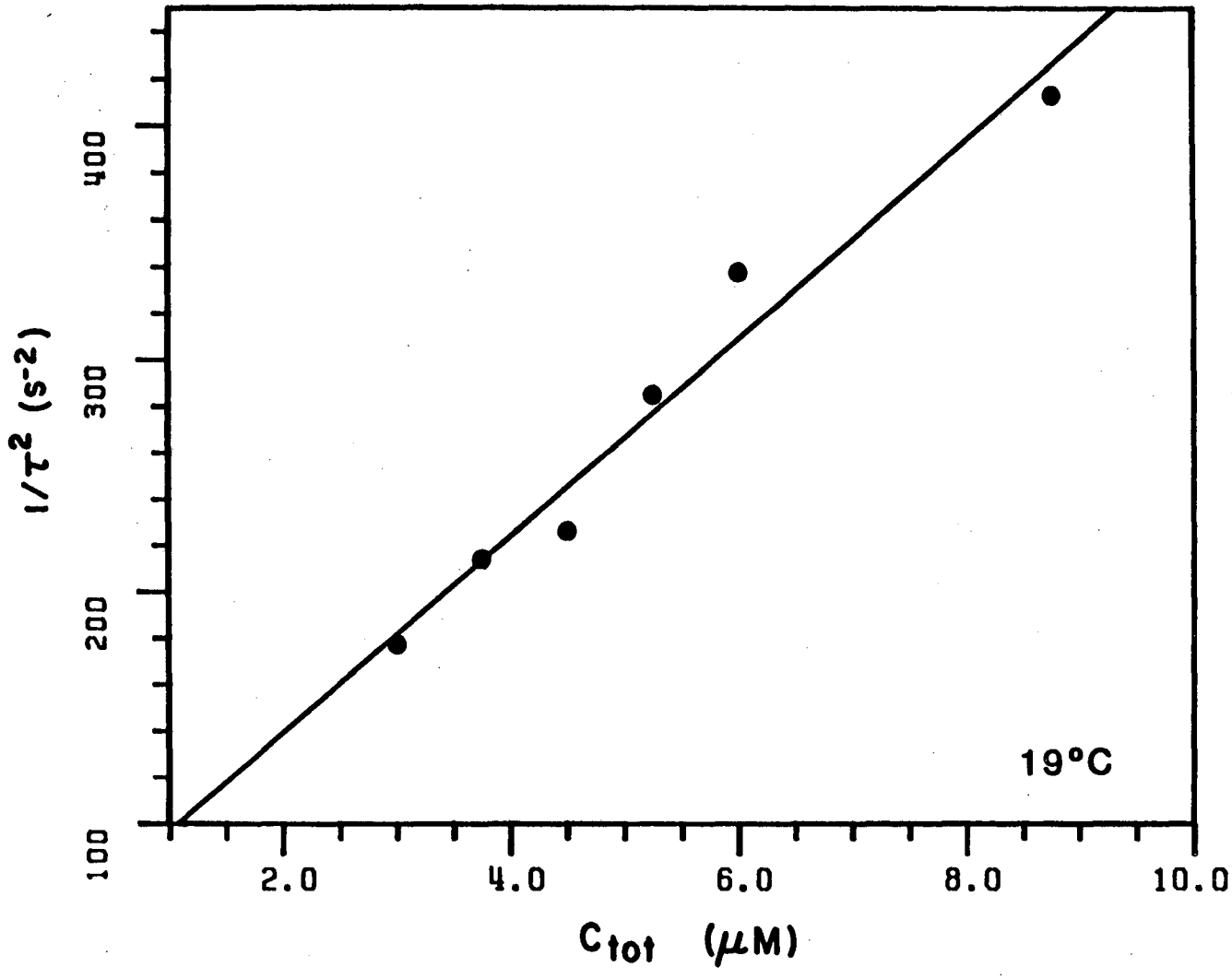
19°C
$1/\tau^2$ (s^{-2})
100
200
300
400
2.0
4.0
6.0
8.0
10.0
C_{tot} (μM)

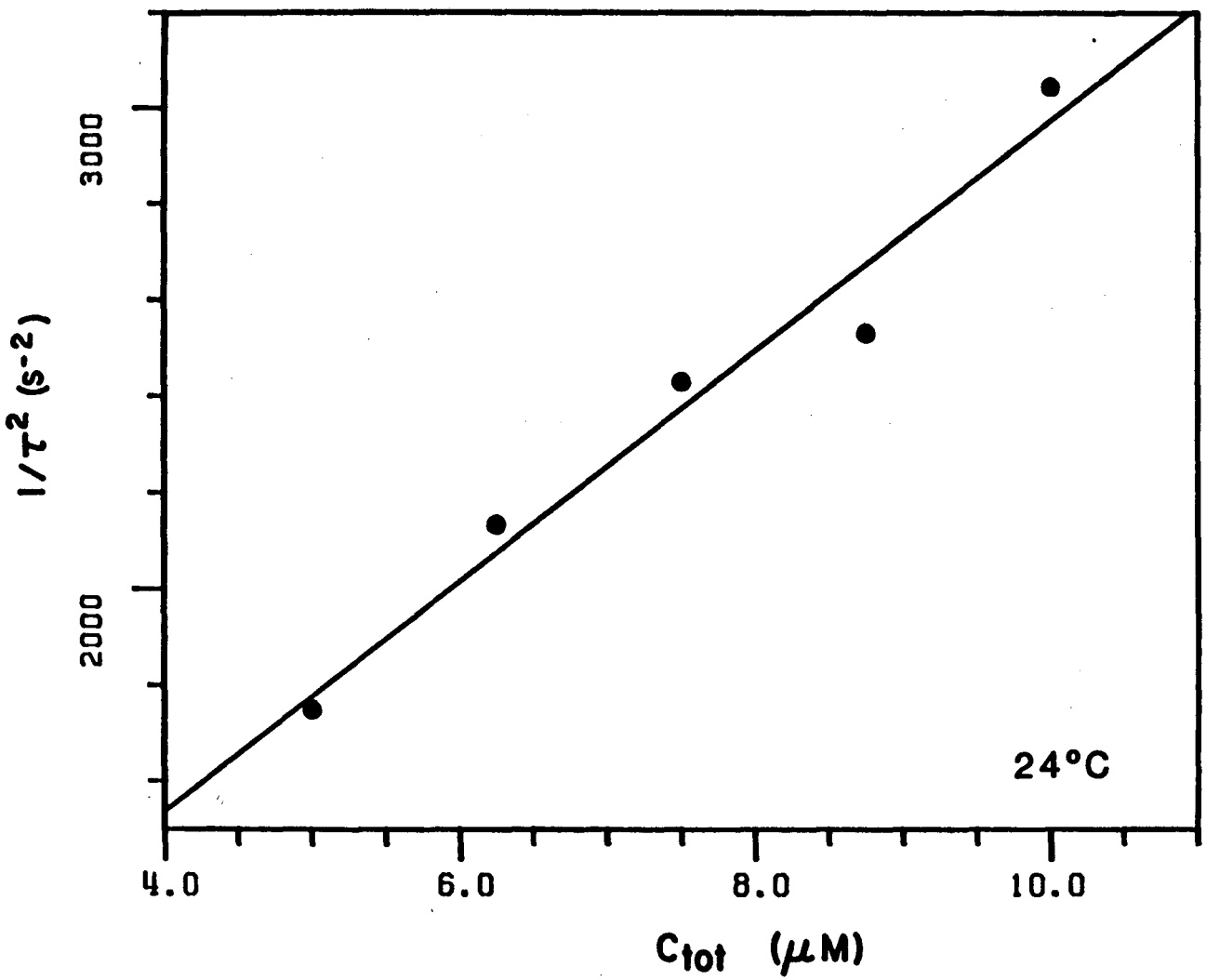
3000
2000
$1/\tau^2$ (s^{-2})
24°C
4.0
6.0
8.0
10.0
C_{tot} (μM)

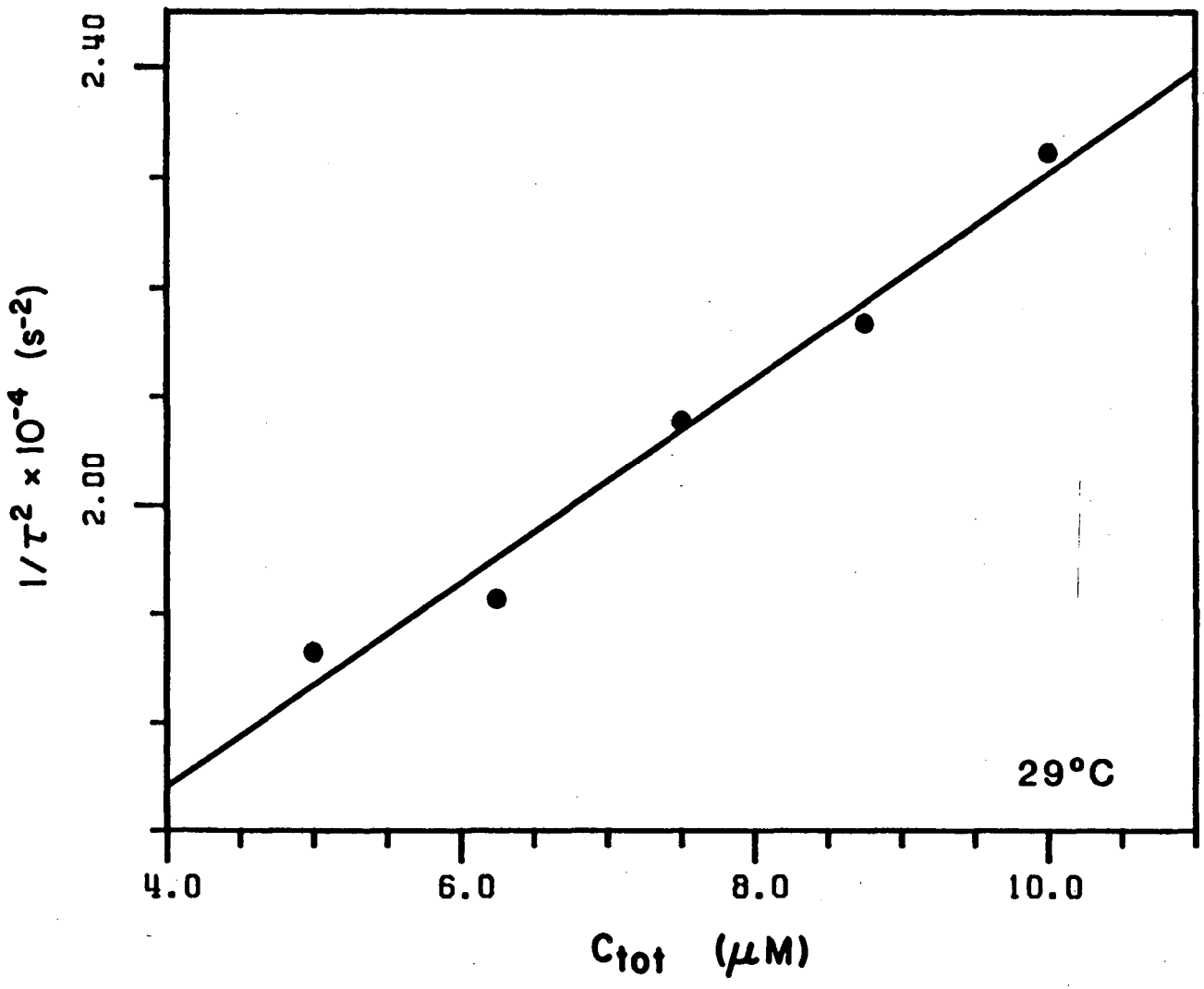
2.40
2.00
$1/\tau^2 \times 10^{-4}$ (s^{-2})
29°C
4.0
6.0
8.0
10.0
C_{tot} (μM)

Figure 2.10-2.13 Plots of $1/\tau$ vs C_s for $dCA_3CA_3G + dCT_6G$ at 5°C, 10°C, 13°C and 15°C, respectively.

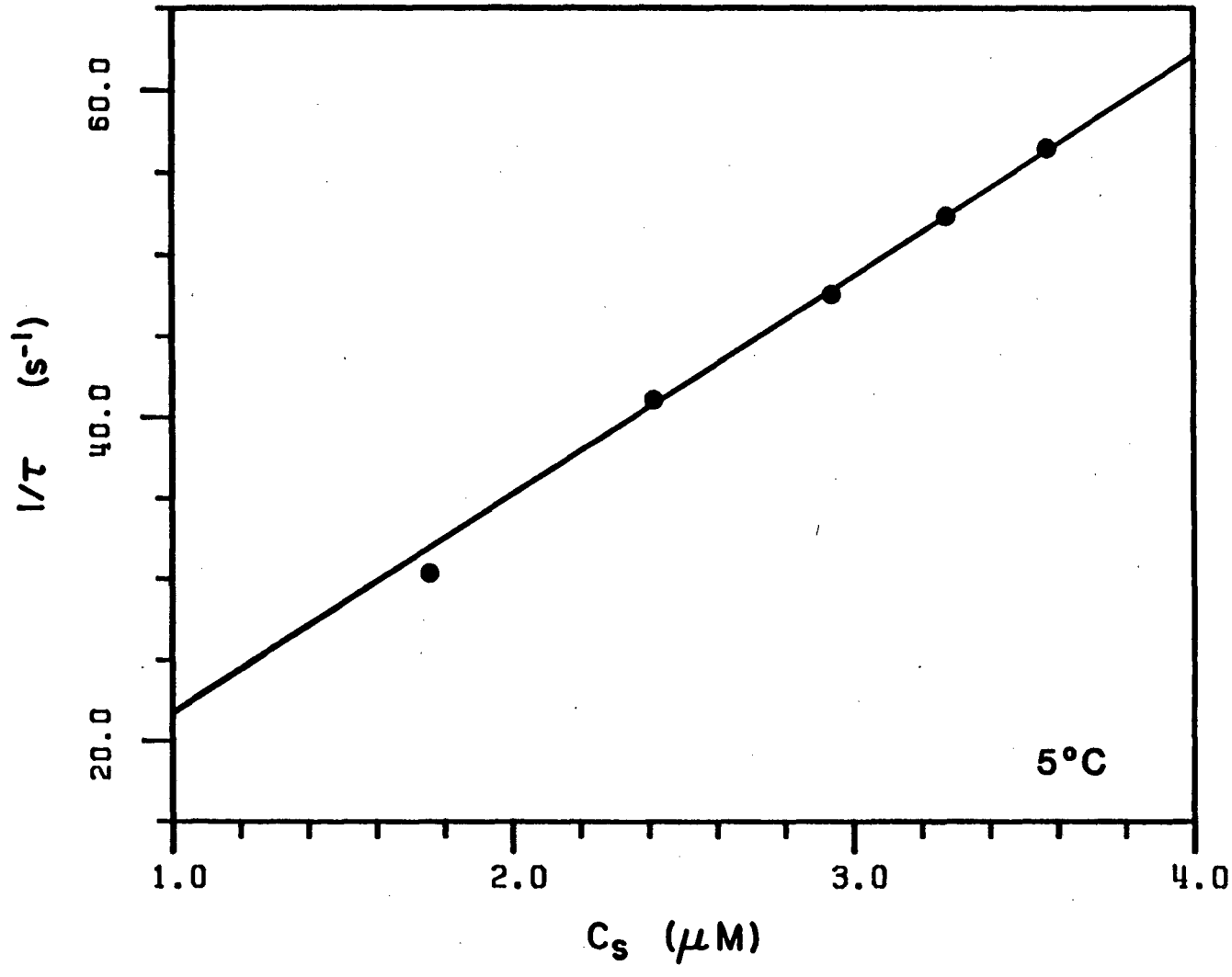
60.0
40.0
20.0
1/τ (s⁻¹)
5°C
1.0
2.0
3.0
4.0
Cs (μM)

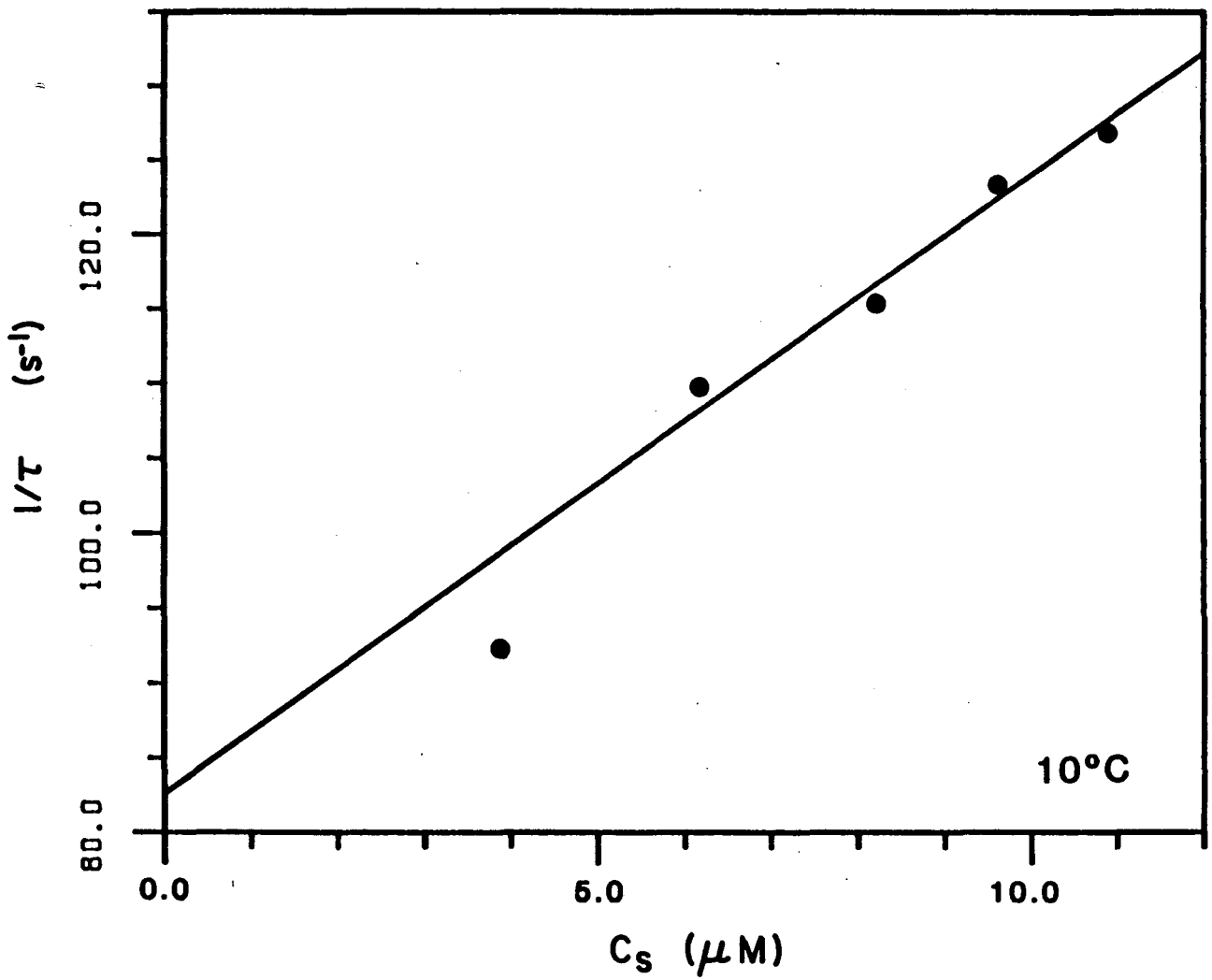
1/τ (s⁻¹)
120.0
100.0
80.0
0.0
5.0
10.0
Cs (μM)
10°C

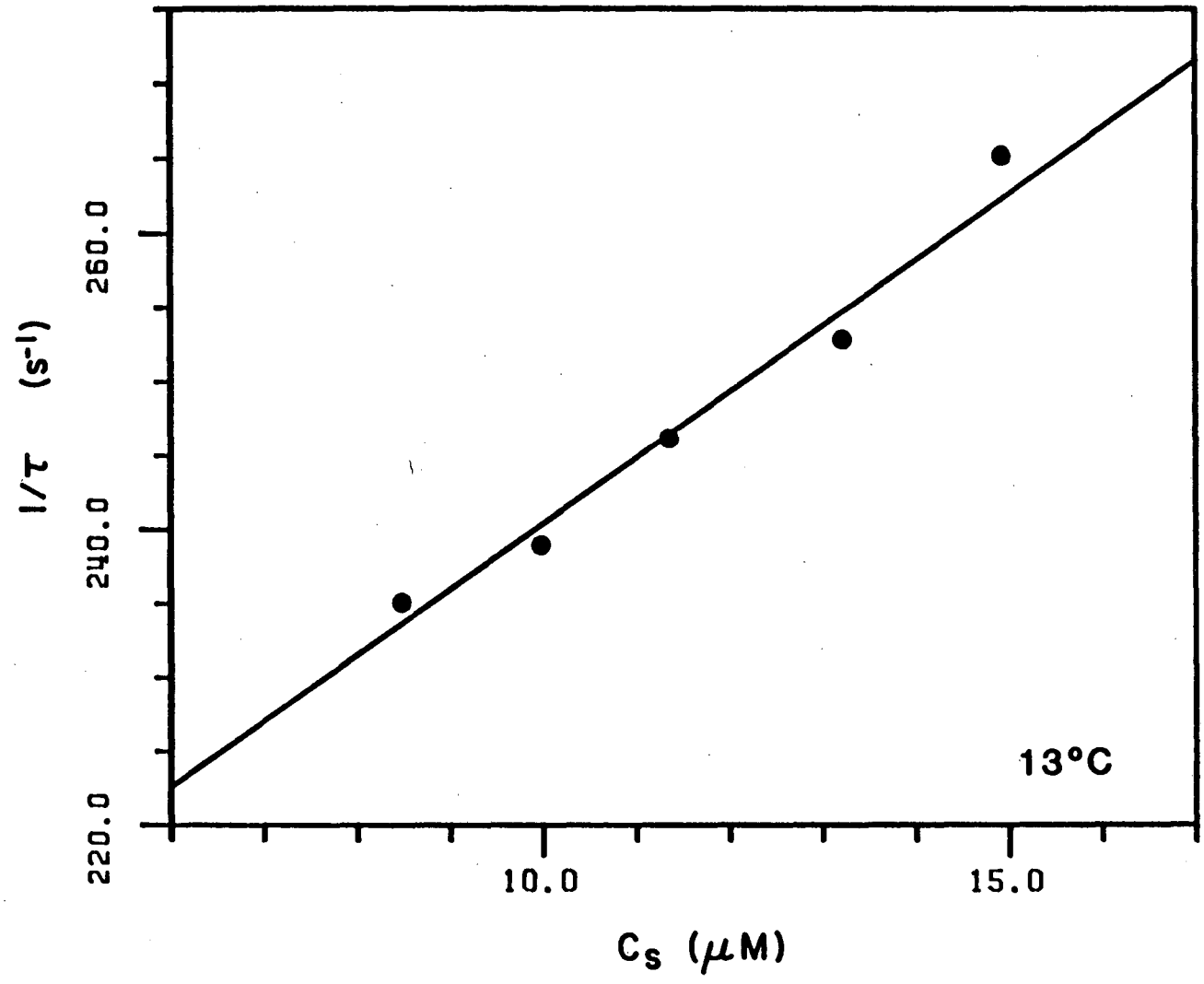
1/τ (s⁻¹)
260.0
240.0
220.0
10.0
15.0
Cs (μM)
13°C

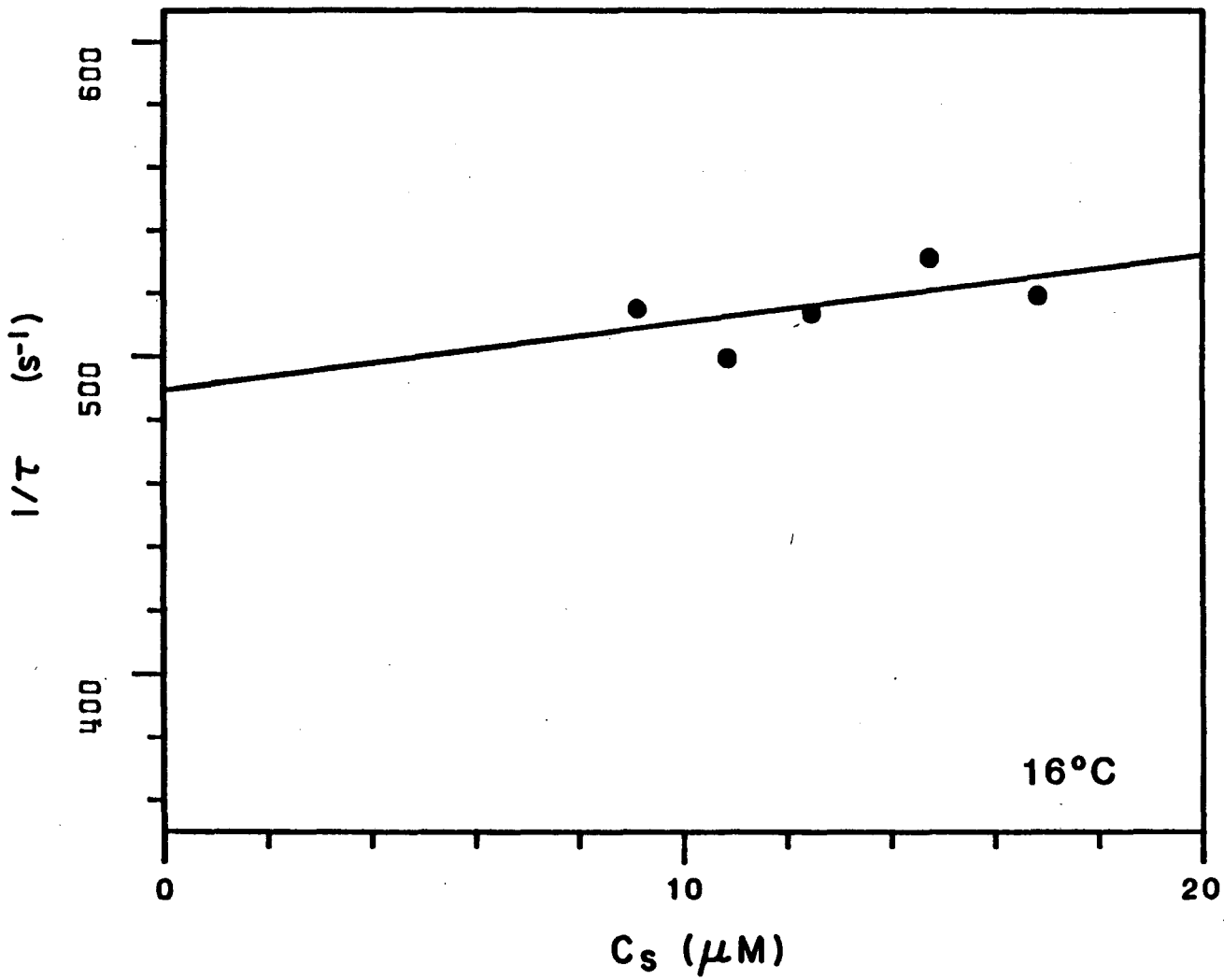
600
500
400
1/τ (s⁻¹)
16°C
0
10
20
Cs (μM)

Figure 2.14-2.17 Plots of $1/\tau^2$ <u>vs</u> C_{tot} for $dCA_3CA_3G + dCT_6G$ at 5°C, 10°C, 13°C and 16°C, respectively.

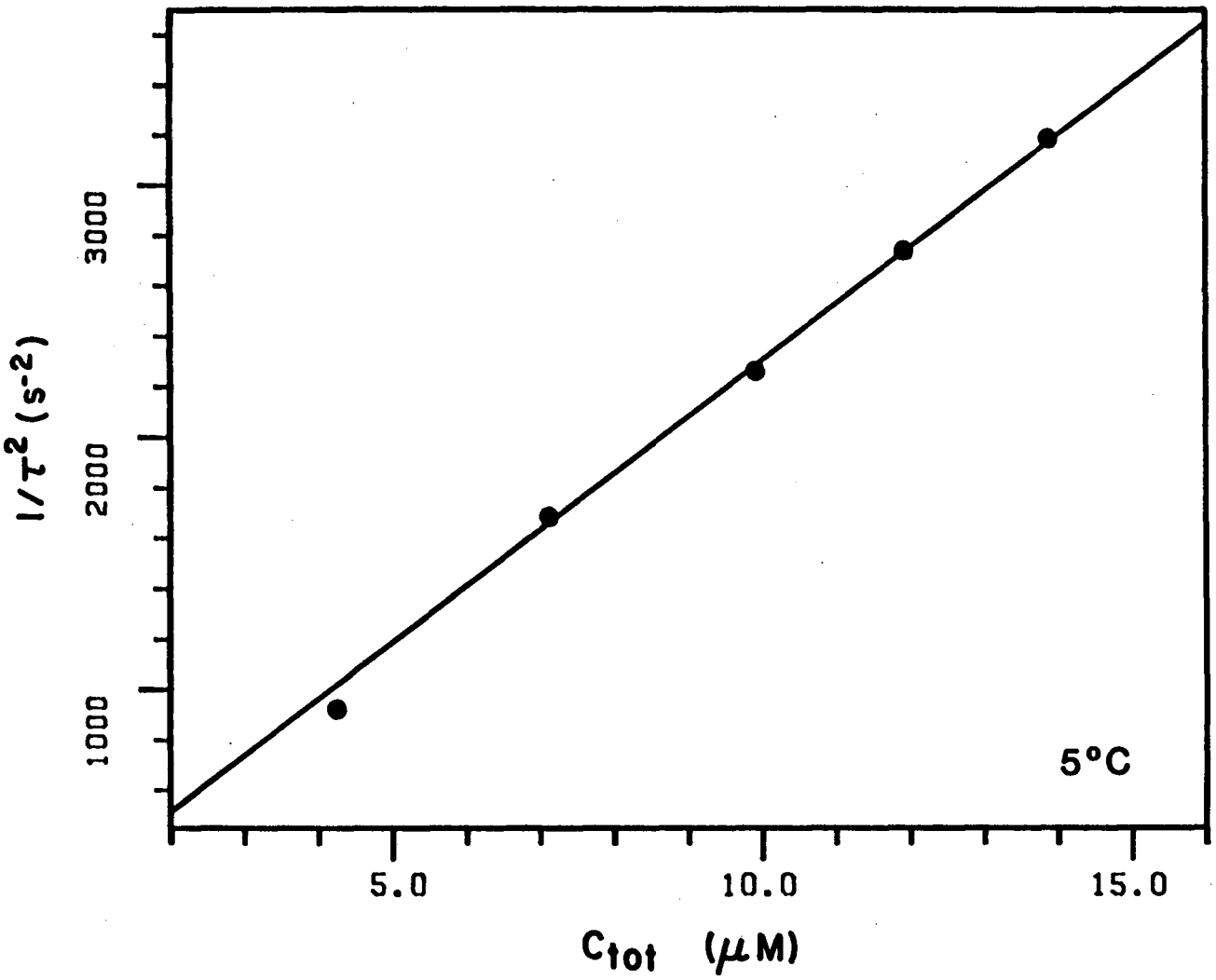
1000
2000
3000
$1/\tau^2$ (s^{-2})
5.0
10.0
15.0
C_{tot} (μM)
5°C

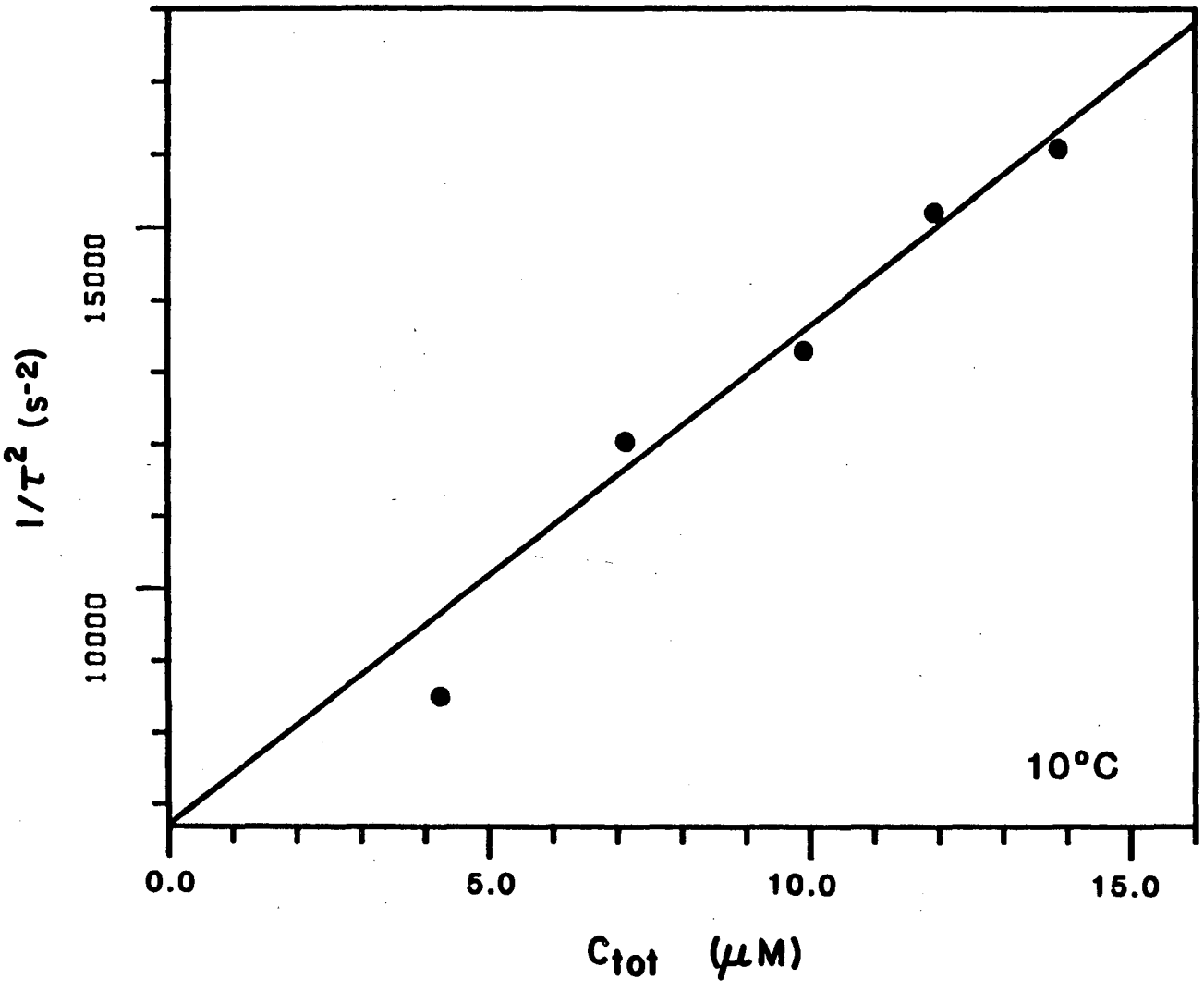
10°C
0.0
5.0
10.0
15.0
C_{tot} (μM)
10000
15000
$1/\tau^2$ (s^{-2})

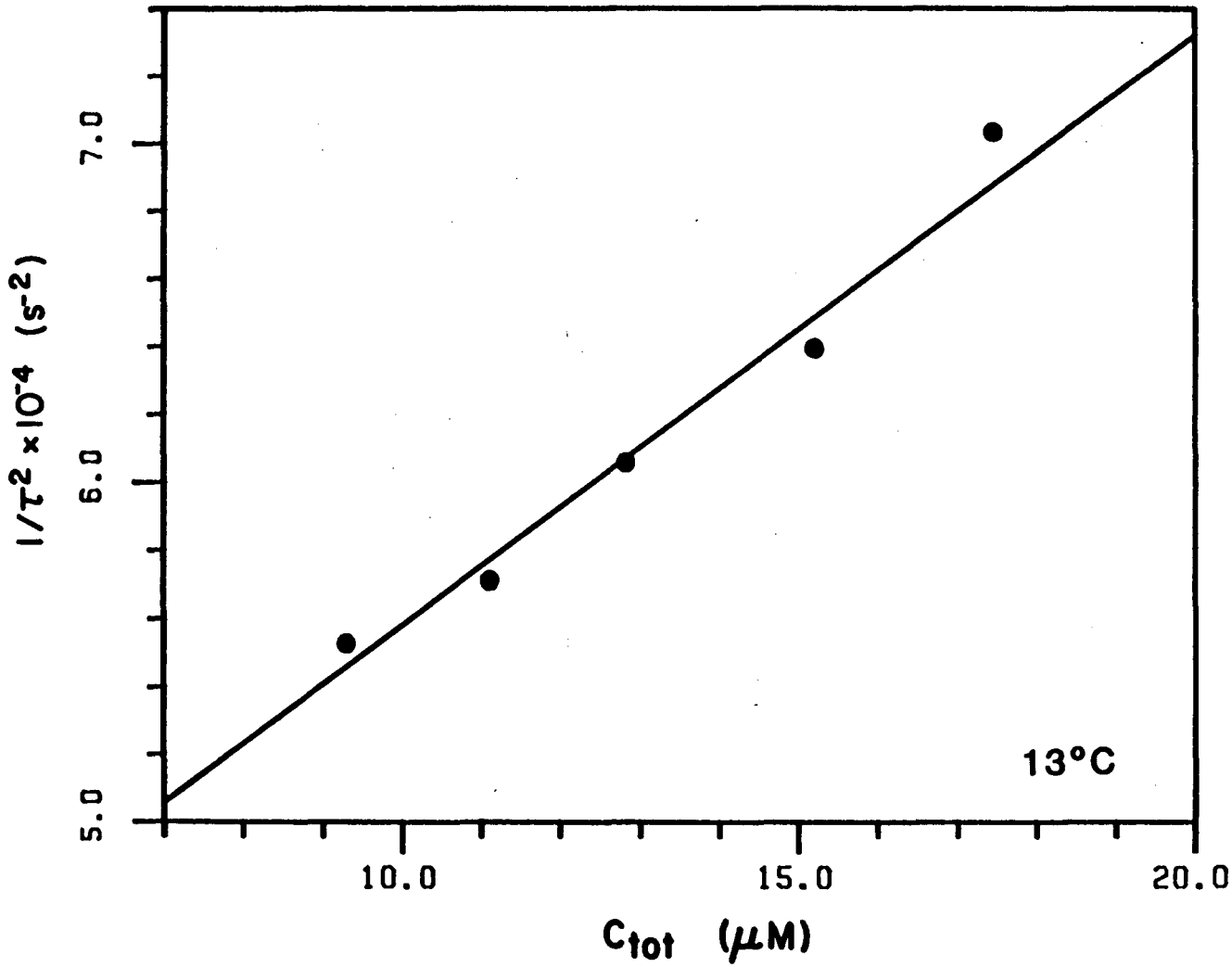
7.0
6.0
5.0
$1/\tau^2 \times 10^{-4}$ (s^{-2})
10.0
15.0
20.0
C_{tot} (μM)
13°C

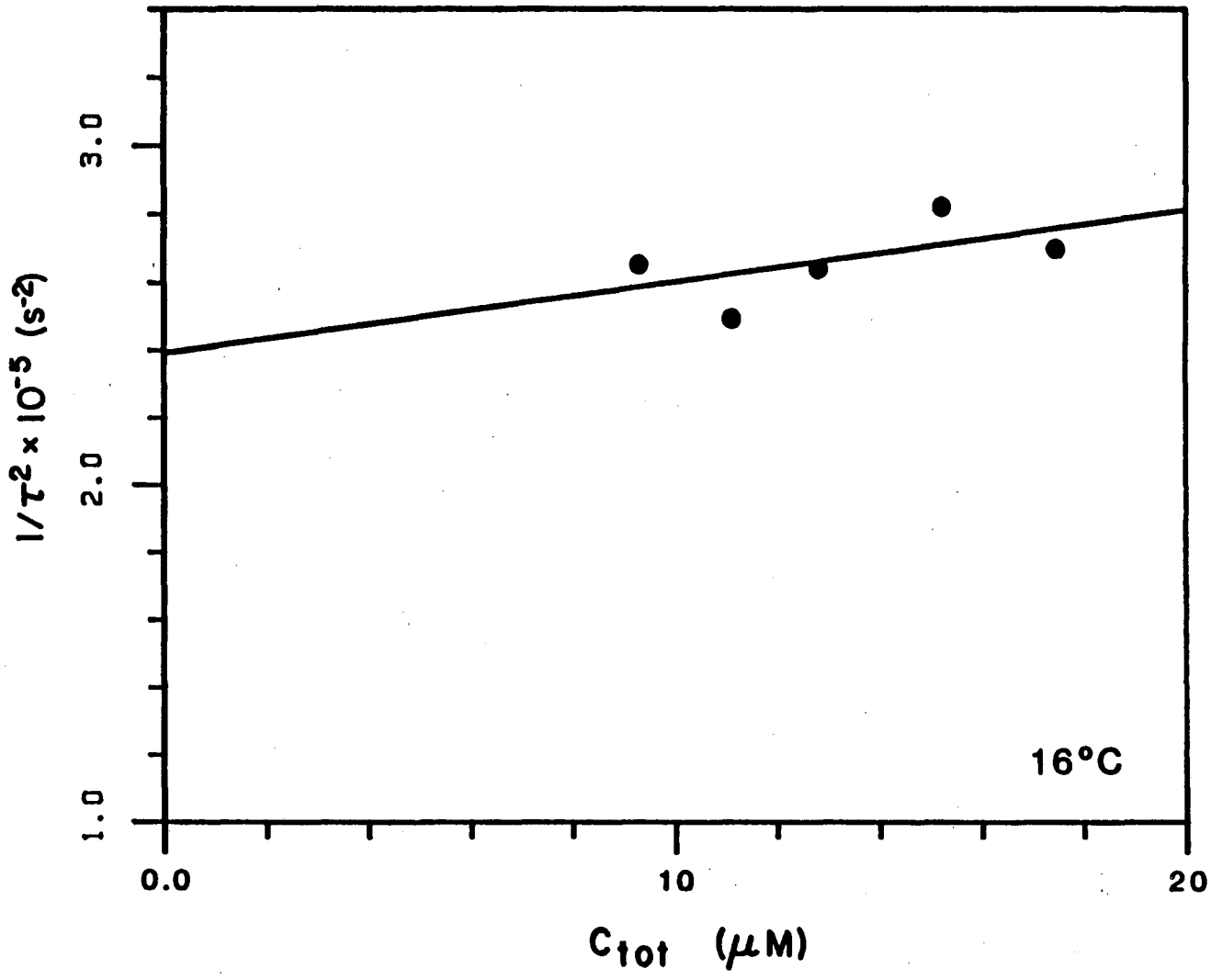
3.0
2.0
1.0
$1/\tau^2 \times 10^{-5}$ (s^{-2})
0.0
10
20
C_{tot} (μM)
16°C

equations 2.3 and 2.4 are shown in Figures 2.2 to 2.17. The kinetic parameters derived from the plots for $dCA_6G + dCT_6G$ and $dCA_3CA_3G + dCT_6G$ are displayed in Tables 2.1 and 2.2.

In principle, the two methods for analyzing relaxation time data (described in the Experimental section) should yield consistent kinetic results. Examining the values listed in Tables 2.1 and 2.2 confirms that the kinetic parameters obtained through the two analyses agree within experimental error.

The plot of $1/\tau^2$ vs C_{tot} gives k_d^2 as the intercept and $4k_rk_d$ as the slope. For these experiments, the value of the intercept is small, thus the k_d determined from the intercept of the $1/\tau^2$ vs C_{tot} plot has a large uncertainty. Since in this method, k_r is not determined independently, the large uncertainty in k_d also contributes to the error in k_r. For these reasons this method of analysis is not as accurate as the iterative procedure. Henceforth, kinetic parameters derived by the iterative method are used in further analyses.

From an Arrhenius plot of the natural logarithm of the rate constants as a function of the inverse temperature, the activation parameters for the kinetic process can be extracted. Arrhenius plots for the perfect and bulged duplexes are shown in Figures 2.18 to 2.21. Table 2.3 lists the kinetic and activation parameters for the two duplexes.

Examining Tables 2.1 and 2.2 reveals that the rate of dissociation of the bulged duplex is greater than that of the

Table 2.3 Kinetic and Activation Parameters for

$dCA_6G + dCT_6G$ and $dCA_3CA_3G + dCT_6G$

	Perfect Helix $dCA_6G + dCT_6G$	Bulged Helix $dCA_3CA_3G + dCT_6G$
$k_{r,15°C}$	1.3×10^6	1.0×10^6
$k_{r,25°C}$	2.0×10^6	1.7×10^5
$E_{a,r}$	+7 ± 2	-29.9 ± 0.4
$\Delta S_r^{\ddagger}$	+4 ± 7	-137 ± 1
$k_{d,15°C}$	2.6	3.7×10^2
$k_{d,25°C}$	41	7.0×10^3
$E_{a,d}$	+47 ± 2	+50.1 ± 0.3
$\Delta S_d^{\ddagger}$	+104 ± 5	+129 ± 1
$\Delta H^{\circ}_{kinetic}$	-40	-80
$\Delta S^{\circ}_{kinetic}$	-100	-266

Units for k_r's: $M^{-1}s^{-1}$

k_d's: s^{-1}

E_a's: kcal/mol

ΔS's: e.u.

ΔH° : kcal/mol

Figure 2.18 Arrhenius plot of the natural logarithm of the recombination rate constant, k_r, for the perfect duplex dCA_6G + dCT_6G, vs 1/T.

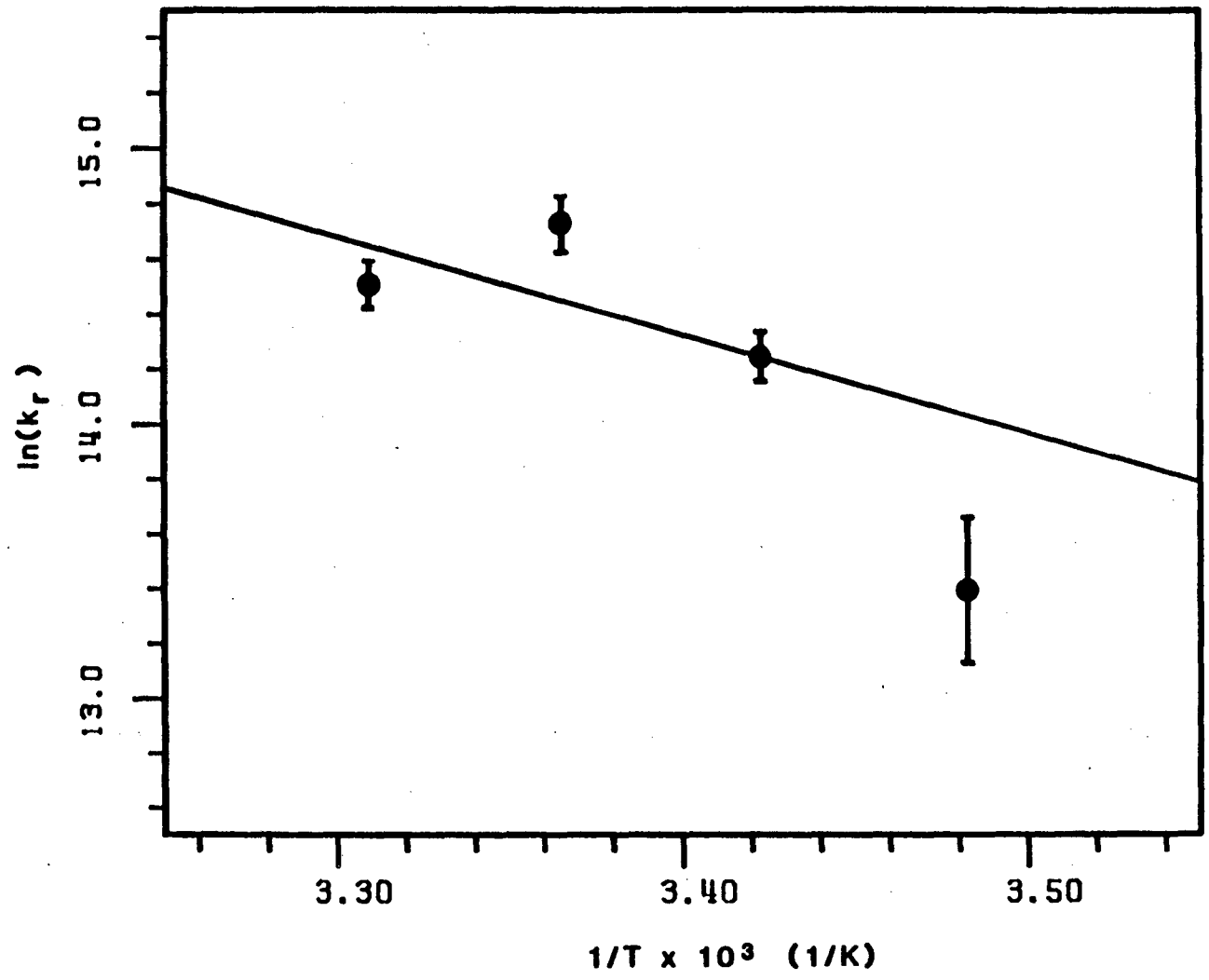
15.0
14.0
13.0
ln(k_r)
3.30
3.40
3.50
1/T x 10³ (1/K)

Figure 2.19 Arrhenius plot of the natural logarithm of the dissociation rate constant, k_d, for the perfect duplex dCA_6G + dCT_6G, vs 1/T.

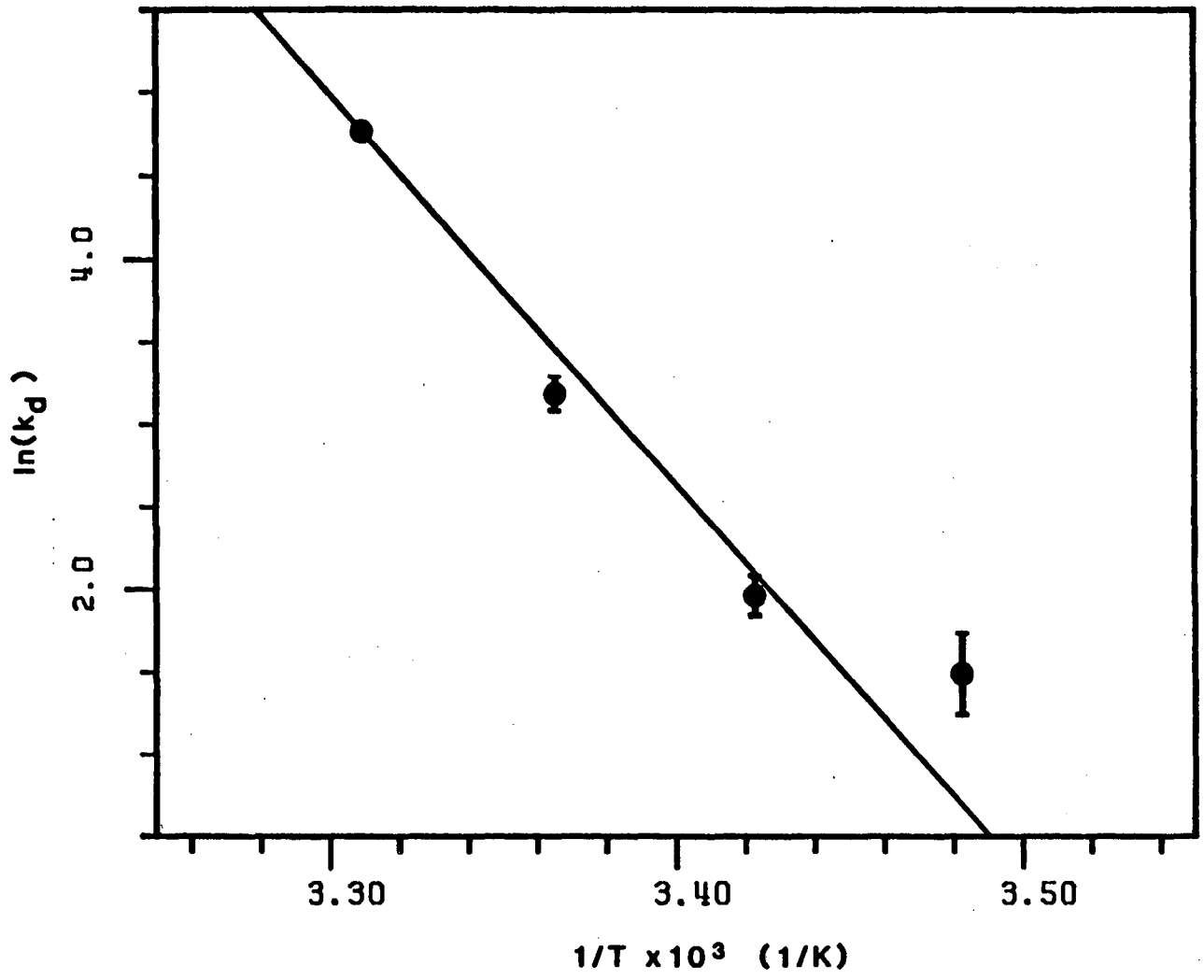
ln(k_d)
4.0
2.0
3.30
3.40
3.50
1/T x10³ (1/K)

Figure 2.20 Arrhenius plot for the recombination rate constant, k_r, of the bulged duplex $dCA_3CA_3G + dCT_6G$.

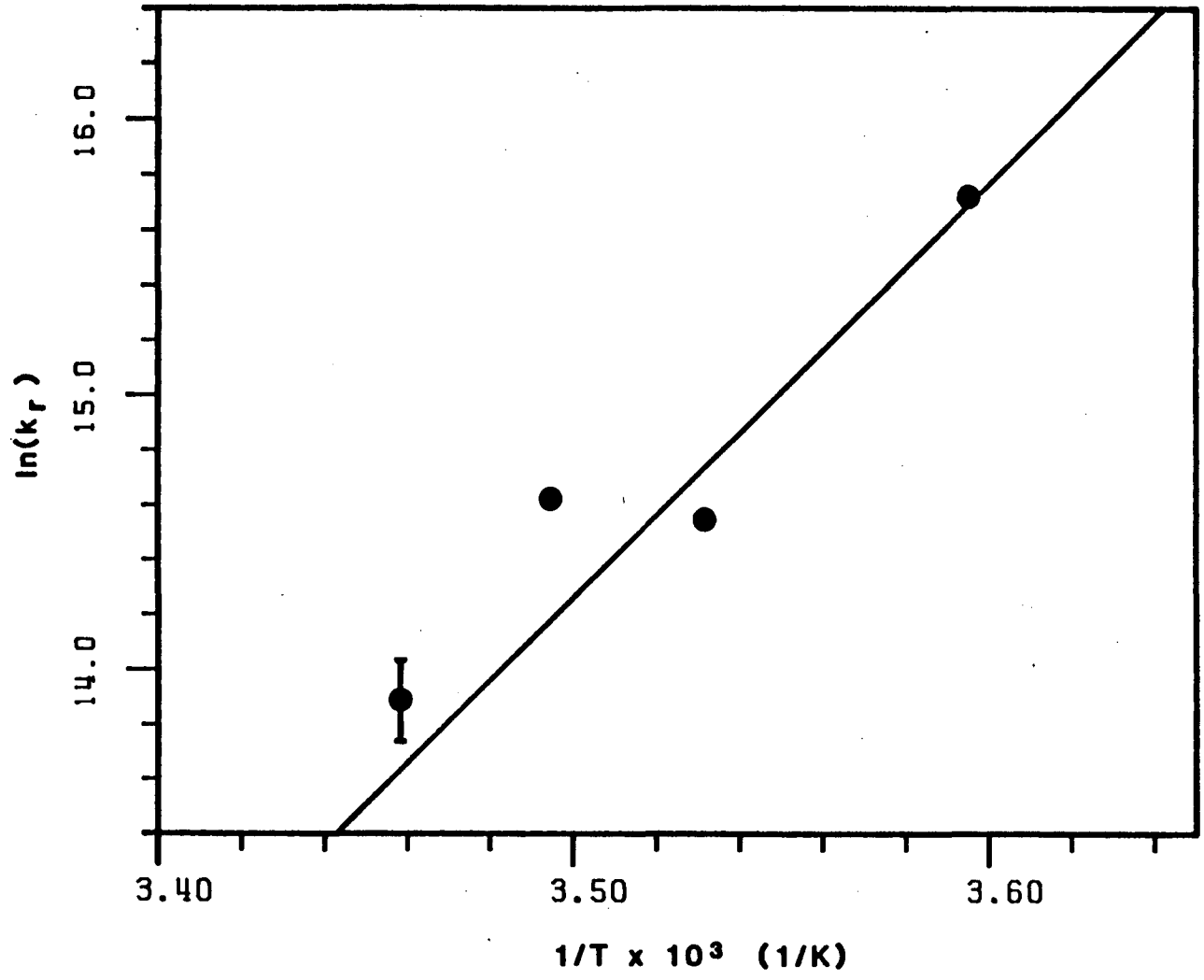
16.0
15.0
14.0
ln(k_r)
3.40
3.50
3.60
1/T x 10³ (1/K)

Figure 2.21 Arrhenius plot for the dissociation rate constant, k_d, of the bulged duplex dCA_3CA_3G + dCT_6G.

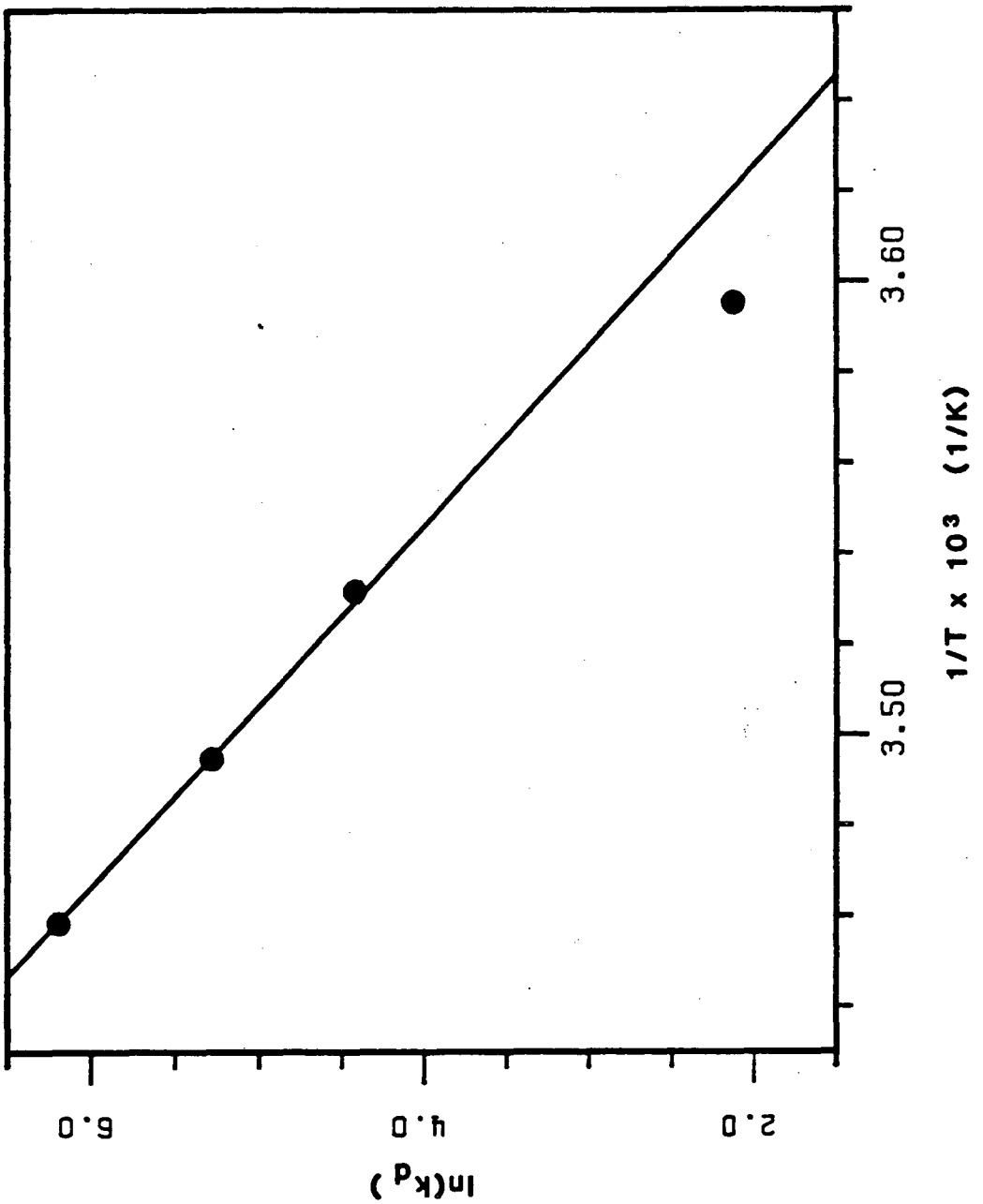
ln(k_d)
6.0
4.0
2.0
3.50
3.60
1/T x 10³ (1/K)

perfect duplex. The behavior of the recombination rate contants is more complex. The recombination rate constants of the two duplexes have opposite temperature dependences. The perfect helix exhibits the familiar trend of larger rate constants with increasing temperature. In the bulged helix, however, recombination rate constants become smaller with rising temperature. This behavior is reflected in the negative activation energy for recombination of the bulged duplex, as shown in Table 2.3. The negative activation energy implies that recombination for the bulged duplex is not an elementary kinetic process. A physical interpretation of the activation parameters will be presented in the Discussion section.

4. Discussion

We begin by comparing the rate constants of the two helices studied. At 15°C, the recombination rate constant of dCA_6G + dCT_6G and dCA_3CA_3G + dCT_6G are comparable at 1.3×10^6 $M^{-1}s^{-1}$ and 1.0×10^6 $M^{-1}s^{-1}$, respectively. At 25°C however, the situation is very different. Now the bulged helix recombines with a rate constant of 0.17×10^6 $M^{-1}s^{-1}$ while the perfect duplex forms more than ten times faster, at 2.0×10^6 $M^{-1}s^{-1}$. This difference in recombination rate constants highlights the tremendous disparity in the activation energies for recombination of the two duplexes. The dissociation rate constants behave in the expected manner. The bulged helix,

containing the extra unpaired cytosine, which is destabilizing, is expected to dissociate faster than its structurally unperturbed counterpart. Indeed, at 15°C the perfect helix has a rate constant for dissociation of 2.6 s^{-1} while the bulged helix dissociates at 370 s^{-1}.

The activation energy for recombination for the perfect duplex is +7 kcal/mol. While most oligoribonucleotides containing G·C base pairs have positive activation energies of several kilocalories per mole for recombination (Pörschke *et al.*, 1973), the same has generally not been found for the limited number of oligodeoxynucleotides studied to date (see Table 2.4). For dissociating the perfect helix, the energy of activation is +47 kcal/mol. Listed in Table 2.5 are the preliminary thermodynamic parameters characterizing base stacking interactons in DNA (I. Tinoco, Jr. K. J. Breslauer, unpublished results). By using these values, we can deduce that the dissociation activation energy of +47 kcal/mol implies the opening of five to six base pairs from either end of the perfect helix to reach the transition state species, which still has intact two to three base pairs. This is in agreement with the results obtained for the homologous duplex dCA_5G + dCT_5G, studied by Jeffrey Nelson in this laboratory (Nelson & Tinoco, 1982). Jeff Nelson determined the activation energy for dissociating the duplex dCA_5G + dCT_5G to be +43 kcal/mol.

Before embarking on a discussion of the activation

Table 2.4 Thermodynamic and Activation Parameters for Oligodeoxyribonucleotide Duplexes

	ΔH°	ΔS°	$E_{a,r}$	$\Delta S_r^\ddagger$	$E_{a,d}$	$\Delta S_d^\ddagger$
$dCA_5G + dCT_5G$[a]	-41	-120	0	-29	+3	+84
dGCGCGC[b]	-57.4	-157.4	-2.55	-101.7	+53.8	+102.9
dATGCAT[c]	-47.6	-147	-3.6	-40	+38.6	+91
$dA_8 + dT_8$[d]	-37	-150	-2.4	-33	+40.8	+95
dCGTGAATTCGCG[e]	-76	-236	+22	+40	+68	+159
dCGCAGAATTCGCG[f]	-70	-215	+16	+20	+74	+180

ΔH° and E_a's given in kcal/mol; ΔS's in e.u.

[a]Nelson & Tinoco, 1982; 1M NaCl.

[b]Albergo, 1981; 1M NaCl.

[c]Drobnies, 1979; 1M NaCl.

[d]Drobnies, 1979; 0.05M NaCl

[e]ΔH°, ΔS° from Patel et al., 1982a; E_a's, $\Delta S^\ddagger$'s from Chu & Tinoco, 1983; 1M NaCl.

[f]ΔH°, ΔS° from Patel et al., 1982b; E_a's, $\Delta S^\ddagger$'s from Chu & Tinoco, 1983; 1M NaCl

Table 2.5 Preliminary Thermodynamic Parameters for Deoxyribonucleotide Stacking Interactions

Values reported for the reaction:

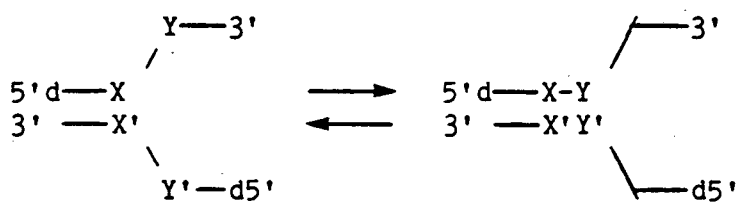

X' and Y' are bases complementary to X and Y, respectively.

X-Y	ΔH°[kcal/mol]	ΔS°[e.u.]
A-A	-8.8 ± 0.4	-23.8
A-C = C-A = A-G = G-A	-6.2 ± 0.4	-16.1
A-T = T-A	-7.3 ± 0.3	-20.8
C-C	-8.1 ± 2.9	-18.5
C-G	-12.0 ± 3.3	-29.5
G-C	-12.8 ± 3.6	-31.2

parameters for the bulged helix, one important structural feature of this helix should be mentioned. The bulged duplex was studied under the same solution conditions as those in this work by NMR and nuclear Overhauser effect (NOE) techniques (Morden et al., 1983). It was found that the extra unpaired cytosine in the molecule was positioned outside the helix and not stacked inside the helix with the other base pairs. Thermodynamic experiments on the bulged and perfect duplexes showed that the extra cytosine contributes +6(±4) kcal/mol to the $\Delta H°$ of duplex formation. The contribution by the unpaired cytosine to the $\Delta S°$ of duplex formation is +11(±13) e.u. The large negative activation energy of -29.9 kcal/mol for recombination of the bulged helix can be explained by invoking a kinetic scheme containing a fast pre-equilibrium:

$$\underset{\text{Single Strands}}{A + B} \underset{}{\overset{K_{PE}}{\rightleftharpoons}} \underset{\text{PE Intermediate}}{A \cdot B} \underset{k_-}{\overset{k_+}{\rightleftharpoons}} \underset{\text{Duplex}}{AB} \qquad (2.5)$$

where $K_{PE} = [A \cdot B]/([A][B])$ is the equilibrium constant for the pre-equilibrium (PE). For this scheme, the rate of duplex formation is given by

$$\left.\frac{d[AB]}{dt}\right|_{\text{formation}} = k_+[A \cdot B] = k_+K_{PE}[A][B] = k_r[A][B] \qquad (2.6)$$

The apparent recombination rate constant derived experimentally

can now be written as

$$k_r = k_+ K_{PE}. \tag{2.7}$$

Replacing the constants with the appropriate exponential expressions yields

$$A_r \exp\left(\frac{-E_{a,r}}{RT}\right) = \left[A_+ \exp\left(\frac{-E_{a,+}}{RT}\right)\right]\left[\exp\left(\frac{\Delta S^\circ_{PE}}{R}\right)\right]\left[\exp\left(\frac{-\Delta H^\circ_{PE}}{RT}\right)\right] \tag{2.8}$$

Differentiating with respect to 1/T after taking the natural logarithm of the expression results in

$$E_{a,r} = \Delta H^\circ_{PE} + E_{a,+}$$

The apparent activation energy for recombination is actually the sum of a true activation energy and the ΔH° for the pre-equilibrium. Since k_+ refers to a kinetic process wherein hydrogen-bonded base pairs are formed in aqueous solution, $E_{a,+}$ must be small and positive. Therefore, ΔH°_{PE} is the cause of $E_{a,r}$ being large and negative.

Now we can begin to examine the nature of the pre-equilibrium. The most natural picture which comes to mind is the following. We imagine that in order to "zip up" the structurally perturbed helix, a sufficient number of base pairs must be formed to lock the unpaired cytosine in its extra-helical conformation. The pre-equilibrium is then simply the nucleation and partial formation of the duplex. G·C base pairs

are more stable than A•T base pairs; we therefore assume that nucleation is more facile with G•C base pairs than with A•T base pairs. Since the bulged duplex is essentially symmetrical, nucleation at either G•C-containing end yields the same result.

We need to find out how much of the helix is involved in the pre-equilibrium. For this we use the thermodynamics presented in Table 2.5 and the fact that the unpaired cytosine contributes +6(±4) kcal/mol to the $\Delta H°$ of duplex formation. The enthalpy of nucleation, i.e., the $\Delta H°$ for making the first base pair, is assumed to be 0 kcal/mol. We find that if we zip up the duplex until we are one A•T base pair beyond the unpaired cytosine, the $\Delta H°_{PE}$ is -26.6(±4.1) kcal/mol. A small positive $E_{a,+}$, e.g. +1-2 kcal/mol, when added to the $\Delta H°_{PE}$ just calculated, yields an apparent $E_{a,r}$ which is <u>less negative</u> than the experimental value, but quite close to it. If we extend the "zipping-up" by one more A•T base pair, we obtain $\Delta H°_{PE}$ = -35.4(±4.1) kcal/mol. In combination with a small positive $E_{a,+}$, this new $\Delta H°_{PE}$ yields an apparent $E_{a,r}$ <u>more negative</u> than the experimental value. Based on these considerations, we conclude that the pre-equilibrium involves closing the duplex to the point of one or two A•T base pairs beyond the unpaired cytosine. The $\Delta H°$ for the pre-equilibrium is somewhere between -26.6 and -35.4 kcal/mol. With such a large enthalpy of reaction, one expects the pre-equilibrium to shift sharply to the left (favoring single strands) with increasing temperature. As a consequence, the

concentration of the partially closed duplex, the critical species from which the full helix is formed, drops markedly with increasing temperature. This accounts for the diminution in the apparent recombination rate constant at elevated temperatures.

Having surmised the nature of the pre-equilibrium, we can now proceed to examine the kinetics of helix growth more closely. As shown previously for the model we have chosen, the experimentally determined recombination rate constant is the product of the elementary rate constant for helix elongation and the equilibrium constant for the pre-equlibrium:

$$k_r = k_+ K_{PE}.$$

Since we have deduced the structure of the critical intermediate generated by the pre-equilibrium, we can use the thermodynamic parameters in Table 2.5 to calculate ΔG^o_{PE} and hence the equilibrium constant, K_{PE}. From the calculated K_{PE} and the observed k_r, we are able to deduce k_+, the unimolecular rate constant for closing the next segment of the bulged helix, which in this case is another A•T base pair. Moreover, we can again use the values of Table 2.5 to calculate an equlibrium constant, $K_{AA\text{-}Stack}$, for closing an A•T base pair next to an existing A•T base pair. If we define k_- to be the rate constant for opening the same A•T base pair, then

$$K_{AA\text{-}Stack} = \frac{k_+}{k_-} \qquad (2.9)$$

Thus, we are also able to calculate k_-. We perform the calculations of K_{PE}, k_+ and k_- twice: once for an intermediate duplex with <u>one</u> A•T base pair closed beyond the extra cytosine and once for <u>two</u> A•T base pairs beyond. The details of the calculations are shown in Schema 2.1. Results of the calculations are presented in Table 2.6.

We see that for forming an intermediate with <u>n</u> base pairs closed beyond the bulged cytosine, we obtain k_- on the order of 2×10^6 s^{-1} for <u>n</u> = 1, whereas for <u>n</u> = 2, k_+ drops to $\sim 5 \times 10^4$ s^{-1}. Since k_+ refers to an elementary kinetic step, $E_{a,+}$ should be small and positive. At <u>n</u> = 1, $E_{a,+}$ is -3.3 kcal/mol, while at <u>n</u> = 2, $E_{a,+}$ becomes relatively high at +5.5 kcal/mol. The implication is that the intermediate is energetically situated somewhere between one and two base pairs closed beyond the unpaired cytosine. The forward rate constant, k_-, should then be between 5×10^4 and 2×10^6 s^{-1}--e.g. $\sim 3 \times 10^5$ s^{-1}. Similarly, the activation energy for opening the A•T base pair should be between +5.5 and +14.3 kcal/mol. The rate constant for the A•T base pair opening, k_-, would be on the order of 10^4 s^{-1}.

The activation energy for dissociation of the bulged duplex is +50.1 kcal/mol. This agrees well with the +55 kcal/mol obtained by Kathy Morden from analyzing the lifetimes of imino proton NMR resonances in the bulged duplex (Kathy Morden, 1983).

Schema 2.1 Calculation of K_{PE}, $K_{AA\text{-}Stack}$, k_+ and k_- using experimentally determined parameters and the thermodynamics presented in Table 2.5.

```
                                   A-A-G                                    A-G
                                  C /                                      C   /
dCA3CA3G   K_PE   dC-A-A-A A   k+   dC-A-A-A A-A
            +      G-T-T-T-T          G-T-T-T-T-T
dCT6G                   \                   k-   \
                          T-T-Cd                   T-Cd
```

For closing up the duplex 1 A•T base pair beyond the bulged C:

$\Delta H^\circ_{PE} = \Delta H^\circ_{nucGC} + \Delta H^\circ_{stack} + \Delta H^\circ_{bulged\ C}$

$\Delta H^\circ_{nucGC} = 0$ kcal/mol

$\Delta H^\circ_{stack} = \Delta H^\circ_{CA} + 3\Delta H^\circ_{AA} = -6.2 + 3(-8.8) = -32.6$ kcal/mol

$\Delta H^\circ_{bulged\ C} = 6$ kcal/mol

$\Delta H^\circ_{PE} = -26.6$ kcal/mol

$\Delta S^\circ_{PE} = \Delta S^\circ_{nucGC} + \Delta S^\circ_{stack} + \Delta S^\circ_{bulged\ C}$

$\Delta S^\circ_{nucGC} = -\Delta G^\circ_{nucGC}/T = -16.77$ e.u. $= -0.01677$ kcal•mol^{-1}K^{-1}

$\Delta S^\circ_{stack} = \Delta S^\circ_{CA} + 3\Delta S^\circ_{AA} = -0.0161 + 3(-0.0238) = -0.1043$ kcal•mol^{-1}K^{-1}

$\Delta S^\circ_{bulged\ C} = 0.011$ kcal•mol^{-1}K^{-1}

Schema 2.1 (continued)

$\Delta S^{\circ}_{PE} = -0.0933$ kcal·mol^{-1}K^{-1}

$\Delta G^{\circ}_{PE} = \Delta H^{\circ}_{PE} + \Delta S^{\circ}_{PE} = -26.6 + 0.0933T$ [kcal/mol]

$K_{PE} = \exp[\ -\Delta G^{\circ}_{PE}/RT\ ]$

Analagously, for closing the duplex 2 A•T base pairs beyond the bulged C, we obtain

$\Delta G^{\circ}_{PE} = -35.4 + 0.1171T$ [kcal/mol]

For $K_{AA\text{-}Stack} = \dfrac{k_+}{k_-}$, the equililibrium constant for forming an A•T on A•T stack:

$\Delta H^{\circ}_{AA\text{-}Stack} = -8.8$ kcal/mol, and

$\Delta S^{\circ}_{AA\text{-}Stack} = -0.0238$ kcal·mol^{-1}K^{-1}

$\Delta G^{\circ}_{AA\text{-}Stack} = -8.8 + 0.0238T$ [kcal/mol]

$K_{AA\text{-}Stack} = \exp[\ -\Delta G^{\circ}_{AA\text{-}Stack}/RT\ ]$

We can now calculate $k_+ = k_r/K_{PE}$ and $k_- = k_+/K_{AA\text{-}Stack}$.

Table 2.6 K_{PE}, $K_{AA\text{-}Stack}$, k_+ and k_- for Closing the Bulged Helix n Base Pairs Beyond Unpaired Cytosine: n = 1, 2

	K_{PE} $[M^{-1}]$		$k_r \times 10^{-6}$	k_+ $[s^{-1}]$		$K_{AA\text{-}Stack}$	k_- $[s^{-1}]$	
	n=1	n=2	$[M^{-1}s^{-1}]$	n=1	n=2		n=1	n=2
5°C	3.23	167	6.54	2.02×10^6	3.92×10^4	51.6	3.92×10^4	758
10°C	1.38	53.9	2.51	1.82×10^6	4.67×10^4	39.0	4.67×10^4	1200
15°C	0.609	18.1	1.00	1.64×10^6	5.53×10^4	29.7	5.53×10^4	1860
20°C	0.276	6.3	0.41	1.49×10^6	6.51×10^4	22.9	6.51×10^4	2850
E_a				$-3.3 \frac{kcal}{mol}$	$+5.5 \frac{kcal}{mol}$		$+5.5 \frac{kcal}{mol}$	$+14.3 \frac{kcal}{mol}$

Compared with $\Delta H° = +53$ kcal/mol for dissociating the bulged duplex (Morden, et al., 1983), the value of +50.1 kcal/mol for $E_{a,d}$ is again in accord with the conventional view of helix dissociation: the duplex has to be opened to the last couple of base pairs before dissociation can occur.

If we attempt to calculate $\Delta H°$ for forming the bulged duplex by taking the difference between the recombination and dissociation activation energies, we find an anomaly. The $\Delta H°_{kinetic}$ ($= E_{a,r} - E_{a,d}$) is -80.0 kcal/mol, which does not agree with the van't Hoff $\Delta H°$ of -53 kcal/mol obtained by analyzing melting curves. Large discrepancies between kinetic and thermodynamic $\Delta H°$ values have been observed before (Chu & Tinoco, 1983), notably for longer oligomers for which melting phenomena can not be analyzed simply. The basic problem which arises by implication from such a discrepancy is that the recombination and dissociation reactions, while they are the same kinetic process, have different transition states. Owing to the principle of microscopic reversibility, the forward and reverse reactions must necessarily have the same transition state. It is rather difficult to come up with a convincing explanation for the discrepancies except to attribute the difference to either large uncertainties normally associated with kinetic values or to some fault inherent in the way in which spectroscopic melting data are analyzed to yield van't Hoff enthalpies.

Finally we wish to examine the mechanistic results from this

study against the background of the behavior of structurally perturbed helices in general. To date, one other duplex containing extra unpaired bases has been studied kinetically. That duplex is formed from the nearly self-complementary tridecamer dCGCAGAATTCGCG. The duplex has a bulged adenine residue beyond the third base pair from either end. Magnetic resonance studies using NOE techniques have shown the unpaired adenines to be stacked inside the helix (Patel et al., 1982b). Interestingly, the recombination of this duplex with intrahelical unpaired adenines proceeds in the usual manner, with a positive energy of activation (Chu & Tinoco, 1983). Mechanistically, no pre-equilibrium is involved in forming the duplex. One may thus postulate that if it is more favorable for the unpaired base to stack with the neighboring base pairs, as in the tridecamer duplex, then the zipping-up of the helix is smooth and continuous once nucleation has taken place. On the other hand, if the energetics are such that the unpaired base must adopt a conformation in which it is outside the body of the duplex, then the structural perturbation will be sufficiently severe to hold up the zipping of the helix. In such cases, an intermediate in which the unpaired base is securely locked outside the helix is necessary for closing the duplex completely. In effect, in addition to spectroscopic probes for structure, we can have a kinetic probe for the conformation of helices containing bulged bases; i.e., "normal" kinetics of

recombination implies intrahelical unpaired bases while a pre-equilibrium with a large negative activation energy signals that the unpaired base is outside the helix. Of course, the validity of this kinetic criterion can only be ascertained through a thorough investigation of other structurally perturbed duplexes for which conformational and mechanistic data can be evaluated together. At present, the idea of a kinetic probe of structure remains an interesting and tantalizing possibility.

CHAPTER III

THE INTERACTION

OF AN UNCHARGED MUTAGEN WITH DNA

1. Introduction

That frameshift mutagens exist is a fact well-known since the early 1960's (Brenner et al., 1961; Crick et al., 1961). In the presence of these chemicals, the frequency of frameshift mutations in prokaryotes can be increased several thousand fold above the natural "background" level (McCann et al., 1975). Frameshift mutagens as a class share certain features, prominent among which are a chemical structure characterized by polycyclic aromaticity and the ability to intercalate into DNA (Lerman, 1961).

Numerous reports have provided information on the equilibrium of binding frameshift mutagens to nucleic acids. A number of studies have characterized, in addition, the kinetics of forming a complex between a mutagen and nucleic acids. The compounds examined in these kinetic studies are acridine derivatives such as proflavin and phenanthridine derivatives such as ethidium. The structures of these compounds were presented in Chapter I, in Figure 1.3. All of the mutagens previously investigated kinetically either are quarternary nitrogen compounds which are permanently cationic, or exist in the

positive protonated form at physiological pH. Under normal conditions, movement of charged species across cell membranes are mediated by specific transport machinery. For this reason, charged frameshift mutagens of non-biological origin may have great difficulty gaining access to the DNA inside a cell. Uncharged chemical agents, in contrast, may enter the organism by simply diffusing through the lipid bilayer membrane. A study conducted with a neutral mutagen is thus desirable in that a neutral agent may be the more biologically relevant choice. Moreover, comparisons with earlier experiments using charged species may give insight into the process of drug-DNA interaction.

Two difficulties hinder any experimental study of DNA interacting with a neutral frameshift mutagen. First of all, the neutral aromatic polycycles have extremely low solubility in the aqueous buffers used for biophysical experiments. Furthermore, the complexes formed between the DNA and the drugs tend to be of rather limited stability. These two facts combined imply that under experimentally accessible conditions, only very small amounts of the drug-DNA complex will actually be formed. This is certainly an obstacle in any attempt to characterize the bound species. Compounds which I tested and rejected for the aforementioned reasons include quinoline N-oxides, acridine N-oxides and a number of anthraquinone dyes.

In this work, the neutral mutagen chosen was a member of the psoralen class: 4'-hydroxymethyl trioxalen (HMT, see Figure 1.3), of which I had a generous supplier. Owing to the presence of the

hydroxymethyl group, HMT has much greater aqueous solubility than other psoralens. In addition, HMT, like other psoralens, is strongly fluorescent in the uncomplexed state in aqueous solution, but the fluorescence is almost completely quenched when the molecule is bound to DNA (Salet et al., 1980). This last feature was important for the success of the relaxation experiments.

The studies here presented are of three types:

1) temperature -dependent equilibrium measurements which yielded thermodynamic information;
2) counterion activity-dependent equilibrium studies which gave clues about the nature of the HMT-DNA complex; and
3) relaxation kinetic experiments leading to rate constants and activation parameters which provided some mechanistic insight into the mutagen binding process.

2. Experimental

Calf thymus DNA (highly polymerized form) from Sigma was mixed with 0.01M Tris, 0.2mM EDTA buffer (pH 7) to give ~80 ml of solution at a concentration of approximately 20 mg/ml. After stirring the mixture for 24 hours in a cold room (5°C), a gel formed. Over the next 24 hours of stirring, the sample was given periodic ten-minute sonications totalling 120 min. During the same period, 20 ml of the Tris buffer were added in several increments. Extraction of the DNA solution with doubly distilled phenol previouly equilibrated with Tris buffer yielded an emulsion which separated after being

centrifuged at 8000 rpm for 10 min. The phenol layer was clear while the DNA layer remained cloudy. At the interface between the two phases a white residue formed. The separated DNA phase was extracted with diethyl ether. The emulsion which resulted from the ether extraction was again broken by centrifugation at 10,000 rpm for 10 min. The ether layer along with more white foam which accumulated at the interface were removed by pipetting. The remaining DNA solution was now quite clear. Portions of the DNA stock so prepared were subsequently dialyzed exhaustively against various NaCl/Phosphate/EDTA buffers used in all the experiments. The densities of all final DNA stock solutions were determined by weighing the solutions in 5-ml or 10-ml volumetric flasks. Subsequent transferring of DNA samples were always made by weight, as the high viscosity of the DNA solutions precluded accurate pipetting. Concentrations of diluted DNA samples were determined optically from the A_{260} and $\varepsilon_{260} = 13100\ cm^{-1}M^{-1}$, with the DNA concentrations expressed in units of moles of base pairs per liter.

Pure samples of crystalline 4'-hydroxymethyltrioxalen (HMT) as well as 4'-[^{3}H]-hydroxymethyltrioxalen (^{3}H-HMT, sealed ampules containing 6.0 mCi in ethanolic solution at a specific activity of 13.2 Ci/mmol) were generous gifts from Steve Isaacs and Prof. John Hearst. All "cold" aqueous HMT stock solutions were prepared by first making a concentrated HMT stock in 95% ethanol and adding small aliquots of this ethanolic stock solution to large volumes of aqueous buffer. The amount of ethanol in the final aqueous solution was

always negligible. A "hot" HMT solution was prepared by adding the ^{3}H-HMT stock ethanol solution to a "cold" aqueous HMT solution to achieve the desired specific activity. All HMT solutions were wrapped in aluminum foil and stored in the cold. HMT concentrations in the "cold" solutions were determined optically using ε_{250}= 2.5 x x10^{4} cm^{-1}M^{-1}.

All equilibrium dialyses were performed in temperature-controlled rooms or constant-temperature baths. Glass scintillation vials of 15 ml capacity were used for dialysis experiments. The dialysis tubing used was prepared and stored prior to use according to conventional procedures (Brewer et al., 1974). In all cases, the DNA solution inside the dialysis tubing was ~2 ml while the external solution volume was ~10 ml. ^{3}H-HMT was added to the internal solution in some cases and to the external solution in others. A small magnetic stirring bar was placed in each dialysis vial. The vials were covered with aluminum foil to protect the samples from light. The entire dialysis assembly was gently agitated on a magnetic stirrer for at least four days. When the dialysis was complete, the internal and external solutions were quickly separated. Liquid scintillation measurements were then made on the internal and external solutions while the absorbance of the internal solution was measured at 260 nm. From these data, the free and bound drug concentration, as well as the DNA concentration could be determined. All experiments were run in duplicate and all individual measurements were also done in duplicate. The liquid scintillation cocktail used was made by

thoroughly mixing 12 grams ofOmniscint, 1 liter of Triton-X 100 and 2 liters of toluene.

The temperature jump instrument used for the relaxation kinetic experiments has been described in detail elsewhere (Rigler el al., 1976; Nelson, 1982). For these studies, fluorimetric detection was used. The wavelength of the exciting light was 365 nm. The fluorescence from the sample, after passing through a 385 nm cut-off filter, was collected with one PMT perpendicular to the path of the exciting light. Appendix 1 gives more detailed specifications for the optical components used for fluorescence measurements on the instrument.

To achieve the temperature jump, a 50nf capacitor charged to 25kV was discharged through the sample. This yielded a jump of 7.1°C. A procedure for calibrating the size of a temperature jump is provided in Appendix 3. The initial temperature of the sample was measured to within 0.2°C using a Fluke 2100A digital thermometer with a copper-constantan thermocouple in contact with the upper electrode of the sample cell.

The instrument was operated most of the time in the zero-suppression mode and sometimes in the DC-mode. For instructions on how to use the special options on the instrument, see Appendix 2. Each relaxation curve was digitized as 2048 points on a Biomation 805 transient recorder. The digitized data were subsequently transferred via a PET microcomputer to a VAX 11/780 minicomputer where all data reduction and analyses were performed. The program DISCRETE

(Provencher, 1976a,b) , provided by S. W. Provencher was used to analyze the raw relaxation data. The program determines the number of expoenential relaxation components which will best fit the digitized data.

Samples for the kinetic studies were made by weighing out a sample of DNA stock solution and adding an aliquot of HMT in aqueous buffer. After shaking briefly on a vortex mixer, the solution was filtered centrifugally through a cellulose membrane of 0.45 μM porosity. The filtered solution was divided into two samples for duplicate kinetic experiments. Prior to loading into the cell, each sample was purged by bubbling water-saturated helium through the solution for 3-5 min.

Two buffer stocks were prepared for the studies. The 0.01M Na buffer comprised 1mM NaCl, 0.5mM $NaH_2EDTA \cdot 2H_2O$ and 4mM Na_2HPO_4; the whole solution was adjusted to pH 7 with HCl. The 0.1M Na buffer consisted of 0.091M NaCl, 0.5mM $Na_2H_2EDTA \cdot 2H_2O$ and 4mM Na_2HPO_4. Likewise, this solution was also adjusted to pH 7 with HCl. The nominal concentration of each buffer (0.01M or 0.1M) refers to the <u>total</u> sodium ion concentration in the buffer. All other buffers used in the studies were prepared by appropriately mixing or diluting the two primary stock buffer solutions.

Samples for the equlibrium fluorescence quenching experiments were prepared in the following manner. A series of six solutions was made in which the total DNA concentration varied from 0 to 1.3×10^{-3} M in base pairs. In each solution, the total HMT

concentration was 1.08×10^{-5} M. The 0.1 M Na buffer was used to prepare the samples for these fluorescence experiments. The fluorescence intensities of the solutions were measured at five different temperatures. From the temperature-dependent quench data, one is able to deduce HMT-DNA binding constants as well as the $\Delta H°$ of binding. The fluorescence measurements were made in a thermostatted cell mount, on a Perkin-Elmer MPF-2A fluorescence spectrometer (courtesy of Prof. Melvin Calvin) operating in the Ratio mode. Light at 340 nm was used for excitation while the fluorescence at 460 nm was monitored. Excitation and emission bandpasses were both set at 6 nm.

3. Results

A) Thermodynamics

The fluorescence quenching data at each temperature were fit to the equation

$$\frac{1}{F_f - F} = \frac{1}{F_f - F_b} \cdot \frac{1}{K} \cdot \frac{1}{[DNA]} + \frac{1}{F_f - F_b} \qquad (3.1)$$

where F_f is the fluorescence of HMT in the absence of DNA,

F_b is the fluorescence of HMT when completely bound to DNA (infinite DNA concentration),

F is the fluorescence of HMT at DNA concentration, [DNA] and

K is equilibrium constant for binding HMT to DNA.

Figures 3.1-3.5 Plots of the fluoresence data with constrained least squares fits to Equation 3.1. Plots are for data at 4.7°C, 13.5°C, 25.1°C, 35.0°C, and 44.9°C, respectively. δF corresponds to $F_f - F$ in Equation 3.1

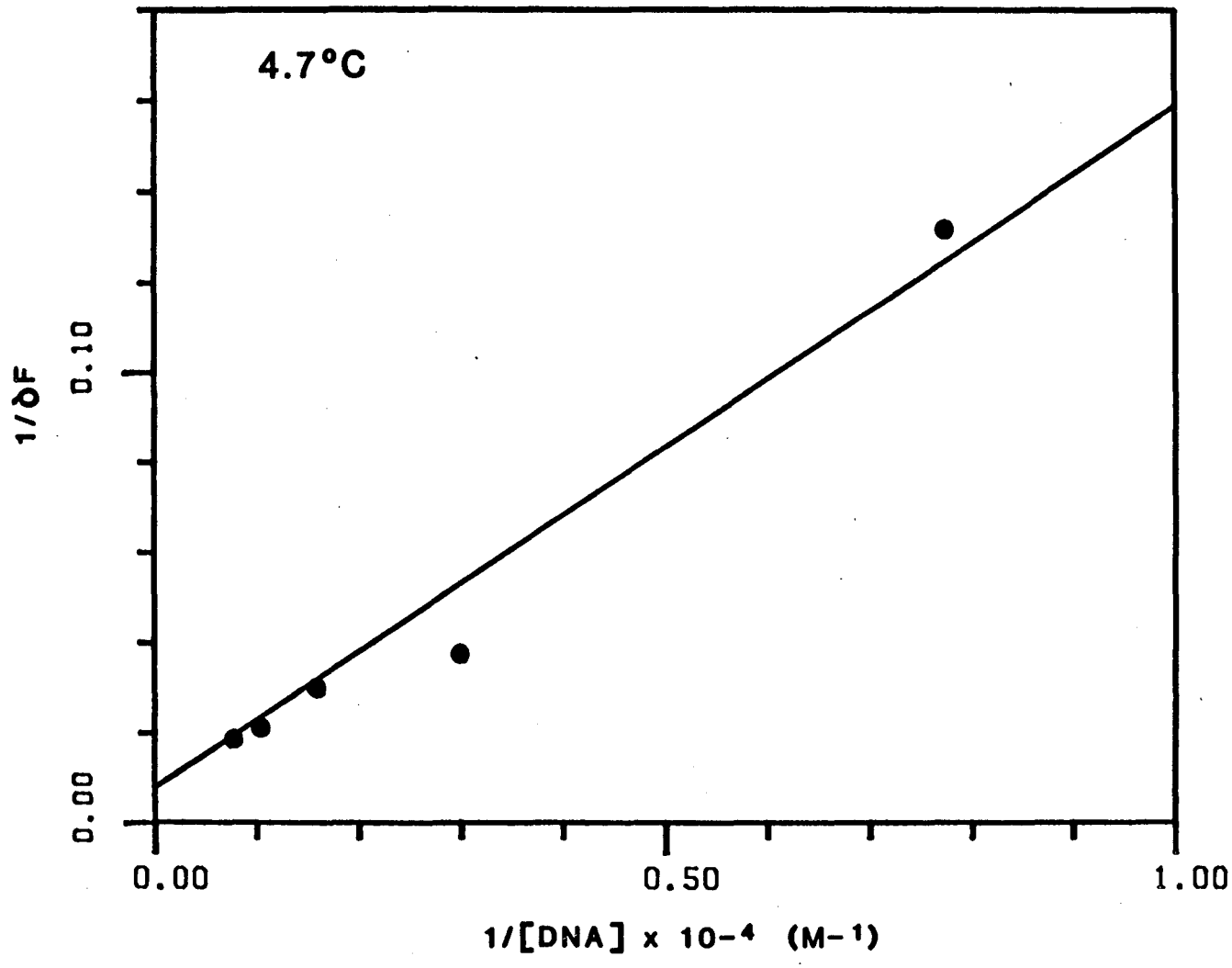
4.7°C
1/δF
0.00
0.10
0.00
0.50
1.00
1/[DNA] x 10-4 (M-1)

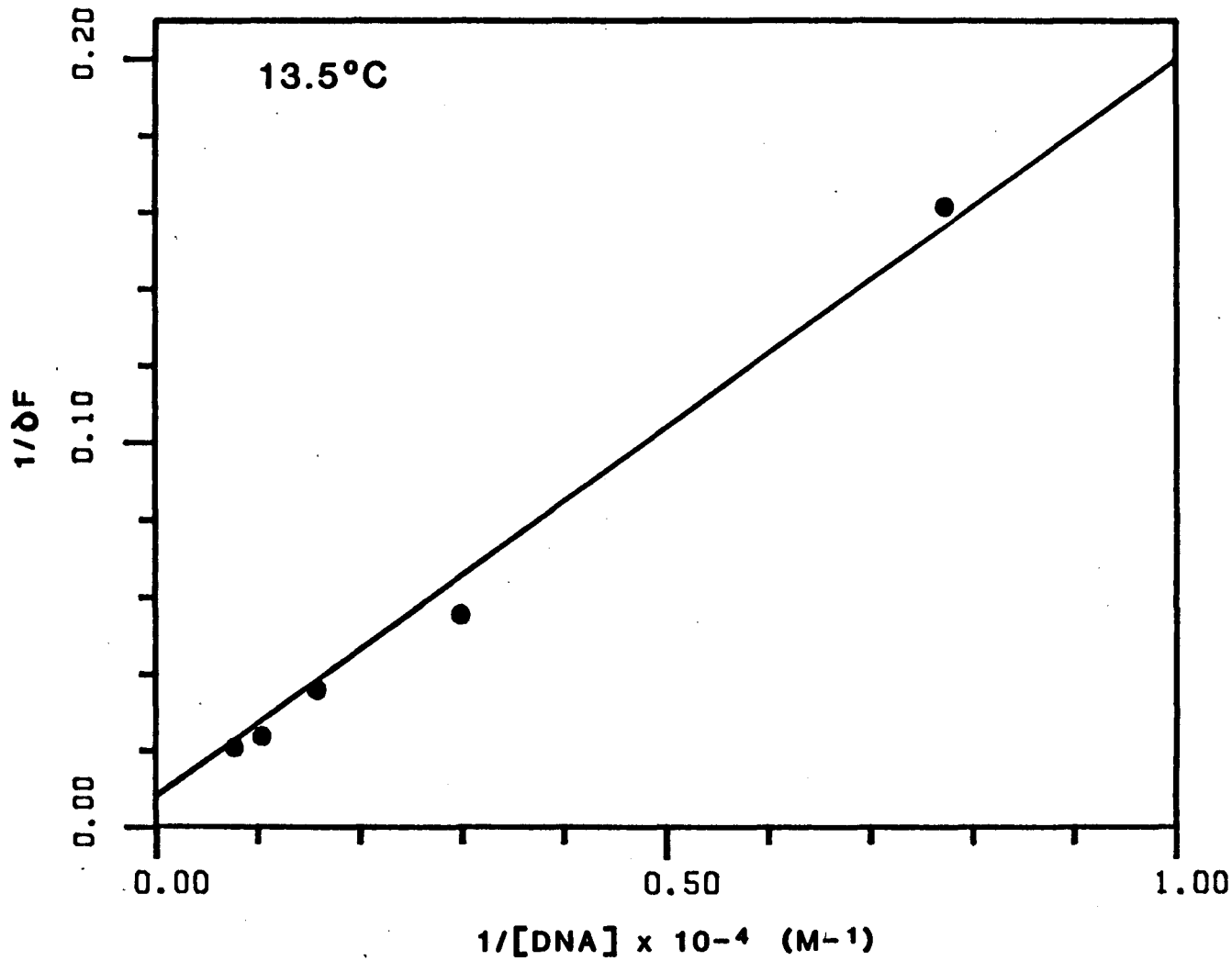
13.5°C
1/δF
0.00
0.10
0.20
0.00
0.50
1.00
1/[DNA] x 10-4 (M-1)

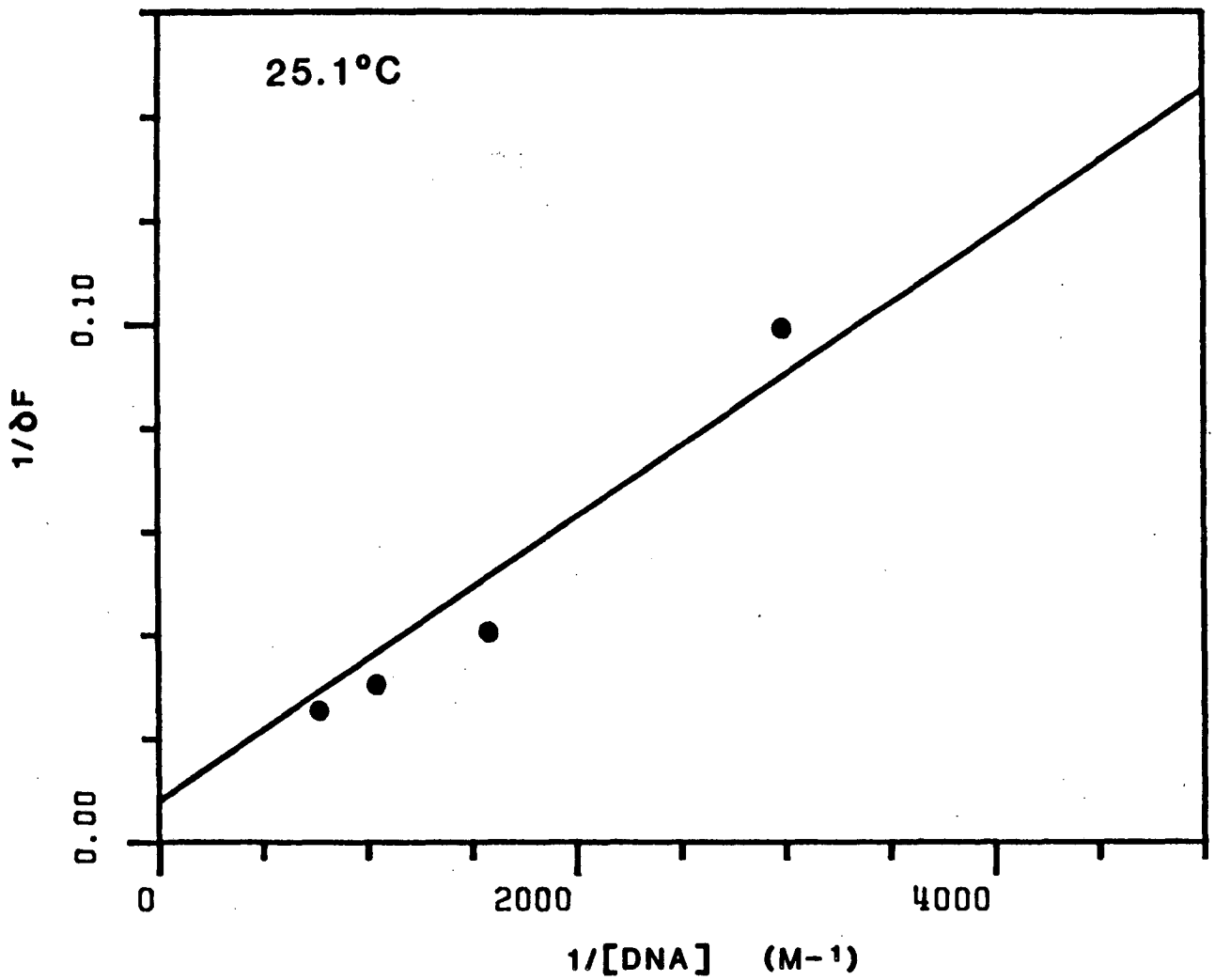
25.1°C
1/δF
0.00
0.10
0
2000
4000
1/[DNA] (M-1)

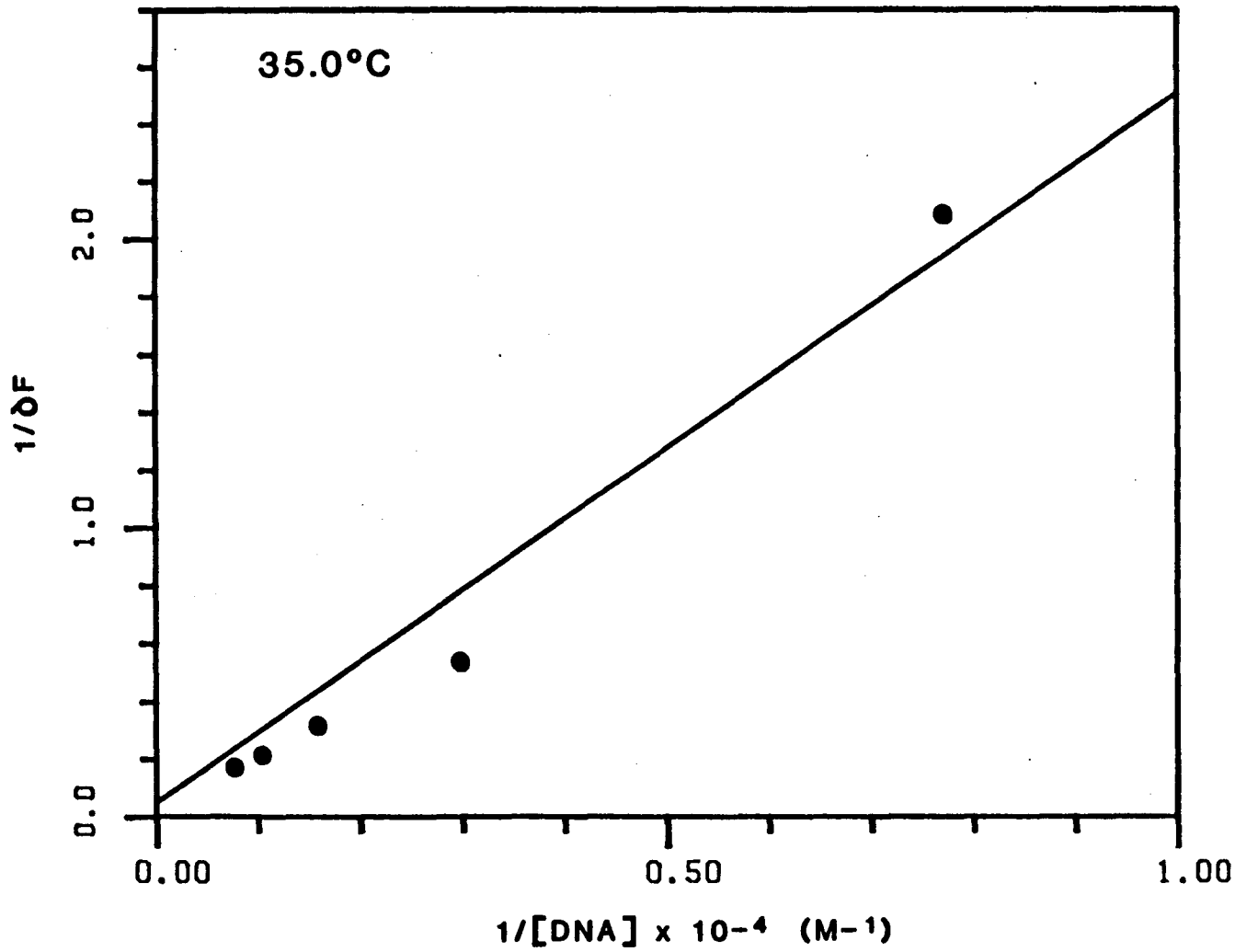
35.0°C
1/δF
0.0
1.0
2.0
0.00
0.50
1.00
1/[DNA] x 10-4 (M-1)

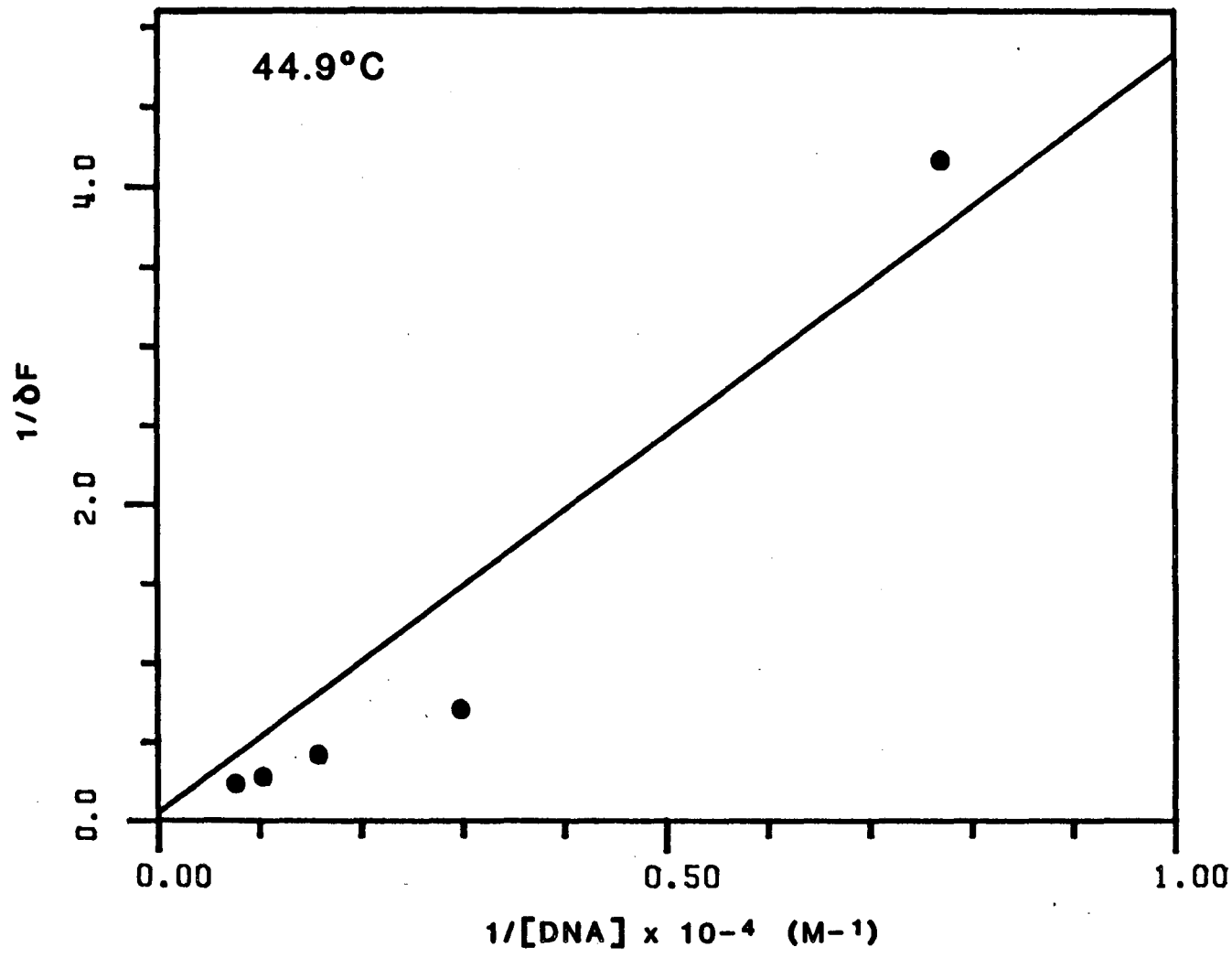
44.9°C
1/δF
0.0
2.0
4.0
0.00
0.50
1.00
1/[DNA] x 10-4 (M-1)

Figure 3.6 Plot of the natural logarithm of the equilibrium binding constant for the system HMT + calf thymus DNA, vs 1/T. The equilibrium constants are derived from the fluorescence quenching data.

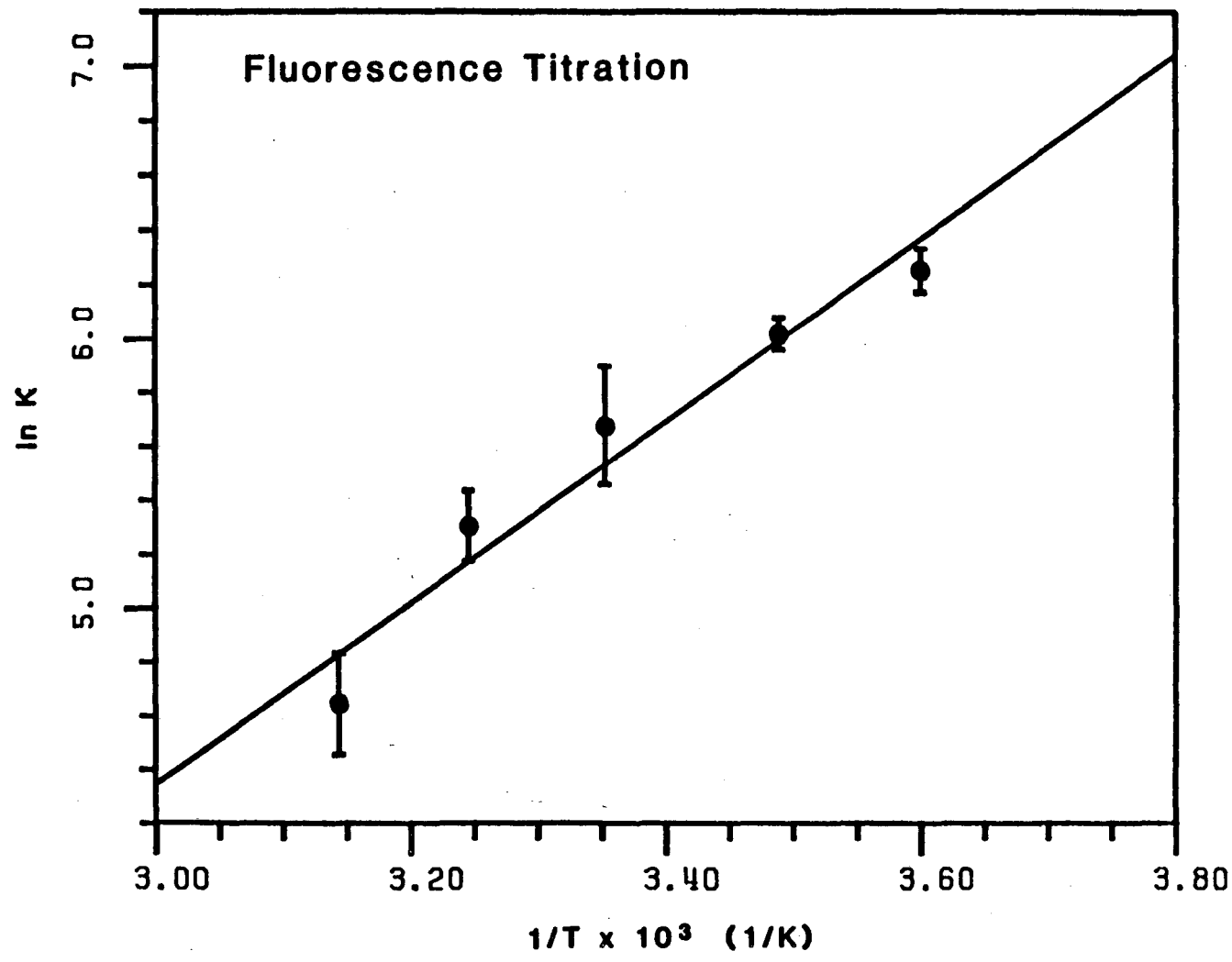
Fluorescence Titration
ln K
7.0
6.0
5.0
3.00
3.20
3.40
3.60
3.80
1/T x 10³ (1/K)

Table 3.1 Thermodynamics of HMT + DNA Derived from Fluorescence Titrations in 0.1 M Na Buffer

T	K, M^{-1}	Estimated % Uncertainty
4.7°C	520	8
13.5°C	410	6
25.1°C	290	22
35.0°C	200	13
44.9°C	100	19
$K_{25°C}$	341	

$\Delta H° = -6.7 \pm 0.9$ kcal/mol

$\Delta S° = -11.5 \pm 3.1$ e.u.

When $1/(F_f-F)$ is plotted against 1/[DNA] and fit by the normal linear least squares method, large errors were associated with intercepts and thus the values of F_b. In fact some of the intercepts were negative in value. The quench data were not good enough to determine the parameters F_b and K. Consequently, the data were fit with a least squares line for which the intercept was constrained to be $1/F_f$. That is, we made the assumption that upon binding to DNA, the fluorescence of HMT is completely quenched. The assumption has support from previous work on psoralen-DNA binding (Salet et al., 1980). Using the constrained fits (see Figures 3.1-3.5), HMT-DNA binding constants were calculated at all the experimental temperatures. A plot of lnK vs 1/T gave a $\Delta H°$ of binding of -6.7(±0.9) kcal/mol (Figure 3.6). The results from these equilibrium fluorescence experiments are shown in Table 3.1.

We now turn to the results from the temperature-dependent dialysis experiments. From the liquid scintillation measurements of the internal and external solutions, one could determine the uncomplexed HMT concentration and the amount of HMT in complex with DNA, given the specific activity of the HMT used. By measuring the A_{260} of the internal solution and correcting for the absorbance of the HMT in the internal solution, one was able readily to determine the total DNA concentration, and hence the concentration of DNA not in complex with HMT. The results combined yield a direct measurement of the equilibrium binding constant. Table 3.2 lists the binding

Table 3.2 Thermodynamics of HMT + DNA Derived from Equilibrium Dialysis in 0.1 M Na Buffer

T	K, M^{-1}	% Uncertainty
5.0°C	650	3.8
15.7°C	560	8.7
27.4°C	270	19.0
44.6°C	190	20.0
$K_{25°C}$	254	

$\Delta H° = -6.1 \pm 0.7$ kcal/mol

$\Delta S° = -8.9 \pm 2.4$ e.u.

Figure 3.7 Plot of the natural logarithm of the HMT-calf thymus DNA equilibrium binding constant, derived from dialysis experiments, vs 1/T.

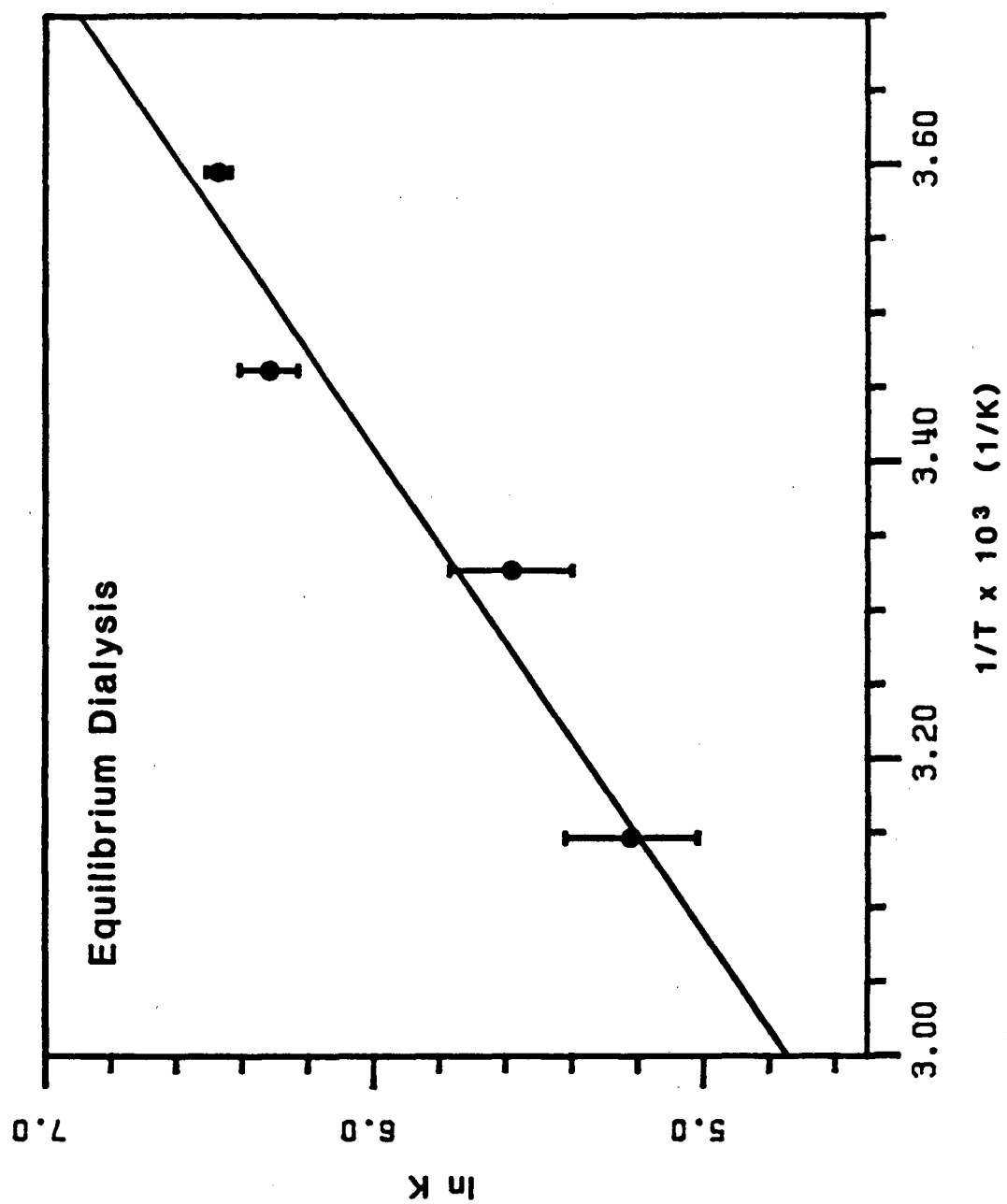
Equilibrium Dialysis
ln K
7.0
6.0
5.0
3.00
3.20
3.40
3.60
1/T x 10³ (1/K)

constants obtained at four temperatures. A plot of lnK against 1/T gave the $\Delta H°$ of HMT-DNA binding as -6.1(±0.7) kcal/mol (Figure 3.7).

The values for $\Delta H°$ determined from the fluorescence and dialysis experiments are seen to be in reasonable agreement. However, in so far as dialysis is a more direct measurement, the results derived from dialyses are more reliable. In subsequent sections, the thermodynamic values used will be those obtained from the dialysis experiments.

B) The Nature of the HMT-DNA Complex

Conventionally, one writes the HMT-DNA binding equilibrium as

$$\text{HMT} + \text{DNA} \underset{}{\overset{K_{app}}{\rightleftharpoons}} \text{HMT}\cdot\text{DNA} \qquad (3.2)$$

with $$K_{app} = \frac{[\text{HMT}\cdot\text{DNA}]}{[\text{HMT}][\text{DNA}]} \qquad (3.3)$$

DNA is, however, a linear polyelectrolyte with regularly spaced negative phosphate groups along its backbone. The phosphate-phoshate repulsion is partially relieved by "condensing" positive counterions onto the linear polymer. The entropic gain from counterion dissociation into the bulk solution prevents complete neutralization of the phosphate charges by condensation. The condensed cations are not bound to specific sites on the polyelectrolyte but rather move freely on the surface of the polymer. Cations condensed on the DNA

are in equlibrium with the cations in the bulk solution. In the theoretical framework developed by Manning (see review by Manning, 1978), the extent of counterion condensation is governed by a dimensionless parameter ξ:

$$\xi = \frac{e^2}{\varepsilon k_B T b} \tag{3.4}$$

where e is the charge on the electron,

ε is the dielectric constant of the bulk solution,

k_B is the Boltzmann constant,

T is the temperature in Kelvins, and

b, with units of Å/charge, is the average distance between negative charges on the polymer.

Under the experimental conditions here, $\xi = 7.08Å/b$. If $\xi < 1$, no counterions condense on the polymer. For $\xi > 1$ (i.e., $b < 7.08Å$), however, counterion condensation will occur. The number of counterions condensed per phosphate is derived by Manning to be

$$\theta_{M+} = 1 - \xi^{-1} \tag{3.5}$$

The theoretical results were confirmed in ^{23}Na-NMR experiments by Anderson and coworkers (Anderson et al., 1978).

HMT is believed to be an intercalator. Intercalators extend and

unwind the DNA to which they bind (Cairns, 1962; Lerman, 1964; Waring 1968). For positively charged intercalators like ethidium, the extent of binding is high and the length increase in the DNA considerable. The effects of unwinding the DNA can be quantitated by sedimentation and gel electrophoretic measurements (Bauer & Vinograd, 1968; Depew & Wang, 1975; Pulleybank et al., 1975). Conversely, a measured degree of unwinding may be used to infer the extent to which a charged drug intercalates into DNA. For the neutral HMT, measuring the extent of unwinding caused by the bound drug is not feasible since so few molecules actually bind to the DNA. An alternative approach based on the polyelectrolye nature of DNA is possible. In view of the earlier discussion, any change in the length of the DNA will change the average distance between phosphate groups on the DNA. The consequence is a change in the amount of counterion condensation. Thus, one might write the HMT-DNA binding equilibrium as

$$\mathrm{HMT} + \mathrm{DNA} \underset{}{\overset{K_b}{\rightleftharpoons}} \mathrm{HMT{\cdot}DNA} + \Delta n\mathrm{Na}^+ \qquad (3.6)$$

for which the equilibrium constant is

$$K_b = \frac{\gamma_{\mathrm{HMT\cdot DNA}}[\mathrm{HMT\cdot DNA}]}{\gamma_{\mathrm{HMT}}[\mathrm{HMT}]\gamma_{\mathrm{DNA}}[\mathrm{DNA}]}\cdot(\gamma_{\mathrm{Na}^+})\cdot[\mathrm{Na}^+]^{\Delta n} \qquad (3.7)$$

where γ_α denotes the activity coefficient for species α. If we assume that the only strongly non-ideal activity coefficient is γ_{Na^+},

Figure 3.8 Plot of $\ln(K_{app})$ <u>vs</u> $\ln(a_{Na^+})$ for the HMT + DNA system.

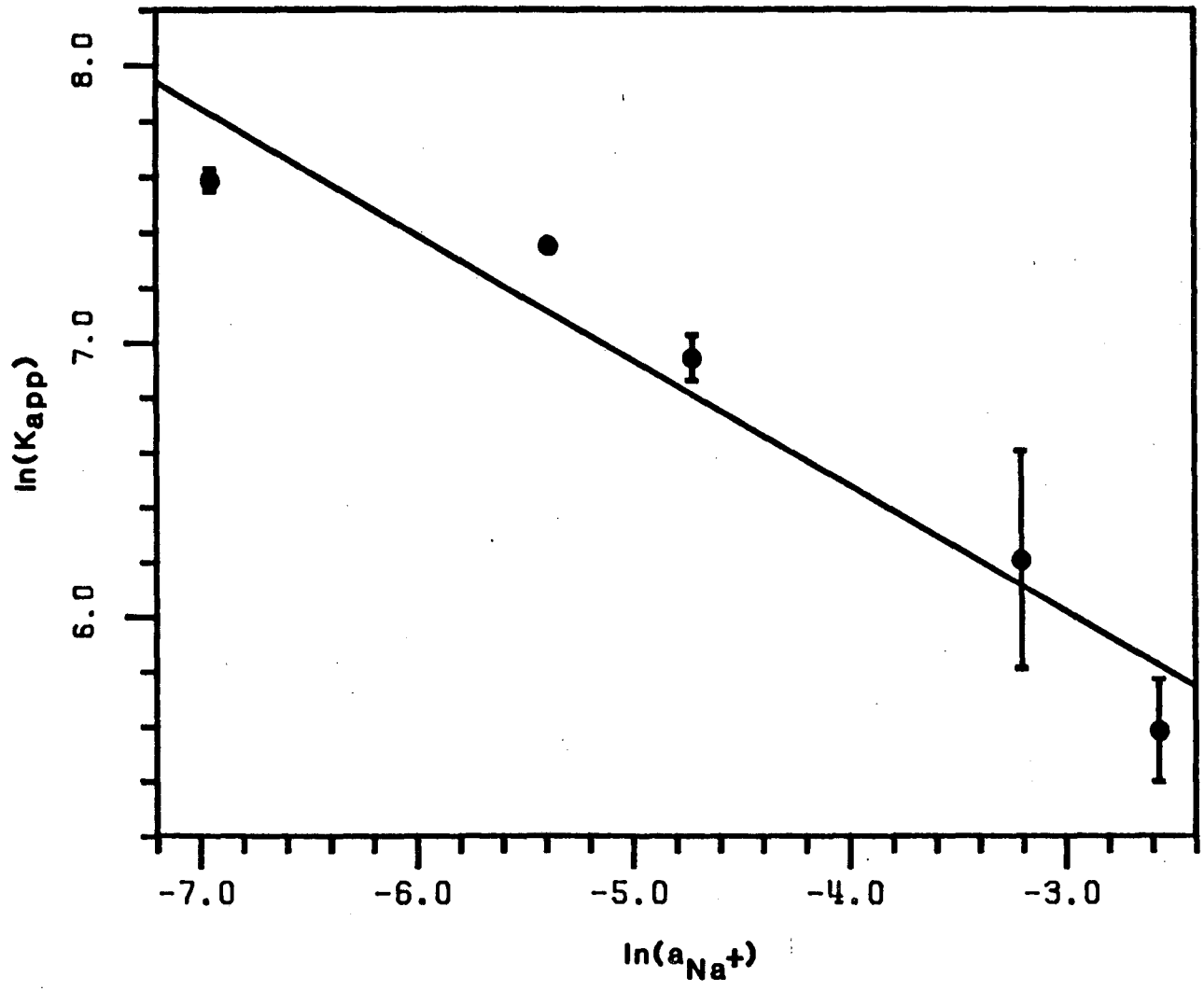
8.0
7.0
6.0
ln(Kapp)
-7.0
-6.0
-5.0
-4.0
-3.0
ln(aNa+)

Table 3.3 Dependence of K_{app} on Sodium Ion Activity[a,c]

C_{Na^+} [M]	γ_{Na^+}[b]	a_{Na^+} [M]	K_{app}(%Uncert.)[M^{-1}]
0.001	0.960	9.60×10^{-4}	1970 (4.1)
0.005	0.917	4.58×10^{-3}	1560 (0.1)
0.010	0.888	8.88×10^{-3}	1030 (8.3)
0.050	0.812	4.06×10^{-2}	490 (40)
0.100	0.767	7.67×10^{-2}	270 (19)

$K_{app,0.1M\ Na^+} = 347\ M^{-1}$

[a]All values reported are for 27.4°C

[b]Calculated using method outlined in Laitinen & Harris, 1975

[c]In an earlier publication (Isaacs et al., 1978), the K_{app} for binding HMT to calf thymus DNA was quoted as 3400 M^{-1}. That value was obtained by dialysis at "room temperature" in a buffer of 0.01 M Tris, 0.001 M EDTA at pH 8.4. Under these conditions $C_{Na^+} \approx 0.002$ M. Results from the present study, when adjusted to the conditions used by Isaacs et al., assuming "room temperature" to be ~22°C, yield a K_{app} of ~2400 M^{-1}. The agreement between the two values is acceptable.

we can write K_b, using the definition of K_{app} from Equation 3.3, as

$$K_b = K_{app} \cdot a_{Na^+}^{\Delta n} \qquad (3.8)$$

K_b is a true thermodynamic equilibrium constant. K_{app}, on the other hand, should show a dependence on the sodium ion activity in the solution. Taking the natural logarithm of Equation 3.8 and rearranging yields

$$\ln K_{app} = -\Delta n \cdot \ln a_{Na^+} + \ln K_b \qquad (3.8a)$$

The negative slope of a plot of $\ln K_{app}$ against $\ln a_{Na^+}$ is the change in the number of condensed sodium ions for each HMT intercalated. Such a plot of the experimental data is shown in Figure 3.8. The data are tabulated in Table 3.3.

What is the expected value of Δn for binding a neutral intercalator? Using the equations of Manning, one gets $\Delta n_{calc} = 0.48$ for binding a neutral intercalator to regular B-DNA (calculation shown in Schema 3.1). The experimentally determined value is $\Delta n_{expt} = 0.46$. The close agreement indicates that HMT binds to DNA by intercalation.

C) Relaxation Kinetics

Displayed in Figure 3.10 is the signal voltage <u>vs</u> time trace from a temperature jump experiment performed on a sample of 1.87×10^{-5}M HMT and 3.42×10^{-4}M DNA. The zero-suppression option was used with a delay time of 50 μs. Final temperature of the sample after the temperature jump was 21.4°C. The initial signal was set equal to 5

Schema 3.1 Change in the Extent of Counterion Condensation upon Binding a Neutral Intercalator

To calculate Δn, the change in the number of counterions condensed per phosphate upon bnding a neutral intercalator, we proceed as outlined below.

The base pairs in B-DNA are separated by 3.4 A. Two negatively charged phosphates are associated with each base pair. The nearest-neighbor exclusion principle dictates that when the DNA lattice is saturated with intercalators, only every other base pair stack along the DNA has an intercalator in it. In other words, an intercalator binding site on DNA may be visualized as two base pairs and their adjoining spaces. Two sites, one empty and the other occupied, are represented in Figure 3.10. With the aid of the diagrams, one can easily determine Δn.

First, we calculate the parameter b for both the empty and the occupied cases. When empty, the site consists of four negative charges and extends over 6.8 A:

$$b_{empty} = 6.8 \text{ A}/4 \text{ charges} = 1.7 \text{ A/charge}$$

The site occupied by a neutral intercalator still carries four negative charges but the total size of the site is expanded to 10.2 A. Thus

$$b_{occupied} = 10.2 \text{ A}/4 \text{ charges} = 2.55 \text{ A/charge}$$

We can now calculate the extent of counterion condensation, θ_{Na^+},

Schema 3.1 (continued)

from Manning theory:

$$\theta_{Na^+} = \frac{n_{Na^+}}{n_{phosphate}} = 1 - \xi^{-1} = 1 - \frac{b}{7.083}, \text{ (at 27.4°C)}$$

Then,

$$\theta_{Na^+}^{empty} = \frac{n_{Na^+}^{empty}}{n_{phosphate}} = 1 - \frac{1.7}{7.083} = 0.760 \qquad \text{(S3.1)}$$

and

$$\theta_{Na^+}^{occupied} = \frac{n_{Na^+}^{occupied}}{n_{phosphate}} = 1 - \frac{2.55}{7.083} = 0.640 \qquad \text{(S3.2)}$$

Since the intercalator under consideration is neutral, the number of negative charges remains at four regardless of the state of occupation of the site. Subtracting Equation S3.2 from S3.1 and substituting $n_{phosphate} = 4$ yields

$$n_{Na^+}^{empty} - n_{Na^+}^{occupied} = 0.48$$

Therefore, for every neutral intercalator bound, the DNA releases $\Delta n = 0.48$ Na^+ ions. The equilibrium for binding HMT to DNA can now be written as

$$HMT + DNA \rightleftharpoons HMT \cdot DNA + 0.48Na^+$$

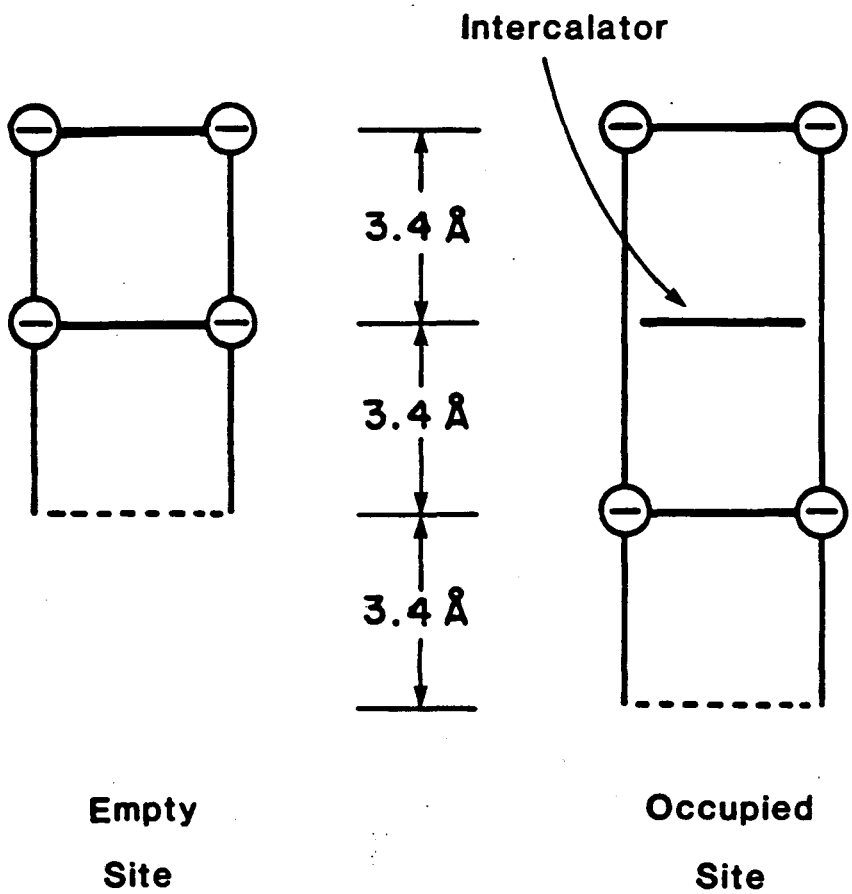

Figure 3.9 Schematic representation of an empty and an occupied intercalator binding site on DNA

Figure 3.10 Relaxation Signal for dCA_6G + dCT_6G

A PMT signal voltage vs time trace obtained from an HMT + calf thymus DNA sample in a temperature jump experiment. See text for conditions of the measurement.

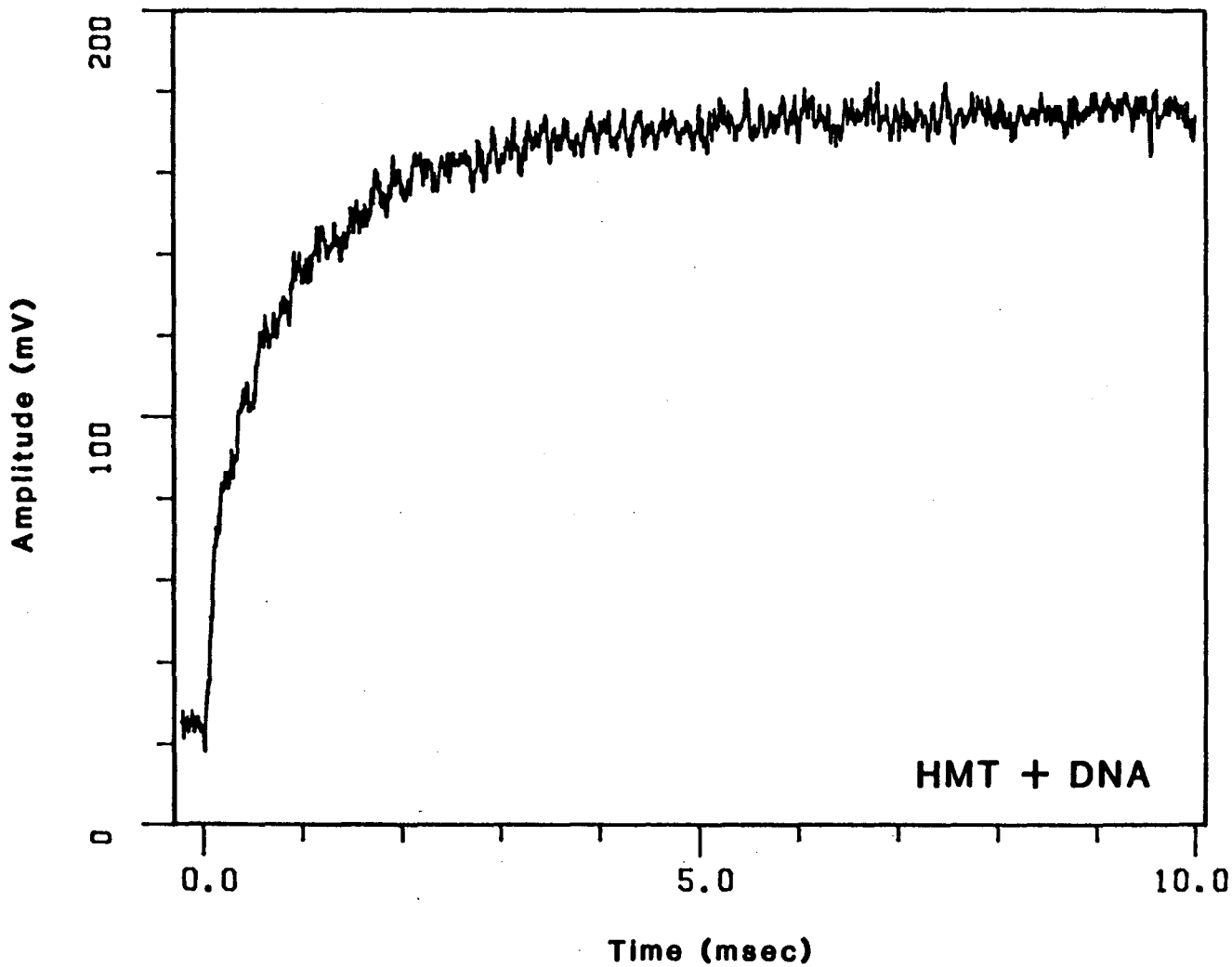
200
100
0
Amplitude (mV)
0.0
5.0
10.0
Time (msec)
HMT + DNA

volts. Analysis of such traces yielded three exponential components.

In the course of a relaxation experiment, an intense beam of light impinges on the sample. In these studies with HMT, exposure of the sample to intense UV light was a problem since HMT is a photoreagent capable of photoreactions with the thymines in DNA as well as photodegradation. It was thus necessary to check the effect of photoreaction on the experiment. To assess the contribution of the HMT-thymine photoadducts on DNA to the fluorescence relaxation signal, one must determine the amount of adducts generated in a typical temperature jump experiment. One must estimate, in addition, the relaxation signal arising from a known amount of adducts. A single temperature jump measurement can be completed with exposure of the sample to UV light limited to ~10 seconds. On the order of ten temperature jumps are made on each sample. Running a set of temperature jumps on a sample made from DNA and ^{3}H-HMT, it was found that after ~100 seconds of cumulative exposure of the sample to UV light at 360nm, approximately four ^{3}H-HMT-DNA adducts were generated per 1000 base pairs. By performing temperature jumps on a purified sample of calf thymus DNA containing ~1 adduct per 100 base pairs, the fluorescence signal was found to be roughly one hundred fold weaker than the signal one gets with a solution containing free HMT and DNA. From these results we conclude that the ~4 adducts per 1000 base pairs generated through the course of a whole set of temperature jumps contribute negligibly to the relaxation signal.

The effect of photodegradation of HMT is best seen by performing

temperature jumps on a solution of HMT without DNA. It was found that a fast relaxation signal appeared with irradiation and grew in amplitude with successive exposures to the exciting light. This signal, since it increased progressively with irradiation, must have arisen from photodecomposition products of HMT in aqueous solution. This degradation product signal corresponded to the fastest component (Component 1) found in analyzing HMT-DNA relaxation curves. Component 1 was in fact faster than the rise time of the instrument. Since it did not have any bearing on the physical binding process in which we were interested, no further attempt was made to characterize the signal arising from the photoproducts.

Out of the analysis, we found that two of the three relaxation components are attributable to physical interactions between HMT and DNA. Of these two components, the faster one (hereon referred to as Component 2) was the only one which varied with DNA concentration. Component 2 could be analyzed using the simple bimolecular scheme

$$\mathrm{HMT} + \mathrm{DNA} \underset{k_{-1}}{\overset{k_1}{\rightleftharpoons}} \mathrm{HMT \cdot DNA} \qquad (3.9)$$

For such a scheme, the inverse relaxation time is expected to have the functional form

$$\tau^{-1} = k_1([\mathrm{HMT}] + [\mathrm{DNA}]) + k_{-1} \qquad (3.10)$$

Since the HMT-DNA interaction is weak, [HMT] + [DNA] is approximately

Figure 3.11-3.14 Plots of $1/\tau_2$ vs C_T (C^o_{HMT} + C^o_{DNA}) for the HMT + calf thymus DNA system at 17.5°C, 21.4°C, 25.6°C and 29.5°C, respectively.

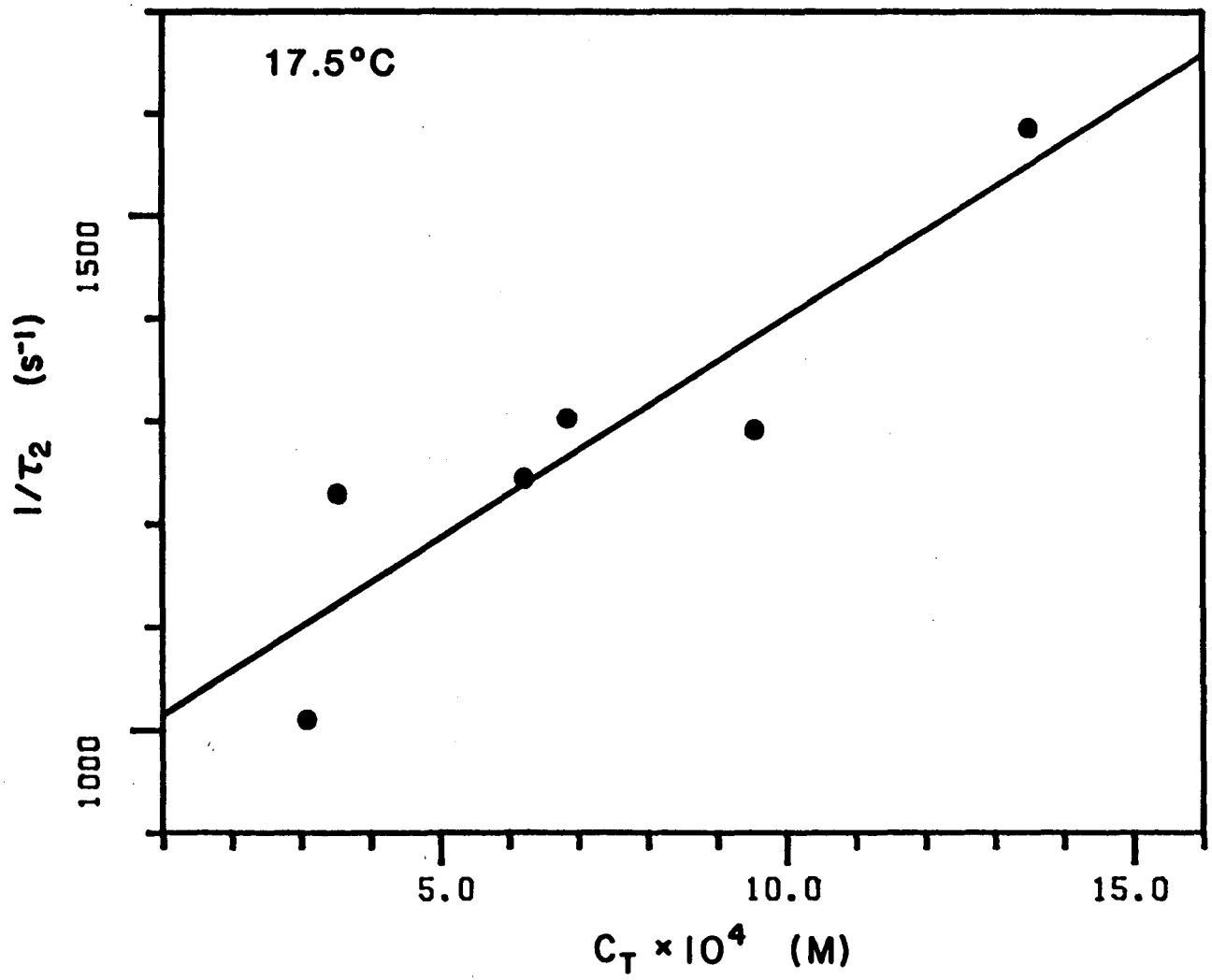
17.5°C
1500
1000
$1/\tau_2$ (s^{-1})
5.0
10.0
15.0
$C_T \times 10^4$ (M)

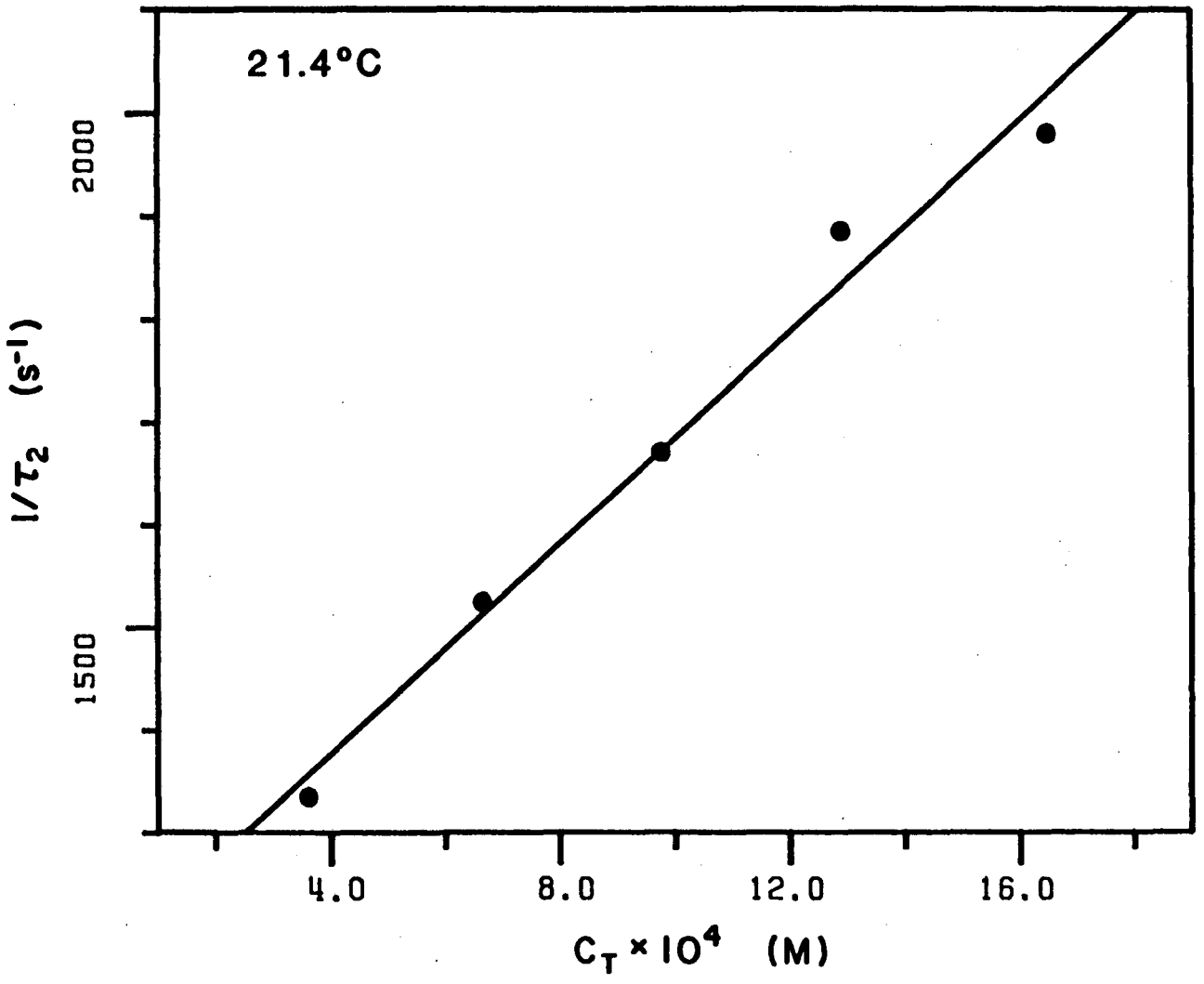
21.4°C
2000
1500
$1/\tau_2$ (s^{-1})
4.0
8.0
12.0
16.0
$C_T \times 10^4$ (M)

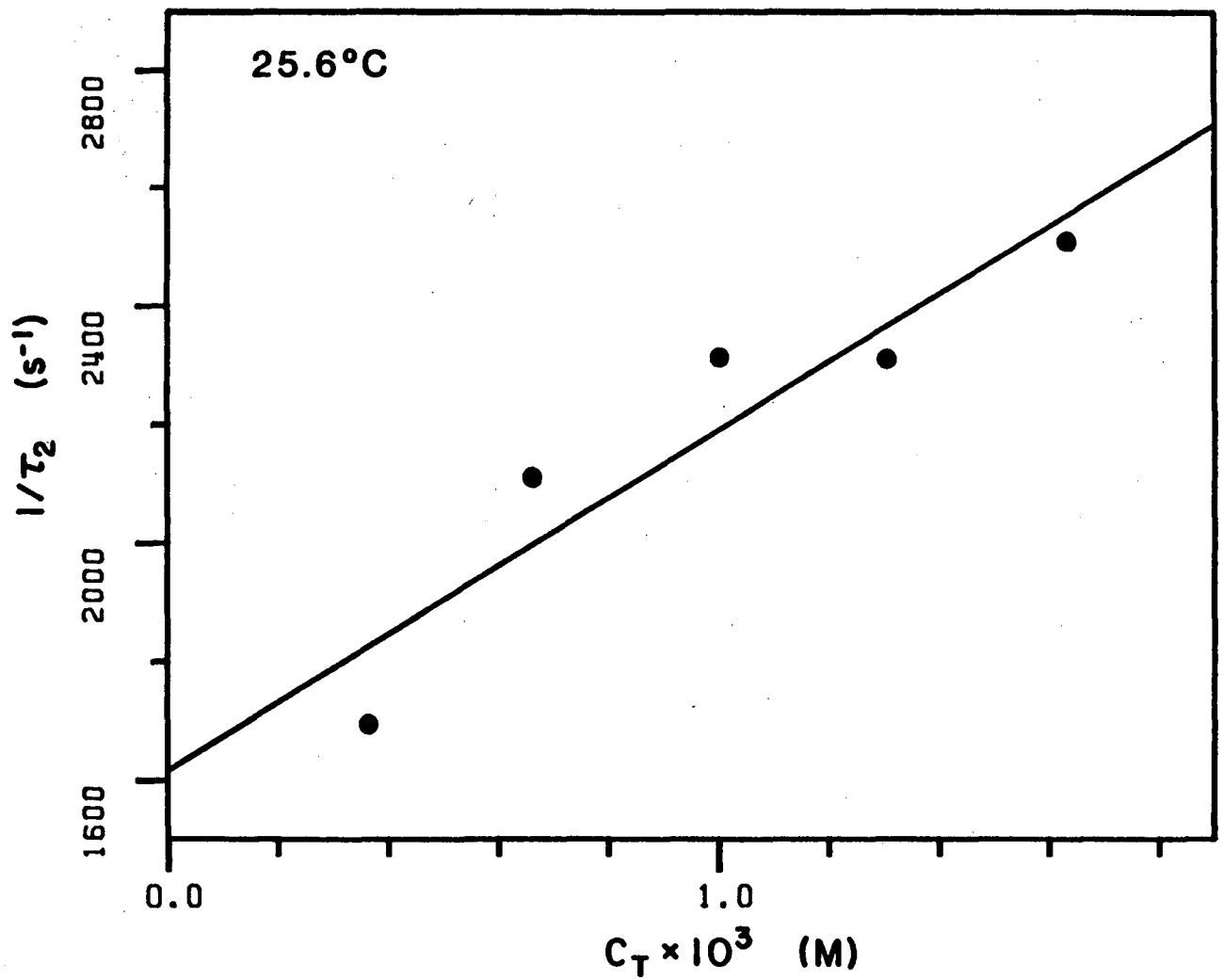
25.6°C
2800
2400
2000
1600
$1/\tau_2$ (s^{-1})
0.0
1.0
$C_T \times 10^3$ (M)

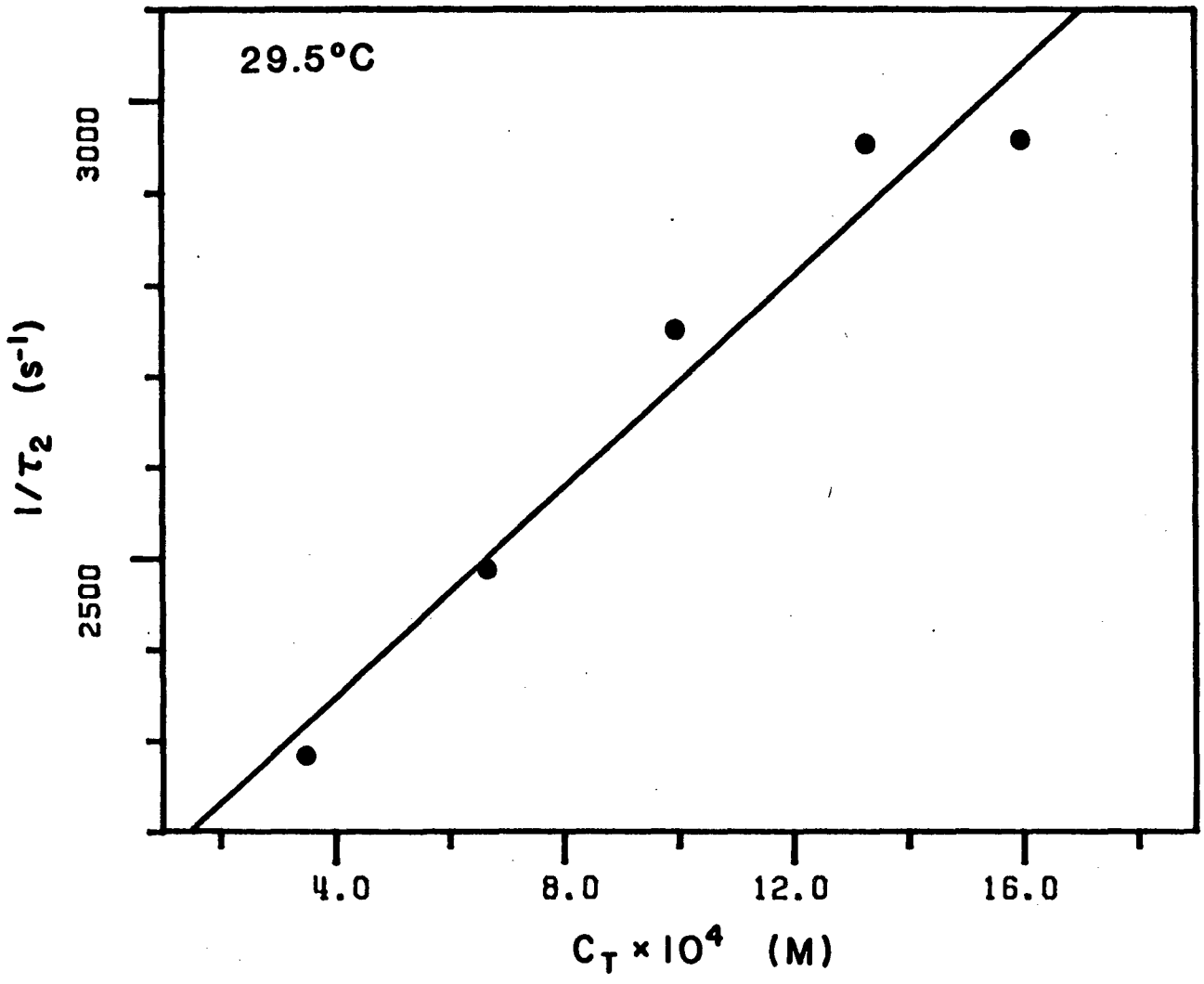
29.5°C
3000
2500
$1/\tau_2$ (s^{-1})
4.0
8.0
12.0
16.0
$C_T \times 10^4$ (M)

$C^{o}_{HMT} + C^{o}_{DNA}$, where C^{o}_{HMT} and C^{o}_{DNA} are the initial total concentrations of HMT and DNA, respectively. Consequently, we can write

$$\tau^{-1} = k_1(C^{o}_{HMT} + C^{o}_{DNA}) + k_{-1} \qquad (3.11)$$

Plots showing the linear least squares fit of Component 2 to Equation 3.11 are displayed in Figures 3.11-3.14 for all the temperatures. Listed in Table 3.4 are the forward and reverse rate constants extracted from the least squares fits. Linear fits of lnk's vs 1/T yielded activation energies and entropies (Figures 3.15-16). The activation parameters are listed in Table 3.4.

The longest relaxation time (Component 3) exhibited no DNA concentration-dependent variation. Values of Component 3 at different temperaures are shown in Table 3.5. The apparent activation parameters, obtained by plotting $\ln(\tau_3^{-1})$ vs 1/T (Figure 3.17), are also given.

4. Discussion

We wish first to compare the thermodynamics of the HMT-DNA system with those of two other well characterized systems, ethidium-DNA and proflavin-DNA. In Table 3.6 we find the pertinent thermodynamic parameters for the three systems. The first striking feature is the disparity in the magnitudes of the equilibrium binding constants. The charged ligands have apparent binding constants which are roughly two orders of magnitude larger than the binding constant of HMT to DNA. In comparing the ΔS^{o} values, it is quite apparent that the

Table 3.4 Kinetic Parameters for the First Step in Binding HMT to DNA

T	$k_1 x10^{-5}$, $[M^{-1}s^{-1}]$	k^{-1} $[s^{-1}]$
17.5°C	4.3 ± 1.0	970 ± 80
21.4°C	5.1 ± 0.4	1170 ± 40
25.6°C	5.7 ± 1.3	1620 ± 140
29.5°C	5.9 ± 0.7	2110 ± 80
$k_{25°C}$	5.44	1561
Ea	4.6 ± 1.1	11.5 ± 0.8
$\Delta S^{\ddagger}$	-19 ± 2	-7 ± 1

$\Delta H^{\circ}_{kinetic}$ = -6.9 ± 1.8 $\Delta S^{\circ}_{kinetic}$ = -12 ± 3

$\Delta H^{\circ}_{equil.}$ = -6.1 ± 0.7 $\Delta S^{\circ}_{equil.}$ = -8.9 ± 2.4

E_a's, ΔH°'s in kcal/mol

ΔS°'s in e.u.

Figure 3.15-3.16 Arrhenius plots for k_1 and k_{-1} in the HMT + calf thymus DNA system.

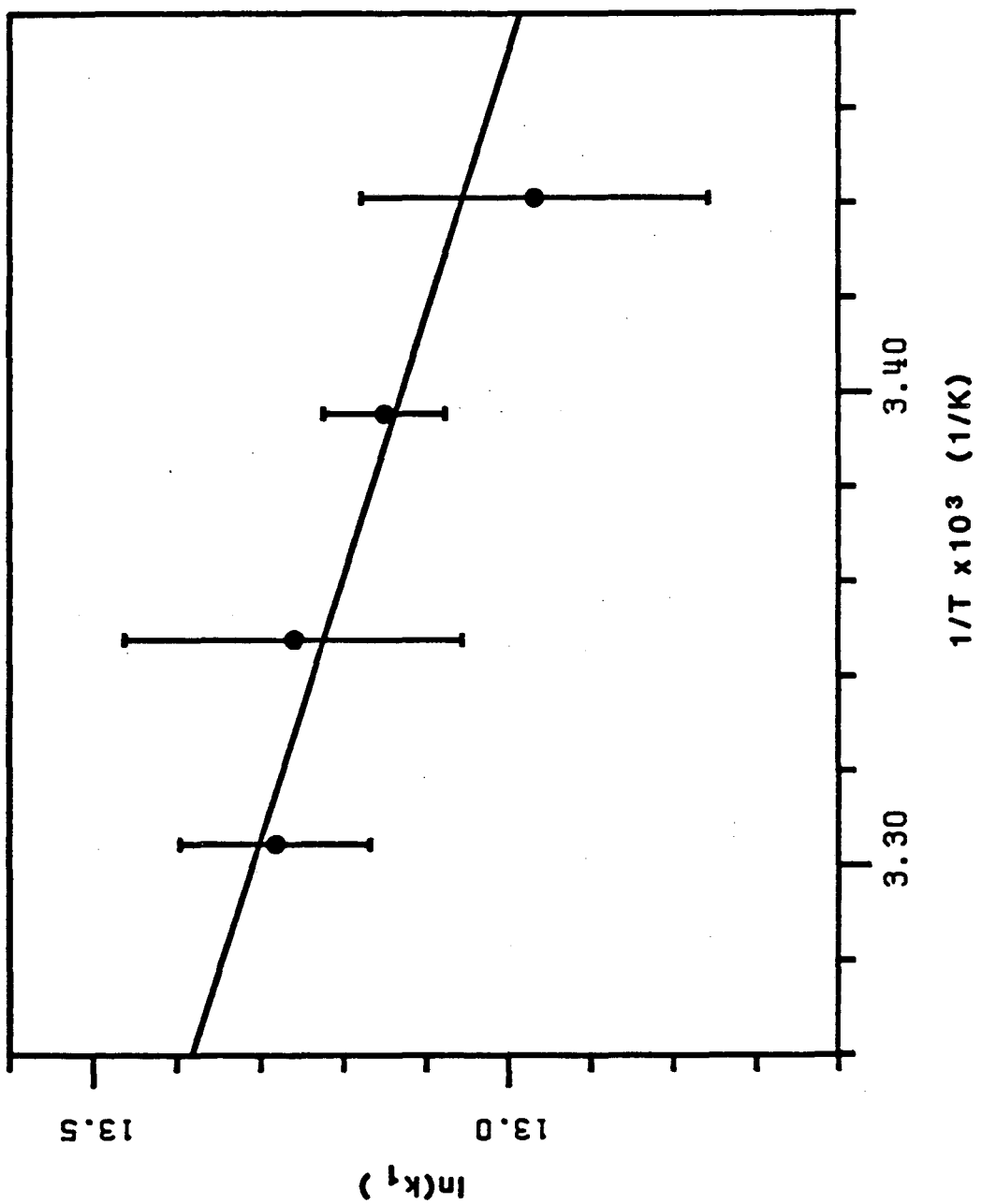
ln(k1)
13.0
13.5
3.30
3.40
1/T x10³ (1/K)

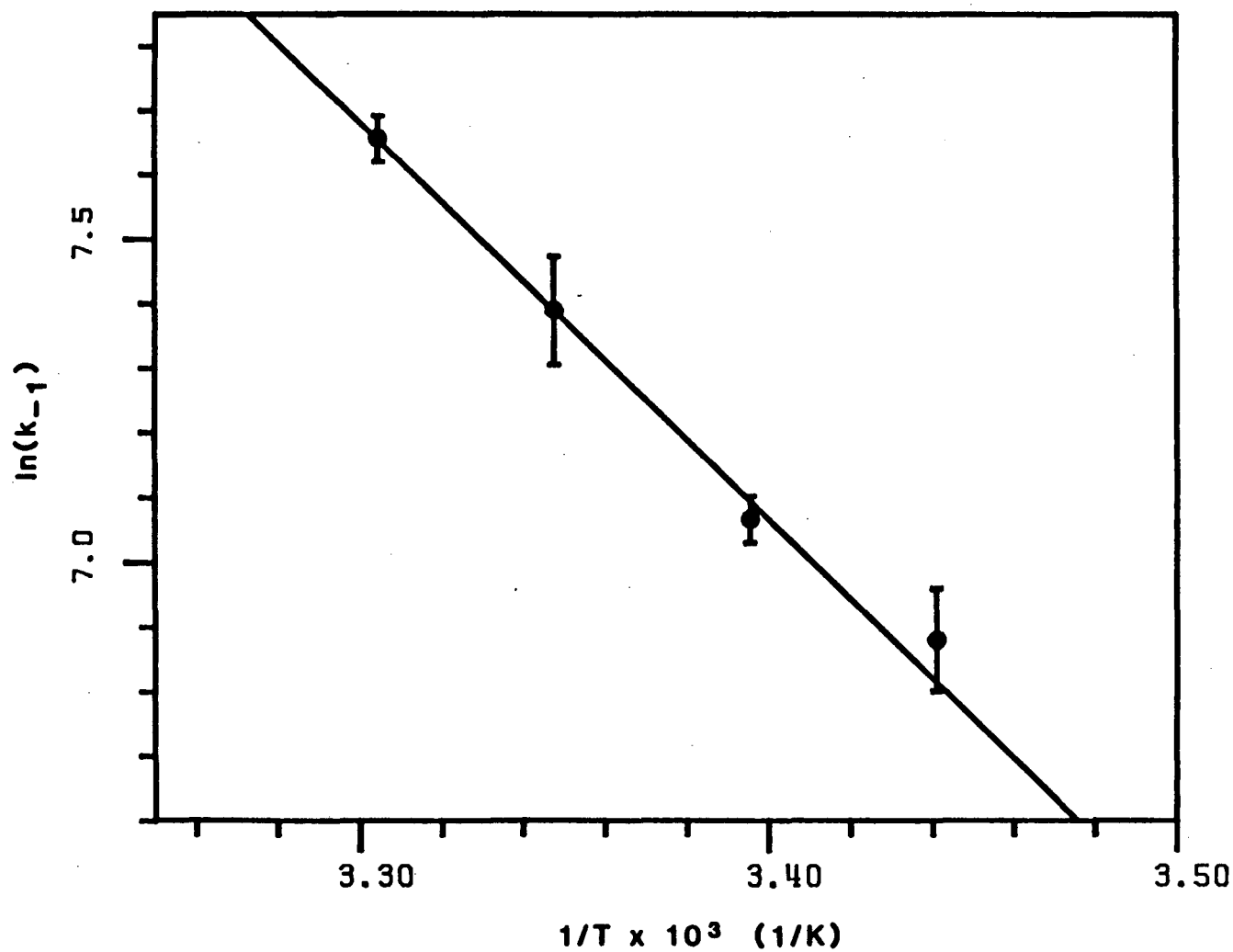
7.5
7.0
ln(k_-1)
3.30
3.40
3.50
1/T x 10³ (1/K)

Table 3.5 Listing of Component 3 and Apparent Activation Parameters[a]

T	τ_3^{-1} [s^{-1}]
17.5°C	479 ± 41
21.4°C	536 ± 27
25.6°C	656 ± 84
29.5°C	688 ± 42
k_{-2}, 25°C	614

E_a = 5.6 ± 0.8 kcal/mol

$\Delta S^{\ddagger}$ = -29 ± 1 e.u.

[a]Following the interpretation in the text, $\tau_3^{-1} = k_{-2}$

Table 3.6 Thermodynamics for Three Ligands Binding to DNA

Ligand	K_{app}	$\Delta H°$	$\Delta S°$	$T\Delta S°$
Ethidium^{+a}	3.8×10^4	-8.4	-7.2	2.1
Proflavin^{+b}	2.0×10^4	-8.4	-8.4	2.5
HMT	340	-6.1	-8.9	2.6

All values for 25°C

K_{app} in M^{-1}

$\Delta H°$ and $T\Delta S°$ in kcal/mol

$\Delta S°$ in e.u.

[a]Bresloff & Crothers, 1975; 1 M NaCl

[b]Li & Crothers, 1968; 0.2 m NaCl

Figure 3.17 Plot of $\ln(\tau_3^{-1})$ <u>vs</u> 1/T for the HMT + calf thymus DNA system.

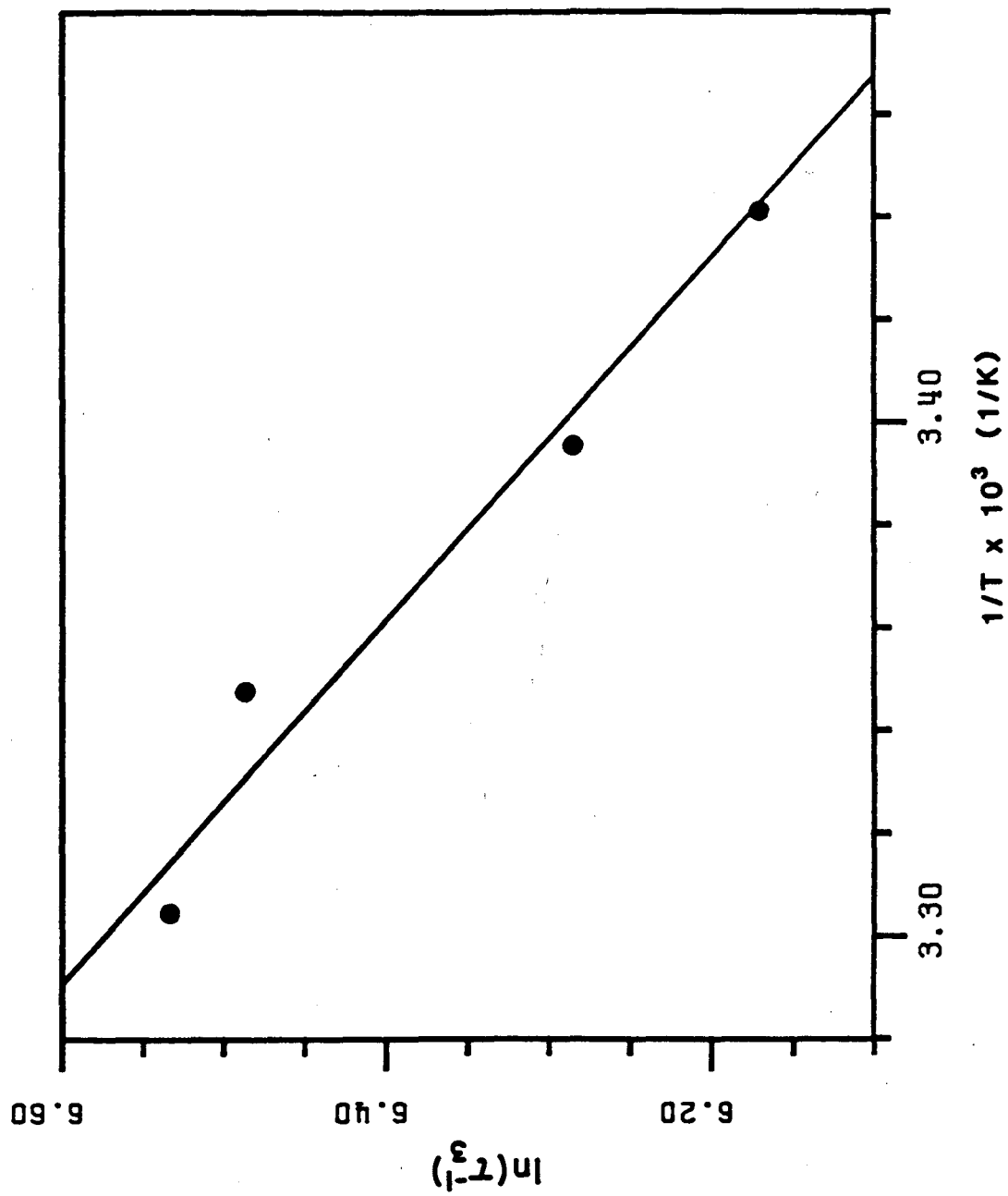
6.60
6.40
6.20
ln(τ3-1)
3.30
3.40
1/T x 10^3 (1/K)

entropy change upon binding a ligand is essentially the same for all three ligands, regardless of charge. The place where the charged and uncharged ligands differ is in the magnitude of the ΔH° of binding. That is, the large influence the positive charge has on the binding constant is exerted through the enthalpy term.

As shown in the Results section, the sodium ion activity dependence of the apparent binding constant, together with the polyelectrolyte theory developed by Manning permitted one to deduce that HMT formed an intercalated complex with DNA. We will now discuss the results of the relaxation kinetic experiments and attempt to characterize the process by which such an intercalated complex is formed.

Once again, the discussion is best presented as a comparison between the present work and previous studies on ethidium and proflavin. Before a comparison is begun, we must ascertain the nature of the slow relaxation component in the HMT-DNA reaction. There are two plausible schemes which may simply describe the binding reaction. Both of these schemes give rise to two relaxation times. We may write a sequential reaction scheme, where a bimolecular step first leads to a complex, $(HMT \cdot DNA)_1$, which subsequently may rearrange to yield $(HMT \cdot DNA)_2$:

$$\mathrm{HMT} + \mathrm{DNA} \underset{k_{-1}}{\overset{k_1}{\rightleftharpoons}} (\mathrm{HMT} \cdot \mathrm{DNA})_1 \underset{k_{-2}}{\overset{k_2}{\rightleftharpoons}} (\mathrm{HMT} \cdot \mathrm{DNA})_2 \qquad (3.12)$$

where $K_1 = k_1/k_{-1}$ and $K_2 = k_2/k_{-2}$. The experimentally measured equilibrium constant is related to the two stepwise constants by

$$K_{app} = K_1(1 + K_2) \tag{3.13}$$

For this linear scheme, the two reciprocal relaxation times are

$$\tau_{fast}^{-1} = k_1([HMT] + [DNA]) \tag{3.14}$$

and

$$\tau_{slow}^{-1} = k_2\frac{K_1([HMT] + [DNA])}{K_1([HMT] + [DNA]) + 1} + k_{-2} \tag{3.15}$$

A parallel scheme is also possible where two bimolecular steps each leads to the formation of a different complex (e.g., one in each groove of the DNA helix):

$$\begin{aligned} HMT + DNA &\underset{k_{-1}}{\overset{k_1}{\rightleftharpoons}} (HMT\cdot DNA)_1 \\ HMT + DNA &\underset{k_{-2}}{\overset{k_2}{\rightleftharpoons}} (HMT\cdot DNA)_2 \end{aligned} \tag{3.16}$$

With $K_1 = k_1/k_{-1}$ and $K_2 = k_2/k_{-2}$, the observed equilibrium constant in terms of the parallel scheme is

$$K_{app} = K_1 + K_2 \tag{3.17}$$

For one step, and for convenience say the first, being much faster than the other, the two relaxation times for the parallel scheme are given by

$$\tau_{fast}^{-1} = k_1([HMT] + [DNA]) + k_{-1} \tag{3.18}$$

and

$$\tau_{slow}^{-1} = k_2 \frac{[HMT] + [DNA]}{K_1([HMT] + [DNA]) + 1} + k_{-2} \tag{3.19}$$

The functional form of the fast relaxation time is identical for the two schemes; the same forward and reverse rate constants would apply for the first bimolecular step of both schemes. Using the value of k_1 and k_{-1} at 25°C, one calculates $K_{1,kinetic} = k_1/k_{-1} = 349$ M^{-1}. The thermodynamic K_{app} determined by equilibrium measurements is 341 M^{-1} at the same temperature. The two values are seen to be essentially equal. In terms of the stepwise equilibrium constants, the expressions for K_{app} are $K_{app} = K_1(1 + K_2)$ for the sequential scheme and $K_{app} = K_1 + K_2$ for the parallel scheme. In either case, since the magnitude of K_1 and K_{app} are essentially identical, the contribution of the second step (K_2) to the total binding process must be very small. Furthermore, since the formation of complex 1 (step 1) dominates the binding equilibrium, and the polyelectrolyte results indicate the bound form to be an intercalated species, we may

conclude that HMT intercalates directly into the DNA helix, in a single bimolecular step, without an intermediate bound form.

The uncertainties in K_1 are on the order of 10%. We can now use this to place limits on the magnitude of K_2 in each scheme. That is, for the sequential scheme, $K_2 \lesssim 0.1$; and for the parallel scheme, $K_2 \lesssim 0.1K_1 = 35\ M^{-1}$, at 25°C. For the slow relaxation component, if we consider the contribution of the forward rate constant, k_2, to the relaxation time to be negligible, then the measured reciprocal relaxation time is simply k_{-2}. This is true for both reaction schemes, as can be seen in Equations 3.15 and 3.19. Since $K_2 = k_2/k_{-2} < 35\ M^{-1}$ for the parallel scheme, $k_{2,para} < 35k_{-2} = 2.1 \times 10^4\ M^{-1}s^{-1}$. For the sequential case, $K_2 = k_2/k_{-2} < 0.1$; therefore, $k_{2,seq} < 0.1k_{-2} = 61\ s^{-1}$. We now wish to check if these values for k_2 do indeed make negligible contributions to the reciprocal relaxation time. Under the conditions of the experiment, $3 \times 10^{-4}\ M < [HMT]+[DNA] < 1.6 \times 10^{-3}\ M$. Over this concentration range, the change in $1/\tau_{slow}$ expected for the parallel scheme is

$$\Delta(\tau_{slow}^{-1})_{para} = 7.5 \times 10^{-4}k_2$$

which, with $k_{2,para} < 2.1 \times 10^4\ M^{-1}s^{-1}$, yields $\Delta(\tau_{slow}^{-1})_{para} < 16\ s^{-1}$. In the sequential scheme, over the same concentration range,

$$\Delta(\tau_{slow}^{-1})_{seq} = 0.27k_2$$

For $k_{2,seq} < 61\ s^{-1}$, the expected change is $\Delta(\tau_{slow}^{-1})_{seq} < 16\ s^{-1}$. A value of $\Delta(\tau_{slow}^{-1})$ of less than $16\ s^{-1}$ is far smaller than the

standard deviations associated with the values of τ_{slow}^{-1} reported in Table 3.5. Thus the k_2's derived from the constraints on K_2 would contribute negligibly to the reciprocal relaxation times. We now proceed to consider the relative plausibility of the parallel and sequential schemes. The rate constant $k_{2,para}$ is less than $2.1 \times 10^4\ M^{-1}s^{-1}$. Since in the parallel scheme k_2 characterizes a <u>bimolecular</u> step, such a value is unreasonably low and would favor rejection of the parallel scheme. In the sequential scheme, however, k_2 is the unimolecular rate constant for rearranging a <u>fully intercalated</u> HMT complex. A value of $k_{2,seq} < 61\ s^{-1}$ is not at all unrealistic. Henceforth, we will interpret the kinetic results in terms of the sequential binding scheme:

$$\text{HMT} + \text{DNA} \underset{k_{-1}}{\overset{k_1}{\rightleftharpoons}} \underset{\text{intercalated}}{(\text{HMT}\cdot\text{DNA})_1} \underset{k_{-2}}{\overset{k_2}{\rightleftharpoons}} \underset{\text{alternative bound form}}{(\text{HMT}\cdot\text{DNA})_2} \qquad (3.20)$$

Now a comparison may be made between this work on HMT and published studies on proflavin and ethidium. Li and Crothers (1968) interpreted the proflavin binding reaction using the following sequential scheme:

$$\text{Pro} + \text{DNA} \underset{k_{21}}{\overset{k_{12}}{\rightleftharpoons}} (\text{Pro}\cdot\text{DNA})_{out} \underset{k_{32}}{\overset{k_{23}}{\rightleftharpoons}} (\text{Pro}\cdot\text{DNA})_{intercalated}, \qquad (3.21)$$

where $(Pro \cdot DNA)_{out}$ represents a proflavin bound to the outside of the DNA helix through electrostatic interactions. Bresloff and Crothers (1975) analyzed the kinetics of ethidium binding to DNA in terms of the rather complex model:

$$\mathrm{Eth} + \mathrm{DNA} \underset{k_{-1}}{\overset{k_0}{\rightleftharpoons}} (\mathrm{Eth} \cdot \mathrm{DNA})_0$$

$$(\mathrm{Eth} \cdot \mathrm{DNA})_2 \underset{k_2}{\overset{k_{-2}}{\rightleftharpoons}} \mathrm{Eth} + \mathrm{DNA} \underset{k_{-1}}{\overset{k_1}{\rightleftharpoons}} (\mathrm{Eth} \cdot \mathrm{DNA})_1 \qquad (3.22)$$

$$(\mathrm{Eth} \cdot \mathrm{DNA})_1 + \mathrm{DNA} \underset{k_{-t}}{\overset{k_t}{\rightleftharpoons}} \mathrm{DNA} + (\mathrm{Eth} \cdot \mathrm{DNA})_2$$

In this model, $(Eth \cdot DNA)_0$ is an externally bound form, while $(Eth \cdot DNA)_1$ and $(Eth \cdot DNA)_2$ are two intercalated forms. Wakelin and Waring (1980) in their follow-up study suggested that forms 1 and 2 are complexes in which the ethidium intercalates <u>via</u> the major and minor groove of the DNA, respectively. In addition to the bimolecular intercalation steps, the process characterized by k_t and k_{-t} is a direct transfer of the ethidium from the major groove on the DNA to

Table 3.7 Kinetics of Three Ligand-DNA Systems

(See text for reaction schemes)

Ligand	Forming[b] External Complex	Direct[c] Intercalation	Rearrangement of Bound Species
Proflavin[a]	$k_{12} = 1.30 \times 10^7$ $k_{21} = 1.19 \times 10^4$	No Comparable Process	$k_{23} = 6.60 \times 10^{-3}$ $k_{32} = 405$
Ethidium	$k_0 = 1.85 \times 10^7$ $k_{-0} = 7.94 \times 10^3$	$k_1 = 1.41 \times 10^6$ $k_{-1} = 171$ $k_2 = 2.64 \times 10^5$ $k_{-2} = 59.3$	No Comparable Process
HMT	No Comparable Process	$k_1 = 5.44 \times 10^5$ $k_{-1} = 1561$	k_2[d] $k_{-2} = 614$

Bimolecular rate constants in $M^{-1}s^{-1}$

Unimolecular rate constant in s^{-1}

[a]Li & Crothers, 1968; 0.2 M NaCl

[b]Original values for ethidium: Bresloff & Crothers, 1975; 1 M NaCl

[c]Revised values for ethidium: Wakelin & Waring, 1980; 1 M NaCl

[d]Could not determine given precision of data

the minor groove on a different segment of DNA. This direct transfer process is absent for both the proflavin and HMT cases.

Table 3.7 displays the rate constants (at 25°C) characterizing various complex forming and rearranging steps in binding the three different ligands to calf thymus DNA. Both proflavin and ethidium form an external complex with DNA. This external complex is formed through a bimolecular step. The forward rate constants for external binding is seen to be quite high. The external complex is believed to be stabilized by electrostatic interactions between the ligand and the DNA. The ligand HMT, lacking any charge, is unable to form such an external electrostatic complex, as evidenced by the absence of a very large bimolecular association rate constant.

The similarity of HMT and ethidium lies in the fact that both ligands exhibit relatively low bimolecular association rate constants. For ethidium, the rate constants k_1 and k_2 are for forming intercalated complexes directly from solution. As previously discussed in connection with the sequential scheme, k_1 for HMT characterizes the direct intercalation of HMT into the DNA. One can see from Table 3.7 that for HMT and ethidium, the forward rate constants for direct intercalation of the ligand are quite similar in magnitude.

Proflavin and HMT share a feature absent in the ethidium situation: a process whereby a bound complex rearranges. In the case of proflavin, the process is the conversion of an external complex to the intercalated form, a process with a relatively small

forward rate constant. On the other hand, for HMT the rearrangement is to some minor alternative species about which little can be deduced. The forward rate constant for rearranging the intercalated HMT is low enough that it could not be determined given the precision of the relaxation kinetic data.

We can gain insight about direct intercalation by examining the activation parameters for proflavin and HMT binding to DNA (Table 3.8). For the bimolecular association step, the activation energies are essentially identical for the two ligands. The reason for the large difference in the forward rate constants between the two is to be found in the activation entropies. $\Delta S^{\ddagger}$ is -10 e.u. for forming the the external proflavin complex and -19 e.u. for directly intercalating HMT. The interpretation is that the positively charged proflavin may approach the DNA in a large number of possible orientations and still be able to form the electrostatic external complex. Being neutral, the HMT does not form and external complex. In order to form the intercalated complex, the HMT must approach the DNA in some very specific orientation with respect to the base pairs. It is this severe restriction on the orientation of approach that entropically lowers the rate constant for direct intercalation.

Table 3.8 Activation Parameters for the Proflavin-DNA and the HMT-DNA Systems

Proflavin	k_{12}	k_{21}	k_{23}	k_{32}
E_a[a], kcal/mol	+4	+14	+16	+14
$\Delta S^{\ddagger}$[b], e.u.	-10	+10	+16	+3

HMT	k_1	k_{-1}	k_2	k_{-2}
E_a, kcal/mol	+4.6	+11.5	---	+5.6
$\Delta S^{\ddagger}$, e.u.	-19	-7	---	-29

[a]As reported in Li & Crothers, 1968

[b]Calculated from results reported in Li & Crothers, 1968

Chapter IV

THE AQUEOUS PHOTOCHEMISTRY OF HMT

1. Introduction

Psoralens (see Figure 4.1) are a class of photoreactive compounds found in a variety of plants. These compounds find their chief medical use as photosensitizing agents in the treatment of skin pigmentation disorders (Scott et al., 1976). Under irradiation with near-UV light, psoralens are capable of forming monoadducts and crosslinks with the pyrimidine bases (predominantly thymine and uracil) in nucleic acids (Musajo et al., 1967; Cole, 1971; Bachellerie et al., 1981). The ability of psoralens to form interstrand crosslinks in nucleic acids is the basis for their use as probes of nucleic acid structure and function (Thamanna et al., 1979; Thompson et al., 1983). The covalent products formed by photoaddition of psoralens to nucleic acid bases have been characterized structurally (Hearst et al., 1984). In previous work, however, one aspect of using psoralens as a reagent in aqueous systems has been neglected: the photochemistry of psoralens by themselves. Characterizing the photodegradation of psoralens is important since whenever a psoralen is used with UV radiation, the reaction system quickly becomes "contaminated" by products arising from psoralen self-reactions. A knowledge of the nature of the psoralen

Figure 4.1 Topmost is the tricyclic psoralen nucleus with the commonly used numbering system. The structure for HMT is shown at the bottom. Also shown are the structures for furan, α-pyrone and coumarin. These structures are useful when one wishes to refer to specific portions of the psoralen molecule.

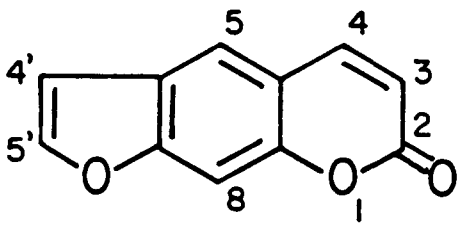

PSORALEN

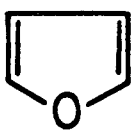

FURAN

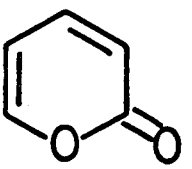

α-PYRONE

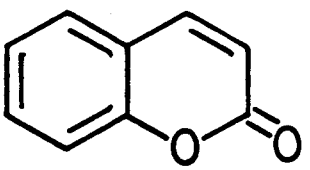

COUMARIN

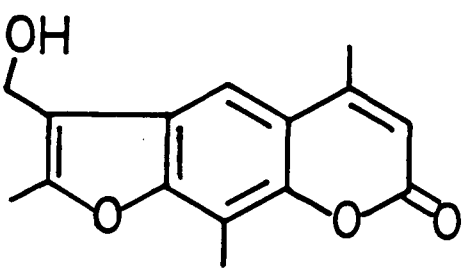

HMT

photodegradation products aids the understanding of experimental results from physical studies. The types of photoproducts found may also give better insight into the clinical effects of psoralen use.

The psoralen chosen in this study is HMT (Figure 4.1). This choice was originally motivated by requirements of the temperature jump relaxation studies presented in Chapter III. HMT is characterized by a relatively high aqueous solubility (of the order of 10^{-5} M), which made collecting analyzable quantities of the photoreaction products possible. The study here reported is concerned with the isolation and characterization of the major photodegradation products of HMT in aqueous solution. Since all psoralens possess the same tricyclic aromatic nucleus, one is optimistic that the reaction patterns found for HMT should apply to furocoumarins as a class.

2. Experimental

Pure samples of HMT and ^{3}H-HMT (specific activity 13.2 Ci/mmol) were generously supplied by Mr. Steve Isaacs and Prof. John Hearst. Solutions to be irradiated were prepared by first making a 0.01 M solution of HMT in 95% ethanol. Small aliquots of this concentrated ethanolic stock diluted into either water or 0.1 M Na buffer (described in the Experimental section of Chapter III) yielded the final solutions used. Irradiations were carried out in an irradation apparatus consisting of two 400 W G.E. Hg-vapor lamps, illuminating a thermostatted Pyrex holder which contained a 40% $Co(NO_3)_2$ solution as

a filter. The transmission profile of this solution filter is shown in Figure 4.2. Small samples (≤ 10 ml) were placed in Pyrex test tubes and irradiated in the apparatus. Large samples of several liters volume were kept at constant temperature in a thermostatted bath and circulated through the inner chamber of a flow cell with the aid of a large peristaltic pump. The outer chamber of the flow cell was filled with the $Co(NO_3)_2$ filter. Small samples were irradiated for 30 minutes unless otherwise indicated. Large circulating samples were irradiated for periods which gave exposures equivalent to 30 minutes of continuous irradiation.

Irradiated samples were concentrated on a Roto-Vap before analysis. Chromatographic analyses were done on a Beckman-Altex HPLC fitted with Altex Ultrasphere ODS reverse phase columns. The column dimensions were 4.6 mm x 25 cm for analytical separations and 10 mm x 25 cm for preparative separations. A 1 cm path length flow cell was used for analytical separations while for preparative runs a flow cell with a path length of 0.5 mm was used. The effluent from the HPLC was monitored spectroscopically at 250 nm. All samples were filtered through membranes with 0.45 μ porosity before being injected onto the HPLC columns. Three solvents were used for the HPLC analyses. A 20 mM phosphate buffer at pH 2.2 was used for washing the column. Water and methanol were used in gradient elution to separate the photoproducts. All solvents were filtered to 0.45 μ and degassed by suction for ~30 minutes before use.

Three types of mass spectra were taken: electron impact (EI),

Figure 4.2 Transmission profile for a 40% $Co(NO_3)_2$ solution in water. The solution is used as a filter in irradiation experiments.

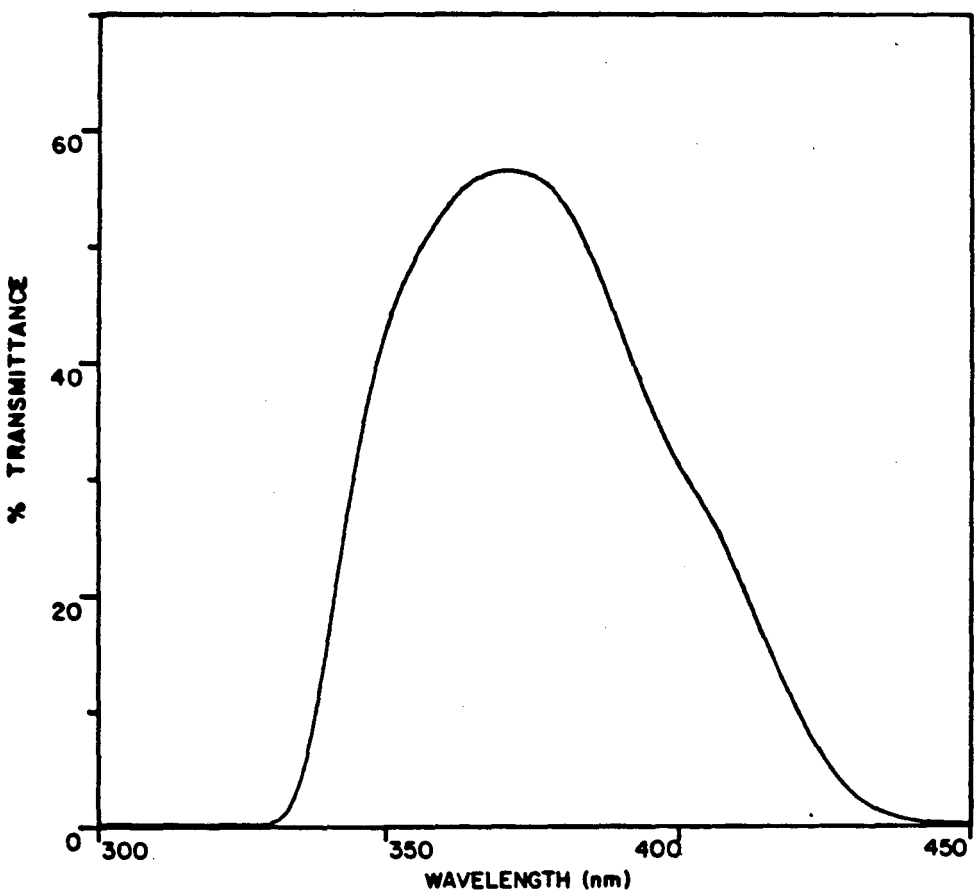

chemical ionization (CI), and fast-atom bombardment (FAB). All mass spectra were run using the mass spectrometry facility in the College of Chemistry at UC Berkeley.

For NMR analysis, HPLC effluent containing the desired compound was first placed under suction to remove methanol. The remaining solution, which was largely aqueous, was lyophilyzed to dryness. The compounds so prepared were kept in a freezer before use. $CDCl_3$ was the solvent used for making all NMR samples. NMR studies were performed at two facilities: the 200 MHz and 250 MHz spectrometers at UC, Berkeley and the 360 MHz instrument on the UC, Davis campus.

3. Results

A. HPLC Analyses

In Figure 4.3 is shown a series of analytical HPLC traces corresponding to a time course study of HMT photodegradation. It can be seen that with increasing irradiation, there is a general decrease in the amount of soluble photoproducts while more and more material becomes insoluble and was removed by filtration.

Figure 4.4 shows a typical record of an HPLC separation of a sample from an irradiated HMT solution. There are four prominent peaks and these are labelled HT, P, I and HM. Portions of four HPLC separations run sequentially on a large-volume irradiated sample are shown in Figure 4.5. We notice that the resolution of peak P and peak I is strongly dependent on the condition of the column. On a

Figure 4.3 Analytical HPLC traces of an aqueous HMT solution irradiated for different lengths of time:
(a) 30 minutes, (b) 60 minutes,
(c) 120 minutes, (d) 180 minutes.
For (a),(b) and (d), gradient elution was used, with eluant being 60% methanol in water at the time of sample injection and 64.4% methanol at the end of 20 minutes. Elution for the sample in (c) was run isocratically, with 60% methanol in water being the eluant. Absorbance of the effluent was monitored at 250 nm.

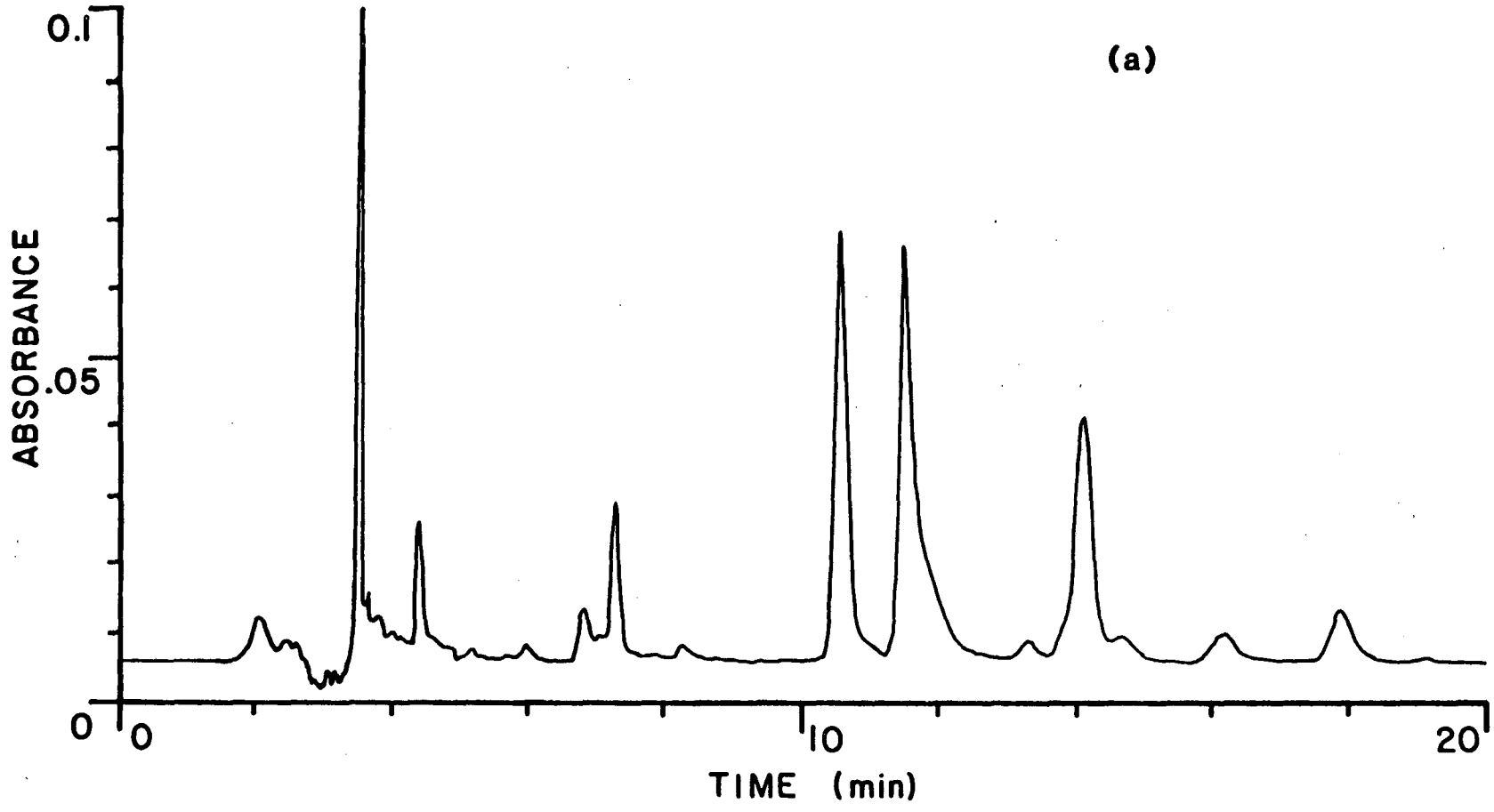
(a)
0.1
.05
0
ABSORBANCE
0
10
20
TIME (min)

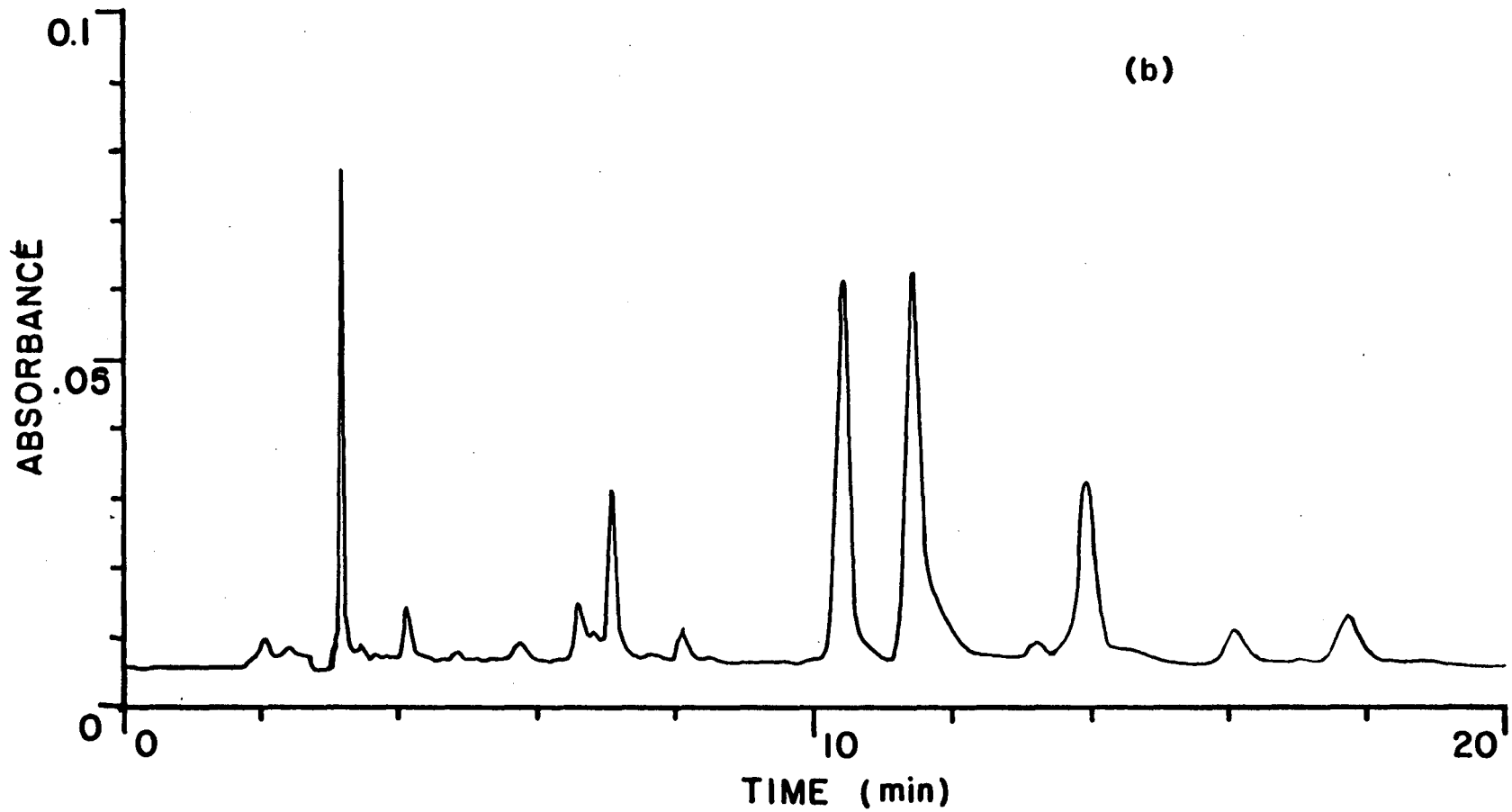
(b)
0.1
.05
0
ABSORBANCE
0
10
20
TIME (min)

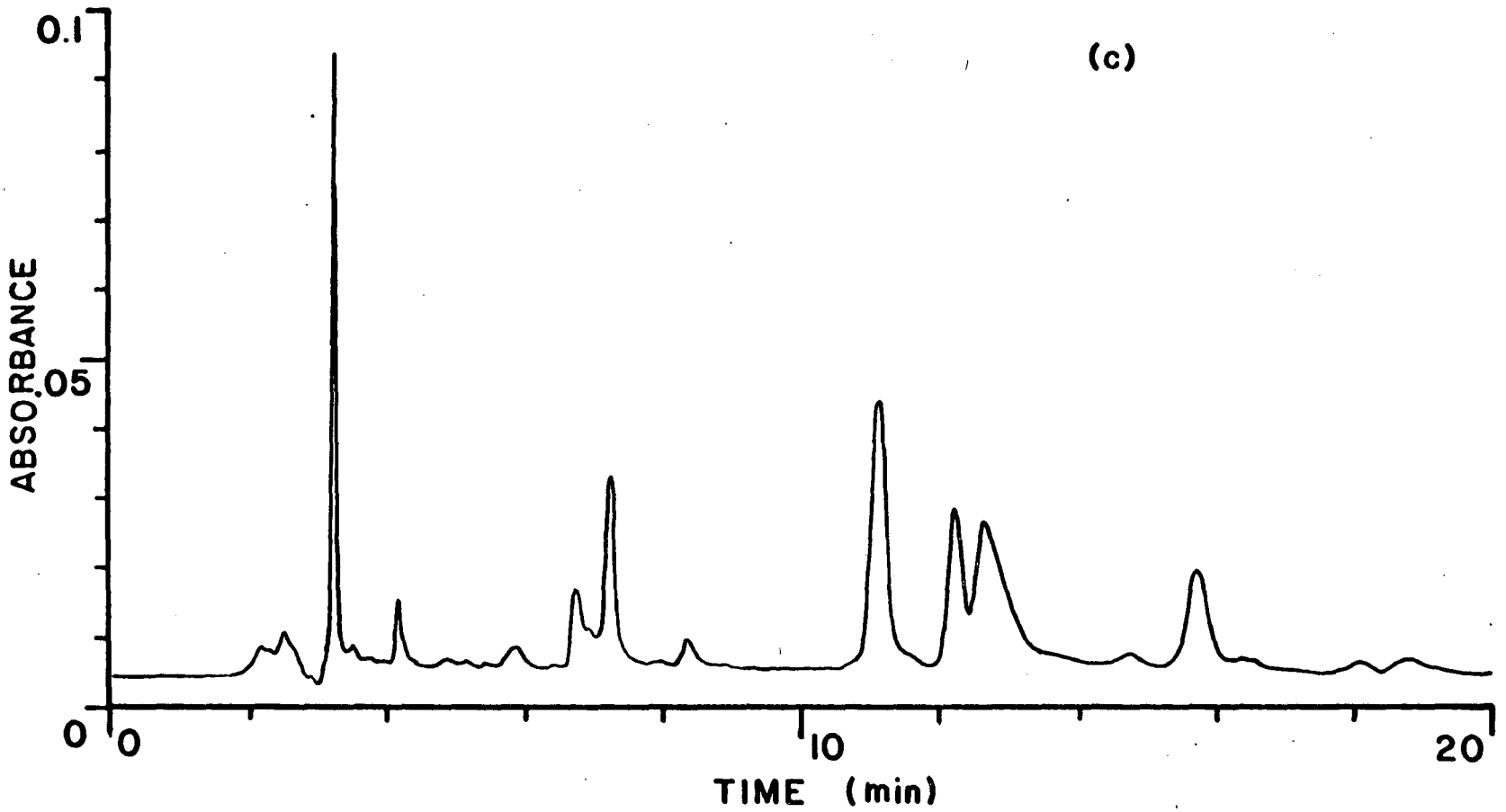
(c)
0.1
.05
0
ABSORBANCE
0
10
20
TIME (min)

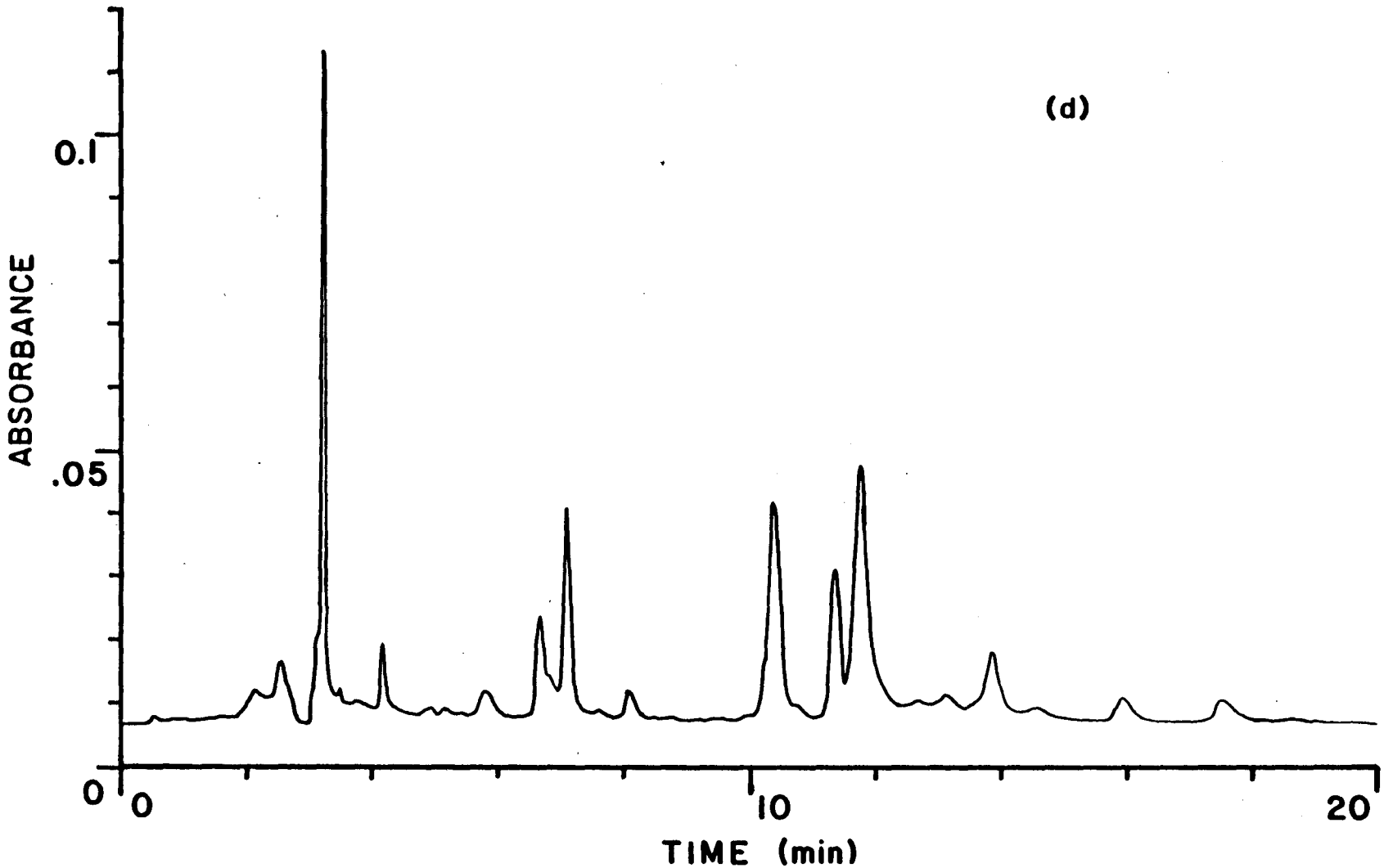
(d)
ABSORBANCE
0.1
.05
0
0
10
20
TIME (min)

Figure 4.4 A typical record of an HPLC separation of an irradiated aqueous HMT sample. Four major peaks are labelled. The dashed line is a record of the percentage of methanol in the eluting solvent as a function of elution time. The HMT solution was exposed to UV light for 30 minutes before being subjected to HPLC analysis.

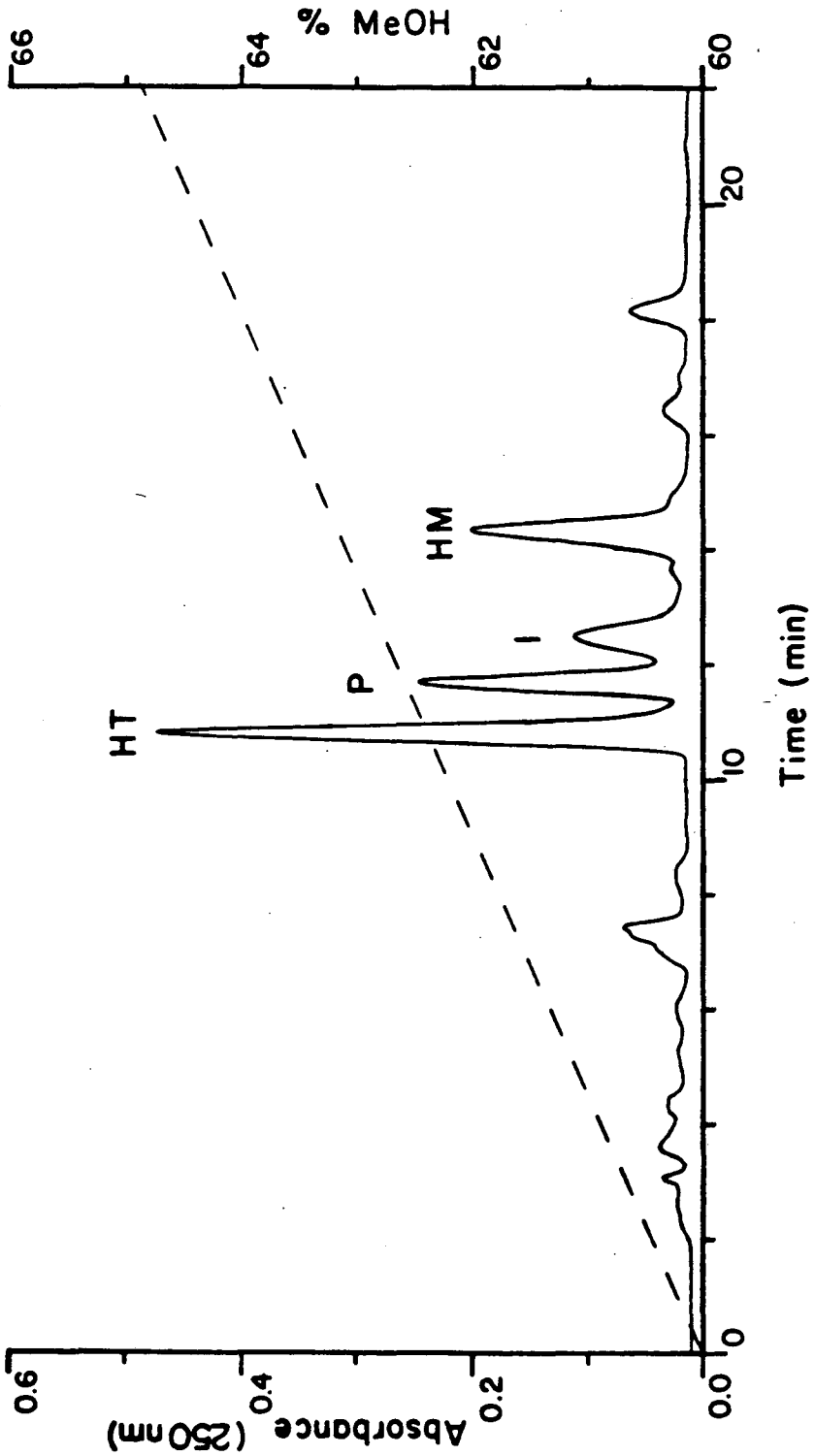
% MeOH
66
64
62
60
HT
P
I
HM
Time (min)
0
10
20
Absorbance (250 nm)
0.6
0.4
0.2
0.0

Figure 4.5 Portions of four HPLC separations run on a large-volume irradiated HMT solution. Trace (1) is the result of one aliquot of sample injected onto a clean column. Traces (2) and (3) are from two injections made immediately after trace (1) was completed. Resolution of peaks P and I is good in trace (1) but quickly deteriorates in (2) and (3). The column was washed with 20 mM phosphate buffer at pH 2.2 in conjunction with methanol immediately after trace (3). Another injection was made after the cleaning cycle and yielded trace (4) which shows excellent resolution of peaks P and I again. The dashed line is the gradient elution profile.

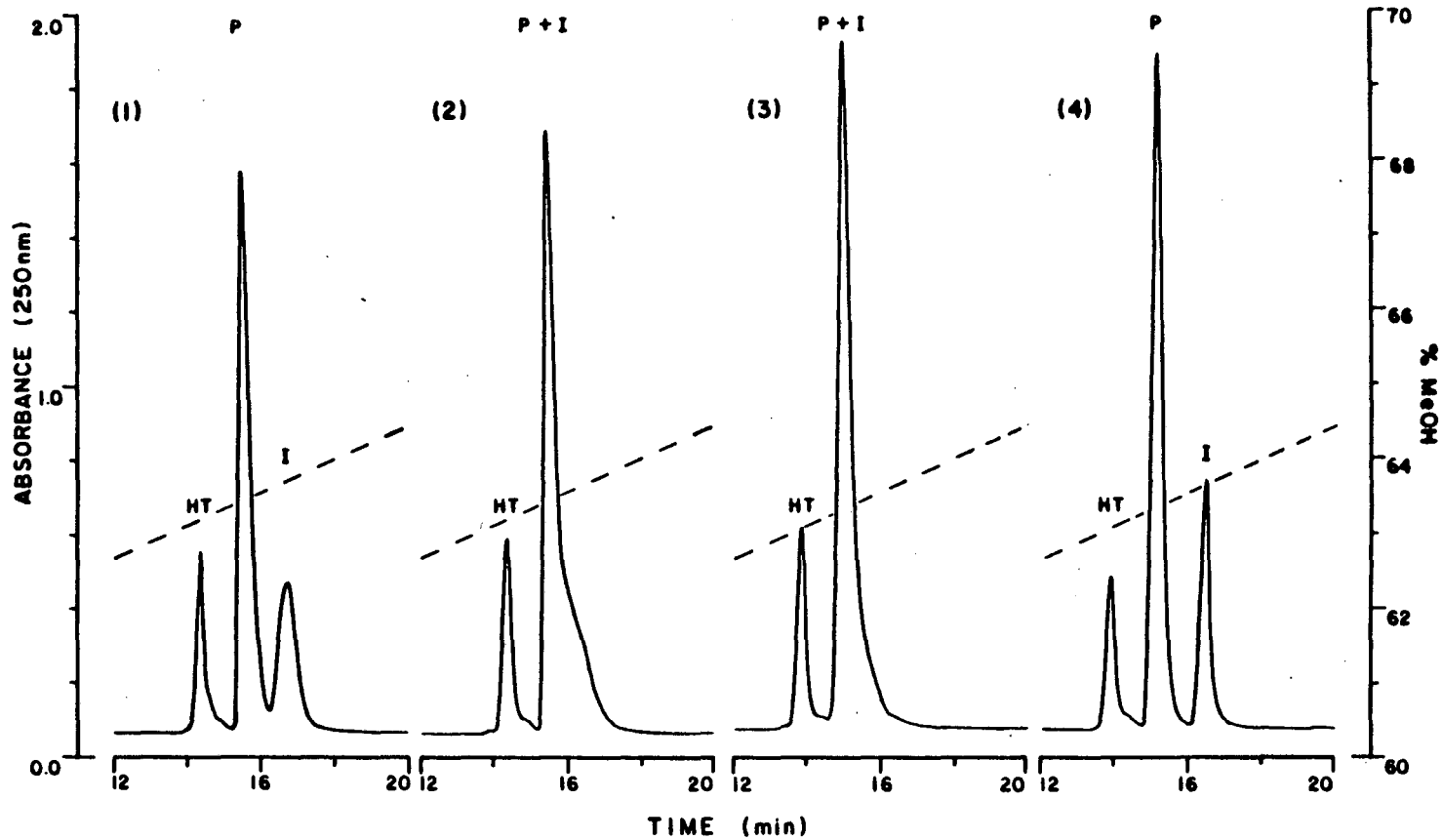
(1)
(2)
(3)
(4)
P
P + I
P + I
P
HT
I
ABSORBANCE (250nm)
2.0
1.0
0.0
% MeOH
70
68
66
64
62
60
12
16
20
TIME (min)

freshly cleaned column, the separation of the two peaks is quite good (Figure 4.5(1)). With each successive injection, however, the right hand peak merges more into peak P (Figure 4.5(2-3)). Rinsing the column with 20 mM phosphate buffer prior to injection caused peaks P and I to be once again resolved (Figure 4.5(4)). Thus, in order to achieve maximal resolution each time, a cleaning gradient cycle using a 20 mM phosphate buffer at pH 2.2 in conjunction with methanol was applied to the column before each injection.

B. UV Spectra

Since HMT itself contains aromatic chromophores which absorb strongly in the UV region and its photoproducts are likely to have similar chromophores, a facile way to get useful information is to examine the UV spectra of the compounds. The UV spectra for the peaks marked HT, P, I, and HM in Figure 4.4 are displayed in Figures 4.6-4.9, respectively In the HPLC trace, P elutes where HMT normally does and comparison of the spectrum of P with a spectrum of pure HMT (Figure 4.10) confirms that P is indeed the parent compound. Shown in Figure 4.11 are the structure and spectrum of a model compound, dihydro-TMP, which has its furan ring hydrogenated, leaving an intact coumarin chromophore. One notices that the spectral band (located between 330 and 340 nm) characteristic of a furocoumarin with a saturated furan ring is prominent in the UV spectrum of HT but entirely absent in the spectrum of HM. The UV spectrum for another

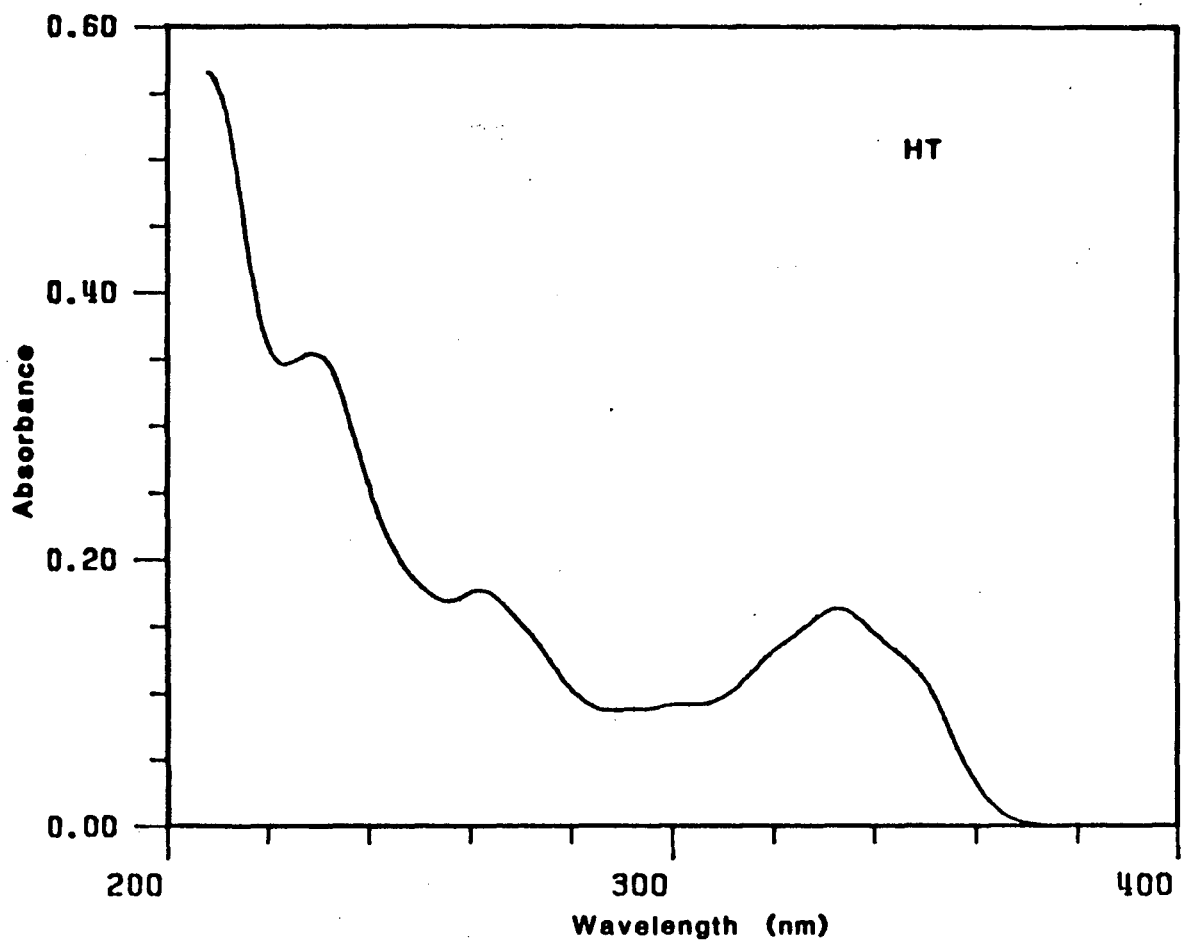

Figure 4.6 UV absorption spectrum of compound HT isolated from irradiated HMT solution. Solvent is 60% methanol in water (by volume).

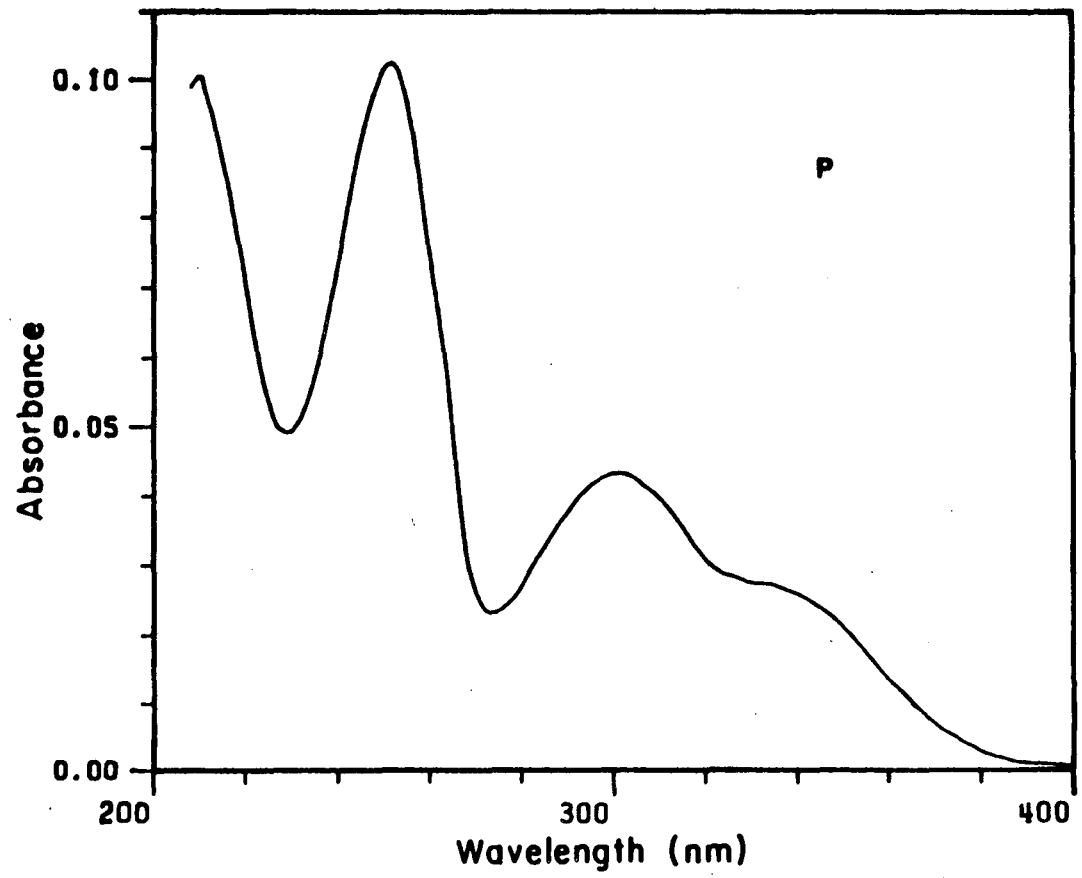

Figure 4.7 UV spectrum of compound P isolated from irradiated sample of HMT. Solvent is 60% methanol in water (by volume).

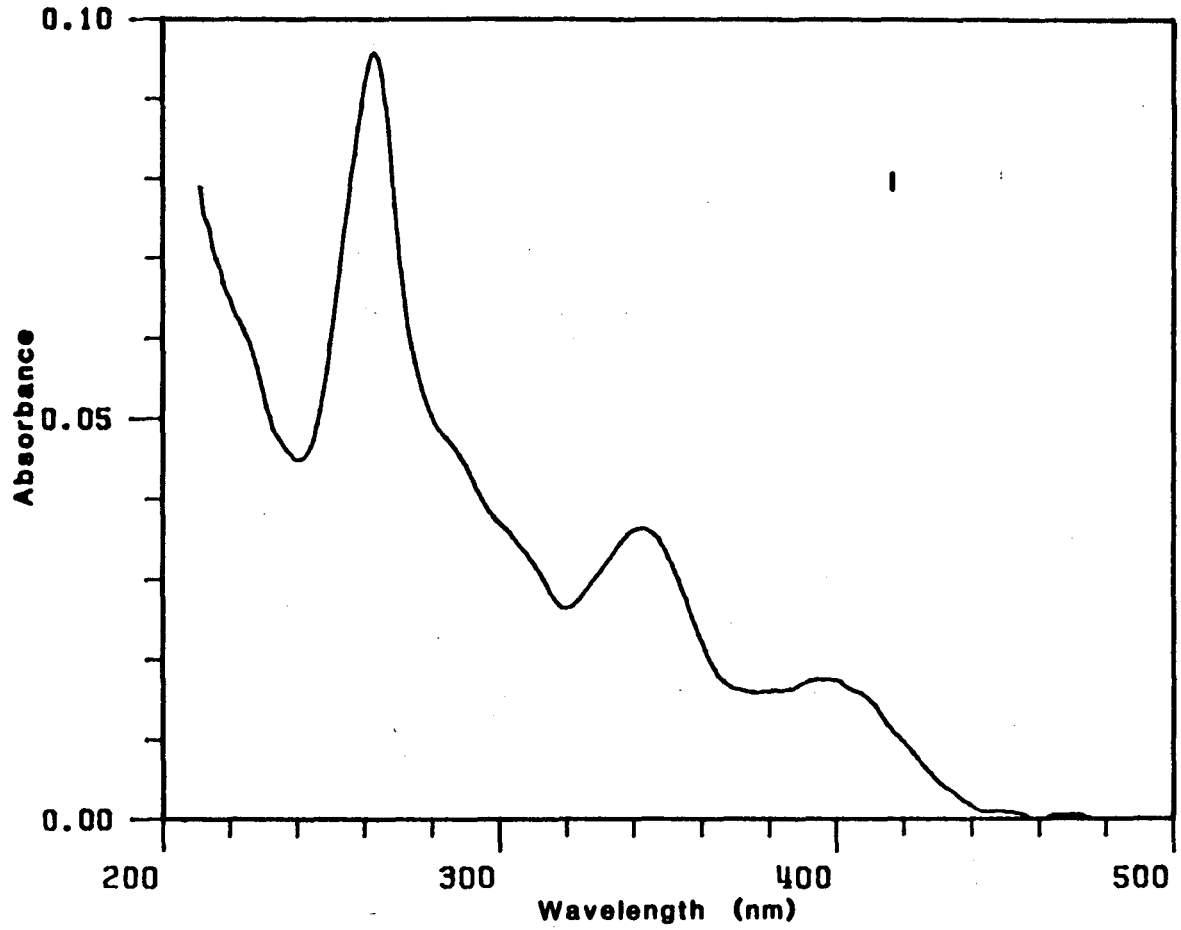

Figure 4.8 UV absorption spectrum of compound I isolated from irradiated HMT solution. Solvent is 60% by volume methanol in water.

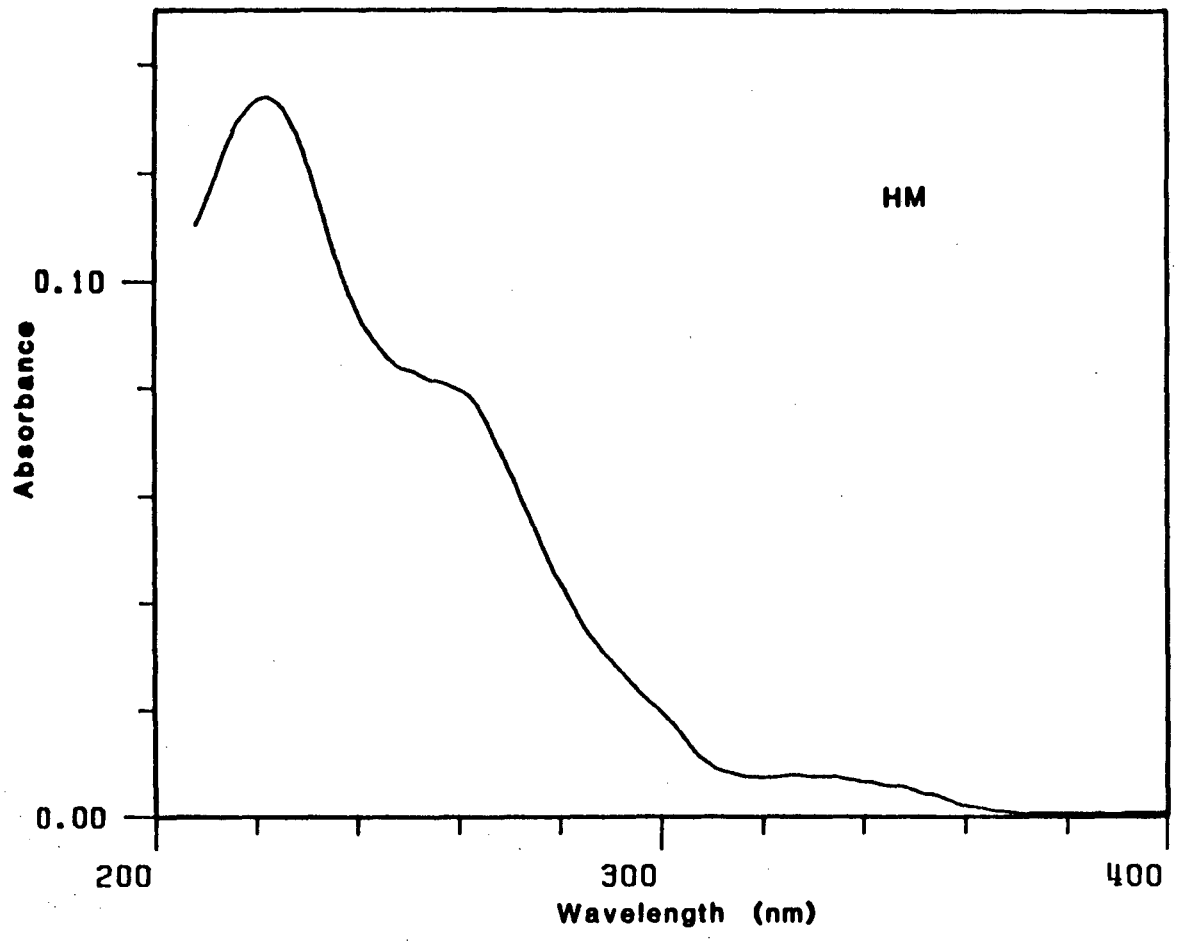

Figure 4.9 UV spectrum of compound HM isolated from irradiated HMT solution. Solvent is 60% by volume methanol in water.

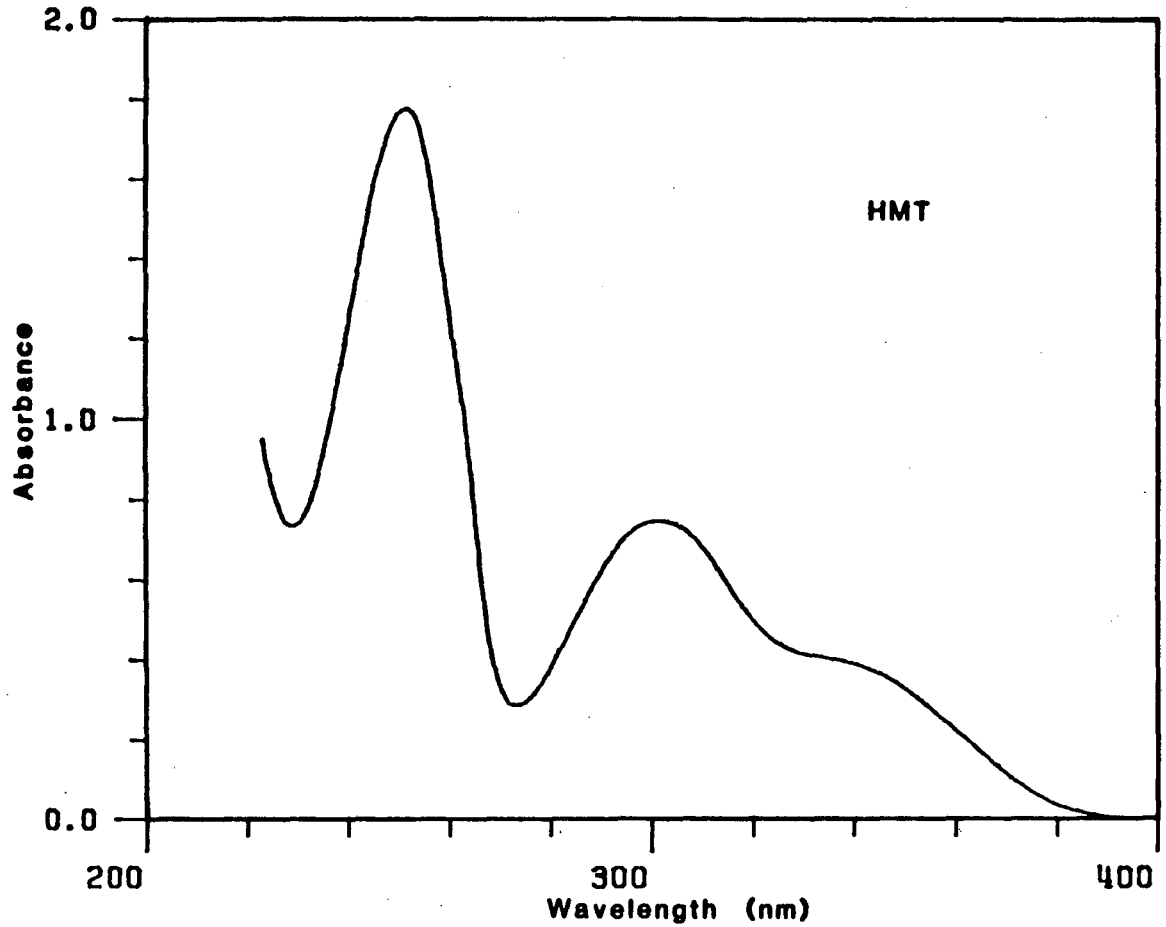

Figure 4.10 UV absorption spectrum of HMT dissolved in 60% by volume methanol in water.

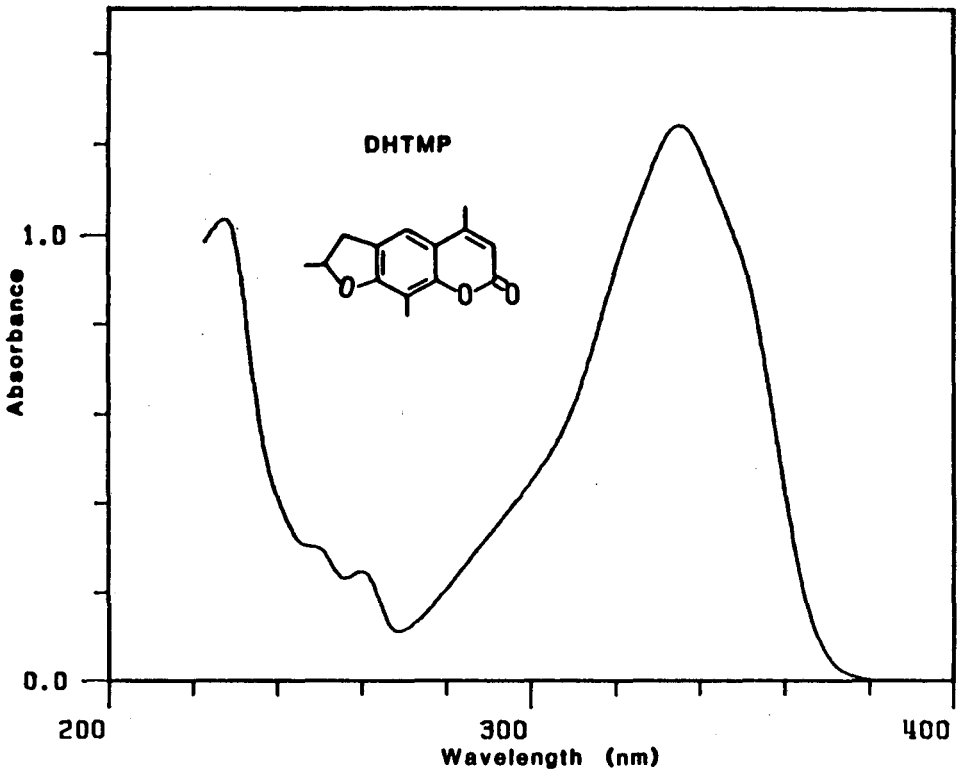

Figure 4.11 UV absorption spectrum of dihydro-TMP in a solvent of 60% by volume methanol in water. The structure of DHTMP is shown.

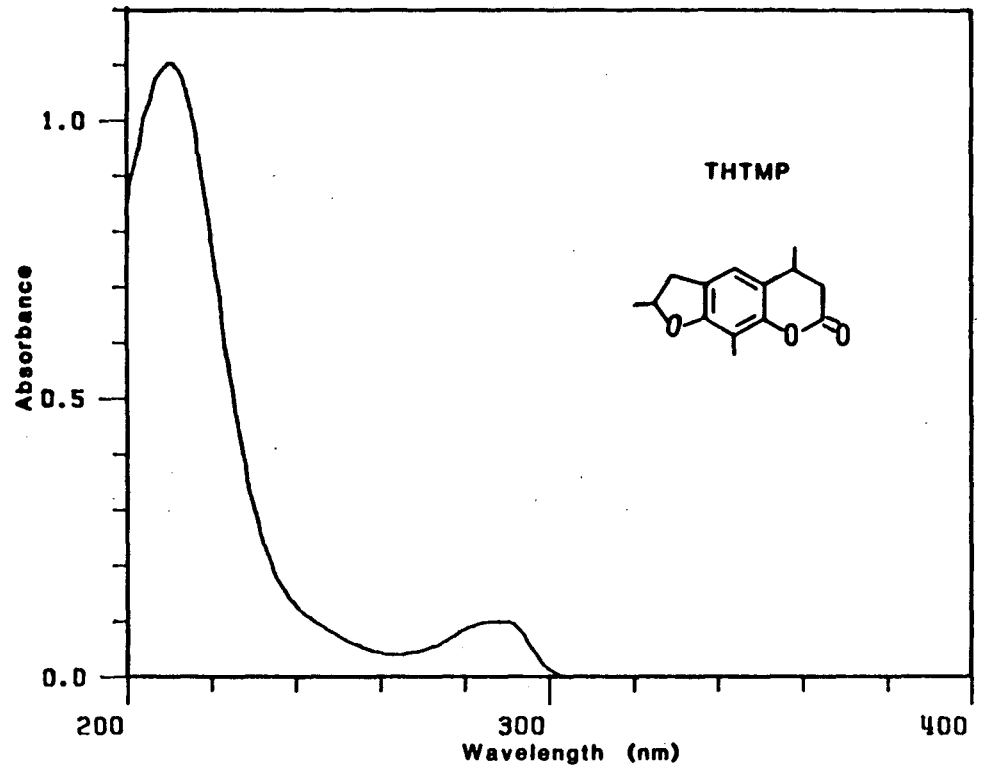

Figure 4.12 UV absorption spectrum of tetrahydro-TMP in a solvent consisting of 60% by volume methanol in water. The structure of THTMP is shown.

model compound, tetrahydro-TMP (THTMP), in which both the furan ring and the pyrone ring of TMP have been reduced, is shown in Figure 4.12, along with the structural formula of THTMP.

A spectral property of compound I is also worthy of note. While the parent compound and the other photoproducts all are colorless, compound I is yellow both in the solid form and in solution. Two possible explanations present themelves. Musajo (Musajo, 1963) has found that yellow products separable by thin layer and paper chromatography were generated as a result of photooxidation of psoralens in the presence of flavin mononucleotide (FMN) and flavin adenine dinucleotide (FAD). While these products were found to be chromatographically distinct, their structures were not determined, owing to their lack of stability. Thus it is possible that the yellow species generated in the present study have their origin in photooxidation as well. An alternative proposal is a mechanism by which the HMT molecule is photochemically rearranged in such a way as to yield a new chromophore whose absorption spectrum extends into the visible region. With the aid of the NMR and mass spectral results, we can choose between the different explanations.

C. Pyrolysis Experiments

In attempting to measure the melting points of compounds HT and HM, it was found that these compounds appear to undergo structural changes in the solid state between 200 and 250 °C before liquefying.

Indeed, no sharp melting point could be determined for either compound. Samples of HT and HM were sealed in glass capillary tubes and pyrolyzed using either the melting point apparatus or a sand bath. When the pyrolyzed samples were taken up into solution and analyzed by HPLC, chromatographic profiles entirely different from those of HT and HM were obtained. In fact, after pyrolysis, both HT and HM yielded primarily a compound which had an HPLC retention time and a UV spectrum identical to that of the parent psoralen, HMT (Figures 4.13 and 4.14). These results clearly indicate that HMT is photochemically converted to HT and HM, which can revert to HMT via thermochemical pathways. Such behavior is well known in [2+2] cycloaddition reactions. One may thus infer that HT and HM are two different dimers generated by the photoaddition of two HMT molecules. The HPLC trace of HT prior to pyrolysis shows that even at room temperature, some thermal reversal can take place to convert HT to HMT (Figure 4.13). The same is not true of HM. HT is thus more thermally labile than HM.

D. Mass Spectral Results

Chemical ionization mass spectra for HMT, HT and HM are shown in Figures 4.15-4.17. Since methane was used as the reagent gas in these CIMS runs, one expects to see an $(M+H)^+$ peak (usually the base peak) as well as $(M+C_2H_5)^+$. In the HMT CI mass spectrum, one finds the base peak to have an m/z of 259, which corresponds to the expected

Figure 4.13 HPLC traces showing a sample of compound HT (a) before pyrolysis and (b) after pyrolysis. Compound HT degrades partially to HMT even at room temperature, as can be seen in trace (a). After pyrolysis, HT is converted to HMT almost quantitatively. Gradient elution used in both HPLC runs. Conditions are the same as in previous traces.

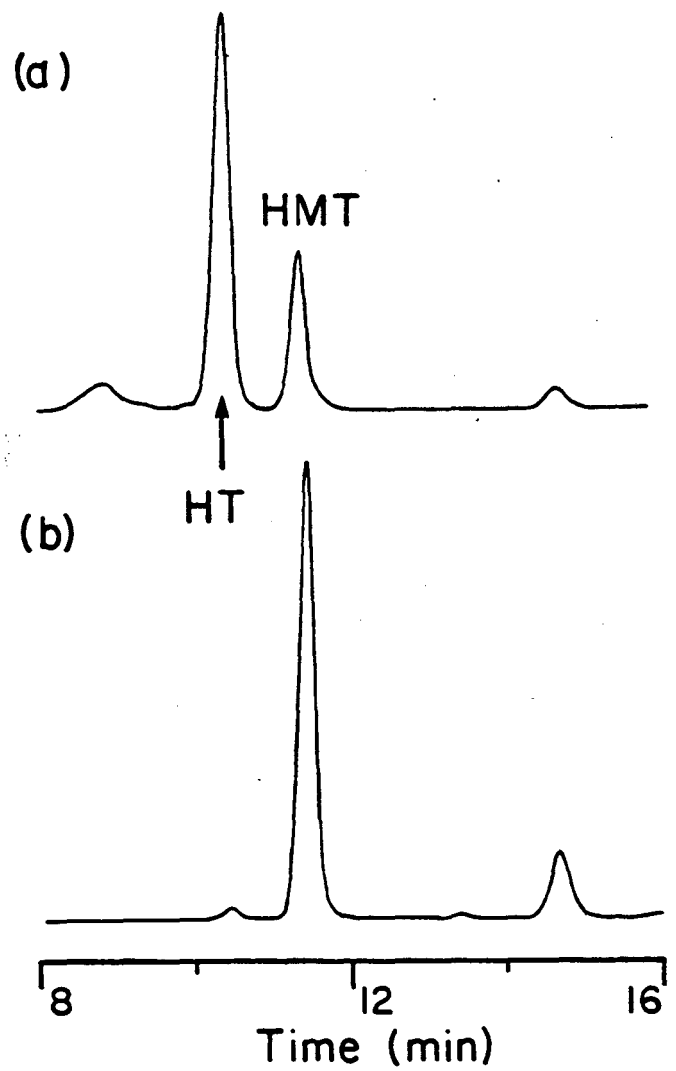

Figure 4.14 HPLC traces showing a sample of compound HM (a) before pyrolysis and (b) after pyrolysis. HM is more stable than HT and does not degrade significantly at room temperature as evidenced by trace (a). After pyrolysis, HM is converted into HMT almost quantitatively. Experimental conditions are the same as those for previous HPLC analyses.

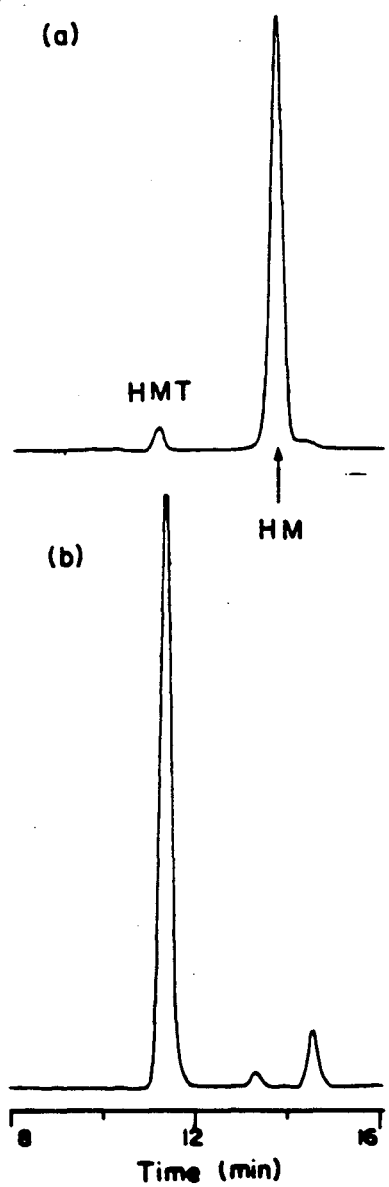

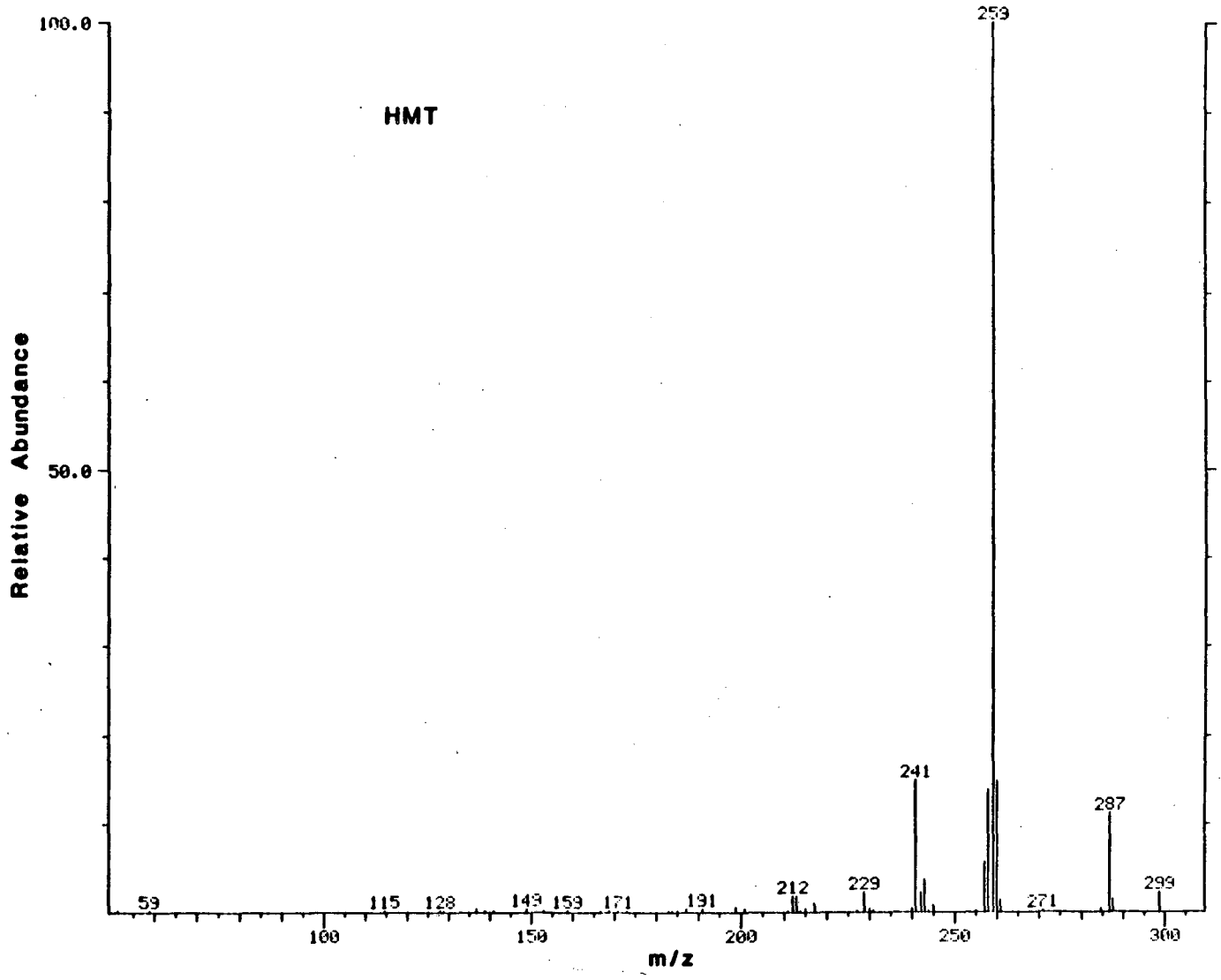

Figure 4.15 Chemical ionization mass spectrum of HMT. CH_4 used as ionizing reagent gas.

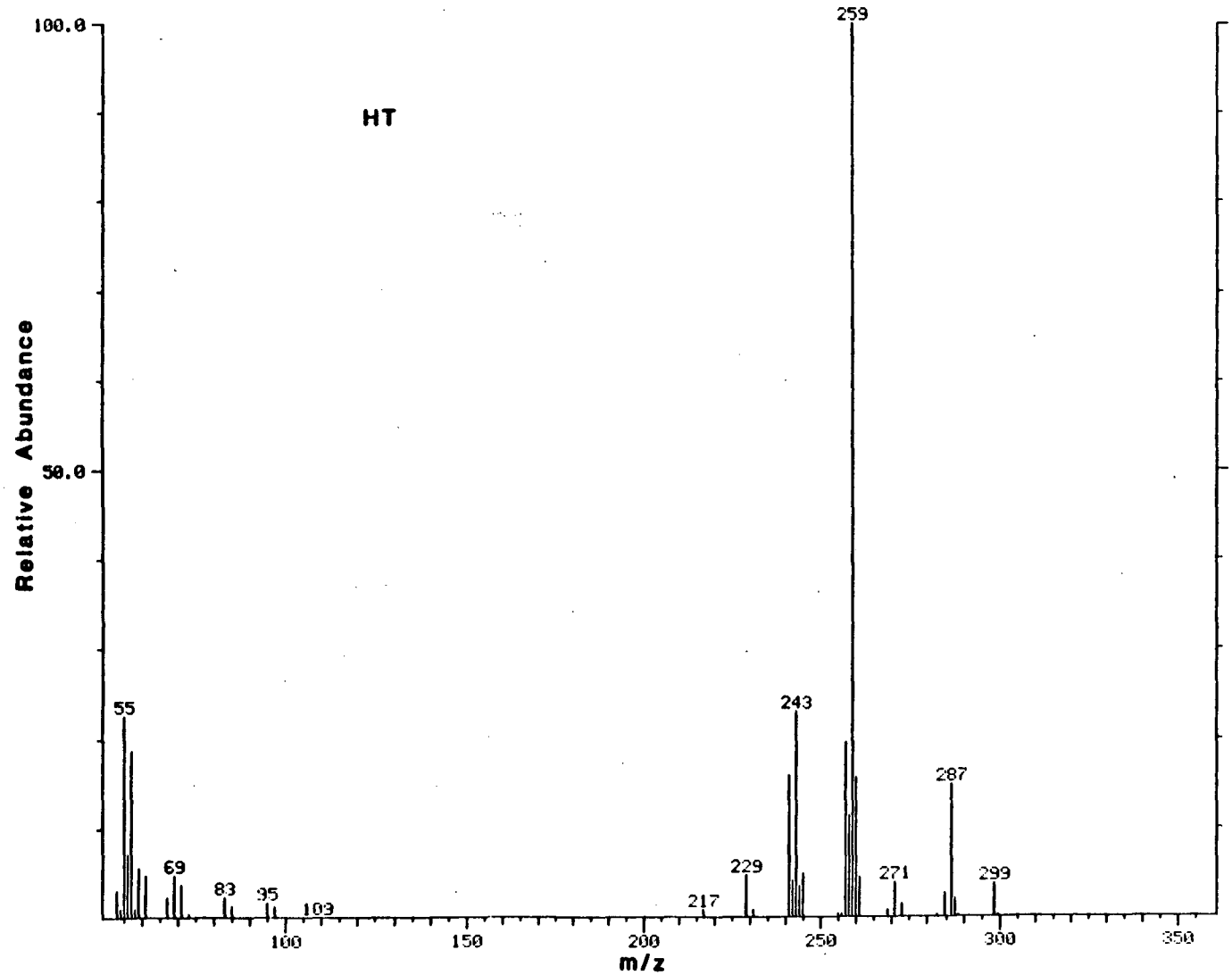

Figure 4.16 Chemical ionization mass spectrum of HT. CH_4 used as ionizing reagent gas.

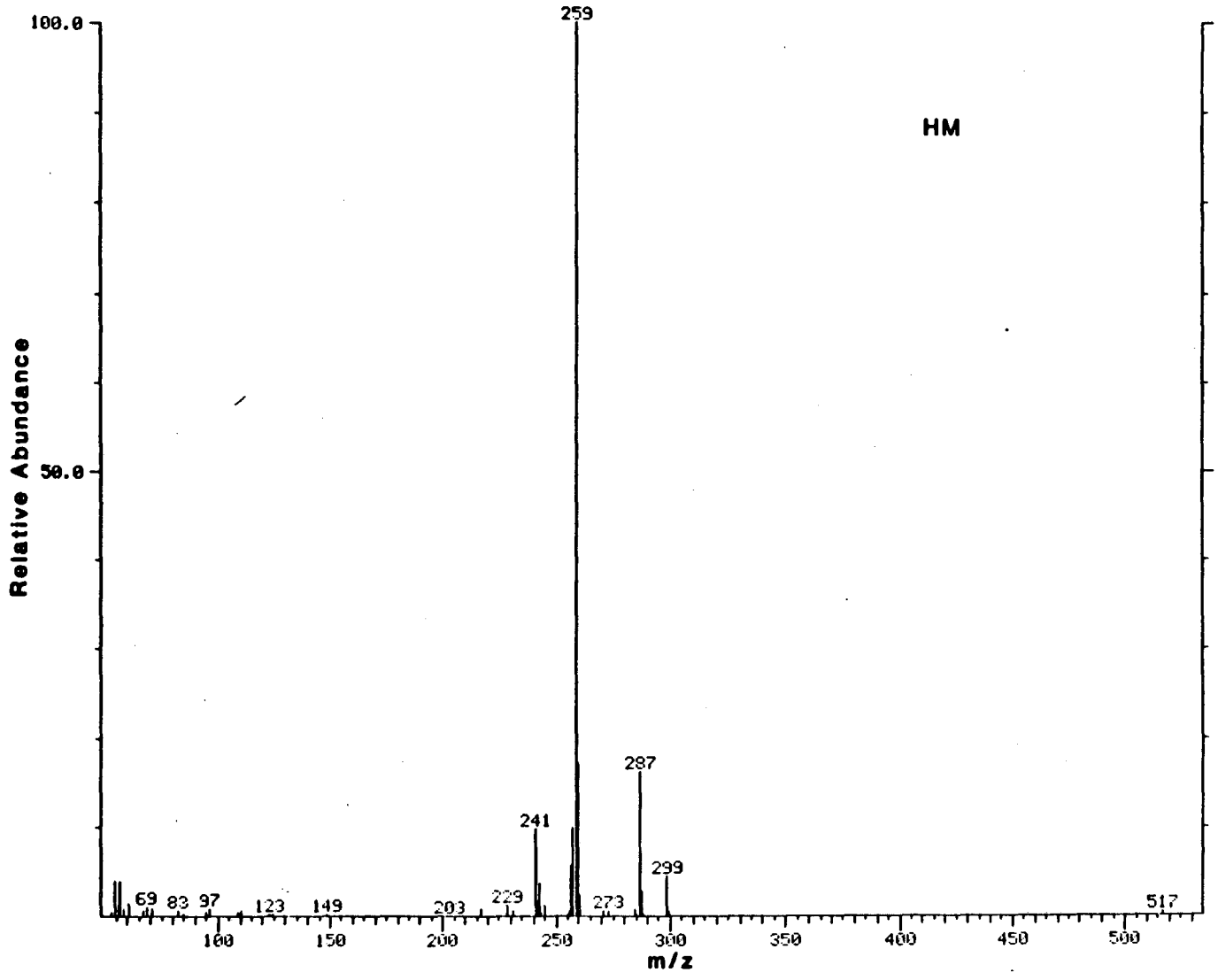

Figure 4.17 Chemical ionization mass spectrum of HM. CH_4 used as ionizing reagent gas.

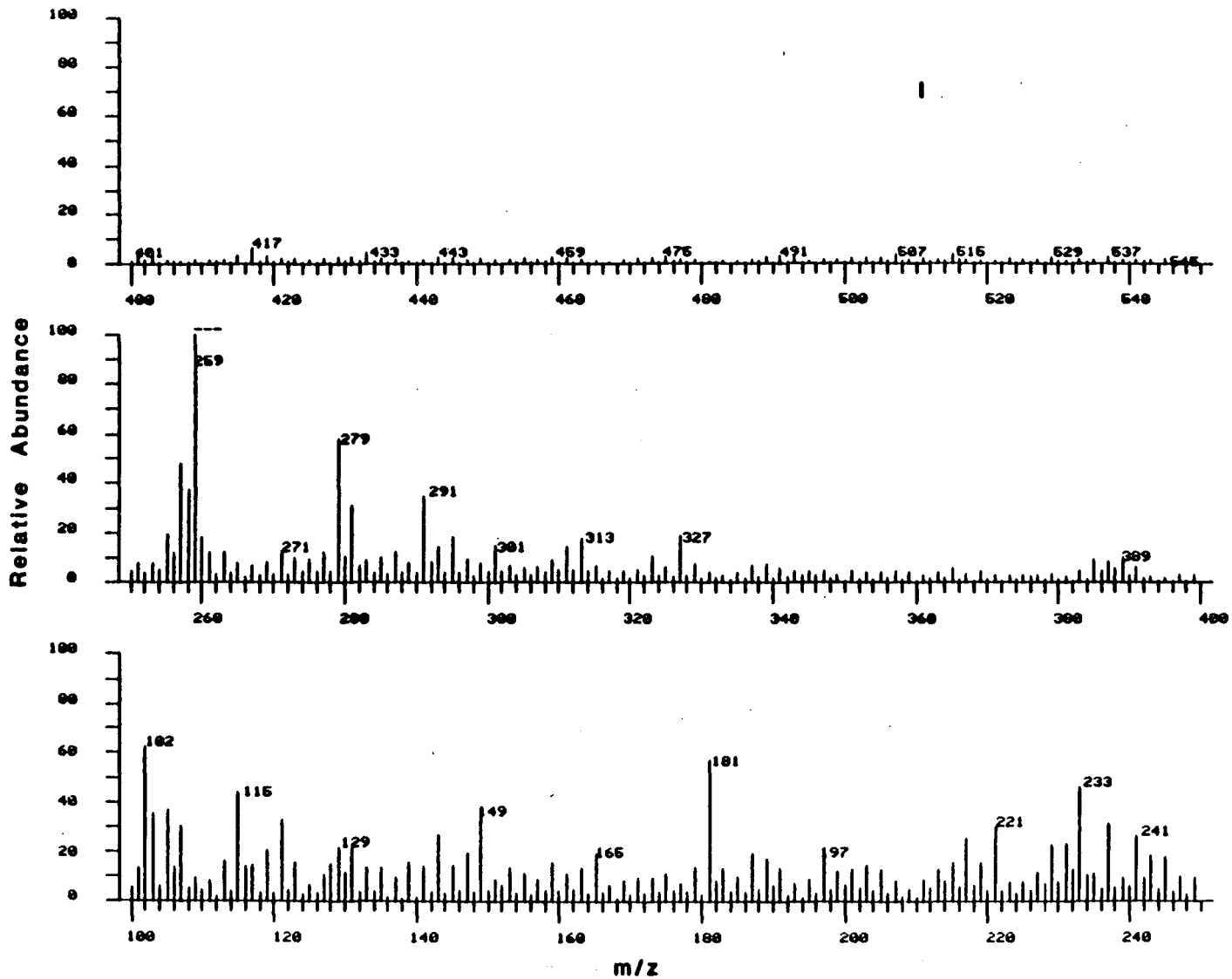

Figure 4.18 Fast atom bombardment mass spectrum of I. Xenon used in neutral beam.

$(M+H)^+$ for HMT, which has a molecular weight of 258. The CI mass spectrum of HM is largely identical to that of HMT except for the existence of a peak at m/z of 517, which can be assigned as the $(M+H)^+$ peak for an HMT dimer. This observation confirms the inference made from the pyrolysis results. The fact that the $(M+H)^+$ is not the base peak for HM as expected in conventional CIMS can be easily understood. In CIMS, while the method for ionizing the sample molecules is relatively gentle and tends not to disrupt molecular structure, the sample is still volatilized into the chemical ionization chamber by raising the temperature of the probe on which the sample is mounted. Since the thermochemical pathway for reversion to HMT is available to HM, one expects that HM would thermally decompose to HMT as the sample probe was rapidly heated. This accounts for the fact that only a small amount of the dimer is seen while the main body of the HM mass spectrum resembles that of HMT.

Comparing the CI mass spectra of HT and HMT shows the two to be essentially identical. No dimer peak is visible at all. In view of the foregoing discussion on the HM mass spectrum and recalling the pyrolysis experiments where it was shown that HT is more thermally labile than HM, one sees that the mass spectral results are consistent with HT being a photodimer of HMT.

Fast atom bombardment mass spectrometry (FABMS) was used to study compound I. For FABMS, the sample is suspended in an inert, high boiling solvent matrix such as one of the glymes or a simple

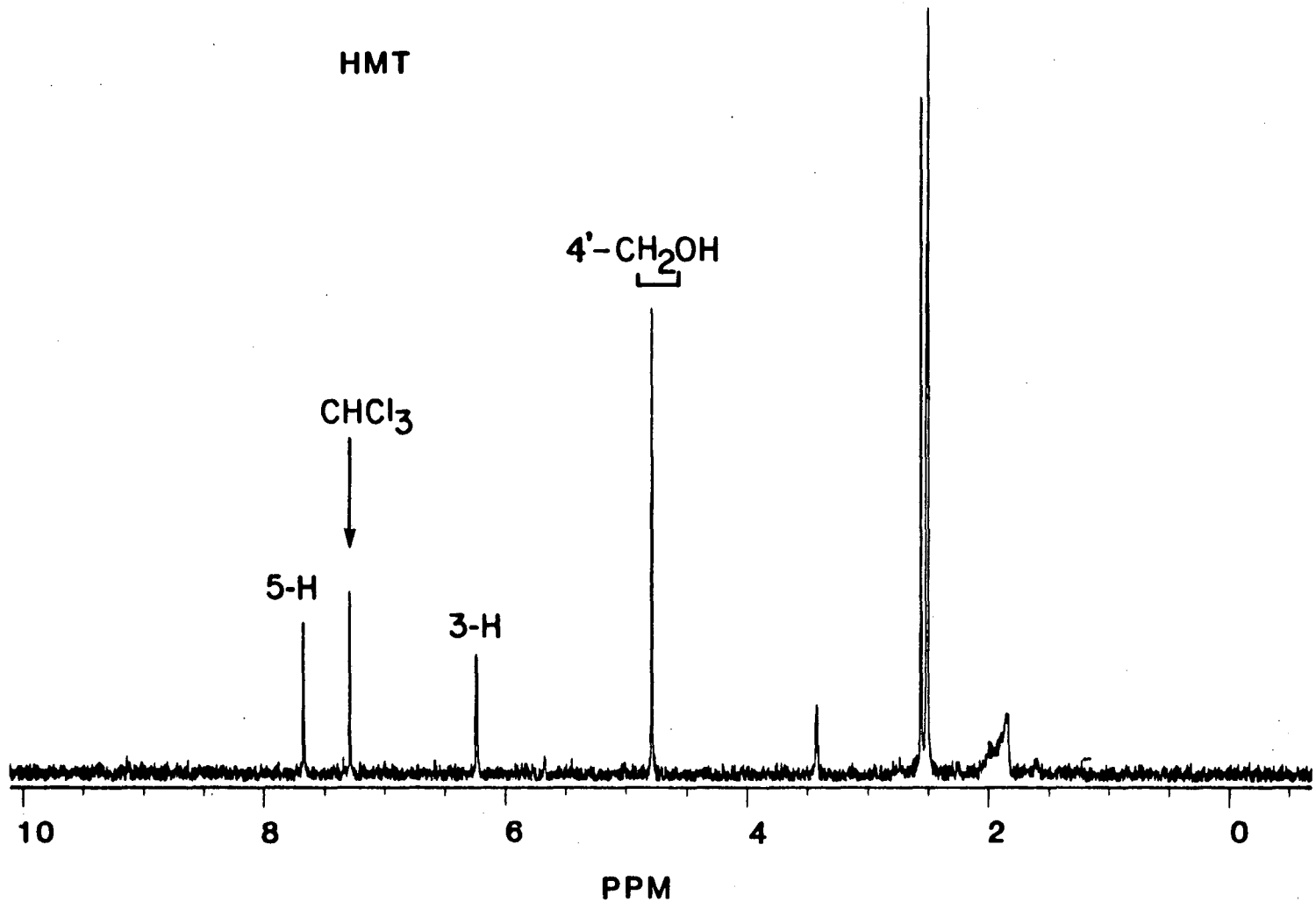

Figure 4.19 Proton NMR spectrum of HMT in $CDCl_3$.

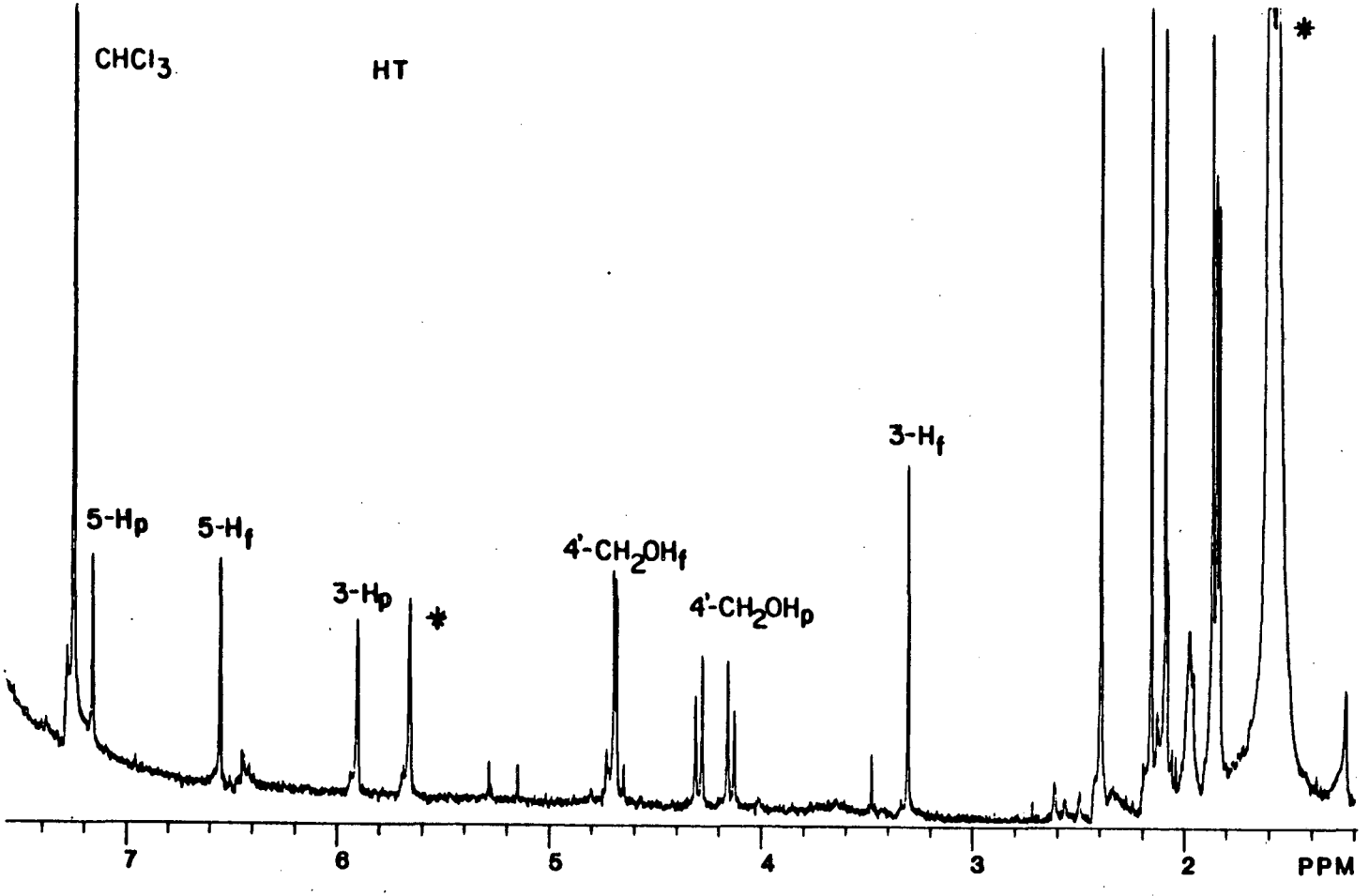

Figure 4.20 Proton NMR spectrum of compound HT in $CDCl_3$.
* marks impurities in the solvent.

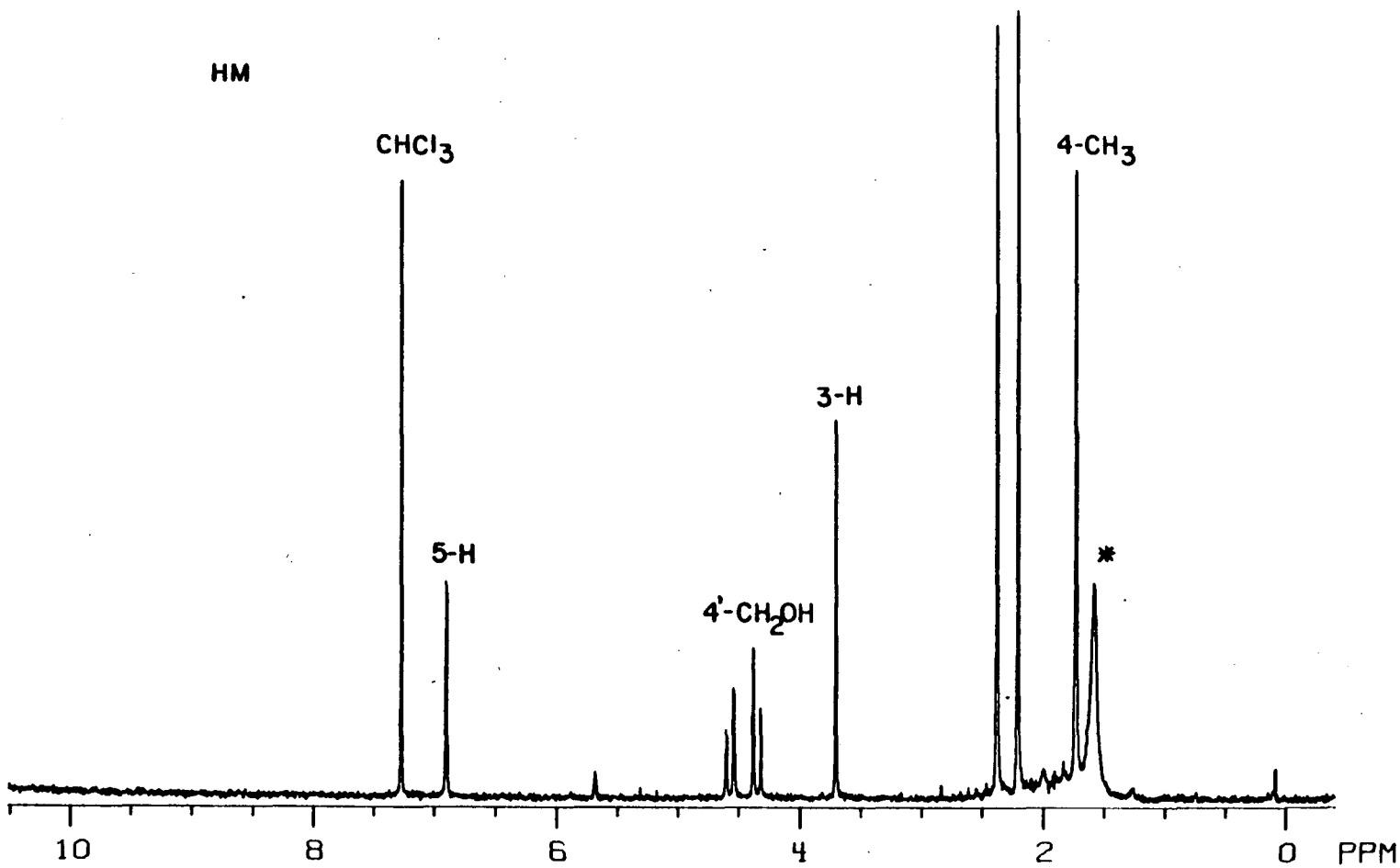

Figure 4.21 Proton NMR spectrum of compound HM in $CDCl_3$.
* marks impurities in the solvent.

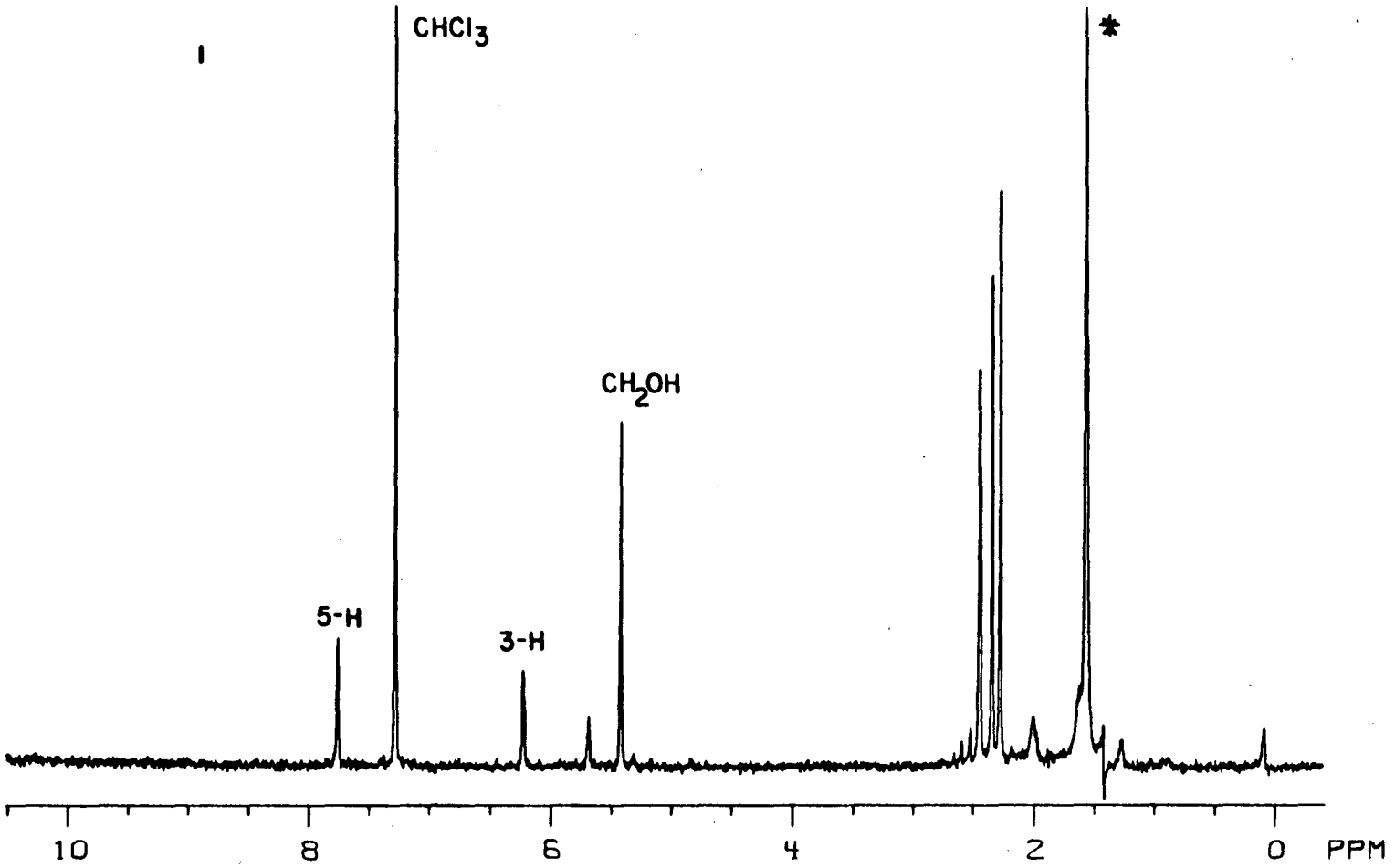

Figure 4.22 Proton NMR spectrum of compound I in $CDCl_3$.
* marks the impurities in the solvent.

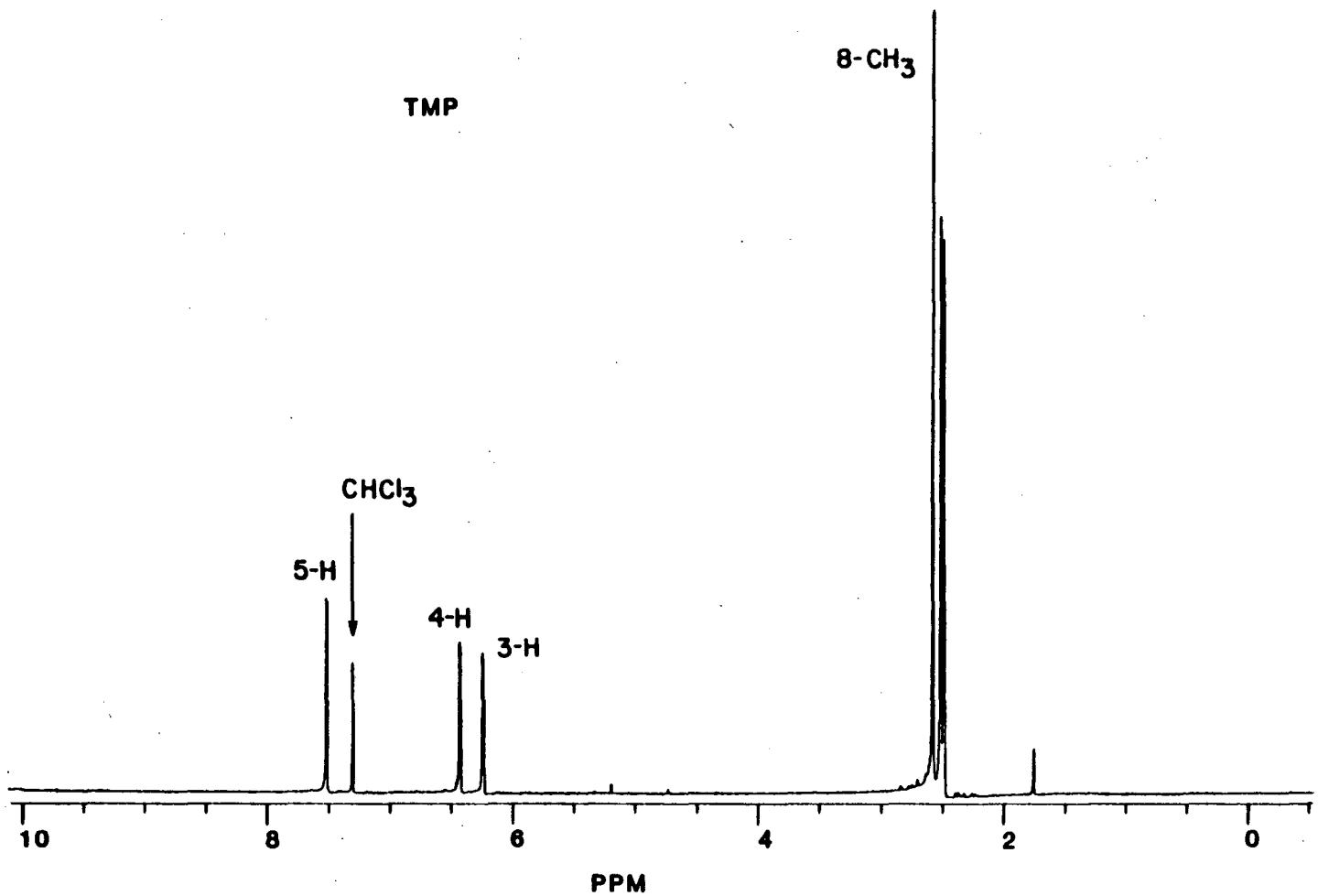

Figure 4.23 Proton NMR spectrum of TMP in $CDCl_3$.

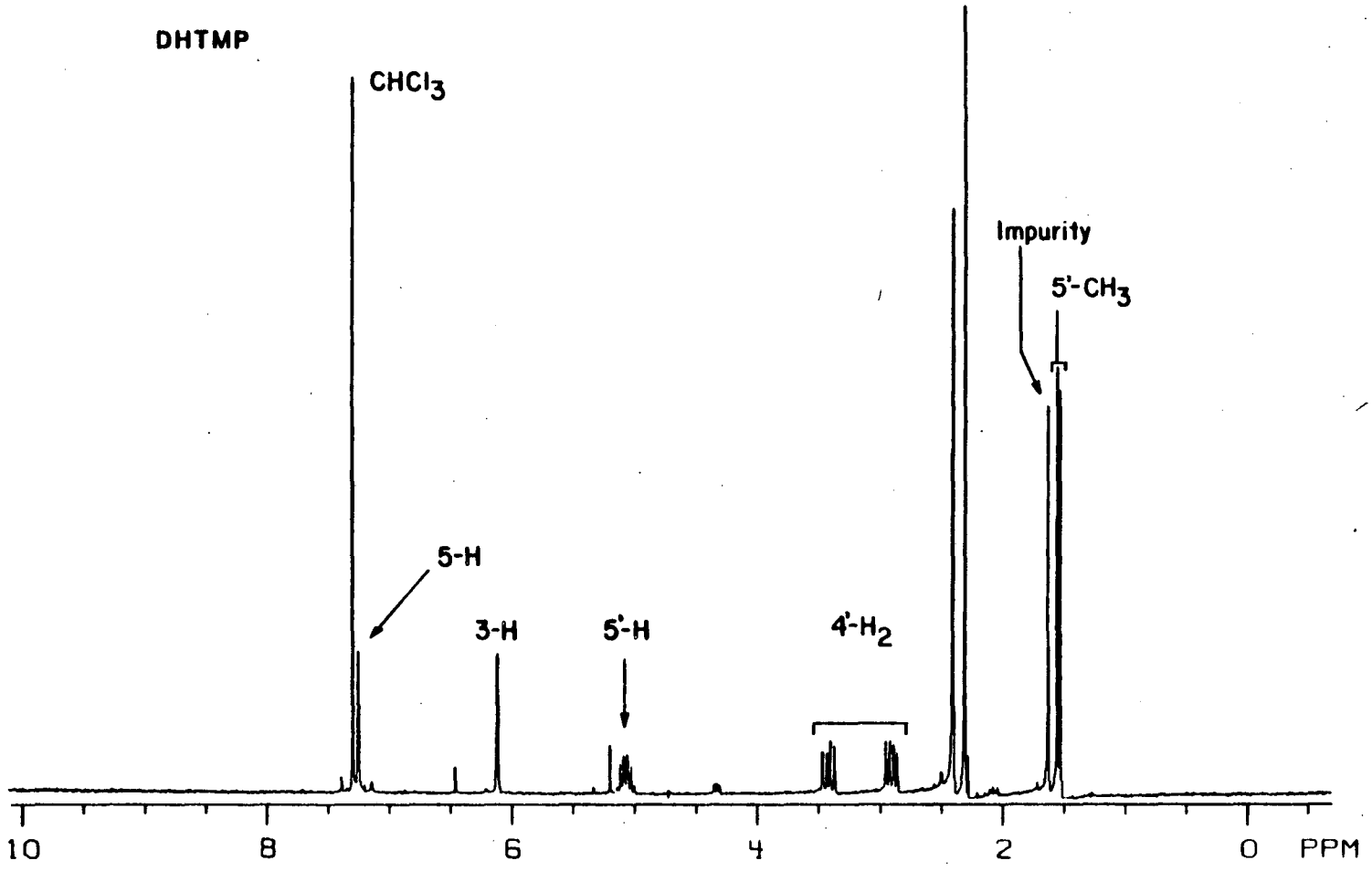

Figure 4.24 Proton NMR spectrum of DHTMP (dihydro-TMP) in $CDCl_3$.

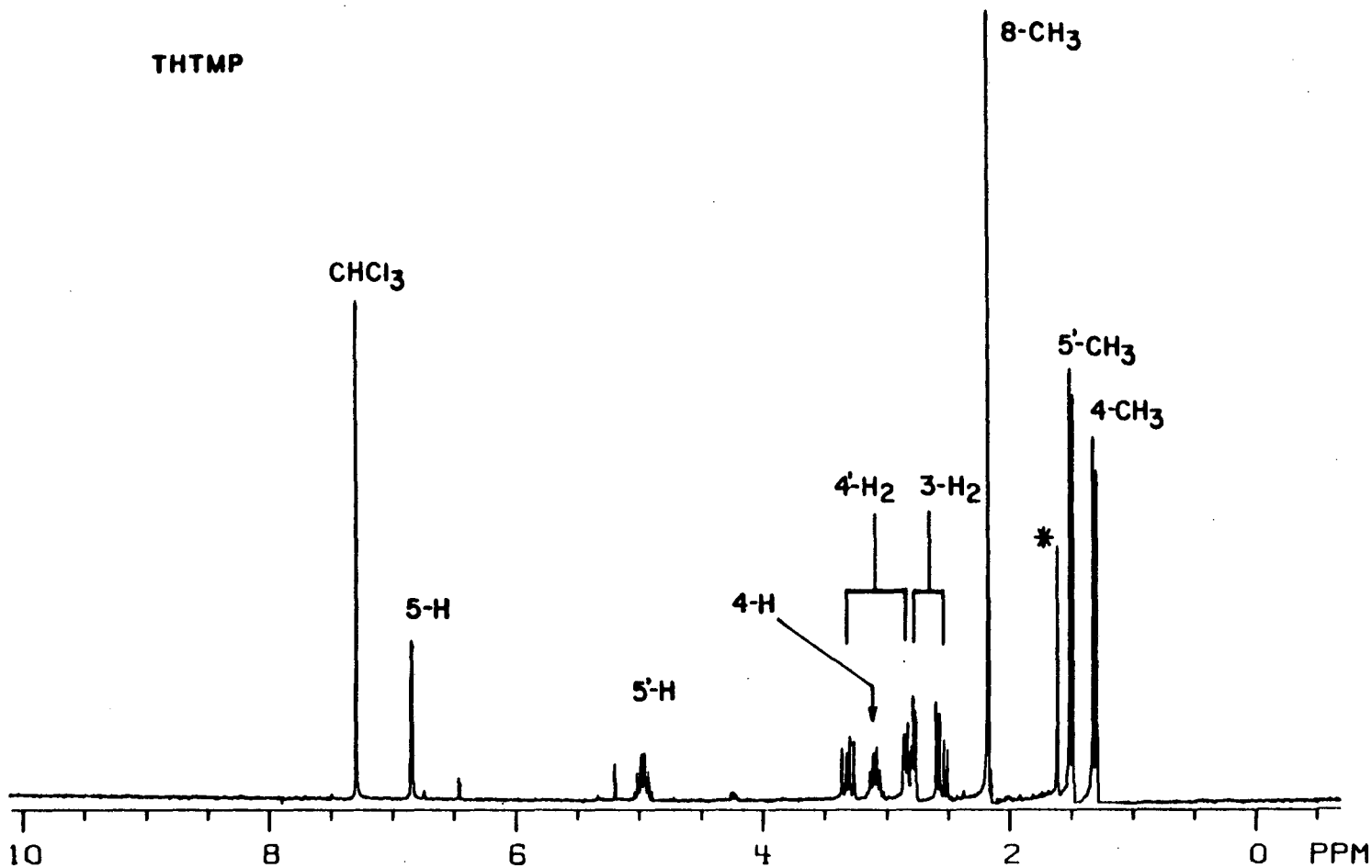

Figure 4.25 Proton NMR spectrum of THTMP (tetrahydro-TMP) in $CDCl_3$. * marks impurity in the solvent.

polyalcohol. A beam of heavy atoms is then directed onto the sample matrix. The fast neutral heavy atoms (xenon, in the present case) serve as a gentle ionizing source. In a FAB mass spectrum the base peak is most often an $(M+H)^+$ peak. Examining the FAB mass spectrum of I displayed in Figure 4.18, one sees that there is an overwhelming abundance of a species with m/z at 259. This means that the compound I has a molecular weight of 258, which is identical to the molecular weight of HMT. Compound I must be an isomer of HMT.

E. NMR Spectral Information

The ^{1}H-NMR spectra of HMT, the photoproducts and some model compounds are shown in Figures 4.19 through 4.25. The NMR spectra of HT and HM are completely consistent with their being photodimers of HMT. A detailed analysis of the spectra will be given in the Discussion. The spectrum of I exhibits precisely the same number of resonances as HMT. The HMT spectrum consists of all singlets. No splittings of any type are observed in the spectrum for I. The only differences between the spectra of HMT and I are differences in chemical shift. This is also in agreement with the previous assignment of I as a photoisomer of HMT.

In the photodimerization of HMT, a number of different products are possible. In order to determine the stereochemistry of HT, NOE experiments were performed. The spectra comprising the NOE experiment are shown in Figures 4.26a through 4.26f.

Figure 4.26 Six NOE difference spectra of compound HT in $CDCl_3$. Experiments were performed using the same sample as the one used to obtain the spectrum shown in Figure 4.20. For each of the spectra (a) - (f) a different methyl group in HT was irradiated. There are six methyl groups in the HT molecule. Only two of the six methyl groups are potentially capable of effecting NOE transfer to the 3-H on the cyclobutane ring. In a difference NOE spectrum a large negative peak is observed at the position at which the irradiated group normally resonates. Positive NOE effects are seen as positive peaks in the difference spectrum. Owing to the low concentration of the sample, solvent impurity peaks are large, relatively. Subtracting these large peaks invariably leave small residuals in the difference NOE spectrum. The peak at the extreme left and the peak at the extreme right are both the result of imperfect subtractions. In each spectrum, the arrow marks the position at which the 3-H on the cyclobutane ring of HT normally resonates.

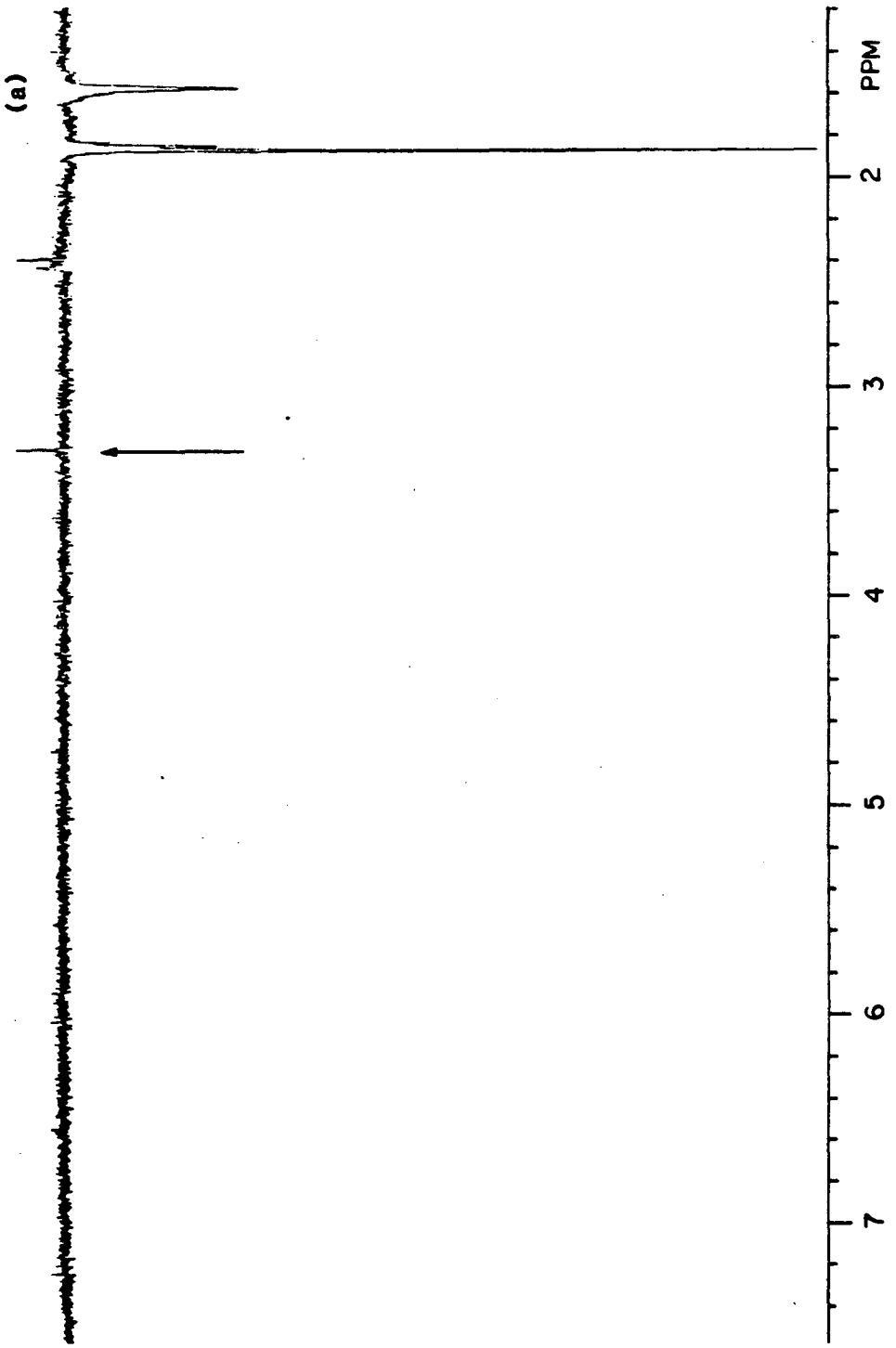
(a)
PPM
2
3
4
5
6
7

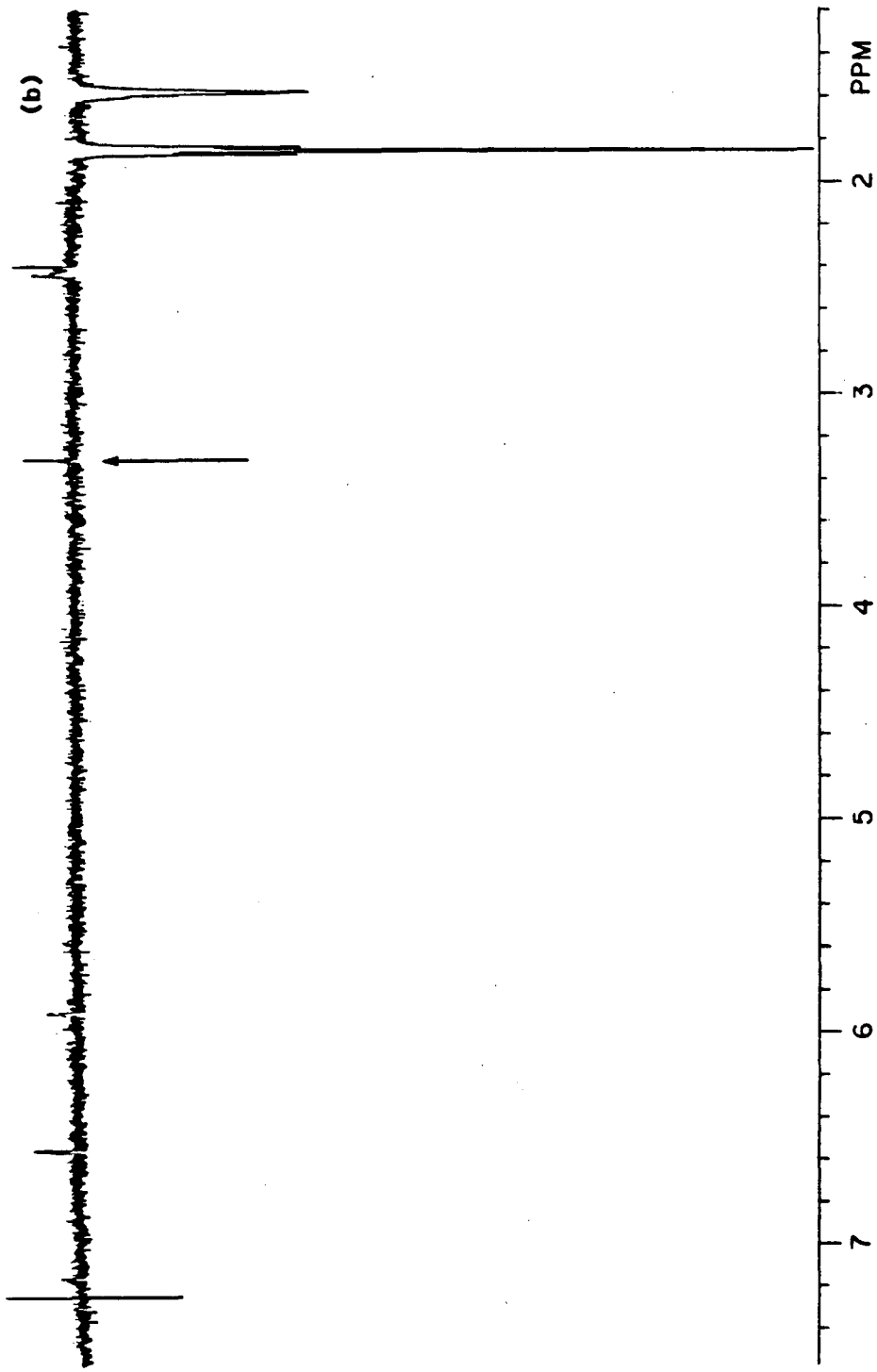
(b)
PPM
2
3
4
5
6
7

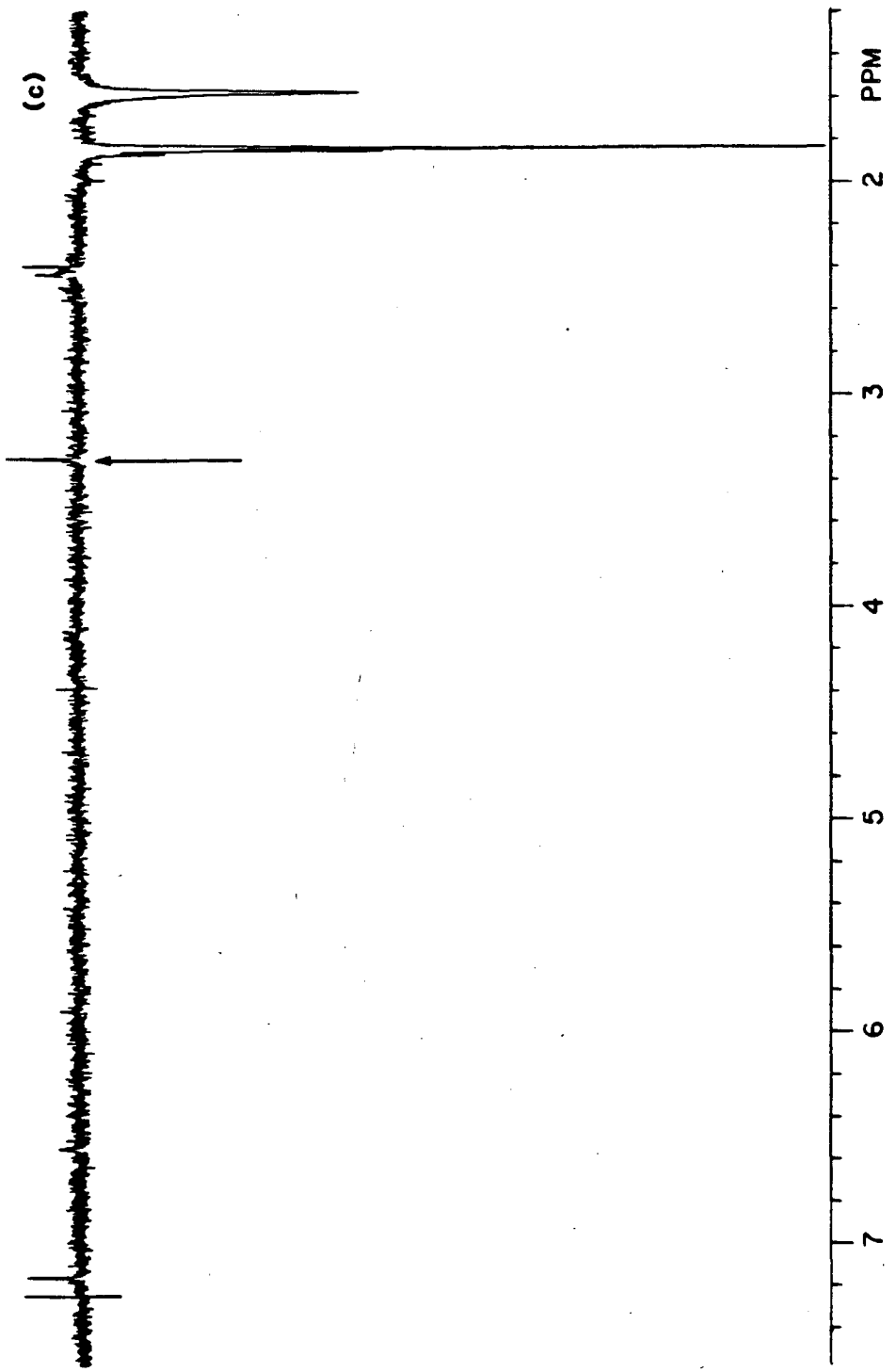
(c)
PPM
2
3
4
5
6
7

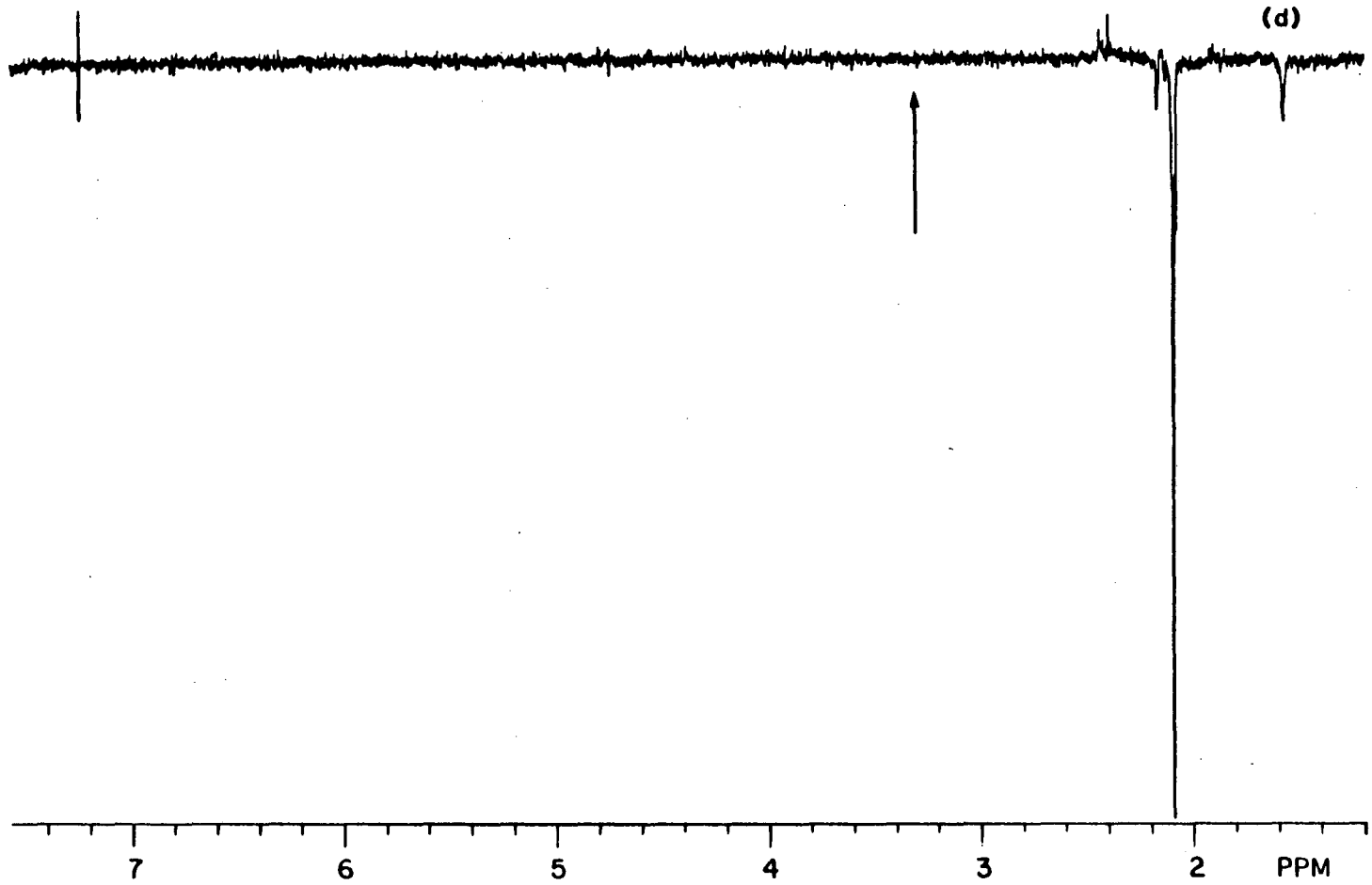
(d)
7
6
5
4
3
2
PPM

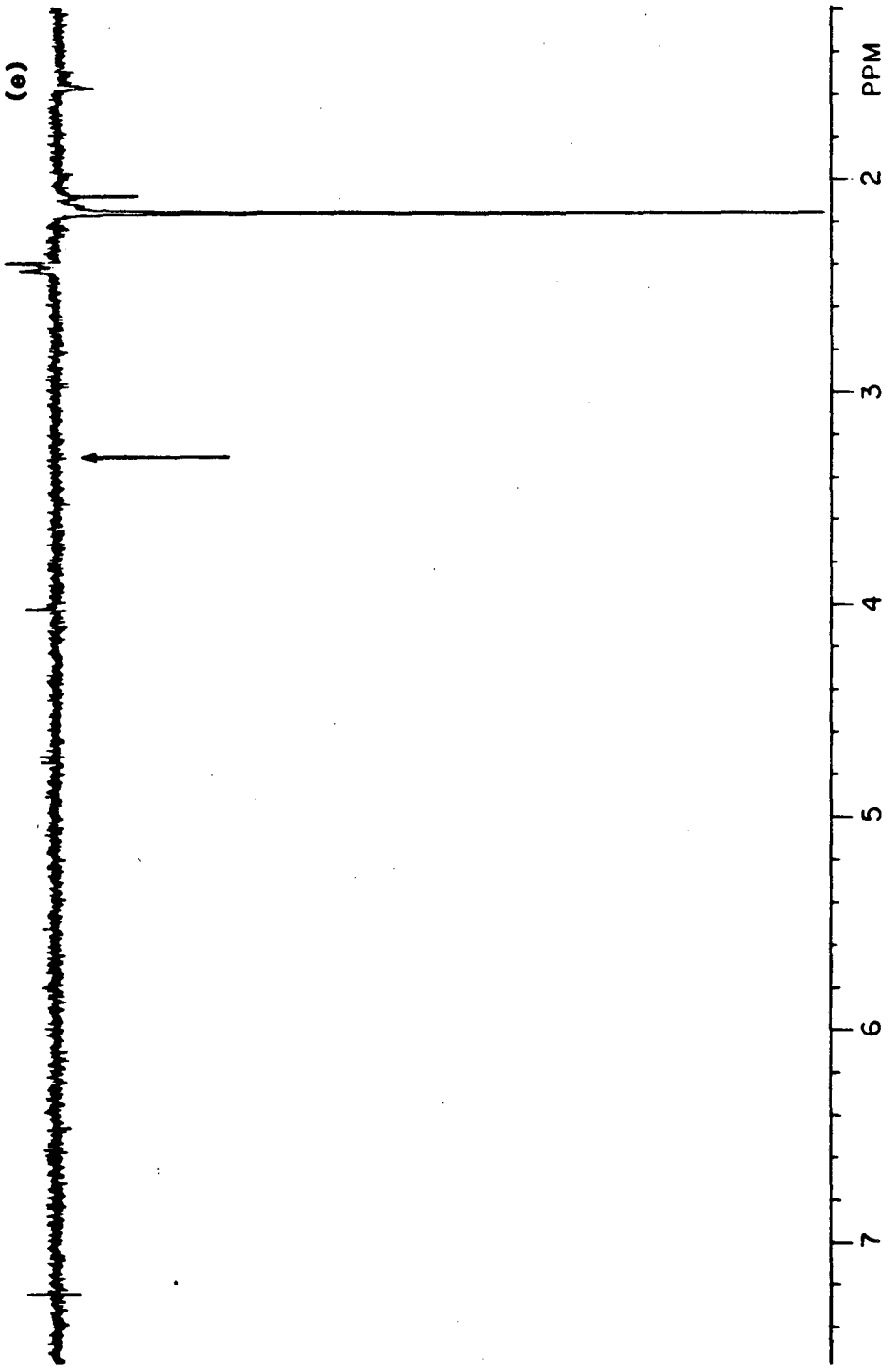
(e)
PPM
2
3
4
5
6
7

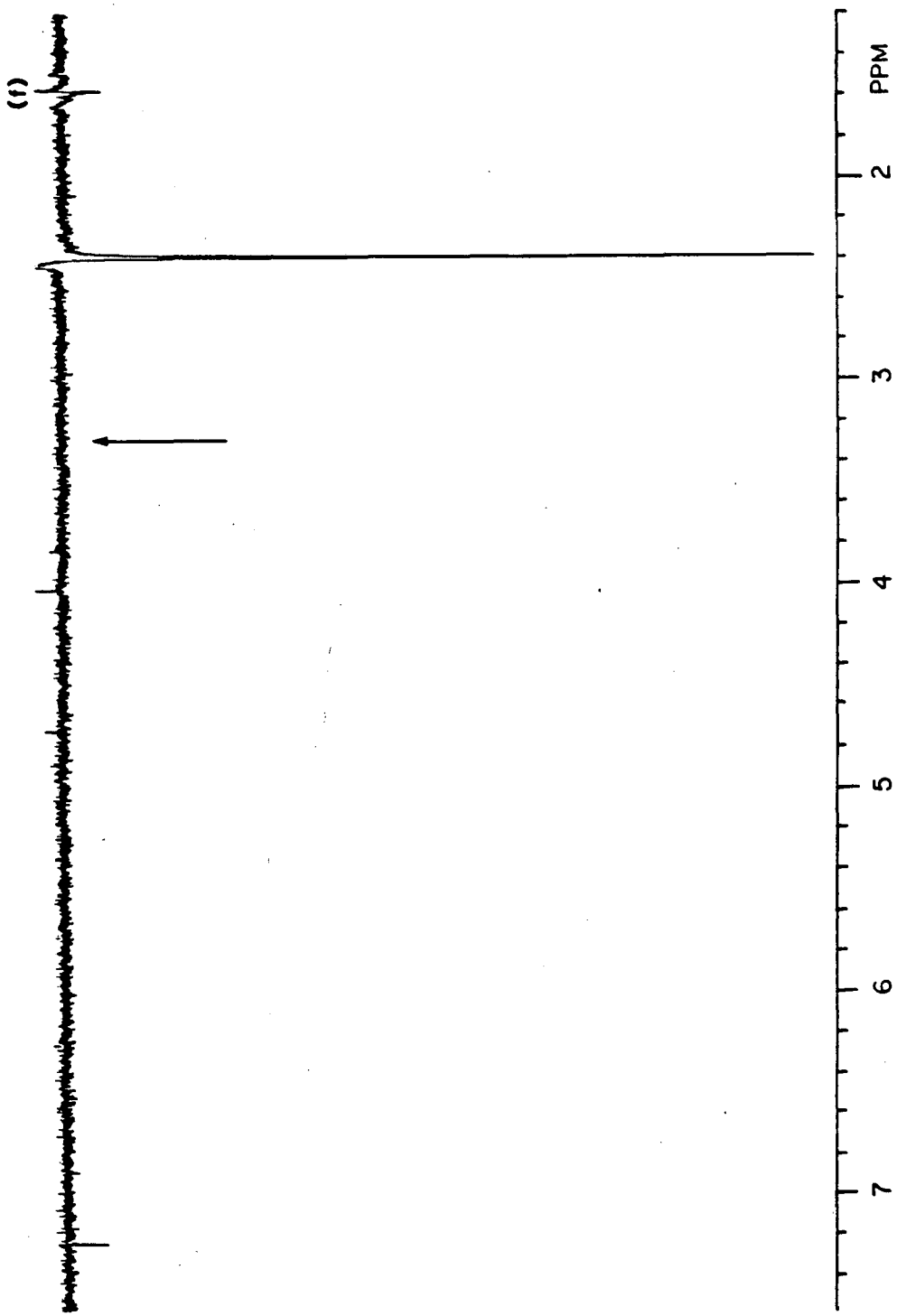
(f)
PPM
2
3
4
5
6
7

4. Discussion

We will first characterize the compounds HT and HM. The mass spectrum of HM showed it as having a molecular weight of 516 and thus permitted us to decide that HM is a photodimer of HMT. As was mentioned in the Results section, while the mass spectrum of HT did not show a species with a molecular weight of 516, it is nevertheless consistent with HT being a photodimer of HMT, when one takes into account the thermal lability of HT. The strongest chemical evidence we have for HT and HM being cycloaddition products is the fact that both compounds can revert to HMT thermochemically. We are thus quite certain that HT and HM are indeed dimeric species generated photochemically from HMT. We now proceed to deduce the structures of the two compounds.

A. Compound HT

Examining the NMR spectrum of HT (Figure 4.20), one notices immediately that there is a proliferation of resonances. Indeed, the number of resonances is exactly twice the number found in the NMR spectrum of HMT (Figure 4.19). HMT is a bifunctional photoreagent. The photochemical addition, which results in a cyclobutane ring, may proceed at either the 3-4 double bond in the pyrone ring or at the 4'-5' double bond in the furan ring. Such being the case, the joining

of two HMT molecules to form a dimer leads potentially to a plethora of stereochemical possibilities. First of all, the HMT molecules in the dimer may be cis or trans with respect to the cyclobutane ring; i.e., they may be on the same or opposite sides of the plane described by the cyclobutane ring. Secondly, HMT being bifunctional, the dimer may be result from head-to-head or head-to-tail joining of the two constituent monomers. Finally, we define a short axis joining the 5 and 8 positions in HMT (see Figure 4.1). We can see that in a dimer, the short axes of the two HMT moieties may be arranged in a roughly parallel or antiparallel fashion. These two alternatives give rise to the syn and anti configurations, respectively. If we were to run through the permutations of the above three binary choices exhaustively, we would generate the complete list of stereochemical possibilities inherent to HMT photodimerization.

In fact, we can come to a solution of the stereochemical problem rather quickly. HMT dimers can be divided into two classes: those with a point, axis or plane of symmetry and those without. In the symmetrical class, the two halves of the dimer are equivalent and the dimer should have the same number of proton resonances in the NMR spectrum as the parent, HMT. As for the non-symmetrical class, the two halves of the dimer are inequivalent, with the result that the NMR spectrum should have twice as many resonances as there are in the HMT monomer spectrum. Thus, HT, with twelve resonances in the NMR spectrum, must be a non-symmetrical dimer. Furthermore, the only way

to obtain a non-symmetrical dimer is by head-to-tail joining of two HMT's. We thus conclude that HT is a head-to-tail dimer. The question of whether the two halves of the dimer are cis or trans to the cyclobutane ring may first be answered qualitatively. Since the photochemistry is carried out in aqueous solution, we expect the stacking of two aromatic molecules like HMT to be favorable. If we assume that dimerization proceeds from the stacked species in aqueous solution, we would expect the dimer to be in the cis configuration, as stacking is not possible in the trans configuration. This assumption is justified in the light of previous work on coumarins (Anet, 1962; Morrison et al., 1966). The only point which remains to be resolved is that of syn vs anti configuration. This last question can be answered by doing Nuclear Overhauser Effect (NOE) experiments. In fact, the NOE results can also be used to assign cis and trans configurations unambiguously.

In Figure 4.27 are displayed the stereochemistries around the cyclobutane rings for the four possible head-to-tail dimers. In each case we find that the 3-H and 4-CH_3 of one monomer and the 4'-$HOCH_2$ and 5'-CH_3 of the other monomer are arranged around the cyclobutane ring. From previous work (most notably Kanne et al., 1982), we know that if we irradiate a methyl group on a cyclobutane ring, we can observe an NOE on another proton on the cyclobutane ring. Such NOE's are observable, PROVIDED that the methyl group and the proton are both on the same face of the cyclobutane ring (i.e., cis) and that they are not located on opposite corners of the ring (i.e., they

Figure 4.27 Stereochemical configurations for the four possible head-to-tail dimers of HMT. For each of the four cases the stereochemistry around the cyclobutane ring is shown. For the two cis structures, projection drawings are also shown. In the cis structures, the two monomers are on the same side of the plane of the cyclobutane ring. The drawing are projections of the monomer moieties onto the plane bisecting the cyclobutane ring and half-way between the two halves of the dimer. (The projection is actually distorted as the planes containing the two monomer units are not completely parallel with each other). In red is the half of the dimer in the "back", in relation to the viewer. In the drawings of the cyclobutane structures, the number (3, 4 or 5') refers to the numbering of the group in the parent HMT molecule.

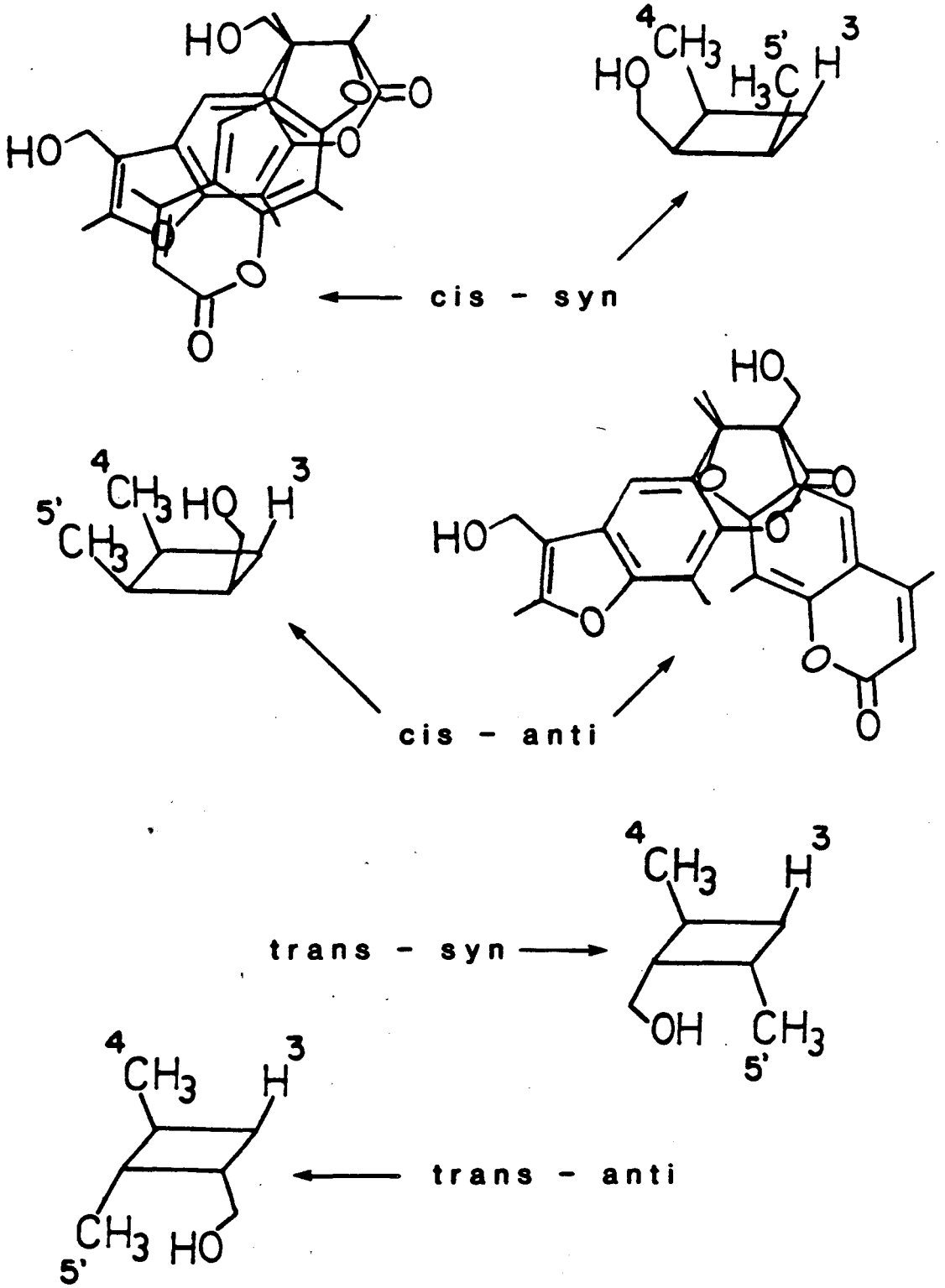
HO
HO
O
O
O
O
O
4 CH3
5' H3C
H 3
HO
cis - syn
HO
HO
O
O
O
O
O
O
4 CH3
HO
H 3
5' CH3
cis - anti
4 CH3
H 3
trans - syn
OH
CH3
5'
4 CH3
H 3
CH3
HO
5'
trans - anti

Table 4.1 Expected Patterns of NOE for the Four Possible Stereochemistries of Head-to-Tail Dimers

Configuration	Methyl on Cyclobutane Ring Irradiated	NOE to 3-H on Cyclobutane Ring
cis - syn	4	+
	5'	+
cis - anti	4	+
	5'	-
trans - syn	4	+
	5'	-
trans - anti	4	+
	5'	-

share an edge). In Table 4.1 are listed, for each of the different configurations, the NOE's we expect to see when irradiating specific methyl groups. The difference NOE spectra from irradiating the six methyl groups in HT are presented in Figures 4.26a through 4.26f. (The spectrum in Figure 4.26b is unreliable because it indicates that NOE is observed on all single protons in the molecule - an impossibility. This may be the result of uncontrollable drift or fluctuations in the NMR spectrometer while the data for the difference spectrum 4.26b were taken). The other difference spectra show that there are two methyl groups which, when irradiated, give rise to NOE's on the 3-H on the cyclobutane ring. This is consistent with only one of the predicted patterns listed in Table 4.1: the two HMT monomers are cis-syn in HT.

One interesting feature of the NMR spectrum of HT merits comment. There are two 4'-hydroxymethyl groups in HT. In HMT, where the hydroxymethyl group can rotate freely, the resonance is a singlet (Figure 4.19). In the HT spectrum however, both hydroxymethyl proton resonances are apparent quartets (Figure 4.20). The answer is to be found in the geometry of HT. In the cis-syn configuration, the hydroxymethyl on the cyclobutane ring is flanked tightly by two methyl groups which hinders rotation. The lack of rotational averaging causes the two methylene protons on the hydroxymethyl group to become inequivalent. Each proton now splits the resonance of its neighbor and a case of geminal coupling results. The apparent quartet is in fact a doublet of doublets. The severely split pair of

upfield doublets can thus be assigned as arising from the hydroxymethyl group on the cyclobutane ring. The marginally split, downfield hydroxymethyl resonance must then be due to the group on that half of HT that still has an intact furan ring. The very slight splitting in this resonance can be attributed to geminal coupling arising from mildly hindered rotation caused by the intact pyrone ring shadowing the hydroxymethyl group on the intact furan ring (see Figure 4.27).

B. Compound HM

By the symmetry argument described in the previous section, HM is a symmetrical dimer, since it has six resonances in the proton NMR spectrum. NOE is of no use in this case since symmetry reduces the number of observable NOE's to one, and it is the same pattern for all symmetrical dimers. By virtue of its being symmetrical, HM must be joined head-to-head (same as tail-to-tail). The question of whether it is the furan side (4'-5' double bond) or the pyrone side (3-4 double bond) that is involved in forming the cyclobutane bridge can be answered by looking at the UV absorption spectrum of HM and DHTMP (Figure 4.9 and 4.11). TMP is HMT sans hydroxymethyl group. DHTMP is TMP with the 4'-5' double bond in the furan ring reduced by hydrogenation. DHTMP should thus be excellent for modelling an HMT which has its furan side engaged in a cyclobutane bridge (the furan would effectively be reduced). The spectrum of DHTMP shows the

angularly shaped absorption band at ~330-340 nm, which is characteristic of substituted coumarins. When we look at the UV spectrum of HM we see that this coumarinic absorption is entirely absent. We may thus infer that in HM, the coumarin chromophore has been disrupted. This is most naturally explained by having the pyrone ring be the end which is locked in the cyclobutane ring.

What then is the location of the monomers relative to the plane of the cyclobutane? If the two HMT monomers were opposite faces of the cyclobutane ring, we would expect the hydroxymethyl groups on the two halves to be unhindered and to give rise to a singlet in the NMR spectrum. This is not so. The NMR spectrum of HM show a hydroxymethyl proton resonance which is a distinct doublet of doublets. This speaks for hindered rotation and would place the monomers cis to each other with respect to the cyclobutane ring.

Syn or anti configuration can be deduced in the same way. Figure 4.28 shows the syn and anti structures for the case where the two halves are cis to each other. It is clear at a glance that the anti structure have hydroxymethyls which are quite free to rotate, whereas in the syn case the two monomers sit on top of each other. Since the doublet of doublets is prominent in the NMR spectrum of HM, we conclude that the stereochemistry is syn.

Since the geminal coupling is so strong for the hydroxymethyl protons in HM, one may justifiably wonder if the furan rings might not also be nailed down in a cyclobutane bridge. That is, perhaps HM is a doubly bridged dimer. We can verify that this is not so.

Figure 4.28 Stereochemistries of the symmetrical dimers in the *cis* configuration. Projection drawings are shown for the *anti* structures. Projections of the *syn* structures essentially have two molecules superimposed.

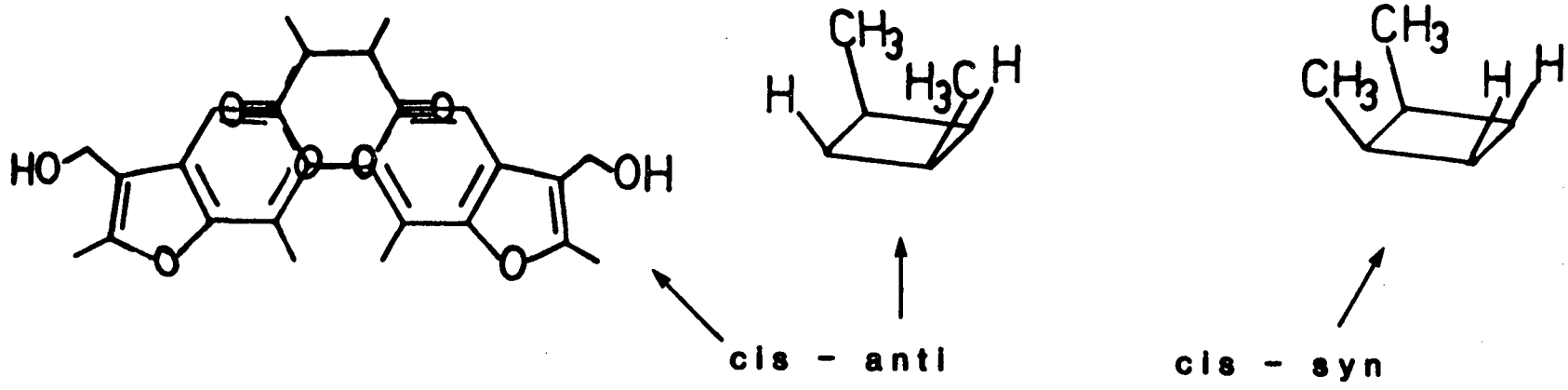

Pyrone-Pyrone Dimer

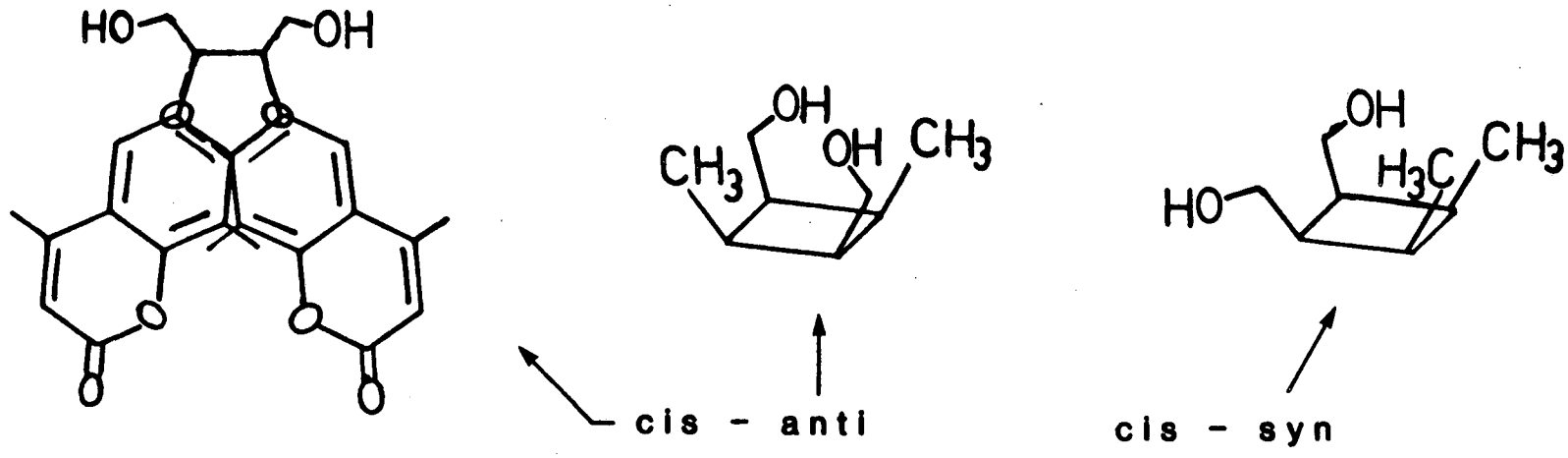

Furan-Furan Dimer

Figure 4.12 shows the UV spectrum of THTMP, i.e., TMP with both the furan and the pyrone rings reduced by hydrogenation. The chromophore in this case is essentially a multiply substituted benzene ring. THTMP shows little absorption between ~230-300 nm. HM, on the other hand, absorbs abundantly below ~270nm. The two spectral profiles are also very different. We thus conclude that HM has retained aromaticity in its furan rings. HM is a head-to-head, cis-syn dimer.

C. Compound I

Compound I is the most elusive of the photoproducts. When it was first isolated from HPLC separations done on the analytical scale, it gave a remarkable absorption spectrum (Figure 4.8). The spectrum of I is odd in having an absorption band which extends to ~440 nm. HMT, the parent compound, does not absorb beyond 400 nm. The long wavelength absorption band of I gives it a distinct yellow color both in solution and in the solid form. As was suggested in the Results section, the yellow compound might actually be a production of photooxidation. Two pieces of evidence argue against this proposition. When oxygen was excluded by purging exhaustively with either argon or helium before irradiation, compound I continued to be generated by exposure to UV light. More unequivocally, when sufficient quantities of I were purified and a FAB mass spectrum was gathered (Figure 4.18), we saw that the molecular weight of I is, at 258, identical to that of HMT. Species I must be an isomer of HMT.

A proton NMR spectrum shows that HMT and I have the same number of resonances (Figure 4.19 and 4.22). But more importantly, the splitting pattern of the resonances are the same for both I and HMT (both spectra consist entirely of singlets). The only resonance which changes significantly is that of the hydroxymethyl group: -0.7 PPM downfield in going from HMT to I. The methyl resonances show less than 0.3 PPM of upfield shift in going from HMT to I.

We are seeking a process by which HMT can be isomerized to yield an extended chromophore which absorbs in the visible. By the NMR data, the isomerization appears to affect mostly the hydroxymethyl group and to a much lesser degree, the methyls. Since coumarins are chemically robust species which do not normally enter into exotic photochemical reactions, attention is probably better directed to the furano segment of the HMT molecule. One possible way to have a new chromophore is by placing an oxygen next to position 6 on the coumarin ring so that the new compound has a chromophore akin to a hydroxydienone system (Figure 4.29). There is published evidence that such a substituted 6-hydroxycoumarin system often gives a yellow coloration (Kaufman et al., 1962). The difficulty lies in not having a ready mechanism by which the furan oxygen in HMT (linked to position 7 on the coumarin) can be transferred to the opposite side of the ring.

The photochemistry of furans and other pentaheterocycles have received some attention in the past. Early workers were able to observe ring-scrambling reaction products from the photolysis of

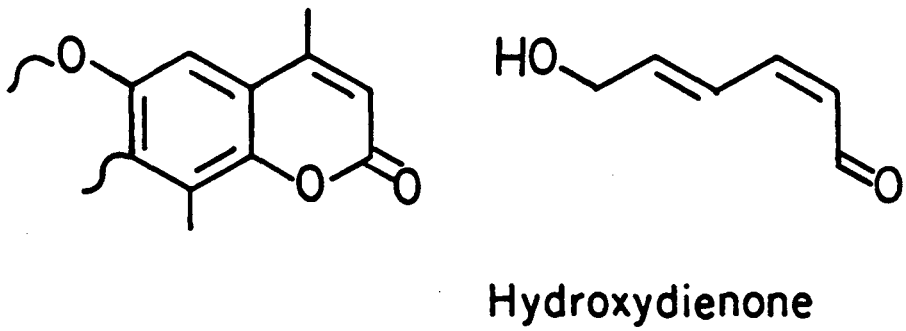

Figure 4.29 Coumarin moiety of HMT with oxygen attached to C_6 instead of C_7. Also shown is the hydroxydienone chromophore generated by such a rearrangement.

furans (Srinivasan, 1967 ; van Tamelen & Whitesides, 1968). These reactions can be represented as

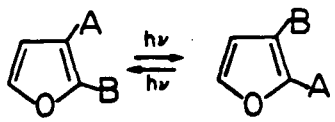

Through trapping studies and solvent incorporation studies, an acylcyclopropene intermediate was postulated:

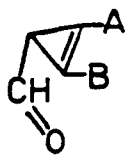

The photorearrangement can be written as a (1,3)-sigmatropic shift:

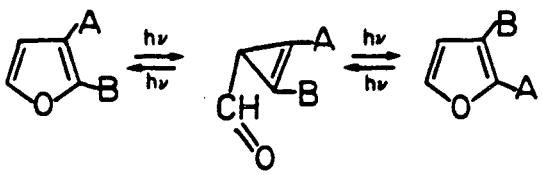

Alternatively, the acylcyclopropene intermediate can be reached by undergoing a homolytic cleavage of the C_1-O bond followed by rearrangement:

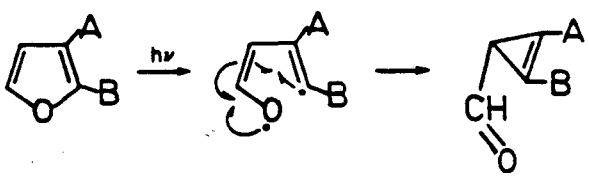

The subsequent ring expansion can be thought of either as another (1,3)-sigmatropic shift or as a cycloaddition of the carbonyl to the σ-bond of the cyclopropene. We can borrow this mechanism for simple furans and apply it to the HMT case at hand. The mechanism for HMT may be written as

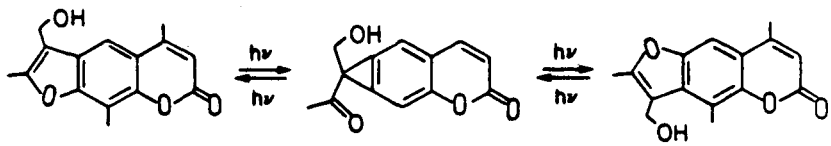

Once the acylcyclopropane intermediate is generated, the carbonyl group (whose oxygen used to be attached to position 7 on the coumarin moiety), is in a position that is at least locally symmetrical. This local symmetry means that when the intermediate undergoes ring expansion, the carbonyl may add either to the 7 position of the coumarin, in which case it regenerates HMT; or the carbonyl may add to the 6 position in which case the entire furan ring is flipped 180° with respect to the coumarin and an isomeric furocoumarin is produced. This scheme is outlined in Figure 4.30. This mechanism is in no way established, but it has grounding in the photochemistry of simple furans.

Potentially, a different acylcyclopropene intermediate can be generated by another route. If, rather than cleaving the C_7-O_1, bond, as above, the $C_{5'}$-$O_{1'}$ bond is cleaved, we can have the reaction below

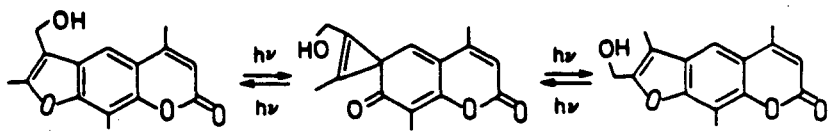

This route is not expected to be favored because to produce the intermediate here requires the aromaticity of the coumarin to be broken. We note also that this mechanism generates an isomer of HMT with only the 4' and 5' substituents reversed. No change is effected

in the tricyclic aromatic nucleus.

We now have a reasonable (though unverified) mechanism consistent with the experimental results on compound I. To furnish absolute proof, one may make use of the extensive chemical craft developed for synthesizing various types of furocoumarins and attempt to synthesize the molecule with the structure shown in Figure 4.30. An encouraging start is the knowledge that the molecule

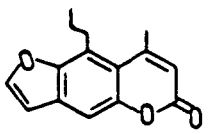

has been synthesized successfully and while detailed spectroscopic data are lacking, we do know it to be yellow (Kaufman et al., 1962).

Appendix 1

MISCELLANEOUS COMPONENTS FOR THE DIALOG TEMPERATURE JUMP INSTRUMENT

1. The Polarizer and Orientational Effects

For experiments involving polymeric nucleic acids or charged biopolymers in general, the polarizer with condensing lense can be used in place of the condensing lense which is normally placed in front of the temperature jump cell, in the path of the light beam. The polarizer is effective in suppressing the fast signal arising from the orientation and orientational relaxation of the biopolymer caused by discharging the capacitor through the sample. These orientation signals are usually of much larger amplitude than the chemical relaxation signals one wishes to study. An orientation signal has the property that the sign and magnitude of its relaxation amplitude are dependent on the polarization of the incoming light. In principle, setting the polarizer at an angle of 55.5° should effectively remove the orientation signal. A series of temperature jump traces illustrating the effect of the polarizer is shown in Figure A1.1. For a detailed discussion of orientational effects observed in temperature jump experiments, one should consult the work of Dourlent (Dourlent et al., 1974).

2. Fluorescence Measurement: Improving the Signal to Noise

When operating the temperature jump instrument in the fluorescence mode, the signal input cable attached to the Photometric Control Box should be disconnected from the PMT used for measuring transmitted light and be connected to the PMT used for collecting fluorescence. The fluorescence PMT should also be connected to its own power supply by the special cable provided. The fluorescence PMT power supply is located on top of the regular PMT power supply. After these obligatory connections are made, three attachments serve to enhance the signal-to-noise ratio.

A. UV-Enhanced High Reflectivity Planar Mirror

The Dialog instrument is equipped with two photomultiplier tubes perpendicular to the path of the incoming light for collecting fluorescence. The control unit of the instrument, however, is only able to receive and process signal from <u>one</u> of the PMT's (either the front or the back tube). Consequently, half of the available fluorescence is lost. One can increase the signal by placing a high quality planar mirror in front of the inactive PMT, with the silvered surface facing the temperature jump cell. This set-up allows the fluorescence previously lost to be reflected into the active PMT. The mirror presently used in the instrument is supplied by Melles Griot, with a part number of 01MFG011/028. This mirror surface has a coating which enhances reflectivity in the ultraviolet region. Both the silvering and the "UV coating" on the mirror are quite soft. Should it become necessary to clean the mirror, gentle streams of

detergent and distilled water are to be used. Drying should be done with a clean jet of nitrogen.

B. Concave Mirror

Dialog supplied a concave mirror for use when making fluorescence measurements. The concave mirror is screwed into the cell mount, with the concave surface facing the back window of the temperature jump cell. The concave mirror reflects the exciting light back through the sample to give increased fluorescence. The signal-to-noise is markedly improved by this set-up.

C. Cut-Off Filters

When the exciting light impinges on the aqueous sample, in addition to the fluorescence, one gets scattered light also. The bulk of the scattered light is due to Rayleigh and Tyndall scattering and is at the same wavelength as the exciting light. A small amount of Raman scattering by water also takes place and the scattered light is slightly red-shifted from the exciting light. The exact amount of red-shift can be calculated from the vibrational frequency of water. The scattered intensity can seriously interfere with the fluorescence temperature jump measurement and should be eliminated. This is done by placing a cut-off filter in front of the fluorescence PMT. Excellent filters are manufactured by Jena^{er} Glaswerk Schott & Gen. of Mainz, West Germany. These filters have sharp cut-off edges and very nearly approach 100% transmittance at wavelengths where they are

supposed to be transparent. Corning glass filters proved to be unsuitable because the cut-offs are broad and the transmission properties poor.

3. The Arc Lamp

The 200-Watt Xe-Hg arc lamp can be purchased from Canrad-Hanovia Inc. The part number is 901B0011. When installing the arc lamp, one should wear a face shield since the lamps have very high internal pressure. Pay attention to the marking "BOTTOM" on the lamp, as the wrong polarity will cause the lamp to melt. During installation, it is better to clamp in the bottom electrode first, since the lead to the bottom electrode is flexible. The clamp to the top electrode is rigid. The flexibility of the bottom clamp is important for relieving stress as one is positioning the lamp into the rigid top clamp. The lamp has a small nodule on its body where the cavity was sealed. This nodule should be facing the back of the lamp housing (toward the installer when being mounted). The smooth side of the bulb should face the small round window on the front of the lamp housing. This orientation makes it possible to see the condition of the arc.

The arc lamp is always operated so as to be current-limited. The power supply should therefore be set to maximum voltage while the current should be set to between 8.5 and 9.5 amperes. A new lamp will usually work fine at 8.5 amp. With increasing age of the lamp, the current may be increased to aid in stabilizing the arc (but not

above 9.5 amp). The working lifetime of the arc lamps is ~200 hours, after which the lamp noise may become too severe. A new lamp needs to burn for ~6-10 hours before the arc is stable enough for temperature jump measurements.

In starting the arc lamp, the power supply should first be on for at least ten seconds, then one should press the START button on the discharge unit for ~1 second. If the arc fails to ignite, just wait for ~10 seconds and try again. Once the lamp is started, the arc should connect the point of the upper electrode to the blunt tip on the bottom electrode. If the arc actually terminates on the helical metal windings on the lower electrode, TURN OFF POWER SUPPLY IMMEDIATELY to avoid danger of explosion. The arc can be re-struck after ~10 seconds.

A large magnetic stir bar is mounted on a rotatable "dip-stick" in the lamp housing. The field of the magnet sometimes helps in reducing arc wander. The best orientation for the magnet is found only through trial and error. On some occasions it is necessary to adjust the magnet before each temperature jump. Arc instability is one the major obstacles to successful temperature jump measurement. Unfortunately, there is no assured way of ridding oneself of the nuisance.

Appendix 2

THE ZERO-SUPPRESSION OPTION

ON THE DIALOG TEMPERATURE JUMP INSTRUMENT

If we wish to "blank out" the relaxation signal from time 0 to time t, then we first connect the intrument and recording equipment as shown in Figure A2.1. We then dial in, on the Photometric Control Unit, the duration of zero-suppression, t. Most importantly, the time base of the Tektronix oscilloscope must be set such that

$$10 \times (\text{Time/Division})_{\text{Tektronix}} > 2048 \times (\text{Time/Channel})_{\text{Biomation}}$$

This is to guarantee that the GATE VOLTAGE supplied by the (Dialog-modified) Tektronix scope will be maintained for the duration of data acquisition. The READY light on the Tektronix time base must be ON before the temperature jump is triggered, otherwise no gate voltage will be applied. Thus it is always a good idea to press the spring-loaded RESET lever on the Tektronix time base before triggering the jump. After data acquisition, the data can be displayed on the Tektronix scope in the normal manner, with the equipment connected as shown in Figure A2.2.

Prior to using the zero-suppression option, it is advisable to check that all the components are functioning properly. Three simple checks can be performed. Since all three tests require the capacitor to be discharged, one must make certain that a T-jump cell containing

Figure A2.1 Instrument set-up when using the zero-suppression option. When the capacitor is discharged, a trigger pulse is sent out by the High Voltage Power Supply.

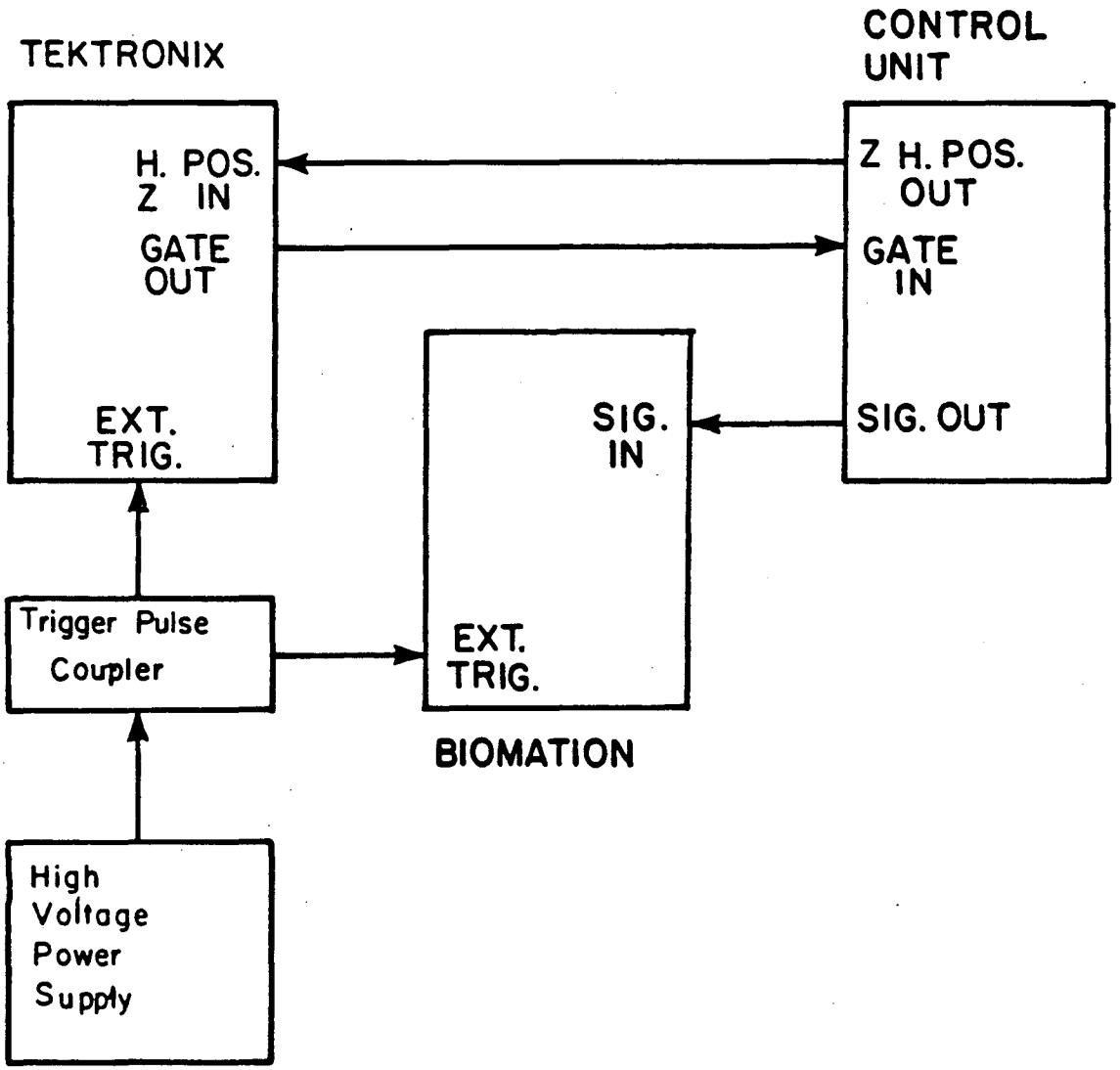

Figure A2.2 Set-up for viewing data stored in the Biomation.

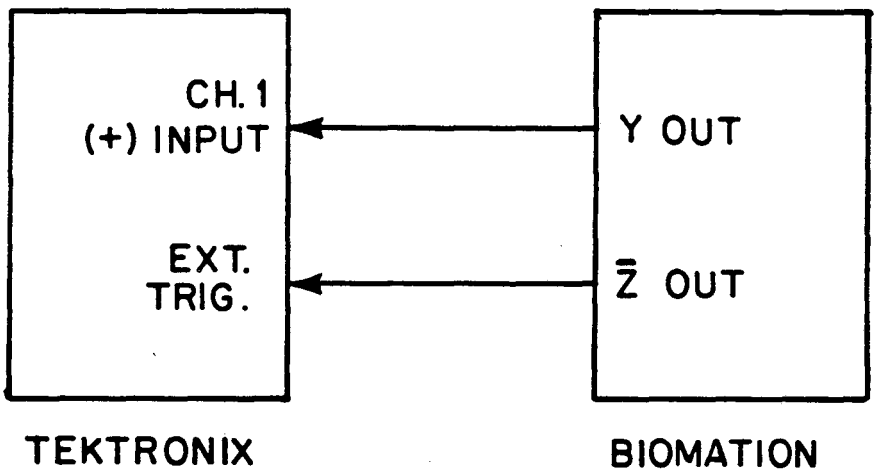

at least a salt solution is placed in the instrument.

1. The Ability of the Discharge to Trigger the Gate Voltage Output of the Tektronix Time Base

Set up the connections as in Figure A2.3. In this configuration, the Biomation records the value of the gate voltage applied by the Tektronix time base. The Biomation should be in Pretrigger mode with 48 points before the trigger and 2000 points after. Data acquisition occurs at 10 μs/channel. The full scale range should be set to 50 V. The Tektronix time base should be set for Single Sweep at 1 ms/division. Since there are 10 divisions on the Tektronix scope, a setting of 1 ms/division in this case amounts to applying the gate voltage for 10 ms. Since the Biomation is set to record for 20 ms, the gate voltage will be maintained for only the first half of the recording period. After the capacitor is discharged, and the equipment is reconnected as in Figure A2.2, we should see a voltage vs time trace corresponding to the diagram in Figure A2.4

2. High-Positive Z Output from the Control Unit as Function of Time in Zero-Suppression Mode

We first make the connections as shown in Figure A2.5. The Photometric Control Unit should be set for 5 ms of zero-suppression. The Biomation settings are precisely as in Section 1. The settings on the Tektronix time base should be Single Sweep at 10 ms/division.

Figure A2.3 Instrument connections for checking the ability of the capacitor discharge-induced trigger pulse from the High Voltage Power Supply to trigger the Gate Voltage Output of the Tektronix Time Base.

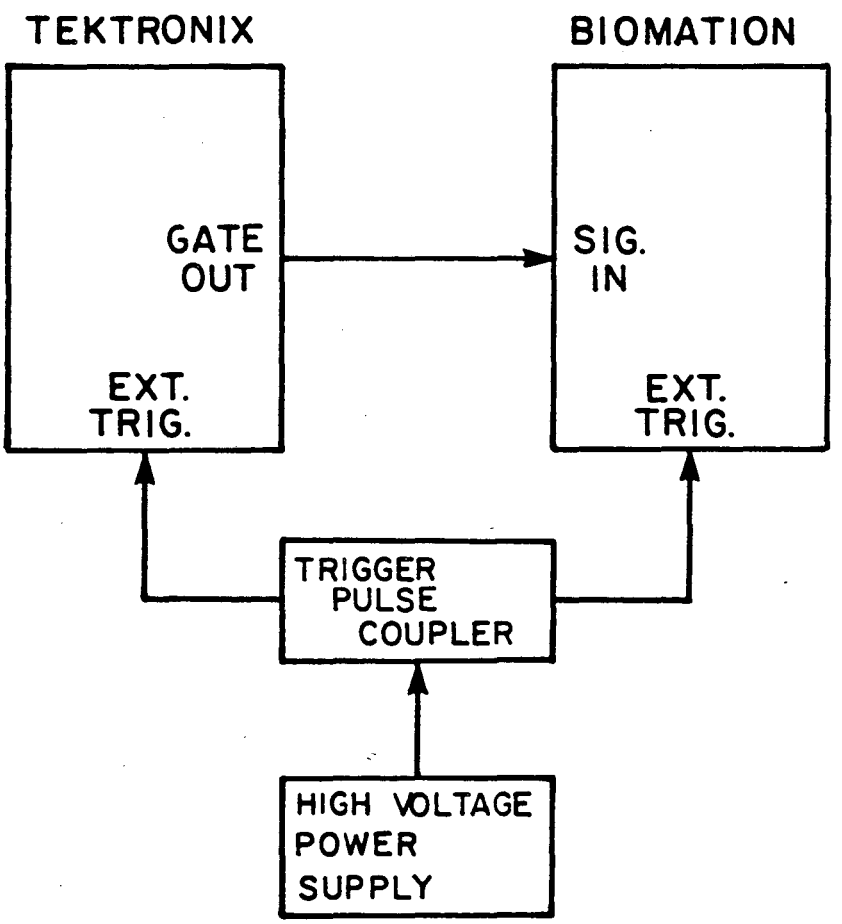

Figure A2.4 Voltage vs time trace obtained when the instrument is operated with the connections shown in Figure A2.3.

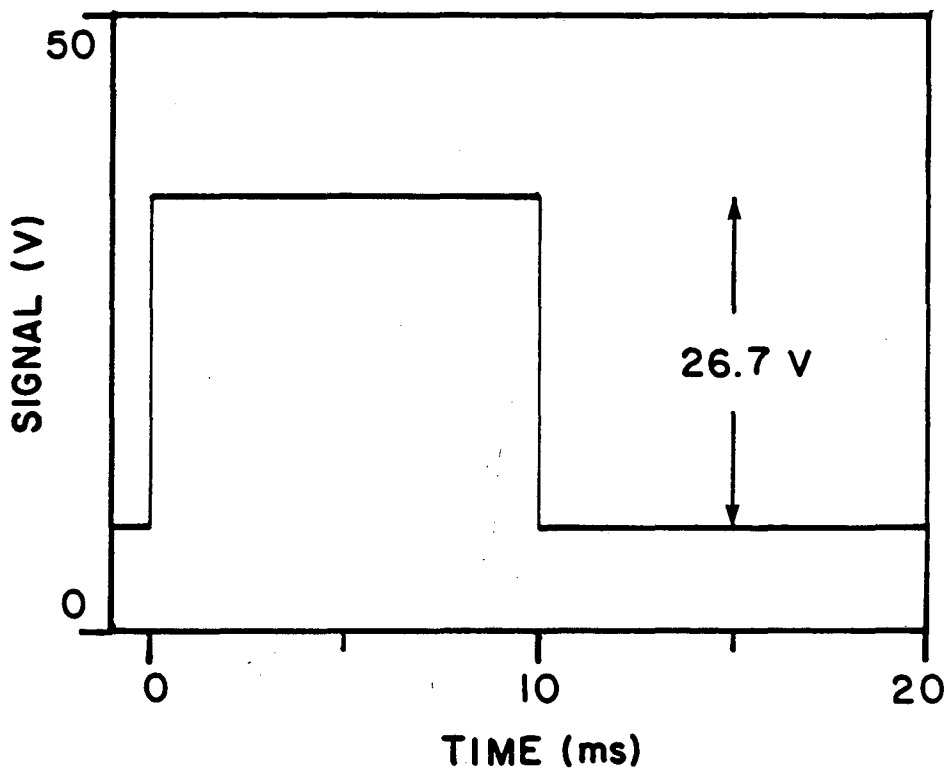

Figure A2.5 Instrument set-up for monitoring the High-Positive Z output from the Control Unit as a function of time, in the zero-suppression mode.

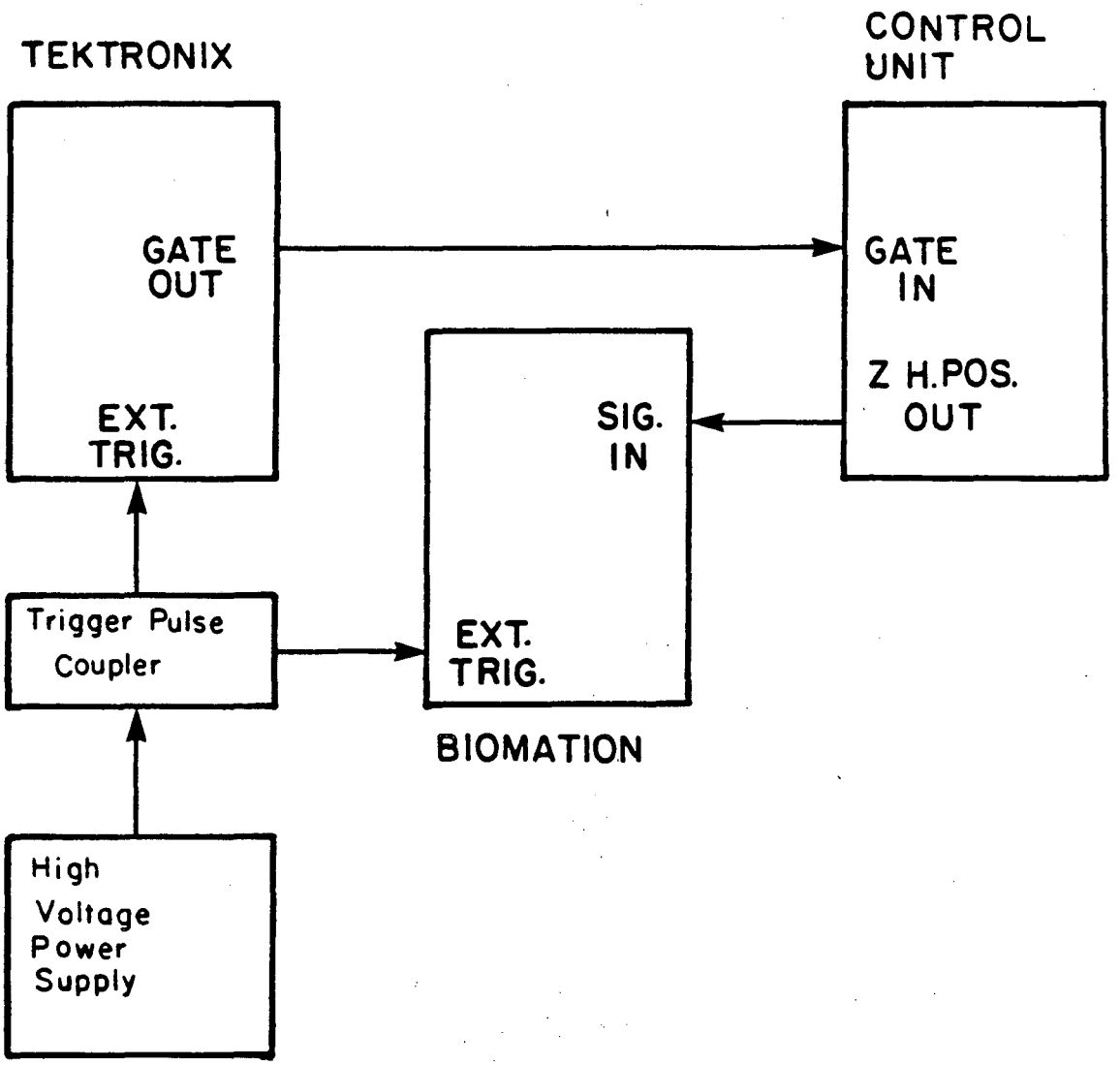

Figure A2.6 Voltage vs time trace obtained when the instrument is operated as set up in Figure A2.5.

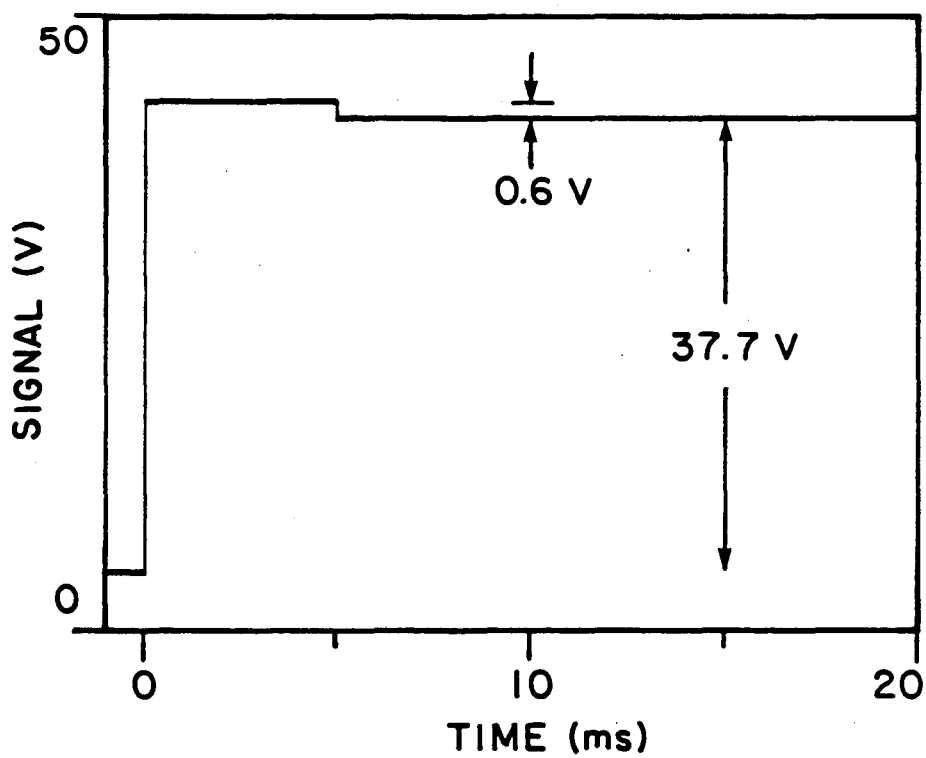

These settings cause the Tektronix to be active for a total of 100 ms. This is "overkill" since Biomation recording ends after 20 ms. The purpose is just to insure that the gate voltage is on for the duration of data collection. The Biomation recording, when viewed in the configuration of Figure A2.2, should look like the trace diagrammed in Figure A2.6.

3. Behavior of the Gate Voltage in Zero-Suppression Mode

The check is made with equipment connected as in Figure A2.7. The settings on the Control Unit, the Tektronix and the Biomation are identical to those in Section 2 above. After triggering, the Biomation record displayed using the set-up of Figure A2.2 should be as shown in Figure A2.8.

4. An Example Illustrating the Use of Zero-Suppression

In Figure A2.9 we find a signal vs time trace recorded with a full scale range of 5 V and a total data acquisition time of 20 ms. Most of the range is taken up by a fast component. With 200 μs of zero-suppression, the fast rising signal can be blanked out (Figure A2.10, still at a full scale range of 5 V). In Figure A2.11 is the record of data collected with the same amount of zero-suppression, but now with 2 V full scale. The slow components now expand to take up most of the range and are more finely digitized. This last fact greatly improves the chances of determining slow, small-amplitude

components with precision.

Figure A2.7 Instrument set-up for checking the behavior of the Gate Voltage in zero-suppression mode.

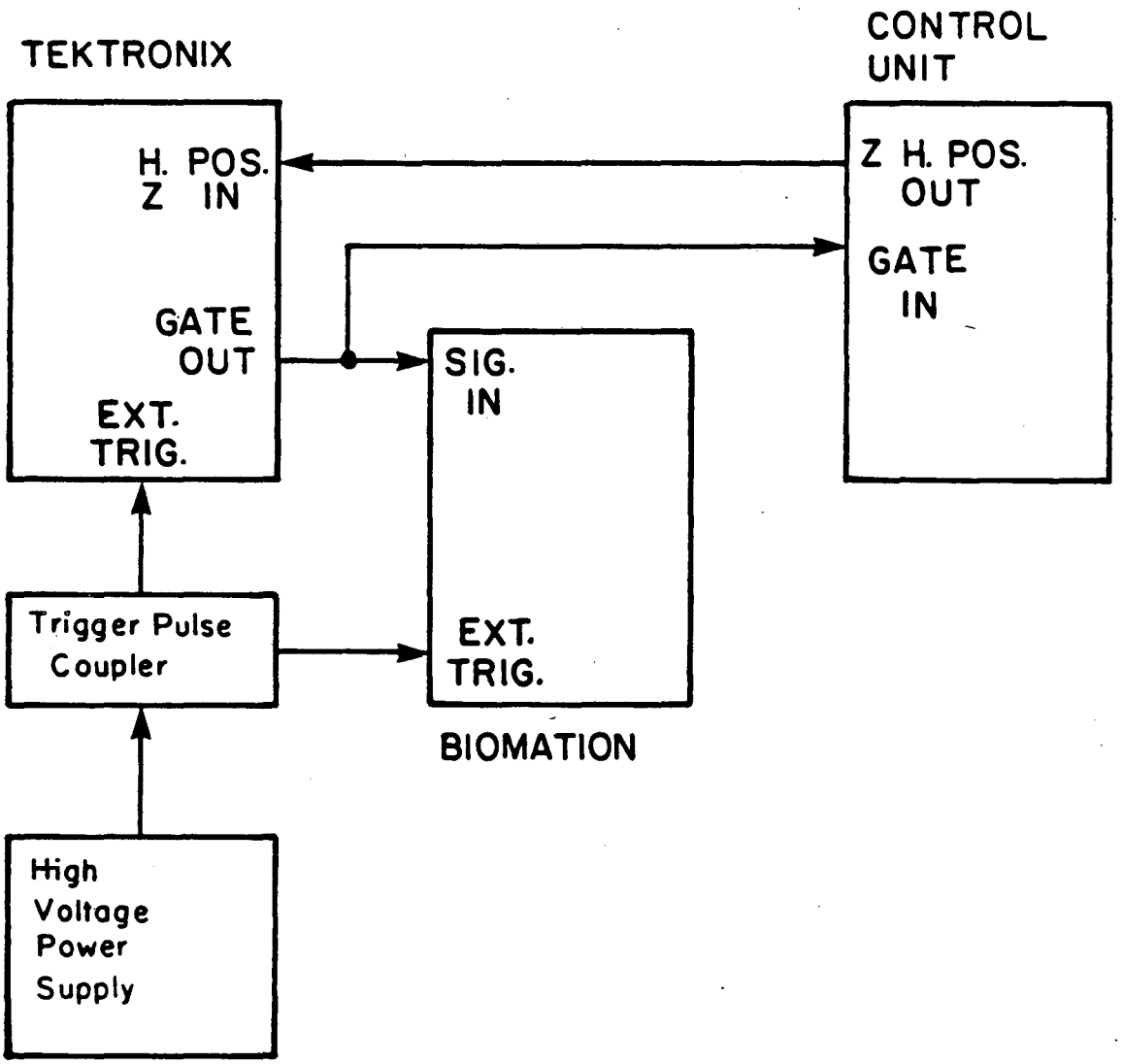

Figure A2.8 Voltage vs time trace obtained when the instrument is operated as shown in Figure A2.7.

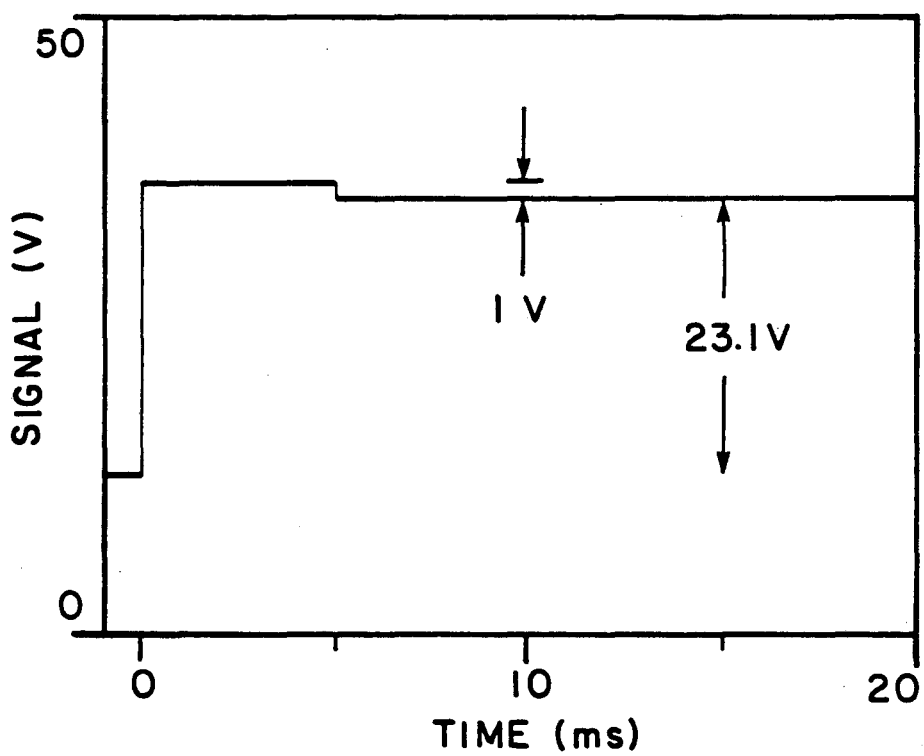

Figure A2.9 A relaxation signal recorded without using the zero-suppression option. Note that much of the vertical range is taken up by a very fast component of large amplitude.

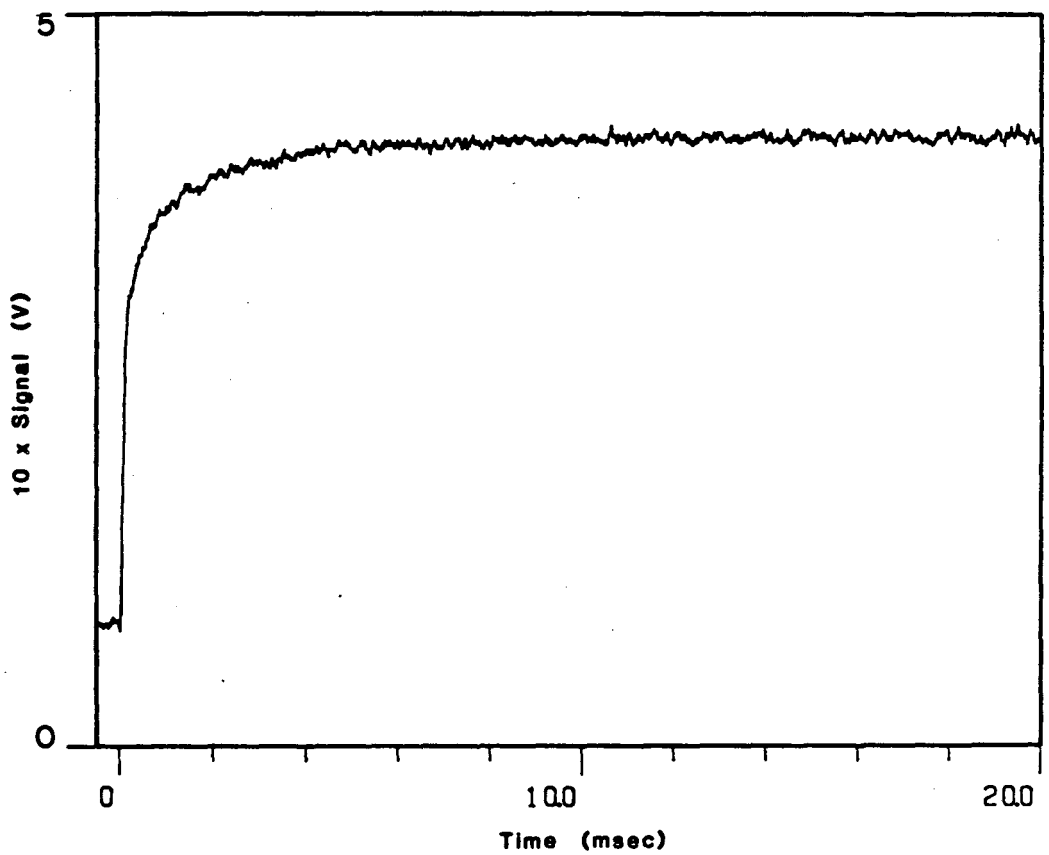

Figure A2.10 When the same signal as that recorded in Figure A2.9 is collected in the zero-suppression mode, with 200 μsec of zero-suppression, the above trace is obtained. Note that the large, fast component has been "blanked out."

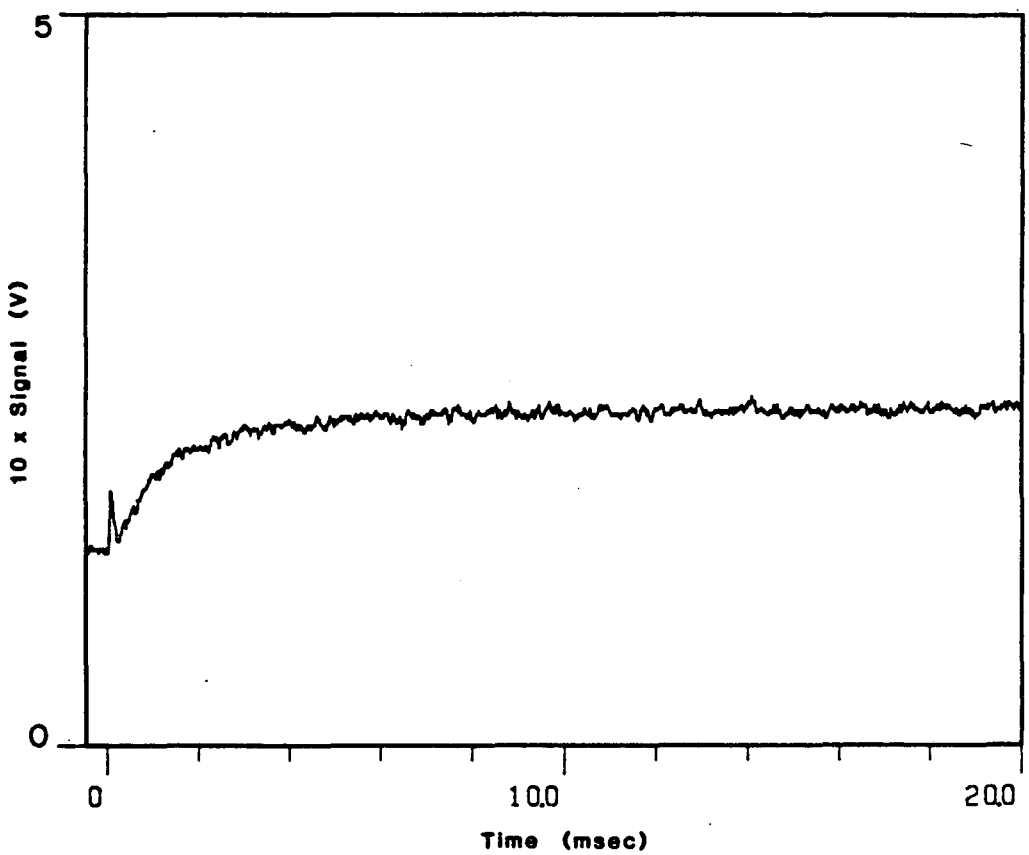

Figure A2.12 The slow, small component left over after zero-suppression is recorded using an expanded scale. The relaxation curve is now recorded with finer digital resolution.

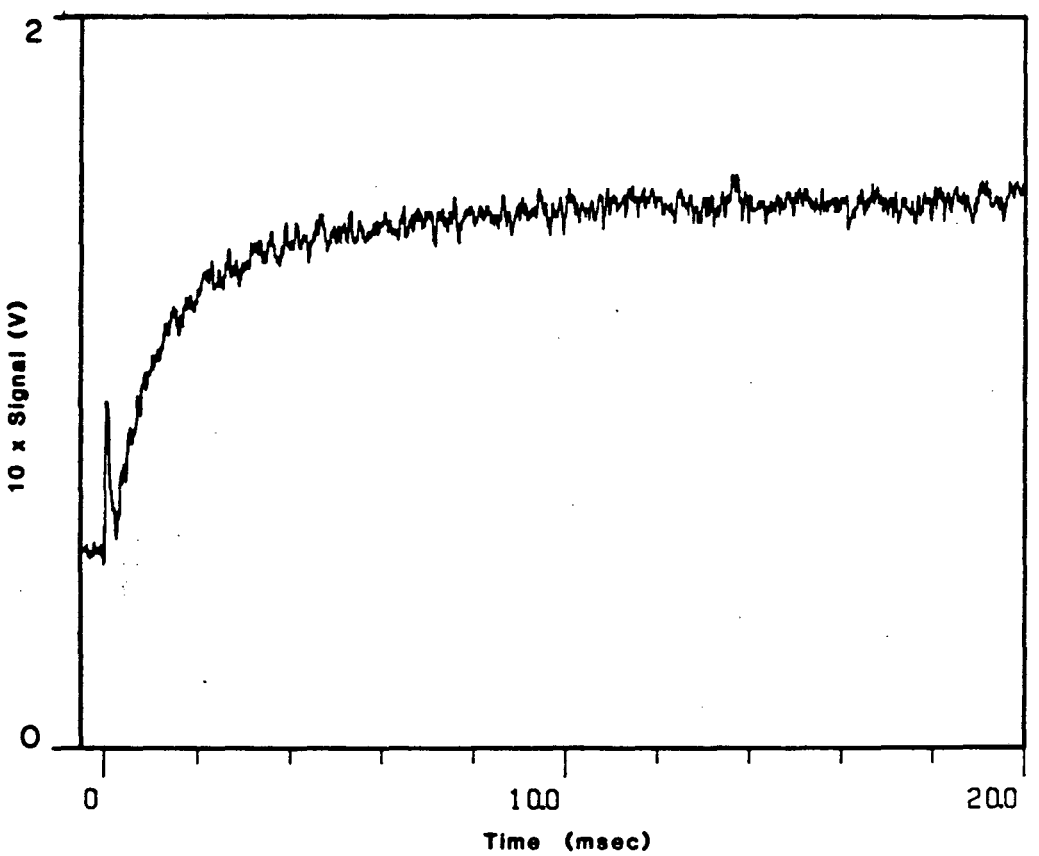

Appendix 3

CALIBRATING THE TEMPERATURE JUMP INSTRUMENT

In a temperature jump experiment, the rapid change in temperature is achieved by discharging a capacitor through the sample solution which contains an inert salt. We can always measure the initial temperature of the sample quite accurately, for it is just the temperature of the sample cell and the cell mount which is maintained at the initial temperature thermostatically. After the capacitor discharge, only the sample is heated to the final temperature by Joule heating. The bulk of the cell and the cell mount remain at the initial temperature. The higher final temperature of the sample lasts at most for ~3-4 seconds before convection develops in the sample and the sample begins its descent back to the initial temperature. It is thus clear that the final temperature of the sample can not easily be measured by conventional means. The final sample temperature is determined by adding the magnitude of the temperature jump to the initial temperature. For this reason it is always necessary to calibrate the size of the temperature jump obtained when one discharges a capacitor through any temperature jump cell.

The analysis of relaxation time data from temperature jump experiments is least mathematically cumbersome when the rise in temperature of the sample occurs in a time much shorter than the

shortest relaxation time in the chemical system under study. This condition is the basis for the term "temperature jump." We require sample heating to be complete long before any process of interest begins to take place in the sample. When this condition is not met, data analysis becomes much more complex or often, impossible. In order to decide whether our data can be analyzed simply, we need to know the heating time of the sample. Since the heating is accomplished by discharging the capacitor through the sample solution which has a certain resistance, the characteristic heating time is just RC/2, where R is the resistance of the sample in ohms and C is the capacitance of the capacitor in farads. We can see that since the heating time is proportional to the resistance in the sample solution, the salt concentration in the sample is important in determining the heating time.

The Tris buffer system (tris(hydroxymethyl)aminomethane and its hydrochloride salt) is used for calibration because its acid-base behavior is strongly dependent on temperature. The rapid change in acidity of the buffer solution caused by a jump in temperature can be rendered measurable optically by adding cresol red indicator to the Tris buffer solution. The large absorbance changes resulting from changes in temperature makes calibrating the size of the temperature jump quite easy.

Equilibration of simple proton transfer processes in solution is extremely rapid and occurs on a time scale of nanoseconds. Typical temperature jump instruments using Joule heating have heating times

on the order of microseconds. The acidity changes in the Tris buffer are thus faster than the capacitor discharge time by two to three orders of magnitude. For this reason, if we discharge a capacitor through the calibration buffer, the changes in the acidity of the buffer will exactly track the progress of heating of the solution. By recording the absorbance change of the cresol red in the Tris buffer as a function of time and analyzing the resultant "relaxation curve", one can extract a "relaxation time" which is the characteristic heating time of the instrument under the experimental conditions.

The calibration solution contains 0.01 M Tris adjusted to pH 8. The solution must also contain at least 0.05 M of a simple binary salt like NaCl or KNO_3. Since it is always advisable to determine the heating time of the temperature jump instrument under the experimental conditions to be used, it is convenient to carry out the calibration using the same salt concentration as that of the experimental samples to be measured. This way the same batch of solution can be used for determining both the jump size (which is not a function of the salt concentration) and the heating time (which is a function of the salt concentration). Typically, the inert salt concentration is between ~0.05 M and ~2 M for most experiments.

1. Determining the Size of the Temperature Jump

A. Absorbance of the Calibration Solution as a Function of

Temperature

We need first to measure the variation of the absorbance of the calibration solution as a function of temperature. This measurement is most easily done on a spectrophotometer equipped with a thermostatted cell mount. The Gilford spectrophotometer equipped with temperature controller is ideally suited for this purpose. With the calibration buffer in a 1-cm pathlength cell, we record the absorbance of the sample at 572 nm over a reasonable range, e.g., 5°C to 30°C. A linear least squares fit of A_{572} as a function of temperature yields a slope which is the change in A_{572} per Celsius degree FOR THIS PARTICULAR CALIBRATION SOLUTION.

B. Size of the Temperature Jump as a Function of the Capacitor Voltage

To calibrate the size of the temperature jump, one filters and degasses the calibration solution according to the normal procedure for sample preparation. The solution is then placed in the instrument and allowed to settle to a stable initial temperature the exact value of which is not important. Since only the total amplitude of the jump is needed, we may set the RC-filter time constant for the instrument at some high value (e.g., ≥1 msec) to get good signal-to-noise ratio. We want to be certain that data acquisition extends over a period long enough for the system to have equilibrated at the new temperature. Since 2000 points are usually recorded at regular time intervals, we can set the recording

intervals, δt ("Time per Channel" on the Biomation recorder), such that $2000\delta t \geq 10\tau_{RC}$, where τ_{RC} is the RC-filter time constant on the instrument. We then perform a series of temperature jumps extending over a range of capacitor voltages. In each case, the PMT voltage is recorded as a function of time on the Biomation recorder. The change in PMT voltage (ΔI) is related to the absorbance change (ΔA) of the solution :

$$-2.303\Delta A = \ln(1 + \Delta I/I) \qquad \text{A3.1}$$

The quantity I is always set to be 5 V on the instrument. For the small absorbance changes normally observed in temperature jump experiments, Equation A3.1 can be approximated as

$$-2.303\Delta A = \Delta I/I \qquad \text{A3.2}$$

and the PMT voltage vs time data can be analyzed directly as if it were absorbance vs time data. But the change in hydrogen ion concentration in the Tris buffer caused by a normal temperature jump is large enough that the PMT voltage changes are no longer proportional to absorbance changes. We need to convert the voltages to absorbances using Equation A3.1. We then divide the absorbance change by the optical pathlength of the T-jump cell to arrive at a value of the absorbance change adjusted to standard pathlength of 1 cm. Using the slope of the least squares line found in Section 1A above, the corrected absorbance change in the temperature jump cell can be converted into a change in temperature, ΔT. We can thus

determine ΔT for a number of capacitor voltages. A least squares fit of ΔT vs $(kV)^2$ yields a linear expression for ΔT as a function of the square of the number of kilovolts across the capacitor. The size of any temperature jump can now be calculated from the linear relationship. One must remember however, that the calibration is valid only for this particular combination of capacitor and T-jump cell. A change of either calls for a different calibration.

2. Determining the Heating Time on the Instrument

To measure the heating time, we proceed essentially as in Section 1 with a few exceptions. Since we are now trying to determine the short time limit of the instrument, we must set the RC-filter time constant to the minimum possible. Furthermore, since the heating time is typically less than 20 μs, the data acquisition time interval should be made small, e.g., 0.5 to 1.0 μs per channel. Once again, the voltage changes need to be converted into absorbance changes as outlined in Section 1. We have now $\Delta A(t)$, which at long times tends to a limiting value ΔA_∞. The difference $\Delta A_\infty - \Delta A(t)$ can be computed for the early time points where $\Delta A(t)$ is still changing significantly. A plot of $\ln|\Delta A_\infty - \Delta A(t)|$ vs time provides a straight line with slope $-1/\tau_h$, where τ_h is the heating time of the instrument. One must again remember that the heating time so determined applies only to the particular combination of capacitor, T-jump cell and salt concentration.

BIBLIOGRAPHY

Ames, B. N. & Whitefield, H. J., Jr. (1966) Cold Spring Harbor Symp. Quant. Biol. 31, 221.

Anderson, C. F., Record, T. M. & Hart, P. A. (1978) Biophys. Chem. 7, 301.

Anet, R. (1962) Canad. J. Chem. 40, 1249.

Bachellerie, J.-P., Thompson, J. F., Wegnez, M. R. & Hearst, J. E. (1981) Nucl. Acids Res. 9, 2207.

Bauer, W. & Vinograd, J. (1968) J. Mol. Biol. 33, 141.

Bauer, W. & Vinograd, J. (1970) J. Mol. Biol. 47, 419.

Bernasconi, C. F. (1976) Relaxation Kinetics, Academic Press, New York, New York.

Bresloff, J. L. & Crothers, D. M. (1975) J. Mol. Biol. 95, 103.

Cairns, J. (1962) Cold Spring Harbor Symp. Quant. Biol. 27, 311.

Chu, Y. G. & Tinoco, I., Jr. (1983) Biopolymers 22, 1235.

Cole, R. S. (1971) Biochim. Biophys. Acta 254, 30.

Crick, F. H. C., Barnett, L., Brenner, S. & Watts-Tobin, R. J. (1961) Nature 192, 1227.

Depew, R. E. & Wang, J. C. (1975) Proc. Nat. Acad. Sci. USA 72, 4275.

Dourlent, M., Hogrel, J. F. & Hèlène, C. (1974) J. Am. Chem. Soc. 96, 3398.

Drobnies, A. E. (1979) Ph.D. Thesis, University of California, Berkeley.

Handbook of Biochemistry and Molecular Biology, Nucleic Acids, 3rd

ed., Vol. I (1975) CRC Press, Cleveland, Ohio, p. 589.

Hearst, J. E., Isaacs, S. T., Kanne, D., Rapoport, H. & Straub, K. (1984) Quart. Rev. Biophys. 17, 1.

Isaacs, S. T., Shen, C. J., Hearst, J. E. Rapoport, H. (1977) Biochemistry 16, 1058.

Kanne, D., Straub, K., Rapoport, H. & Hearst, J. E. (1982) Biochemistry 21, 861.

Kaufman, K. D., Keana, J. F. W., Kelly, R. C., McBride, D. W. & Slomp, G. (1962) J. Org. Chem. 27, 2567.

Khorana, H. G. (1968) Pure Appl. Chem. 17, 349.

Lerman, L. (1961) J. Mol. Biol. 3., 18.

Lerman, L. (1964) J. Cellular Comp. Physiol. 64, Suppl. 1, 1.

Li, H. J. & Crothers, D. M. (1969) J. Mol. Biol. 39, 461.

Manning, G. (1978) Quart. Rev. Biophys. 11, 179.

Matteucci, M. D. & Carruthers, M. H. (1981) J. Am. Chem. Soc. 103, 3185.

McCann, J., Choi, E., Yamasaki, E. & Ames, B. N. (1975) Proc. Nat. Acad. Sci. USA 72, 5135.

Morden, K. M., Chu, Y. G., Martin, F. H. & Tinoco, I., Jr. (1983) Biochemistry 22, 5557.

Morden, K. M. (1983) Ph.D. Thesis, University of California, Berkeley.

Morrison, H., Curtis, H. & McDowell, T. (1966) J. Am. Chem. Soc. 88, 5415.

Musajo, L. (1963) Pure Appl. Chem. 6, 369.

Musajo, L., Bordin, F., Caporale, G., Marciani, S. & Rigatti, G.

(1967) Photochem. Photobiol. 6, 711.

Nelson, J. W. (1982) Ph.D. Thesis, University of California, Berkeley.

Nelson, J. W. & Tinoco, I., Jr. (1982) Biochemistry 21, 5289.

Okada, Y., Terzaghi, E., Streisinger, G., Emrich, J., Inouye, M. & Tsugita, A. (1966) Proc. Nat. Acad. Sci. USA 56, 1692.

Okada, Y., Streisinger, G., Owen, J. E., Newton, J., Tsugita, A. & Inouye, M. (1972) Nature 236, 338.

Orgel, A. & Brenner, S. (1961) J. Mol. Biol. 3, 762.

Patel, D. J., Koslowski, S. A., Marky, L. A., Rice, J. A., Broka, C., Dallas, J., Itakura, K. & Breslauer, K. J. (1982a), Biochemistry 21, 437.

Patel, D. J., Koslowski, S. A., Marky, L. A., Rice, J. A., Broka, C., Itakura, K. & Breslauer, K. J. (1982b) Biochemistry 21, 445.

Pörschke, D., Uhlenbeck, O. C. & Martin, F. H. (1973) Biopolymers 12, 1313.

Provencher, S. W. (1976a) Biophys. J. 16, 27.

Provencher, S. W. (1976b) J. Chem. Phys. 64, 2772.

Pulleybank, D. E., Shure, M., Tang, D., Vinograd, J. & Vosberg, H.-P. (1975) Proc. Nat. Acad. Sci. USA 72, 4280.

Ramstein, J., Ehrenberg, M. Rigler, R. (1980) Biochemistry 19, 3938.

Record, M. T., Jr., Mazur, S. J., Melancon, P., Roe, J. H., Shaner, S. L. & Unger, L. (1981) Annu. Rev. Biochem. 50, 997.

Rigler, R., Rabl, C.-R. & Jovin, T. M. (1974) Rev. Sci. Instrum. 45, 580.

Ripley, L. S. (1982) Proc. Nat. Acad. Sci. USA 79, 4128.

Salet, C., Macedo de sa e Melo, T., Bensasson, R. & Land, E. J. (1980) Biochim. Biophys. Acta 607, 379.

Schmechel, D. E. V. & Crothers, D. M. (1971) Biopolymers 10, 465.

Scott, B. R., Pathak, M. A. & Mohn, G. R. (1976) Mutat. Res. 39, 29.

Srivnivasan, R. (1967) J. Am Chem. Soc. 89, 1758.

Streisinger, G., Okada, Y., Emrich, J., Newton, J., Tsugita, A., Terzaghi, E. & Inouye, M. (1966) Cold Spring Harbor Symp. Quant. Biol. 31, 77.

Thammana, P., Cantor, C. R., Wollenzien, P. L. & Hearst, J. E. (1979) J. Mol. Biol. 135, 271.

Thompson, J. F. & Hearst, J. E. (1983) Cell 32, 1355.

Van Tamelen, E. E. & Whitesides, T. H. (1968) J. Am. Chem. Soc. 90, 3894.

Wakelin, L. P. G. & Waring, M. J. (1980) J. Mol. Biol. 144, 183.

Wang, J. C. (1974) J. Mol. Biol. 89, 783.

Waring, M. (1968) Nature 219, 1320.

This report was done with support from the Department of Energy. Any conclusions or opinions expressed in this report represent solely those of the author(s) and not necessarily those of The Regents of the University of California, the Lawrence Berkeley Laboratory or the Department of Energy.

Reference to a company or product name does not imply approval or recommendation of the product by the University of California or the U.S. Department of Energy to the exclusion of others that may be suitable.

TECHNICAL INFORMATION DEPARTMENT
LAWRENCE BERKELEY LABORATORY
UNIVERSITY OF CALIFORNIA
BERKELEY, CALIFORNIA 94720